Nonlinear Transport Properties of Quantum Dot Systems

vorgelegt von

Diplom-Physiker

Gerold Kießlich

aus Berlin

von der Fakultät II – Mathematik und Naturwissenschaften
der Technischen Universität Berlin
zur Erlangung des akademischen Grades

Doktor der Naturwissenschaften
– Dr. rer. nat. –

genehmigte Dissertation

Promotionsausschuss:

Vorsitzender:	Prof. Dr. Christian Thomsen
Berichter:	Prof. Dr. Eckehard Schöll, PhD
Berichter:	Prof. Dr. Andreas Wacker

Tag der wissenschaftlichen Aussprache: 21. Oktober 2005

Berlin 2005
D 83

Zusammenfassung

Diese Arbeit beschäftigt sich mit der theoretischen Untersuchung und Beschreibung des nichtlinearen elektronischen Transports durch gekoppelte Quantenpunktsysteme mit Hilfe verschiedener Modelle. Wesentlich hierbei ist zum einen die Berücksichtigung der Coulomb-Wechselwirkung zwischen den Ladungsträgern und zum anderen die Quantenkohärenz im resonanten Tunnelprozess. Beide sorgen für zeitliche Korrelationen im Tunnelstrom, die sich auf charakteristische Weise in den Stromfluktuationen offenbaren. D.h. für ein tieferes Verständnis des Transportprozesses ist es notwendig, nicht nur den mittleren Strom, sondern auch das Stromrauschen zu studieren.

Charakteristisch für Strom-Spannungs-Kennlinien von gekoppelten Quantenpunktsystemen ist das Auftreten von Peaks. Deren physikalischer Ursprung und die Abhängigkeit von systemspezifischen Parametern wird ausführlich in einem Mastergleichungsmodell diskutiert. Darüberhinaus werden systematisch Szenarien für Sub-Poisson- und Super-Poisson-Rauschen aufgezeigt und analysiert. Dabei tritt das Wechselspiel zwischen Coulomb-Wechselwirkung und Pauli-Prinzip in den zeitlichen Korrelationen des Tunnelprozess deutlich zutage. Für die quantenkohärente Beschreibung des Transports unter der Berücksichtigung der Coulomb-Wechselwirkung wird die Hartree-Fock-Näherung betrachtet. Es zeigt sich, dass sie zwar für den nichtlinearen Strom zuverlässige Ergebnisse liefert, aber auf Grund der Vernachlässigung von Quantenfluktuationen das Rauschen nicht hinreichend wiedergibt.

Um die Verbindung zwischen sequentiellem und kohärentem Tunneln herzustellen, wird der Mechanismus der Dephasierung des kohärenten Transports untersucht. Im Vordergrund steht hierbei der Vergleich verschiedener Modellansätze ohne Coulomb-Wechselwirkung. Im Speziellen zeigt sich, dass der mittlere Strom durch zwei seriell gekoppelte Quantenpunkte unabhängig ist vom Grad der Kohärenz im Transportprozess. Für schwache und starke Kopplung zwischen den Quantenpunkten gilt dies auch für das Nullfrequenz-Stromrauschen. Demgegenüber ist es für mittlere Kopplungen sensitiv auf Kohärenz. Dephasierung durch elastische Streuung im Streumatrixformalismus führt in diesem Bereich zwar zum Verschwinden der kohärenten Merkmale, im Limes hinreichend starker Dephasierung weicht es allerdings vom Rauschverhalten des sequentiellen Tunnelns ab.

Um in diesem Zusammenhang den Transportprozess vollständig zu charakterisieren, wird das moderne Konzept der Elektronen-Zählstatistik benutzt. Insbesondere zeigt die Kumulante dritter Ordnung ein qualitativ ähnliches Verhalten bezüglich des Dephasierens wie das Schrotrauschen.

Abstract

This work deals with the theoretical investigation and description of nonlinear electronic transport through coupled quantum dot systems by means of various approaches. The essential aspects are the consideration of the Coulomb interaction between the carriers and the quantum coherence during the resonant tunneling process. Both provide temporal correlations in the tunneling current which manifest themselves in a characteristic manner in the current fluctuations. This means that for a deeper understanding of transport processes it is necessary not only to consider the average current, but also the shot noise behavior.

Typical for current-voltage characteristics of coupled quantum dot systems is the emergence of peaks. Their physical origin and dependencies on the system parameters is elaborately discussed by means of a master equation model. Furthermore, scenarios of sub-Poissonian and super-Poissonian noise are systematically presented and analyzed. Therein, the interplay between the Coulomb interaction and Pauli's exclusion principle clearly emerges. For the quantum coherent description of transport with Coulomb interaction the Hartree-Fock approximation is considered. It provides reasonable results for the average current, but due to the neglect of quantum fluctuations the noise proves to be inadequate.

In order to establish the connection between sequential and coherent tunneling, the mechanism of dephasing of the coherent transport process is investigated. The main focus here is on the comparison of different approaches without Coulomb interaction. In particular, the average current through two quantum dots coupled in series turns out to be independent of the degree of quantum coherence in the transport process. For weak and strong coupling between the quantum dots this also holds for the zero-frequency shot noise. However, for intermediate coupling strengths the noise is sensitive to coherence. Dephasing by elastic scattering in the framework of scattering matrix formalism indeed leads to the loss of the coherent features in the noise, but for sufficiently strong dephasing the limit of sequential tunneling cannot be reached within this approach.

In order to fully characterize the transport process in this context the modern concept of full counting statistics is utilized. Particularly the third order cumulant shows a qualitatively similar dephasing behavior as the shot noise.

Contents

List of important Symbols, Functions, and Abbreviations

Symbol	Description
$e > 0$	elementary charge
$f_{e/c}$	Fermi distribution for emitter/collector contact
$\underline{\underline{j}}_{e/c}$	current operator at the emitter/collector barrier
n_i	occupation number of single-particle state i
$t_{k\sigma\eta}$	tunnel matrix element (contact state k, spin $\sigma \in \{\uparrow, \downarrow\}$, contact $\eta \in e/c$)
$C_{ab}(t)$	correlation function of current between contacts a and b
C_k	k-th order cumulant
C^{-1}	inverse capacitance matrix
Diag[.]	diagonal matrix with entries .
$F(\chi)$	characteristic or cumulant generating function
H	Hamiltonian
$I_a, \langle I_a \rangle$	stationary current at contact a
Im	imaginary part
$\underline{\underline{M}}$	transition matrix in master equation
$\overline{P}(N, t_0)$	full counting statistics (FCS) distribution function
$\underline{P}$	probability vector
$\underline{P}^0$	stationary probability vector
Re	real part
$S_P(\omega)$	total spectral power density
$S_{ab}(\omega)$	spectral power density between contacts a and b
S_{Poisson}	spectral power density for Poissonian noise
T	temperature
$\hat{T}, \hat{T}^{\text{anti}}$	time-ordering operator, anti time-ordering operator
$\hat{T}_C$	contour-ordering operator
$T_{ab}(\varepsilon)$	transmission function between contacts a and b
$\underline{\underline{T}}(t)$	time propagator for master equation
Tr[.]	trace of .
U	Coulomb interaction strength
V	external bias voltage

Symbol	Description
α	Fano factor
$\delta(.)$	delta distribution
ε	energy
ε_i	energy of single-particle state i
η_i	leverage factor for single-particle state i
χ_i	counting field at contact/terminal i
ω	frequency
$\Gamma_{e/c}^{(i)}$	emitter/collector tunneling rates of single-particle state i
Γ_{φ}	dephasing rate
$\Theta(.)$	Heaviside function (step function)
Ω	tunnel matrix element (between quantum dots)

	Description
AFM	atomic force microscopy
CVC	current-voltage characteristic
DOS	density of states
EOM	equation of motion
FCS	full counting statistics
FWHM	full width at half maximum
ME	Master equation
NDC	negative differential conductance
NEGF	nonequilibrium Green's functions
QD	quantum dot
SMF	scattering matrix formalism
SPD	spectral power density
SPI	Stochastic path integral approach
2DEG	two-dimensional electron gas

1. Introduction

1.1. General context

Nanotechnology deals with the manufacturing of functional materials, devices and systems through control of matter on the nanometer length scale (1-100 nanometers), and exploitation of novel phenomena and properties (physical, chemical, biological, mechanical, ...) at that length scale. In particular, computational nanoelectronics is probably one of the most prominent and quickly developing areas. In the meantime a large variety of nanostructures serve as basic modules for electronic or opto-electronic devices in this field. Most of them are made up of semiconductor materials. Very new technologies which certainly will come into commercial operation in the very near future even use single organic or anorganic molecules as the active part of devices and electronic circuits.

The smallest mesoscopic nanostructure in use is typically termed **quantum dot** (QD) - therein "quantum" refers to the specific physical properties of electrons caged in all three spatial dimensions on the nanometer length scale. This spatial confinement gives rise to the term "dot". These structures are frequently denoted as "artificial" atoms since their electronic structure very much resembles those of real atoms [MCE97, REI02]. Primarily the discrete density of states (DOS) implies such an analogy, but moreover shell-filling effects as an important property of real atoms described by Hund's rules can be found in QDs as well [TAR96].

The electronic transport through QDs is based on the mechanism of *resonant tunneling*. Since the pioneering work of Esaki a huge amount of scientific work has considered this fascinating phenomenon mainly in the so-called resonant tunneling diode which consists of a double barrier heterostructure with an electronic confinement in transport direction. The *negative differential conductance* (NDC) in the respective current-voltage characteristic (CVC) is the fingerprint of resonant tunneling [CHA74]. In contrast to the resonant tunneling diode, semiconductor QDs provide a countable number of electronic states energetically separated by up to tens of meV. Moreover, the typically small spatial extension of QDs causes a strong Coulomb interaction strength in the order of meV which yields the striking effect of *Coulomb blockade* in transport through QDs and the corresponding phenomenon of *single electron tunneling* [MEI95a]. Experimentally this becomes manifest in the *Coulomb blockade oscillations* of the linear response conductance by tuning the electrostatic potential of the QD[1] or in the *Coulomb staircase* i.e. the step-like increase of the

[1] This is realized by changing the voltage applied to a metallic gate capacitively coupled to the

CVC (first measurement in Ag nanoparticles [2] [BAR87]). For single QDs the theoretical description of these experimental facts concerning the stationary current is well-elaborated in the 1990s: in the regime of weak coupling between the QD and the contacts (*sequential tunneling* regime) for linear response e.g. in [BEE91a, MEI91] and for nonlinear transport e.g. in [AVE91, HEN94, KLI94a, STA96b]; at very low temperatures Kondo correlations between contact and QD electrons take place as considered theoretically for nonlinear transport e.g. in [MEI93, SWI03].

The fabrication of single semiconductor QDs typically comes about in a sophisticated combination of growth techniques, lithographical and etching methods (for some details see Chap. 2). But there are also technologies available which are based on the effect of self-organization, i.e. the QDs are formed by themselves during the growth process [BIM99, STA04]. Ensemble of millions of more or less homogeneous QDs in a small volume can be obtained in this manner and naturally systems of coupled QDs arise. This predestines them for a wide range of optical applications, including diode lasers, optical amplifiers, infrared detectors, mid-IR lasers, and quantum-optical single-photon emitters [GRU02]. Their optimal performance can be guaranteed by the fundamental understanding of the interplay between the electronic properties and the morphology of individual QDs [STI01] but also ensemble effects e.g. caused by Coulomb interaction can play a role. Spectroscopy by means of electronic transport measurements is one of the successful diagnostic facilities especially if the QDs are buried within a device. For instance the average position of QD levels and broadening mechanisms due to Coulomb interaction can be revealed by capacitance-voltage spectroscopy [WET03, WET03a, WET03b, WET04b] (and references therein). Beyond this, by means of the resonant tunneling current through a QD ensemble individual QDs can be addressed and the respective wave function can be mapped [EAV02]. The CVCs of a layer of self-organized QDs [NAR97] and self-organized QD stacks [BOR01] can exhibit multiple peaks with pronounced NDC. Their origin is not fully understood yet. In the present work, the sequential tunneling description [AVE91, BEE91a] is generalized to coupled QDs, either tunnel-coupled in series or electrostatically in parallel, and the emergence of NDC in the CVC of such systems will be examined. In this context it will turn out that the Coulomb interaction plays a crucial role.

Beyond the characterization of QDs via the average tunneling current the consideration of **current fluctuations** can provide additional information e.g. about tunneling barrier geometries of buried self-organized QDs [NAU02, KIE03a]. Since the beginning of the 1990s the consideration of current fluctuations has been a very active field of research on transport through mesoscopic conductors (for a representative snapshot of the current state see [NAZ03]). The granular nature of particles (or quasi-particles) and the stochasticity of transport processes where they

QD - single electron transistor.

[2] Note that pure Coulomb staircases are only observable in metallic QDs with asymmetric barriers. In semiconductor QDs the steplike CVC is due to the complicated interplay of the discrete level spectrum and charging effects.

are involved in are responsible for the so-called *shot noise*[3] (for a brilliant review see [BLA00, BEE03]). It turns out that it contains detailed information about temporal correlations in the stochastic transport process caused by e.g.

- (Quasi)[4] particle statistics (e.g. for fermions: Pauli's exclusion principle)
- Coulomb interaction
- Scattering processes, e.g. electron-phonon scattering
- Quantum coherence - decoherence

which cannot be extracted from the stationary current alone. The first measurements of shot noise in tunneling through a single metallic QD were examined in Ref. [BIR95] with the respective theoretical analysis in [HER93], for semiconductor QDs the first shot noise experiments were published in [NAU02] which mainly triggered the theoretical investigations of current fluctuations in the present work. A comprehensive analysis of the shot noise behavior in semiconductor QDs with the emphasis on the effect of Coulomb interaction is presented here.

At the moment a very controversial debate is taking place concerning the influence of quantum coherence on the current fluctuations in tunneling through QDs, i.e. the link between quantum and classical noise. Particularly there is no consensus about the emergence of Fano factors below one half for tunneling through a symmetric QD which is believed to be an indicator of coherent transport [ALE03, ALE04, BLA04b]. This issue will be addressed in this work.

Furthermore, the transport through tunnel-coupled QDs ("artificial"molecule) is strongly governed by quantum coherent effects (for a review see [WIE03]). Therefore, it can serve as an ideal system to study the effect of dephasing which provides the link between quantum coherent and incoherent transport (sequential tunneling). From the point of view of applications two tunnel-coupled QDs can be used for quantum computation according to the proposal of Loss et al. [LOS98]: they can constitute a two-level quantum system prepared in a pure state $|\Psi\rangle = c_1|1\rangle + c_2|2\rangle$ which provides the basic memory unit of quantum computers called "qubit". The maintenance of this superposition over large times requires a very high degree of quantum coherence so that the investigation of decoherence mechanisms is indispensable. For this purpose it turns out that the analysis of the current fluctuations in the tunneling current can serve as a very convenient tool as it will be shown in this work.

However, shot noise is not the only feature of current fluctuations. The transport through a conductor is basically a stochastic process where electrons arrive at a

[3] This term traces back to W. Schottky who called the noise caused by the random emission of electrons from the hot cathode in a vacuum tube "Schrotrauschen" [SCH18].

[4] e.g. fractional Quantum Hall effect - fractions of elementary charges directly measurable in shot noise signal [GRI00] (and references therein)

certain contact randomly in time. Hence, for a fixed measuring time interval this electron number is a random variable and the transport process is fully characterized by its probability distribution (the average electron number gives the current and the variance is connected to the shot noise.) Its determination is the aim of *full counting statistics* (FCS). Levitov adopted this concept for electronic transport from quantum optics where the temporal correlations of emitted photons are investigated [LEV93]. In recent years there has been an increasing interest in FCS in mesoscopic conductors. Several systems have been addressed theoretically (for a review see [NAZ03]) and the corresponding statistics yield the complete insight into the nature of transport. However, the measurement of cumulants higher than second order (i.e. beyond shot noise) is a difficult task and up to now there is only one measurement of the third-order cumulant in transport through a tunnel junction [REU03] so that at the moment most theoretical results have predictive character. Here, the FCS is utilized to fully characterize the process of tunneling through tunnel-coupled QDs with respect to quantum coherence and the mechanism of dephasing.

1.2. This work

The goal of this work is the systematic investigation of tunneling processes through coupled QD systems. Two main questions will be addressed in this context: How does the Coulomb interaction, which is crucial in QDs, affect the nonlinear transport? What is the influence of quantum coherence on the transport process and particularly on the current fluctuations? For that purpose, parallel QDs coupled via an electrostatic potential due to the Coulomb interaction or tunnel-coupled QDs in series are considered. These systems will be connected to two electron reservoirs (emitter and collector) with different chemical potentials given by an applied bias voltage which can drive the QD system into a non-equilibrium state - electrons can enter and leave this state by means of resonant tunneling as the basic transport mechanism. Throughout this thesis QD systems with at most four levels will be studied in order to elaborate and discuss the physical effects in a clear and explicit manner.

In particular, the occurrence of NDC and multiple peaks as observed experimentally in self-organized QD systems is examined. Triggered by the experiments of A. Nauen et al. [NAU02] we focus on the shot noise and systematically investigate the possibilities of super- and sub-Poissonian noise.

In principle, there are two different ways to treat transport through QD systems depending on the degree of quantum coherence whilst the tunneling process: sequential and coherent tunneling. The crossover between them is accomplished by dephasing. In order to treat their connection systematically different methods will be applied: master equation technique (ME), density matrix approach, non-equilibrium Green's functions (NEGF), scattering matrix formalism[5](SMF) (see

[5]also widely called Landauer-Büttiker formalism

Fig. 1.1). Here special attention will be laid on the question, how these methods relate to each other.

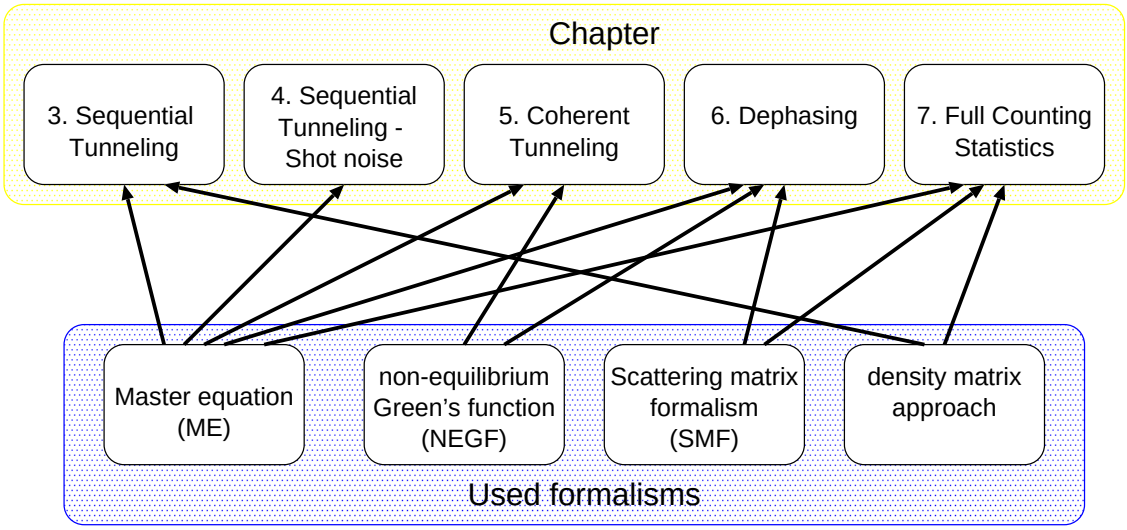

Figure 1.1.: Appearance of the used formalisms in the chapters.

This thesis is organized as follows: Chap. 2 introduces the manufacturing of semiconductor QDs and transport experiments conducted on these. Particulary the fabrication of self-organized QDs and nonlinear transport through ensemble of self-organized QDs is considered. The important features of transport regarding the experimental average current and shot noise will be outlined. Chap. 3 contains the theoretical analysis of sequential tunneling through capacitively coupled QDs and tunnel-coupled QDs with respect to the average current. The shot noise within sequential tunneling is considered in Chap. 4. Chap. 5 provides an elaborate analysis of coherent tunneling through single and coupled QDs and within the framework of nonequilibrium Green's functions. The link between sequential and coherent tunneling will be tried to be established in Chap. 6 for tunneling through single and coupled QDs namely the influence of dephasing on the current and the shot noise. In the last Chap. 7 the full information about the transport process through QDs is obtained by means of FCS. The transport statistics of sequential and coherent tunneling through tunnel-coupled noninteracting QDs is compared and the concept of pure dephasing in FCS is discussed.

2. Semiconductor Quantum Dots

Quantum dots (QDs) are mesoscopic objects where electrons or holes can be confined in all three spatial dimensions. If the spatial extension of the confinement potential is of the order of the Fermi wavelength of the carriers or even smaller a discrete DOS results. Depending on the level spacing one distinguishes between semiconductor QDs and metallic QDs. Throughout this thesis we will focus on semiconductor QDs where the level spacing is such that we can deal with a small number of states in the energy range of interest. In contrast, for metallic QDs there is an infinite number of possible many-particle states of the QD which are relevant due to the very dense level spectrum.

There exist several technologies to manufacture semiconductor QDs. In general, lateral and vertical structures are available [KOU97]. The starting point for the former is the growth of a two-dimensional electron gas (2DEG). On top of the wafer, metallic gates are patterned using electron beam lithography. Biasing them leads to a depletion of the electron gas underneath and defines the potential landscape of the QD. Limited by the resolution of the lithographical process the extension of such a QD is in order of $\sim$ 100nm. One advantage of this method is the external calibration of the confinement potential of the QD by tuning the gate voltages. Furthermore, the QD can be coupled to the rest of the electron-gas via point contacts so that carriers can enter the QD and transport measurements in the plane of the 2DEG are conducted. The list of references which consider such a type of QDs is far too large to be given here. For an overview see e.g. [KOU97, KOU97a].

The transport through vertical QDs is parallel to the growth direction of the 2DEG. Here, the heterostructure containing the 2DEG is etched down so that a pillar with a diameter in order of tens of nm remains. In contrast to lateral QDs, the vertical QD can contain a very small number of electrons so that e.g. shell-filling effects in transport measurements can be studied [TAR96]. A very prominent type of vertical QD structures are self-organized grown QDs. A large part of this thesis deals with transport through such systems. Consequently, we dedicate the next section to the technology of self-organized QDs and their experimental transport properties.

2.1. Self-organized quantum dots

The growth of two semiconductor materials with different lattice constants on top of each other provides strain at the interface of both constituents [BIM99, SHC03].

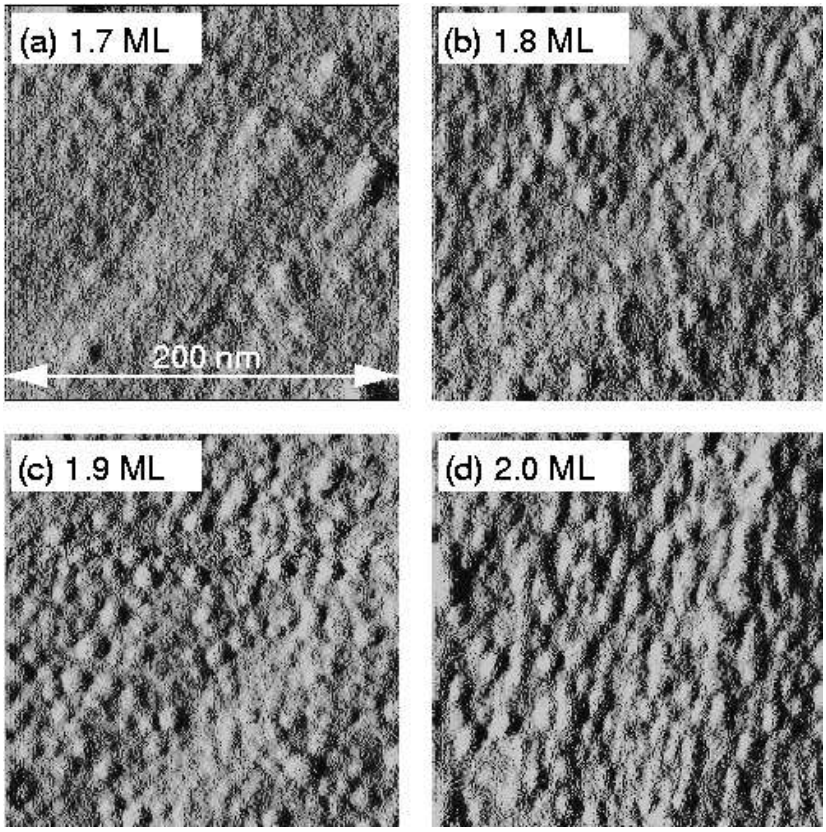

Figure 2.1.: AFM measurement of InAs islands on AlAs substrate for various InAs coverages. Source [HAP02]

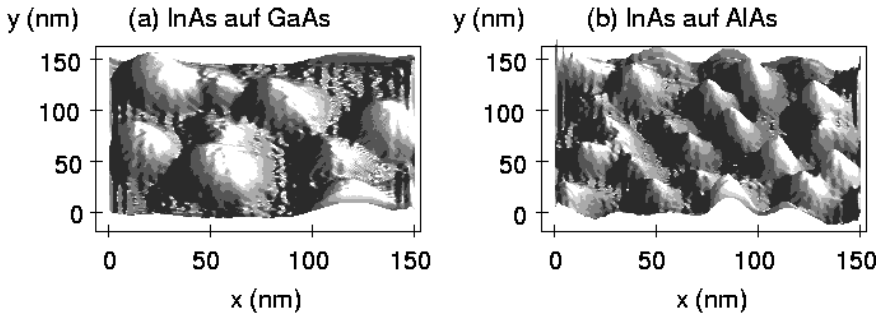

Figure 2.2.: AFM measurement of 1.8 ML InAs quantum dots on (a) GaAs substrate and (b) AlAs substrate. Source [HAP02]

Widely used combinations of such materials are InAs on AlAs or InAs on GaAs with a lattice mismatch of almost 7 %. In the Stranski-Krastanov growth mode first a wetting layer emerges which can be considered as a disordered 2DEG. With increasing layer thickness the strain energy increases and leads to the formation of islands wherein the strain is relaxed. One obtains an array of randomly distributed self-organized grown QDs as one can observe in the AFM images in Fig. 2.1 (taken from [HAP02] by the courtesy of I. Hapke-Wurst). Increasing coverages of InAs on AlAs are depicted from a) to d). Remarkable is that for low coverage the density of QDs is higher than for high coverage. Further growth parameters such as deposition rate and temperature strongly influence the QD density, the size distribution and the spatial distribution of the islands. A thorough theoretical study by kinetic Monte-Carlo simulations of the growth kinetics can be found in [MEI02b, MEI03a]. Note, in Fig. 2.1a there are a few QDs visible which are larger than a most others. As it will outlined in the next section a few individual QDs can be selected by resonant tunneling through the QD ensemble which may be caused by this heterogeneity of the QD array.

A closer AFM look at the QDs is presented in Fig. 2.2 (taken from [HAP02]) for InAs on GaAs (a) and InAs on AlAs (b). From these pictures one can extract the QD densities: $2.5 \times 10^{10}\mathrm{cm}^{-2}$ for GaAs and $1 \times 10^{11}\mathrm{cm}^{-2}$ for AlAs. The height of the almost pyramidal shaped islands is in both cases almost 4 nm. The lateral extension of InAs islands on GaAs is approximately 20 -30 nm whereas for the AlAs substrate it is almost a factor one half smaller.

2.2. Transport experiments

For the measurement of an electronic current through the QD ensemble considered in the previous section the layer of self-organized QDs is embedded in a diode structure as schematically shown in Fig. 2.3a [KIE03a]. Here the active region consists of InAs QDs surrounded by AlAs which acts as tunneling barriers. A 15 nm undoped GaAs spacer layer and a GaAs buffer with graded doping on both sides of the tunneling structure provide three-dimensional emitter and collector contacts. In Fig. 2.3b the respective conduction band edge without an applied bias voltage can be seen. It forms a double-barrier structure where resonant tunneling through the zero-dimensional QD states can take place.

2.2.1. Current-voltage characteristics

2.2.1.1. Single layer quantum dot array

Applying a bias voltage V between the ohmic contacts (Fig. 2.3a) induces a difference in chemical potentials of the contacts and therefore the band scheme tilts as shown in inset b) of Fig. 2.4. Electronic states in the QDs then shift energetically downwards with increasing bias voltage. For InAs QDs in AlAs the ground

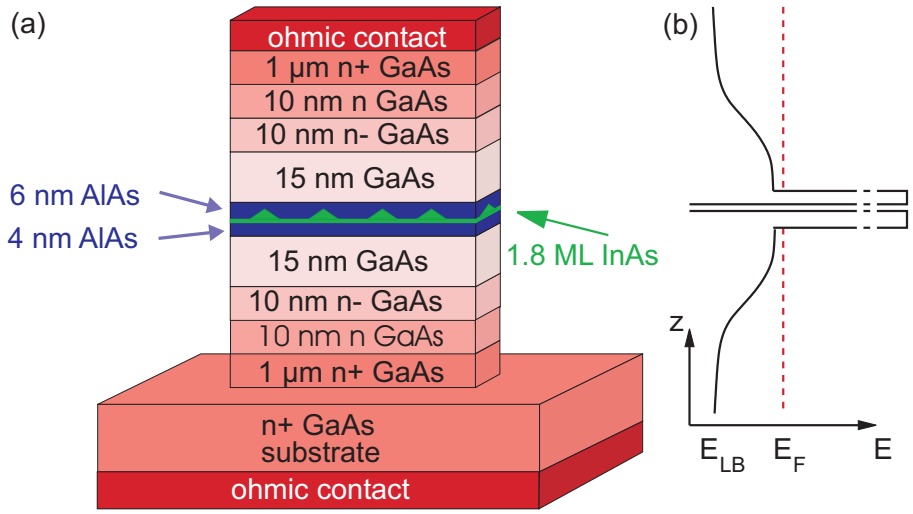

Figure 2.3.: a) Growth scheme of a diode comprising a layer of self-organized quantum dots of InAs. b) The band structure of the sample with Fermi energy E_F for zero-bias. Taken from [KIE03a].

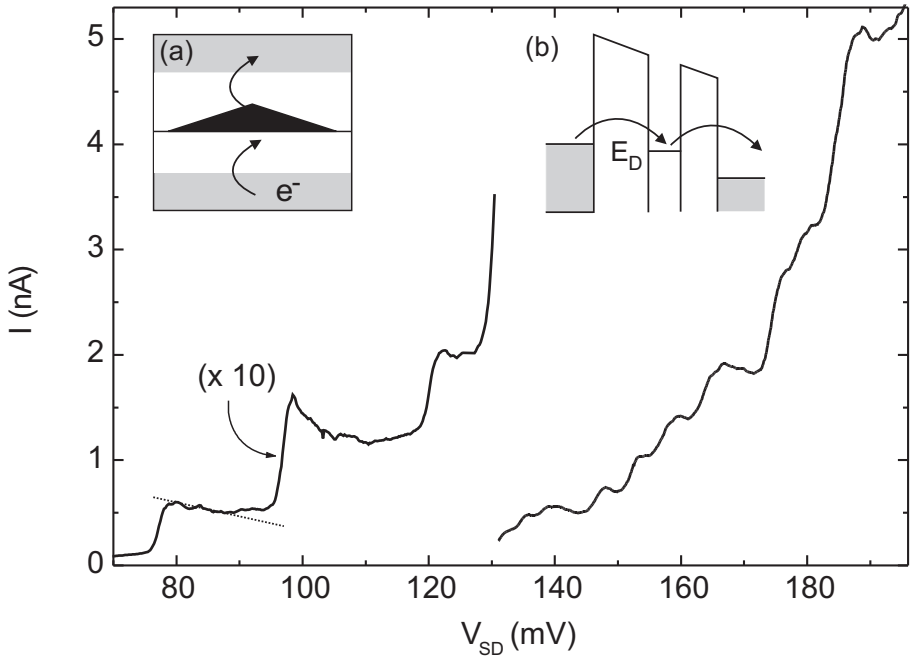

Figure 2.4.: Current-voltage characteristic of an InAs quantum dot array measured at T =1.7 K. The current for bias voltages below 130 mV is magnified by a factor of 10. The dotted line is a guide of the eye representing the expected current (see text). Insets: a) Principal sample structure of a single InAs quantum dot (black) embedded in a AlAs barrier (white). b) Schematic band profile at positive bias with quantum dot level E_D. Taken from [NAU02].

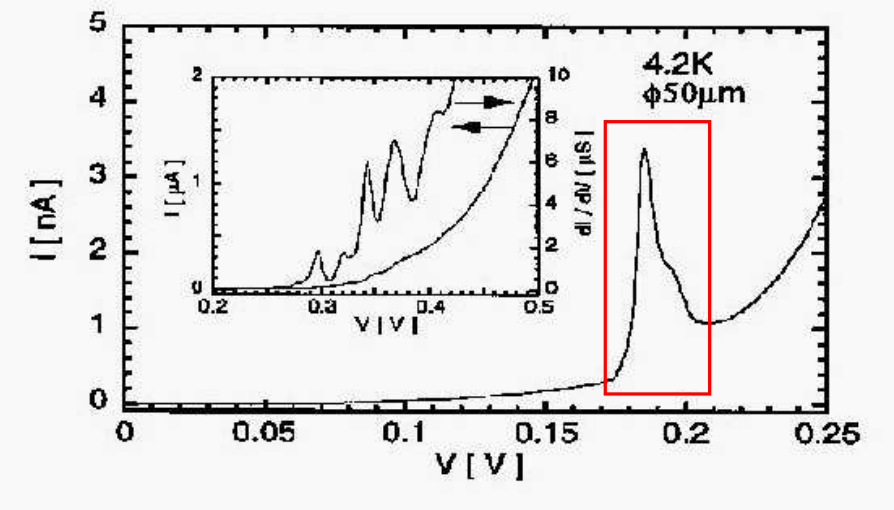

Figure 2.5.: Measured current voltage characteristic at T =4.2 K. Inset: $I(V)$ and $dI/dV(V)$ for higher bias voltages. Taken from [NAR97].

state energies lie above the emitter chemical potential for zero-bias, i.e. one starts with empty QDs and at a certain bias voltage the ground states pass the emitter chemical potential so that electrons can enter the QDs[1]. The typical diameter of diodes in experiments of microns allow to have millions of QDs in the active region. Due to the statistical size distribution of the QDs their ground state energies are almost continuously distributed over a certain energy range. This is confirmed e.g. by photoluminescence measurements [HAP02]. Therefore, one would expect a continuous increase of the current by increasing the bias voltage since more and more QDs contribute to the current flow. Experimentally this is not the case. In Fig. 2.4 a typical current-voltage characteristic (CVC) is shown [NAU02]. There is a sharp current onset at about 78 mV followed by a current staircase with non-equidistant steps. This result suggests that the QD ground state energy spectrum has gaps corresponding to constant current plateaus. An estimation of the current through a single QD ground state reveals that each step corresponds to tunneling through an individual QD with slightly different ground state energies. This very counterintuitive behavior was also found in the CVCs of many other samples [HAP99, HAP02] and the comparison with a reference sample without QDs relates this effect uniquely to QD tunneling. Obviously there is a selection mechanism which only allows the tunneling through few individual QDs for low bias. Even though it is not fully clarified which mechanism is responsible there are some explanations on the market. One will be discussed in Sec. 3.2 and is based on the Coulomb interaction between electrons in different QDs and inhomogeneities in the collector coupling of the QDs. This can lead to negative differential conductance and consequently to peaks in

[1]This mechanism is widely termed as *resonant tunneling*.

the CVC as observed e.g. by [NAR97] shown in Fig. 2.5 and in [ITS96][2], [SUZ97]. Another explanation is proposed in [VDO00, LEV01]. The authors investigated samples with a 50 nm spacer layer (in contrast to Fig. 2.3a). Caused by a locally inhomogeneous emitter the local DOS is strongly fluctuating so that only QDs are selected which are close to regions with a high DOS. Nevertheless, for a small spacer layer this argument is not very convincing.

As shown in [LIU89] tunneling from a three-dimensional emitter to a zero-dimensional QD state generates a linear decrease of the current plateaus in the CVC: In a simple picture they consider the conservation of total energy during the tunneling process which leads to the condition $k_1^2 + k_2^2 + k_3^2 = k_r^2$ with k_i $(i = 1, 2, 3)$ being the momenta of electrons in the emitter and k_r corresponds to the energy of the resonant QD state as $E_r = \hbar^2 k_r^2/(2m^*)$. By increasing the bias voltage the resonant level E_r is decreased so that the radius k_r of the hemisphere reduces. The current is proportional to the number of states on this sphere i.e. on its surface area $I \propto 4\pi k_r^2 \propto E_r$. Hence, the current linearly decreases with increasing the bias voltage. This behavior can be clearly seen on the first current plateau in Fig. 2.4. In the theoretical investigations of the following chapter this effect is not included since we assume bias-independent tunneling rates.

At the second current step an overshoot is visible which is known as the *Fermi edge singularity*. It is caused by the influence of the Coulomb interaction between emitter electrons and QD electrons on the tunneling process which is very pronounced at the Fermi edge and for low temperatures [MAT92a]. In all theoretical discussions throughout this work we neglect this effect and assume ideal contacts.

2.2.1.2. Stacked quantum dots

In [BOR01, BRY02, BRY03] the tunneling through two layers of self-organized QDs were reported. Due to the effect of strain the QDs in the second layer tend to form on top of a QD in the first layer [MEI02b, MEI03] so that a QD stack emerges where both QDs are separated by a small tunnel barrier. Astonishingly, the authors of [BOR01, BRY02, BRY03] are able to fabricate samples with a very low density of QD stacks so that the macroscopic contact covers only a few stacks. The respective CVC is shown in Fig. 2.6 [BOR01]. A sharp current peak with a high peak-to-valley ratio can be observed in the low-bias region. The emergence of such a current peak can be simply understood by the fact that energy levels or excitations of different QDs in one stack energetically align. If these resonances take place in the range of the emitter Fermi sea electrons are able to enter the first QD and can further tunnel through the stack. An elaborate discussion of the influence of the tunnel coupling between the QDs and their coupling to the contacts on the CVC of a single stack

[2] In contrast to the other mentioned experiments here a 2DEG in front of the emitter barrier forms due to charge accumulation. Hence, resonant tunneling occurs if an electronic state of a QD is resonant with a state in the 2DEG. If the QD state passes the subband ground energy of the 2DEG a sharp current drop is caused.

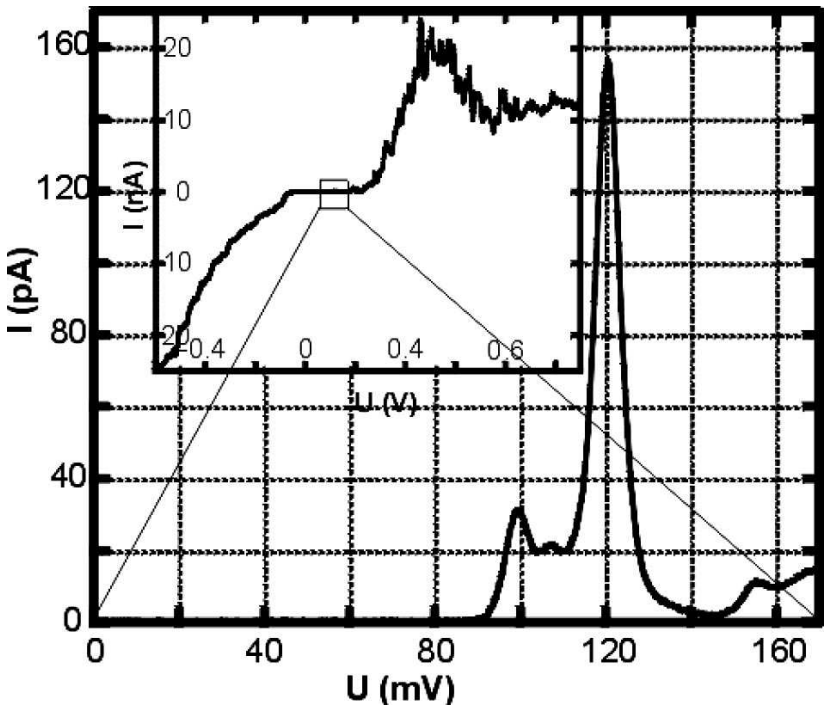

Figure 2.6.: Measured current voltage characteristic at $T = 7$K of an InAs quantum dot stack. Inset: $I(V)$ for a larger bias voltage range. Taken from [BOR01].

will be done in Sec. 3.3. The Lund group also reports on the frequent observation of double current peaks as can be seen in Fig. 2.6. As we show in Sec. 3.3.3 they are caused by the Coulomb interaction.

2.2.2. Current fluctuations - Shot noise measurements

In Refs. [NAU02, KIE03a, NAU03] measurements of the low-frequency[3] spectral power density (SPD) S_P of the tunneling current through self-organized QDs were reported. The current fluctuations contain information about correlations in the tunneling current. For uncorrelated tunneling (e.g. through a single barrier, Poissonian statistics of tunneling events - for details see Chap. 4 and Chap. 7) the SPD is given by the charge e and the stationary current $\langle I \rangle$ as $2e\langle I \rangle$. Normalizing the actual SPD by this value yields the **Fano factor** α (for the definition see also (4.1.9)) which gives a measure for correlations in the current. In Fig. 2.7 the CVC

[3]I.e. in the range of few kHz where the spectrum of the power density is flat apart from 1/f noise far below frequencies of the order of the tunneling rates (Sec. 4.1.3).

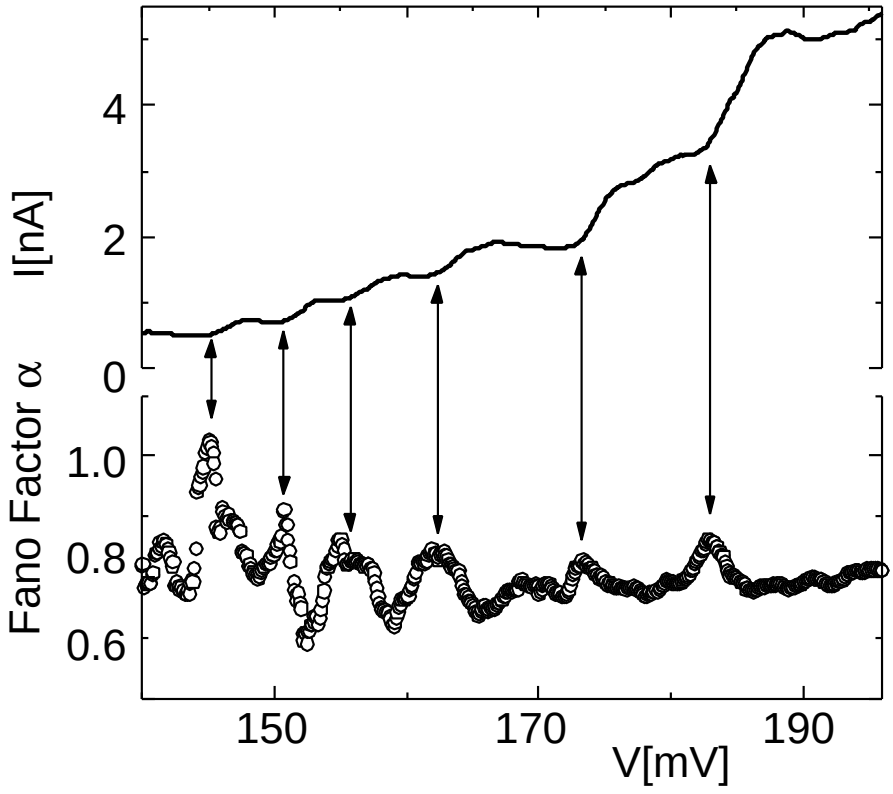

Figure 2.7.: Upper trace: measured current voltage characteristic. Lower trace: Fano factor α vs. bias voltage V. Temperature $T = 1.6$ K. Taken from [KIE03a].

and the respective Fano factor vs. bias voltage is presented [NAU02, KIE03a]. The CVC (upper trace) shows steps as already discussed with respect to Fig. 2.4. The Fano factor is always reduced below unity, i.e. there are only negative correlations present. They are caused by Pauli's exclusion principle as we discuss in detail in Chap. 4 and the corresponding average Fano factor of around 0.8 then gives informations about the barrier geometry. The enhancement of the Fano factor at the current steps is also an effect of Pauli's exclusion principle [KIE03a] which we are going to discuss analytically in Sec. 4.2.1. Its temperature dependence could provide information about the spatial distribution of QDs which are active in transport at this bias voltage (Sec. 4.2.1).

With the recent improvement of the equipment, the measurement of the SPD for currents of the order of pA became feasible so that the noise at the current onset of the CVC can be resolved [MAI03, NAU04a]. It turns out that the linear decrease of the current plateau (Fig. 2.4) is accompanied by a linear increase of the Fano factor underlining the effect of 3D-0D tunneling of the electrons. Furthermore, the first current plateau corresponds to tunneling through a Coulomb correlated state since the ground state of the QD is spin-degenerate. This causes an additional correlation

in the tunneling current and consequently to a modified Fano factor as considered in Sec. 4.2.1. The lifting of the spin-degeneracy by a magnetic field (Zeeman splitting) was considered in [MAI03] and the Fano factor vs. bias voltage at the current onset is shown in Fig. 2.8. Below the current onset the Fano factor is unity due to the tunneling of thermally activated emitter electrons which happens rarely. Hence the corresponding statistics of tunneling events is Poissonian. Each step in the Fano factor corresponds to an increasing step in the current. At the first step one QD spin state becomes occupied. The Fano factor of 0.67 is given by Pauli's exclusion principle and determines the ratio of the collector to the emitter tunneling rate. At the next step the second spin state gets filled. But now, a Coulomb correlated state emerges since double occupation of the ground state is forbidden because of the Coulomb repulsion (Coulomb blockade). Due to the additional correlations the Fano factor is reduced (see Sec. 4.2.1).

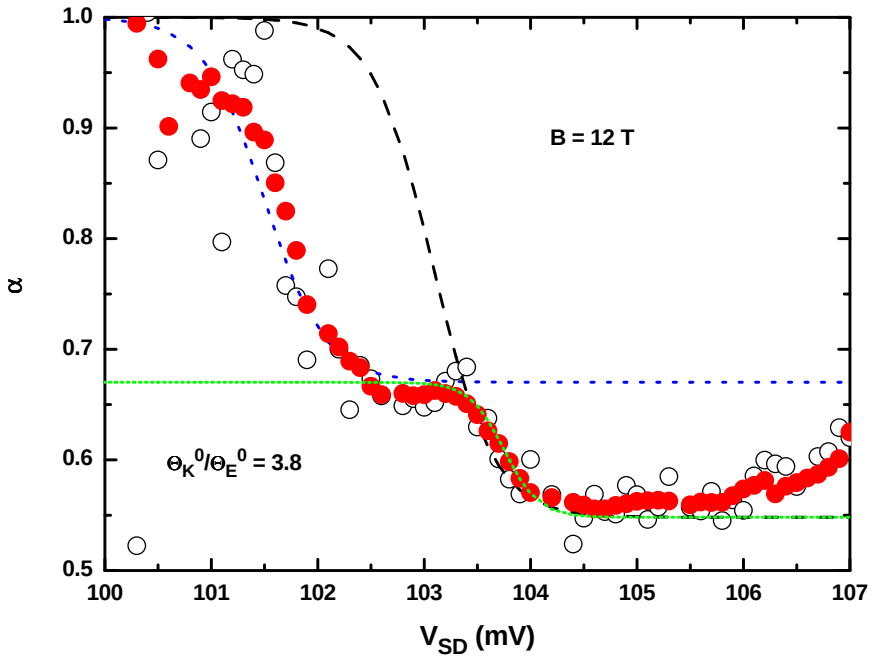

Figure 2.8.: Measured Fano factor vs. bias voltage for quantum dots in a magnetic field $B = 12$T and temperature $T = 1.5$K (tunnel rates $\Theta^0_{E/K} = \Gamma_{e/c}$ in our notation). Taken from [MAI03].

In Ref. [BAR04] the noise of tunneling through QD stacks was measured. Interestingly, super-Poissonian noise corresponding to a Fano factor larger than unity was found close to the peaks in the CVC. Unfortunately the experimental data does not exclusively refer to shot noise[4] so that we just give a description of predictive

[4]There are probably also 1/f noise contributions.

character in Sec. 4.2.2.2 for the observation of super-Poissonian noise in tunneling through coupled QDs.

3. Sequential Tunneling - Stationary Current

3.1. Theoretical framework: Master equation

A large class of stochastic processes in physics are characterized by the Markov property. A Markov process is defined as a stochastic process where the transitions in successive time intervals are statistically independent or in other words the transition between two states does not take into account the prehistory of the process. Defining the conditional probability for a transition from state ν to a state ν' at times t and t', respectively: $p(\nu' t'|\nu t)$, the Markov property can be quantified as [KAM81, ROE87]

$$p(\nu_3 t_3|\nu_1 t_1) = \sum_{\nu_2} p(\nu_3 t_3|\nu_2 t_2) p(\nu_2 t_2|\nu_1 t_1) \tag{3.1.1}$$

$(t_1 < t_2 < t_3)$ which is the famous Chapman-Kolmogorov equation. From (3.1.1) a differential form can be derived which is called *Master equation* (ME)[1]

$$\frac{\partial}{\partial t} P_\nu(t) = \sum_{\nu' \neq \nu} [W_{\nu\nu'} P_{\nu'}(t) - W_{\nu'\nu} P_\nu(t)] \tag{3.1.2}$$

for the occupation probabilities P_ν of state ν. The $W_{\nu\nu'}$ are the rates for the transition from state ν' to state ν per unit time. This equation is the basis for the considerations in this chapter and can be interpreted quite easily: the first term in (3.1.2) describes the "gain" of state ν due to transitions from other states ν' and the second term is due to the loss from state ν into other states ν' (therefore the minus sign).

The concept of a ME description for sequential or single electron tunneling through QDs was introduced in [BEE91a, AVE91] and will be briefly outlined in the next section.

3.1.1. Single electron tunneling

The QD system is described by a Fock state $\nu = (n_1, \ldots, n_N)$ with the occupation numbers $n_i \in \{0, 1\}$ and N single particle states. The single particle states i may

[1] This term may occur in several contexts, e.g. sometimes for the Liouville equation. Throughout this thesis it is used in the way introduced here.

correspond to different energy levels in the same QD, or in different QDs. The time evolution of these occupation probabilities P_ν is determined by sequential or single electron tunneling of an electron into or out of the emitter/collector contact. We use the ME (3.1.2) and write it in the compact matrix form as[2]

$$\underline{\dot{\mathbf{P}}} = \underline{\underline{\mathbf{M}}}\,\underline{\mathbf{P}} \tag{3.1.3}$$

The diagonal elements $M_{\nu\nu}$ of the transition matrix $\underline{\underline{\mathbf{M}}}$ contains the loss term and the non-diagonal elements correspond to the gain term in (3.1.2). In order to fulfill the probability normalization $\sum_\nu P_\nu = 1$ the sum of the matrix elements in a column of $\underline{\underline{\mathbf{M}}}$ has to be zero. This guarantees that at least one vanishing eigenvalue of this matrix always exists so that a steady state solution of (3.1.3) can be found by

$$\underline{\underline{\mathbf{M}}}\,\underline{\mathbf{P}}^0 = 0 \tag{3.1.4}$$

The matrix $\underline{\underline{M}}$ entering the ME (3.1.3) contains the transition rates $M_{\nu\nu'}$ between the Fock states $\nu' \to \nu$. Since we are dealing with single electron tunneling all elements $M_{\nu\nu'}$ are zero if the total particle number $N(\nu) = \sum_i n_i(\nu)$ differs by more than one from $N(\nu')$. This leads to a structure of $\underline{\underline{M}}$ which is not completely reducible or decomposable [KAM81] so that only one stationary state can occur.

The central quantity of interest in the following Sects. 3.2 and 3.3 is the mean current through the respective QD system. With (3.1.4) and current operators $\underline{\underline{\mathbf{j}}}_{e/c}$ for the emitter and collector barriers, respectively, the stationary mean current is

$$\langle I \rangle = \sum_\nu [\underline{\underline{\mathbf{j}}}_c\,\underline{\mathbf{P}}^0]_\nu = \sum_\nu [\underline{\underline{\mathbf{j}}}_e\,\underline{\mathbf{P}}^0]_\nu \tag{3.1.5}$$

In the stationary limit the mean current at the collector barrier equals the mean current at the emitter barrier. For the calculation of the stationary current in (3.1.5) the current operators $\underline{\underline{j}}_{e/c}$ can be either defined in diagonal or in non-diagonal matrix form without changing the result (3.1.5). As shown later on in Chap. 4 for the determination of the current-current correlator the exact definition of the current operators $\underline{\underline{j}}_{e/c}$ becomes crucial: there these operators project the occupation probability to the state after an electron has traversed the barrier. An explicit non-diagonal form of these operators is presented in (3.2.2).

[2]Note that this approach holds only for QDs which are weakly coupled to the contacts such that $\Gamma \ll k_B T$ (Γ is the largest tunneling rate which enters the transition rates $M_{\nu\nu'}$), and cannot account for co-tunneling processes [GRA92a], i.e. coherent tunneling which we discuss in detail in Chap. 5.

3.1.2. Coupled quantum dots: Notations

The transition matrix elements $M_{\nu\nu'}$ in the ME (3.1.3) contain the tunneling rates $\Gamma^i_{e/c}$ to the emitter/collector, respectively, and the occupations of the contacts. These are assumed to be in local equilibrium characterized by Fermi functions $f_{e/c}(E) = 1/(1+\exp((E-\mu_{e/c})/k_BT))$ with chemical potentials $\mu_{e/c}$, respectively, and temperature T. An applied bias voltage $V = (\mu_e - \mu_c)/e$ drives the QD system out of equilibrium. For a transition which increases the total particle number by one, i.e. an electron enters the QD single particle state i via the emitter/collector barrier, respectively, the transition rate reads $M_{\nu\nu'} = \Gamma^{(i)}_{e/c} f_{e/c}(\Delta E_{\nu\nu'})$ where $\Delta E_{\nu\nu'} = E(\nu) - E(\nu')$ is the difference of total energies (see below). For the inverse tunneling processes the transition rate is $M_{\nu\nu'} = \Gamma^{(i)}_{e/c}[1 - f_{e/c}(\Delta E_{\nu'\nu})]$. Throughout this thesis we choose the sign of the elementary charge $e > 0$ so that $V > 0$ means $\mu_e > \mu_c$ and $I > 0$ describes a net particle current from emitter to collector. The single particle energies ε_i in the QDs are assumed to shift linearly with respect to the bias voltage V: $\varepsilon_i(V) = \varepsilon_i - e\eta_i V$ with the leverage factor η_i $(0 < \eta_i < 1)$ for the i-th QD. The leverage factor is one half for symmetric barrier structures. The total energy of the state ν is

$$E(\nu) = \sum_i n_i(\nu)(\varepsilon_i - e\eta_i V) + U(\nu) \tag{3.1.6}$$

where $n_i(\nu)$ is the occupation number of the i-th single particle state for state ν and $U(\nu)$ is the charging energy for state ν which is given by

$$U(\nu) = \frac{e^2}{2}\sum_{i,j} n_i(\nu)\left[C^{-1}\right]_{ij} n_j(\nu) - \frac{e^2}{2}\sum_i \left[C^{-1}\right]_{ii} n_i(\nu) \tag{3.1.7}$$

with the inverse of the capacitance matrix C, where the last term subtracts the self-interaction.[3] For states in different QDs i and j at positions $\mathbf{r}_i$ and $\mathbf{r}_j$ the inverse capacitance matrix can be written as [WHA96]

$$[C^{-1}]_{ij} = \frac{1}{4\pi\epsilon r_{ij}} \tag{3.1.8}$$

with $r_{ij} \equiv |\mathbf{r}_i - \mathbf{r}_j|$ and ϵ is the dielectric constant. (3.1.8) is simply the electrostatic potential between two point charges at $\mathbf{r}_i$ and $\mathbf{r}_j$. In experiments the contacts are typically highly-doped and nearby to the layer of QDs so that they screen the Coulomb potential in the array of QDs. If a is the distance of the QD array to both

[3] Since the n_i enter the Fermi functions via the charging energy the transition rates depend strongly nonlinear on the occupation numbers. For that reason it is not possible to obtain rate equations for $\langle n_i \rangle$ starting from the ME in the presence of Coulomb interaction. For noninteracting electrons it will be shown in Sec. 3.3.2.

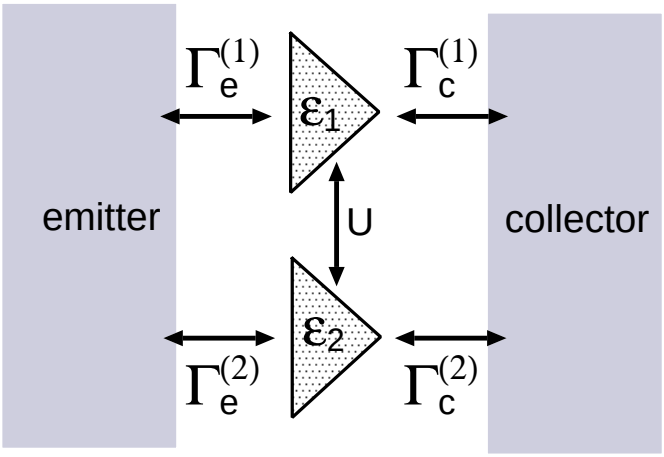

Figure 3.1.: Scheme of the tunneling structure with rates $\Gamma_{e/c}^{(i)}$ $(i = 1, 2)$ between two QDs and the emitter/collector, respectively; single particle levels $\varepsilon_{1/2}$, and Coulomb interaction energy U. Taken from [KIE03b].

contacts the inverse capacitance matrix then has to be modified. For $r_{ij} \gg a$ it becomes (for details see Appendix A)

$$[C^{-1}]_{ij}^{s} = \frac{1}{4\pi\epsilon} \frac{\exp\left(-\frac{r_{ij}}{2a}\right)}{\sqrt{\pi a r_{ij}}} \tag{3.1.9}$$

Note, that the screened potential is not simply (3.1.8) multiplied by an exponential of $-\lambda r_{ij}$ with a screening parameter λ. The electrostatic interaction of carriers in states of the same QD can be treated in first-order perturbation in the Coulomb potential considering the QD wave functions [WAR98]. This and the effect of screening is elaborately discussed in [KIE02b, KIE03] regarding bipolar transport through QD arrays. The impact of the Coulomb interaction on the unipolar CVC of large QD arrays is studied in [KIE02, KIE02a]. There the emergence of NDC caused by Coulomb interaction between different QDs was shown. In the following section we examine the generic case of two parallel QD states capacitively coupled to each other in order to give the physical picture of the mechanism leading to the NDC.

3.2. Parallel quantum dots: negative differential conductance

We consider two single particle states $\varepsilon_{1/2}$ which are connected to the emitter/collector contact and are coupled electro-statically by a Coulomb interaction of strength U (see Fig. 3.1). This could either correspond to the spins of the QD

ground state (compare Secs. 5.2 and 5.3) or to two spatially separated QD states without spin degeneracy. In this sense the following considerations are generic for any larger QD array considered in [KIE02, KIE02a]. Then the vector of the occupation probabilities is $\underline{\mathbf{P}} = (P_{(0,0)}, P_{(1,0)}, P_{(0,1)}, P_{(1,1)})^T$ and the transition matrix in (3.1.3) reads

$$\underline{\underline{\mathbf{M}}} = \begin{pmatrix} -\Gamma_e^{(1)} f_e^{(1)} - \Gamma_e^{(2)} f_e^{(2)} & \Gamma_e^{(1)}(1-f_e^{(1)}) + \Gamma_c^{(1)} \\ \Gamma_e^{(1)} f_e^{(1)} & -\Gamma_e^{(1)}(1-f_e^{(1)}) - \Gamma_c^{(1)} - \Gamma_e^{(2)} f_e^{(2,U)} \\ \Gamma_e^{(2)} f_e^{(2)} & 0 \\ 0 & \Gamma_e^{(2)} f_e^{(2,U)} \end{pmatrix}$$
$$\begin{pmatrix} \Gamma_e^{(2)}(1-f_e^{(2)}) + \Gamma_c^{(2)} & 0 \\ 0 & \Gamma_e^{(2)}(1-f_e^{(2,U)}) + \Gamma_c^{(2)} \\ -\Gamma_e^{(1)} f_e^{(1,U)} - \Gamma_e^{(2)}(1-f_e^{(2)}) - \Gamma_c^{(2)} & \Gamma_e^{(1)}(1-f_e^{(1,U)}) + \Gamma_c^{(1)} \\ \Gamma_e^{(1)} f_e^{(1,U)} & \Gamma_e^{(1)} f_e^{(1,U)} + \Gamma_e^{(2)} f_e^{(2,U)} - \Gamma \end{pmatrix} \tag{3.2.1}$$

with $\Gamma \equiv \Gamma_c^{(1)} + \Gamma_c^{(2)} + \Gamma_e^{(1)} + \Gamma_e^{(2)}$ and the Fermi functions in the emitter $f_e^{(i)} = (1 + \exp((\varepsilon_i - e\eta V)/(k_B T)))^{-1}$ and $f_e^{(i,U)} = (1 + \exp((\varepsilon_i + U - e\eta V)/(k_B T)))^{-1}$. V is the bias voltage, ηV is the voltage drop across the emitter barrier, and $f_e^{(i,U)}$ includes the Coulomb interaction energy U of the occupied QDs. For $eV \gg k_B T$ we neglect tunneling from the collector into the QDs, setting the collector occupation probability $f_c^{(i)} = f_c^{(i,U)} = 0$.

The current operators at the collector barrier and at the emitter barrier, respectively, are given by

$$\underline{\underline{\mathbf{j}}}_c = e \begin{pmatrix} 0 & \Gamma_c^{(1)} & \Gamma_c^{(2)} & 0 \\ 0 & 0 & 0 & \Gamma_c^{(2)} \\ 0 & 0 & 0 & \Gamma_c^{(1)} \\ 0 & 0 & 0 & 0 \end{pmatrix}$$
$$\underline{\underline{\mathbf{j}}}_e = e \begin{pmatrix} 0 & -\Gamma_e^{(1)}(1-f_e^{(1)}) & -\Gamma_e^{(2)}(1-f_e^{(2)}) & 0 \\ \Gamma_e^{(2)} f_e^{(2)} & 0 & 0 & -\Gamma_e^{(1)}(1-f_e^{(1,U)}) \\ \Gamma_e^{(1)} f_e^{(1)} & 0 & 0 & -\Gamma_e^{(2)}(1-f_e^{(2,U)}) \\ 0 & \Gamma_e^{(1)} f_e^{(1,U)} & \Gamma_e^{(2)} f_e^{(2,U)} & 0 \end{pmatrix} \tag{3.2.2}$$

For the following examination we assume $\varepsilon_1 = \varepsilon_2$ and set $\Gamma_e^{(1)} = \Gamma_c^{(1)} = \Gamma_e^{(2)}$, i.e. both single particle states have the same energy, the single particle state $i = 1$ is symmetrically coupled to the emitter and collector contact, and the collector tunneling rate $\Gamma_c^{(2)}$ of the single particle state $i = 2$ we will allow to vary. For

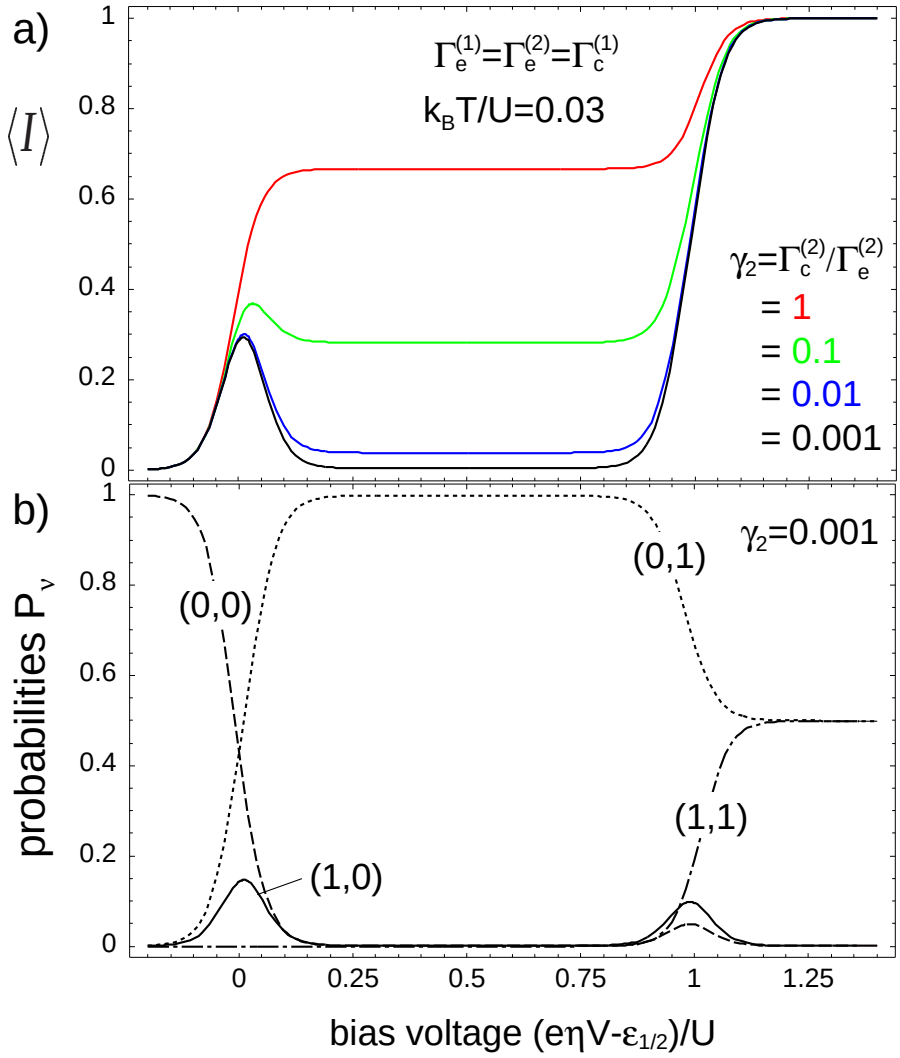

Figure 3.2.: a) Normalized stationary current vs. bias voltage for various $\gamma_2 = \Gamma_c^{(2)}/\Gamma_e^{(2)}$. b) Occupation probabilities P_ν for $\gamma_2 = 0.001$. $k_BT/U = 0.03$, $\Gamma_e^{(1)} = \Gamma_e^{(2)} = \Gamma_c^{(1)}$

that purpose we introduce the ratio $\gamma_2 \equiv \Gamma_c^{(2)}/\Gamma_e^{(1)}$. In Fig. 3.2a the normalized stationary current vs. bias voltage is shown for various ratios γ_2 ($k_BT/U = 0.03$). For both single particle states symmetrically coupled to the reservoirs ($\gamma_2 = 1$, red curve) the CVC exhibits two steps whose shape is defined by the thermal occupation of the emitter states. The current step at low bias voltage arises from the tunneling through the single particle states $(1,0)$ or $(0,1)$ - in the same time only one electron can be in the system (single electron tunneling). In order to fill the two-particle state $(1,1)$ the Coulomb repulsion given by the charging energy U has to be overcome by the emitter electrons so that a second step occurs for $(e\eta V - \varepsilon_{1/2})/U = 1$. This is known as the *Coulomb blockade* effect and the red curve in Fig. 3.2a represents the simplest example for a *Coulomb staircase* [CHE91a]. The tunneling current through one single particle state i is the series connection of the resistances arising from the emitter/collector tunneling barrier which are proportional to the inverse tunneling rates $\Gamma_{e/c}^{(i)}$, respectively. I.e. $\langle I_i \rangle = e[(\Gamma_e^{(i)})^{-1} + (\Gamma_c^{(i)})^{-1}]^{-1}$. The total current one obtains by $\langle I \rangle = \sum_i \langle I_i \rangle = 2e\Gamma_e^{(1)}\Gamma_c^{(1)}/(\Gamma_e^{(1)} + \Gamma_c^{(1)})$ which corresponds to the second current plateau in Fig. 3.2a. The current in the Coulomb-blockade regime (first plateau, red curve) becomes $\langle I \rangle = e2\Gamma_e^{(1)}\Gamma_c^{(1)}/(2\Gamma_e^{(1)} + \Gamma_c^{(1)})$ which takes into account that only the single particle channels are open (this will also be discussed in Sec. 4.2.1.3) so that it appears to be a factor of 1/3 smaller than the total current on the second plateau. Now, let us decrease the collector coupling of the single particle state $i = 2$. The ratio $\gamma_2 = 0.1$ results in the green CVC in Fig. 3.2a. The first current plateau drops with respect to the total current on the second plateau. For electrons which enter the single particle state $i = 2$ from the emitter the tunneling into the collector is delayed so that electrons spend a longer time in this state. During this time interval the other single particle state is blocked, i.e. electrons cannot enter this state. Therefore the current is reduced. For a very low γ_2 the current can be even exponentially small as can be seen in the black CVC of Fig. 3.2 ($\gamma_2 = 0.001$). At the onset of the first plateau a peak develops for decreasing γ_2 and consequently a pronounced NDC becomes observable in the CVC (also observed in [HET02]). For its explanation in Fig. 3.2b the occupation probabilities P_ν for $\nu = (0,0)$ (dashed line), $\nu = (1,0)$ (solid line), $\nu = (0,1)$ (dash-dotted line) vs. bias voltage for $\gamma_2 = 0.001$ are shown. At the current onset the occupations of the single particle states $(1,0)$ and $(0,1)$ start to increase for increasing bias voltage due to the tunneling of thermally activated emitter electrons. Since the state $(1,0)$ is only partially filled its Coulomb blocking effect on state $(1,0)$ is less effective so that $P_{(1,0)}$ can also increase but weaker as $P_{(0,1)}$. As soon as $P_{(0,1)}$ exceeds a certain value, the state $(1,0)$ gets blocked and $P_{(1,0)}$ starts to drop. For those reasons the pronounced precursor peak in the black CVC of Fig. 3.2 and the corresponding NDC are caused by the effect of mutual Coulomb blocking of the single particle states in the QD system and by tunneling of thermally activated emitter electrons into these states. In Sec. 4.2.2.1 it will be shown that this Coulomb blocking effect is accompanied with bunching of tunneling events, i.e. positive temporal correlations

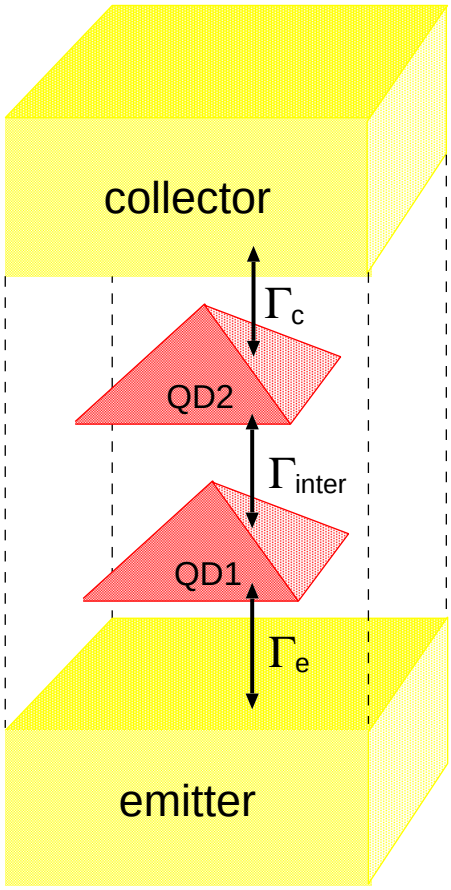

Figure 3.3.: Scheme of the quantum dot stack connected to an emitter/collector contact with tunneling rates $\Gamma_{e/c}$, respectively, and tunneling rate Γ_{inter} between the quantum dots.

in the tunneling current.

Note that NDC in nonlinear transport through QDs can also be caused by spin blockade as investigated by Weinmann et al. [WEI95].

The NDC in the CVC of double barrier resonant tunneling diodes can come along with the phenomenon of bistability. Due to the probabilistic nature of the ME approach used here, bistability should become manifest in a bimodal distribution e.g. of the particle number in the system Such a behavior was not found for the unipolar tunneling through coupled QDs as considered above. But for bipolar transport through large QD arrays [KIE02b, KIE03] the author observed bimodal distributions which are accompanied with NDC behavior.

3.3. Stacked quantum dots

The results of this section are published in [SPR04]. In the following we investigate the tunneling current through a single QD stack as mentioned in Sec. 2.2.1.2 regarding the experiment. In Fig. 3.3 the double QD system is sketched: QD1 is connected to an emitter contact with a tunneling rate Γ_e, QD2 is connected to a collector contact with a tunneling rate Γ_c, and both QDs are tunnel-coupled mutually with a rate Γ_{inter} (for the definition see below). We consider one spin degenerate single particle state per QD. Then the many-particle (Fock-) states of the QD stack are characterized by occupation numbers $n_{i\sigma}^{(\nu)} \in \{0,1\}$, where $i = 1,2$ labels the QD and $\sigma = \uparrow, \downarrow$ labels the spin degree of freedom. Thus $\nu = (n_{1\uparrow}^{(\nu)}, n_{1\downarrow}^{(\nu)}, n_{2\uparrow}^{(\nu)}, n_{2\downarrow}^{(\nu)})$ gives 16 different Fock states.

3.3.1. Fermi's golden rule

Setting up the transition matrix $\underline{\underline{M}}$ in (3.1.3) for tunneling processes into or from the emitter/collector contacts is performed in the same manner as in the previous section. Here we additionally deal with transitions which do not change the total particle number in the QD system - they describe tunneling between QD1 and QD2: Taking into account the broadening of the transition due to the finite lifetime in the QDs, Fermi's golden rule provides us with

$$\begin{aligned} M_{\nu\nu'} =& 2\pi|\Omega|^2 \left[\frac{1}{\pi}\frac{\Gamma/2}{(\Delta E_{\nu\nu'})^2 + (\Gamma/2)^2}\right] \\ =& \Gamma_{\text{inter}}\, L(\Delta E_{\nu\nu'}, \Gamma) \end{aligned} \tag{3.3.1}$$

Here Ω is the tunneling matrix element and $\Gamma \equiv \Gamma_e + \Gamma_c$. The maximum tunneling rate is $\Gamma_{\text{inter}} = 4|\Omega|^2/\Gamma$ and $L(x,w) \equiv [1 + (2x/w)^2]^{-1}$ is a Lorentzian function in x with a full-width-half-maximum (FWHM) of w. For convenience we measure rates and energies in the same units in this section, i.e. we set $\hbar = 1$.

3.3.2. Noninteracting quantum dots: The width of current resonances

If the energies of single particle states in two different QDs are resonant, a current flows through the QD stack and a peak arises in the CVC. In this section we give an analytical derivation of the current for noninteracting electrons, i.e. setting $U(\nu) \equiv 0$ in Eq. (3.1.6). Then both spin directions decouple and we can restrict ourselves to a single spin direction here. For the single particle levels in QD1 and QD2 it is assumed that $\varepsilon_1 - \mu_e \gg k_B T$ and $\mu_c - \varepsilon_2 \gg k_B T$ such that $f_e \approx 1$ and $f_c \approx 0$. With $\underline{P}^0 = (P^0_{(0,0)}, P^0_{(0,1)}, P^0_{(1,0)}, P^0_{(1,1)})^T$ the matrix $\underline{\underline{M}}$ explicitly reads

$$\underline{\underline{M}} = \begin{pmatrix} -\Gamma_e & \Gamma_c & 0 & 0 \\ 0 & -(\Gamma_e + \Gamma_c + Z) & Z & 0 \\ \Gamma_e & Z & -Z & \Gamma_c \\ 0 & \Gamma_e & 0 & -\Gamma_c \end{pmatrix} \tag{3.3.2}$$

with $Z \equiv \Gamma_{\text{inter}} L(\Delta E_{(1,0)(0,1)}, \Gamma)$. The stationary ME can be rewritten in a rate equation for the average occupation numbers $\langle n_1 \rangle$ and $\langle n_2 \rangle$ which results in the following stationary solution

$$\begin{pmatrix} \langle n_1 \rangle \\ \langle n_2 \rangle \end{pmatrix} = \frac{\Gamma_e}{\Gamma_e \Gamma_c + \Gamma Z} \begin{pmatrix} \Gamma_c + Z \\ Z \end{pmatrix} \tag{3.3.3}$$

The current (3.1.5) then becomes

$$I = e \left[\frac{1}{\Gamma_e} + \frac{1}{\Gamma_c} + \frac{1}{Z} \right]^{-1} \tag{3.3.4}$$

which can be physically interpreted quite easily: the three barriers in the QD stack act as a series connection of resistors corresponding to the inverse of tunneling rates. After a straightforward transformation of (3.3.4) one obtains

$$I = e\Gamma_w \, L \left(\Delta E, \Gamma \sqrt{1 + \frac{4|\Omega|^2}{\Gamma_e \Gamma_c}} \right) \tag{3.3.5}$$

with $\Gamma_w \equiv \left[\frac{1}{\Gamma_e} + \frac{1}{\Gamma_c} + \frac{1}{\Gamma_{\text{inter}}} \right]^{-1}$. Due to the assumption of a linear dependence of the single particle levels on the bias voltage it follows for the energy difference $\Delta E = \varepsilon_1 - e\eta_1 V - (\varepsilon_2 - e\eta_2 V) = e(\eta_2 - \eta_1)(V - V_R)$ with the bias voltage for the resonance between the levels $eV_R \equiv \frac{\varepsilon_2 - \varepsilon_1}{\eta_2 - \eta_1}$. Substituting this in Eq. (3.3.5) leads to

$$I(V) = e\Gamma_w \, L \left(V - V_R, \frac{\Gamma}{e(\eta_2 - \eta_1)} \sqrt{1 + \frac{4|\Omega|^2}{\Gamma_e \Gamma_c}} \right) \tag{3.3.6}$$

As expected, the CVC shows a Lorentzian peak at the bias voltage V_R. Interestingly, its broadening is not just given by the tunnel-coupling to the contacts Γ, but by a line width modified by the correction factor $\sqrt{1 + \frac{4|\Omega|^2}{\Gamma_e \Gamma_c}}$. This factor provides a significant increase of the FWHM for the current peak if the tunneling matrix element $|\Omega|$ is larger than the geometric mean $\sqrt{\Gamma_e \Gamma_c}$ of the contact tunneling rates.

To discuss Eq. (3.3.6) let us assume that $\Gamma_c > |\Omega| > \Gamma_e$: the current is limited by the lowest rate $\Gamma_{\text{inter}} L(\Delta E, \Gamma)$ for bias voltages V far away from V_R. If the bias approaches V_R this rate is increased until it equals the emitter coupling Γ_e. Now, the emitter barrier starts to limit the current, i.e. the current flattens close to the

resonance so that the FWHM value of the current is reached for larger distances from the resonance voltage V_R. The smaller the ratio of $\Gamma_e/|\Omega|$ the broader the current peak.

The peak (maximum) current is given by $I(V_R) = e\Gamma_w$. It has a non-monotonic dependence on the collector tunneling rate Γ_c: for weak collector coupling the peak current increases linearly, it shows a maximum at $\Gamma_c = 2|\Omega|$ which corresponds to the highest transparency through the triple-barrier structure and drops as $1/\Gamma_c$ for strong collector coupling. (The same holds for the emitter coupling.) On the basis of the coherent description this was interpreted in Ref. [WEG99] as a competition between enhanced tunneling for weak collector coupling and destructive interference in the opposite limit [4] . Hence, it is worth to note that one obtains the same effect in a Fermi's golden rule treatment where no interference is taken into account. In this picture increasing Γ_c enhances the transport over the collector barrier but limits the transport between the dots by broadening the transition.

The expression (3.3.5) for the stationary current was also found in [GUR96c, GUR96d, GUR98, WEG99] where a density matrix approach was used. In the next Sec. 3.3.2.1 we show that both approaches give identical results in the stationary state if electron-electron interaction is neglected.

3.3.2.1. Link to coherent tunneling: Density matrix approach

We start with the modified Liouville equation for the double QD system (Fig. 3.3) derived in [GUR96c]. The following abbreviations for the Fock states $|\nu\rangle$ will be used: $|a\rangle \equiv |0,0\rangle$, $|b\rangle \equiv |1,0\rangle$, $|c\rangle \equiv |0,1\rangle$, and $|d\rangle \equiv |1,1\rangle$. Then the time evolution of the corresponding density-matrix elements is given by

$$\begin{aligned}
\dot{\rho}_{aa} &= -\Gamma_e\rho_{aa} + \Gamma_c\rho_{cc} \\
\dot{\rho}_{bb} &= \Gamma_e\rho_{aa} + \Gamma_c\rho_{dd} + i\Omega(\rho_{bc} - \rho_{cb}) \\
\dot{\rho}_{cc} &= -\Gamma\rho_{cc} - i\Omega(\rho_{bc} - \rho_{cb}) \\
\dot{\rho}_{dd} &= -\Gamma_c\rho_{dd} + \Gamma_e\rho_{cc} \\
\dot{\rho}_{bc} &= i\Delta E\rho_{bc} + i\Omega(\rho_{bb} - \rho_{cc}) - \frac{1}{2}\Gamma\rho_{bc}
\end{aligned} \tag{3.3.7}$$

with $\Delta E \equiv \varepsilon_2 - \varepsilon_1$ and $\Gamma \equiv \Gamma_e + \Gamma_c$. Additionally, probability conservation is demanded: $\sum_\nu \rho_{\nu\nu} = 1$ and $\rho_{cb} = \rho_{bc}^*$ holds. Eq. (3.3.7) can be transformed into a matrix equation of the form $\underline{\dot{u}} = \underline{\underline{A}} \cdot \underline{u}$ with $\underline{u} \equiv (\rho_{aa}, \rho_{bb}, \rho_{cc}, \rho_{dd}, \mathrm{Re}(\rho_{bc}), \mathrm{Im}(\rho_{bc}))^T$ and

[4] The interference mechanism can be applied e.g. for anti-reflection coating in ballistic transport through superlattices [PAC01].

$$\underline{\underline{A}} \equiv \begin{pmatrix} -\Gamma_e & \Gamma_c & 0 & 0 & 0 & 0 \\ 0 & -\Gamma & 0 & 0 & 0 & -2\Omega \\ \Gamma_e & 0 & 0 & \Gamma_c & 0 & 2\Omega \\ 0 & \Gamma_e & 0 & -\Gamma_c & 0 & 0 \\ 0 & 0 & 0 & 0 & -\frac{1}{2}\Gamma & -\Delta E \\ 0 & \Omega & -\Omega & 0 & \Delta E & -\frac{1}{2}\Gamma \end{pmatrix} \tag{3.3.8}$$

In order to derive the ME for the occupation probabilities $P_\nu = \rho_{\nu\nu}$ one has to get rid of the non-diagonal elements ρ_{bc} in (3.3.7) by truncating the 6×6 matrix (3.3.8) to the 4×4 matrix (3.3.2). This can be accomplished by setting the time derivatives of $\mathrm{Re}(\rho_{bc})$ and $\mathrm{Im}(\rho_{bc})$ to zero. Then one can solve the algebraic equations for $\rho_{bc}^{\mathrm{stat}} = \Omega(\rho_{cc} - \rho_{bb})/(\Delta E + i\Gamma/2)$ and substitute this expression in the equations for $\dot{\rho}_{bb}$ and $\dot{\rho}_{cc}$. This immediately leads to the terms $Z = \frac{\Omega^2\Gamma}{\Delta E^2 + (\Gamma/2)^2}$ in (3.3.2) as introduced by Fermi's golden rule in Sec. 3.3.1.

The necessary assumption $\dot{\rho}_{bc} = 0$ is justified if one of two conditions is met: (i) In the limiting case $\Omega \ll \Gamma$ the relaxation of $\rho_{bc}(t)$ to $\rho_{bc}^{\mathrm{stat}}$ occurs on a fast time scale. This is the condition for sequential tunneling which underlies our derivation of the ME. (ii) In the stationary case $\dot{\rho}_{bc} = 0$ holds independently of the magnitude of Ω. Therefore, the ME provides reliable results also in the strong coupling limit if one restricts oneself to the stationary current.

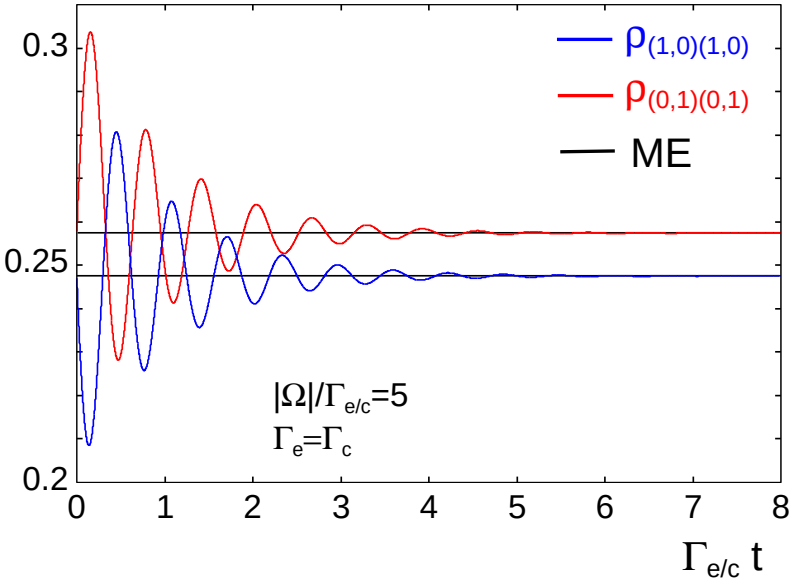

Figure 3.4.: Time evolution of the occupation of QD1 (blue curve) and of QD2 (red curve) with density matrix approach and with master equation (black curves). Initial conditions are given by the stationary occupations and $\mathrm{Re}(\rho_{bc})(t=0) = \mathrm{Im}(\rho_{bc})(t=0) = 0$.

Nevertheless, the time evolution of the occupations in the density matrix approach is governed by Rabi oscillations [KIE98] which are missing in the description by the ME as shown in Fig. 3.4. This essential difference is revealed e.g. in the noise behavior as studied in Sec. 5.4 or more fundamentally in the full counting statistics considered in Chap. 7.

3.3.3. Coulomb interaction: Appearance of double current peaks

Now, our considerations will be extended to the more realistic situation of Coulomb interacting electrons. We describe the interaction of electrons inside QD1 and QD2 with charging energies $e^2[C^{-1}]_{11} = U_1$ and $e^2[C^{-1}]_{22} = U_2$, respectively. The Coulomb interaction strength of electrons in different QDs is given by $e^2[C^{-1}]_{12} = U_{\text{inter}}$.

3.3.3.1. Current dependence on emitter Fermi energy

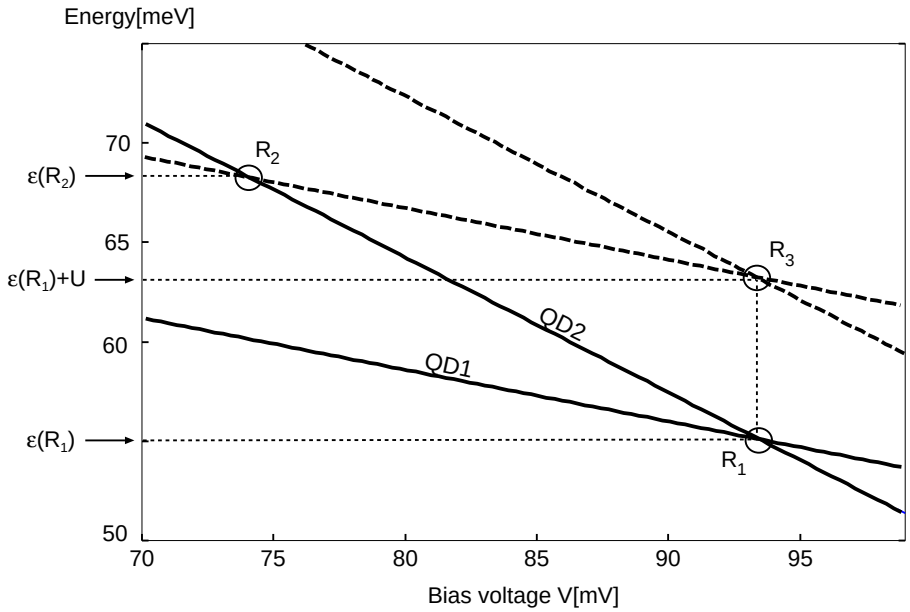

Figure 3.5.: Linear bias voltage dependence of the single particle energy levels in QD1 (η_1 =0.26, $\varepsilon_1(V = 0)$ =79.5 meV) and in QD2 (η_2 =0.68, $\varepsilon_2(V = 0)$ =118.7 meV). Dashed lines: addition energies for doubly occupied QD states ($U = U_1 = U_2$ =8meV, U_{inter} =0). Taken from [SPR04].

In Fig. 3.5 the bias voltage dependence of the QD energies are depicted. The zero-bias single particle energies ε_i and leverage factors η_i were obtained from the calculation of the transmission through a two-dimensional geometry as depicted

in Fig. 3.5 without scattering processes [SPR04] (method very similar to [KIE99a] where the transmission through a quantum wire geometry was examined). In order to describe the experiment, we use the geometry in [BRY03] which gives η_1 =0.26, ε_1 =79.5 meV, and η_2 =0.68, ε_2 =118.7 meV.

Due to the different slopes, the single particle levels of QD1 and QD2 (full lines in Fig. 3.5) intersect at the point R_1. Further resonances can occur by considering the double occupancy of the QDs. Assuming equal charging energies for both QDs ($U = U_1 = U_2 = 8$meV) parallel lines with the additional charging energy U emerge (dashed lines in Fig. 3.5). The resonance R_2 is due to the intersection of the energies of the doubly occupied QD1 and the singly occupied QD2. The resonance of the doubly occupied states R_3 occurs at the same bias voltage as for R_1 if the charging energies for both QDs are equal.

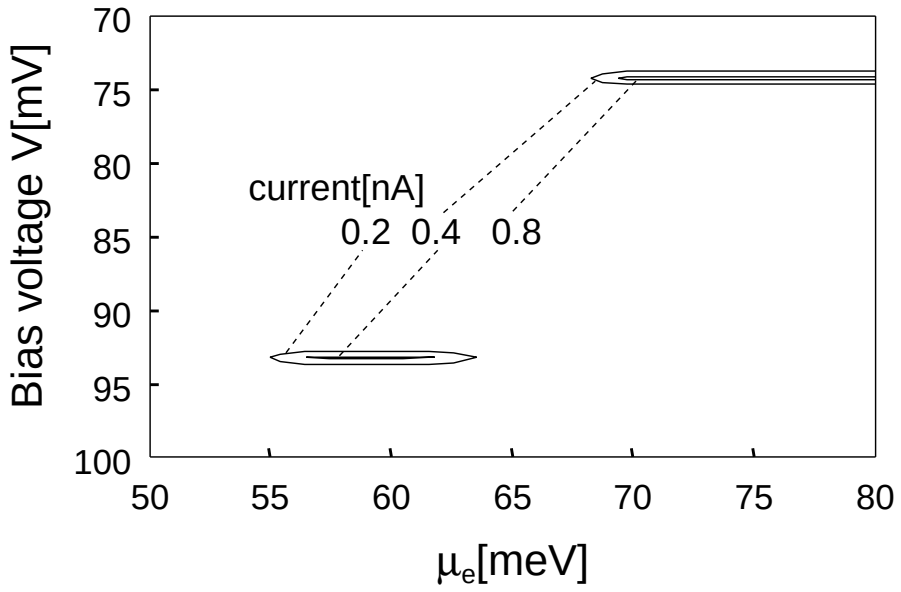

Figure 3.6.: Contour plot: current I vs. emitter chemical potential μ_e and bias voltage V for $U = U_1 = U_2 = 8$meV, $U_{\text{inter}} = 0$, $\Gamma_e = \Gamma_c = 100\mu$eV, $|\Omega|$ =10μeV, $T = 4.2$ K. Taken from [SPR04].

A current flow through the QD system is possible at the resonance energies $\varepsilon(R_1)$ and $\varepsilon(R_2)$ providing that electron states in the emitter contact are occupied at these energies. (Typically, these resonances occur at energies far above the chemical potential of the collector, so that the electrons can always leave the QD system via the collector barrier.) In Fig. 3.6 the dependence of the current on the emitter chemical potential μ_e and the bias voltage V is shown as a contour plot. Here we assume that the tunnel coupling between the dots is rather weak, i.e. $|\Omega| \ll \Gamma_e, \Gamma_c$, so that the occupation of the dots is determined by the respective reservoirs. The conduction band edge in the emitter is the zero-point of the energy scale. Different scenarios for the stationary current depending on μ_e arise:

(i) $\mu_e < \varepsilon(R_1)$: there is only an exponentially small current due to thermally activated electrons in the emitter.

(ii) $\varepsilon(R_1) < \mu_e < \varepsilon(R_1) + U = \varepsilon(R_3)$: in this case the current shows a peak due to the resonance R_1 of the single particle levels, the second resonance R_2 is energetically available for thermally activated electrons from the emitter and gives rise to an additional current peak at lower bias voltage which increases with increasing temperature (this scenario was experimentally investigated in [BRY03] and was used to determine the charging energy U).

(iii) $\varepsilon(R_1)+U < \mu_e < \varepsilon(R_2)$: no current peak appears. In this regime it is possible to add a second electron in QD1. Since the coupling between the QDs is weaker than the coupling to the emitter contact, QD1 is mostly occupied with two electrons. They leave QD1 with the energy $\varepsilon_1 + U$ so that they cannot fulfill the resonance condition for R_1.

(iv) $\mu_e > \varepsilon(R_2)$: a current peak due to the resonance R_2 occurs with twice the peak height than in the case (ii) because two electrons contribute to the current here. A current peak for resonance R_1 is suppressed for the same reasons as in (iii).

3.3.3.2. Current dependence on tunnel coupling

Now we want to study the behavior with increasing tunnel coupling $|\Omega|$. In particular we consider the regime (iv) of the last section but now we allow the tunneling rates to the contacts to be different ($\Gamma_e = 17\mu$eV, $\Gamma_c = 400\mu$eV).

Fig. 3.7 shows the bias voltage dependent current for varying couplings $|\Omega|$ between the QDs. For low $|\Omega|$ one observes a current peak at $V = 75$mV corresponding to the resonance R_2 in Fig. 3.5 (compare regime (iv) in the last section). According to Eq. (3.3.6) the current peak broadens with increasing $|\Omega|$ but one has to consider the double occupancy of QD1 which modifies the current peak width such that the correction factor becomes now $\sqrt{1 + 2 \cdot \frac{4|\Omega|^2}{\Gamma_e \Gamma_c}}$. With increasing $|\Omega|$ a second current peak at the bias voltage of R_1 appears in Fig. 3.7. Due to the stronger coupling between the QDs single occupancy of QD1 becomes more likely, since the second electron in QD1 can tunnel into QD2 off-resonantly because of the finite line-width of the levels. Hence, electrons with energy E_1 can leave QD1 and contribute to resonance R_1 which generates a current peak at $V(R_1)$. Hence, the possibility of the observation of a double current peak in the experiment depends mainly on the tunnel matrix element Ω between states in different QDs. Its sensitivity on the spatial separation of the QDs within the stack could explain the frequent observation of the double current peaks [BOR01].

Note that for $|\Omega| \geq 260\mu$eV a small third current peak at almost 110 mV appears due to the resonance of the energies of the doubly occupied QD2 and single occupied QD1 (out of the bias range depicted in Fig. 3.5).

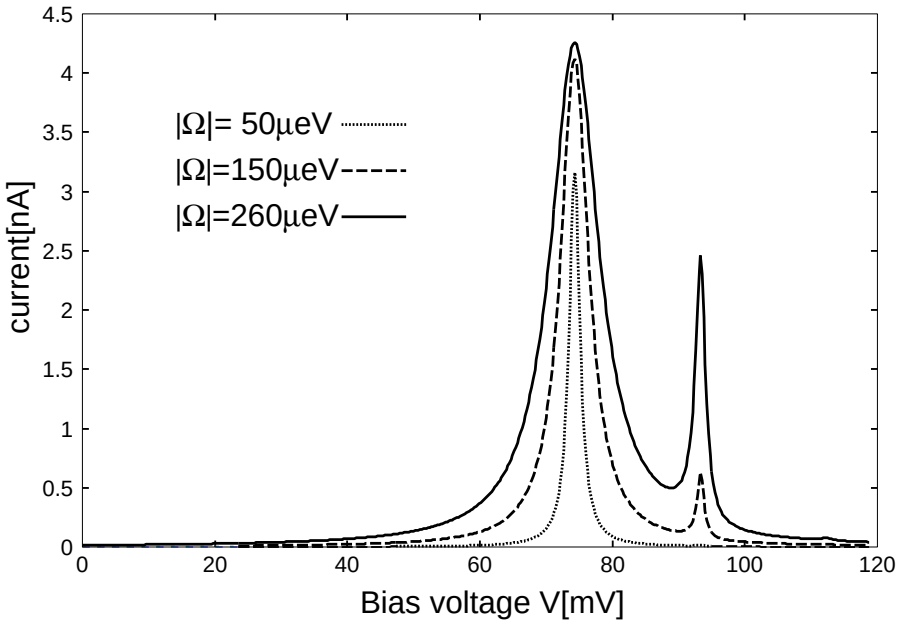

Figure 3.7.: Current I vs. bias voltage V for varying coupling between QDs $|\Omega|$. $\Gamma_e = 17\mu$eV, $\Gamma_c = 400\mu$eV, $T = 4.2$K, $U = U_1 = U_2 = 8$meV, $U_{\text{inter}} = 0$, $\mu_e = 90$meV. Taken from [SPR04].

Underlining the corresponding mechanisms which lead to the current peaks in Fig. 3.7 we show the current-voltage characteristics for different charging energies U_1 with fixed $U_2 = 8$meV in Fig. 3.8a (the other parameters are the same as for the full curve in Fig. 3.7). As one can see, with decreasing U_1 the low bias current peak shifts to higher bias voltages and the second current peak remains at the same bias voltage position: Reducing U_1 leads to a parallel shift of the dashed line with smaller slope in Fig. 3.5 so that the intersection point R_2 shifts to higher bias voltages and the resonance R_1 is left unchanged. In Fig. 3.8b the values of Γ_e and Γ_c were interchanged so that a different physical situation emerges. Here, both current peaks shift to higher bias voltages by the same amount with decreasing U_1, i.e. the resonance R_3 is now mainly responsible for the current peak at higher bias voltage. Due to the weaker collector coupling the double occupancy of both QDs becomes more likely.

Note that for equal charging energies in QD1 and QD2 the current-voltage characteristics are invariant with respect to an interchange of Γ_e and Γ_c. This is due to the electron-hole symmetry in the considered QD system. The necessary condition for this symmetry is that the resonances occur at energies deep in the Fermi sea on one contact side and unoccupied states on the other side.

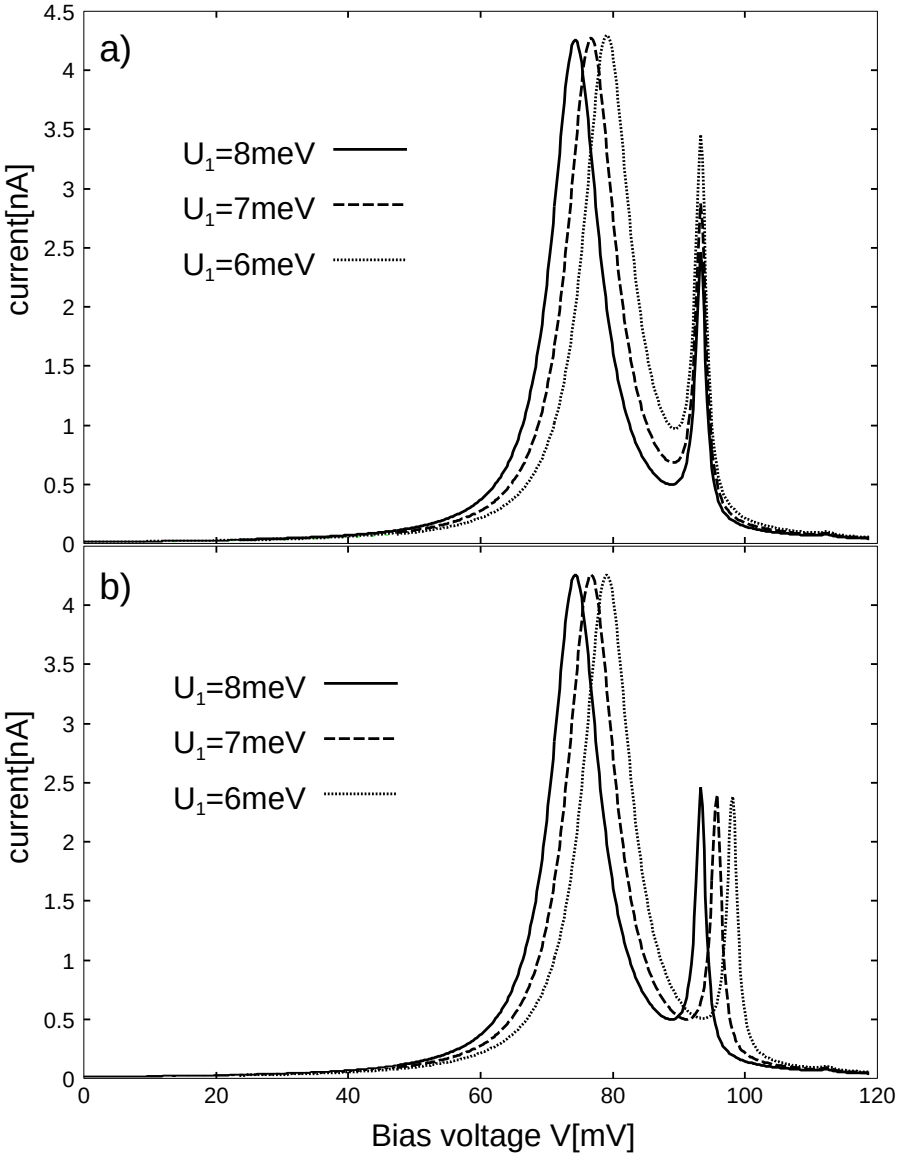

Figure 3.8.: Current I vs. bias voltage V for different charging energies of QD1: $\Delta U_{\text{intra}} \equiv U_2 - U_1$; $U_2 = 8\text{meV}$; other parameters are the same as for the full curve in Fig. 3.7. Taken from [SPR04].

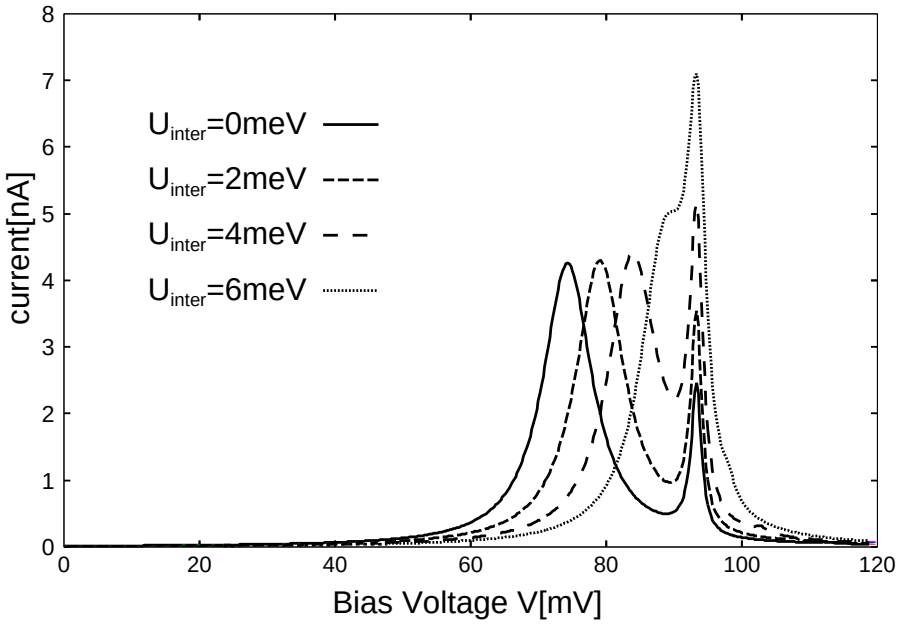

Figure 3.9.: Current I vs. bias voltage V for different Coulomb interaction strengths between QD1 and QD2: U_{inter}, other parameters are the same as for the full curve in Fig. 3.7. Taken from [SPR04].

3.3.3.3. Coulomb interaction between neighbouring quantum dots

The self-organized QDs within one stack grown in [BOR01, BRY02, BRY03] have a spatial separation of few nm so that the Coulomb interaction between electrons in different QDs is a crucial ingredient in a theoretical examination. Fig. 3.9 shows the CVC for different interaction strengths $U_{\text{inter}} = 0$, 2, 4meV.

Again a double peak appears whereas the distance of the maxima diminishes with increasing U_{inter}. If QD1 is filled with one electron the single particle level of QD2 is shifted by U_{inter} so that the low-bias resonance R_2 moves to higher bias voltages. The resonance R_1 stays at the same bias voltage since QD2 filled with one electron generates a shift of the single particle level of QD1 by the same amount U_{inter}. This leads to the current peak separation

$$\Delta V = \frac{U - U_{\text{inter}}}{e(\eta_2 - \eta_1)} \tag{3.3.9}$$

Another feature can be seen in the dotted curve in Fig. 3.9: if ΔV becomes smaller, the height of the high-bias peak increases. This peak structure is quite similar to that observed in the experiment (Fig. 4 in Ref. [BOR01]).

4. Current Fluctuations within Sequential Tunneling - Shot Noise

"The noise is the signal" [LAN98]

Due to the granularity of the electron charge in units of the elementary charge, tunneling through barriers is a discrete stochastic process. Therefore the tunneling current is a fluctuating quantity and this gives rise to shot noise [SCH18]. In the previous chapter we considered the stationary current through QD systems in the sequential tunneling regime. Even though important aspects of the physics of transport through coupled QDs is provided by this quantity, a lot of information is missing, but can be revealed by the consideration of the current fluctuations. In this chapter, the shot noise for double-barrier and triple-barrier QD geometries will be investigated in the sequential tunneling regime, i.e. by utilizing the ME technique introduced in Sec. 3.1. First, we will show how one can obtain the autocorrelation function of the tunneling current through an arbitrary QD system starting from the ME. The frequency dependent shot noise intensity, i.e. the spectral power density (SPD) is then obtained from the autocorrelation function by means of the Wiener-Khinchin theorem. Beside shot noise an additional source of fluctuations is thermal noise which predominatly exhibits in the linear response regime. We will briefly discuss its relevance for nonlinear transport. While a lot of information for temporal correlations in nonlinear transport is already contained in the low-frequency SPD which is one of the central observables throughout this work, we nevertheless give a short characterization of the full SPD spectrum for double-barrier tunneling.

In this chapter, one particular aim is the investigation of the temporal correlations in the tunneling current through QDs caused by the interplay of Pauli's exclusion principle and the Coulomb interaction. This will be examined for a generic two-level QD system. It will turn out that the shot noise is able to reveal detailed information about tunneling barrier geometries and Coulomb interactions in coupled QDs.

Furthermore, it will be examined how Coulomb repulsion can cause positive correlations (super-Poissonian noise) in the tunneling current through QDs which in some cases can be accompanied by NDC as discussed in Sec. 3.2.

4.1. Current fluctuations

4.1.1. Correlation function and spectral power density

The SPD of the current fluctuations is related to the autocorrelation function of the current by the Wiener-Khinchin theorem (for $a = b$ see Appendix B):

$$S_{ab}(\omega) = 2\int_{-\infty}^{\infty} dt\, e^{i\omega t}\left[\langle I_a(t)I_b(0)\rangle - \langle I_a\rangle\langle I_b\rangle\right] \tag{4.1.1}$$

where $a, b = e, c$ (emitter/collector) and $\langle\cdot\rangle$ denotes the ensemble average. To obtain the autocorrelation function of the current entering Eq. (4.1.1) the explicit time evolution of the occupation probabilities given by the ME (3.1.3) is needed. It can be obtained by the time propagator $\underline{\underline{\mathbf{T}}}(t)$ which is introduced as follows:

$$\underline{\underline{\mathbf{T}}}(t) \equiv \exp\left(\underline{\underline{\mathbf{M}}}t\right) \quad \text{with} \quad \underline{\mathbf{P}}(t) = \underline{\underline{\mathbf{T}}}(t)\,\underline{\mathbf{P}}(0) \tag{4.1.2}$$

Note, that the elements of the time propagator (4.1.2) are transition probabilities from a state at time $t = 0$ to a state at time t.

With the stationary solution of the ME (3.1.4) and the time propagator (4.1.2) the current-current correlator in (4.1.1) can be defined as [HER93]

$$\begin{aligned} C_{ab}(t) \equiv \langle I_a(t)I_b(0)\rangle \;=\; & \theta(t)\sum_{\nu}[\underline{\underline{\mathbf{j}}}_a\,\underline{\underline{\mathbf{T}}}(t)\,\underline{\underline{\mathbf{j}}}_b\,\underline{\mathbf{P}}^0]_\nu + \\ & +\theta(-t)\sum_{\nu}[\underline{\underline{\mathbf{j}}}_b\,\underline{\underline{\mathbf{T}}}(-t)\,\underline{\underline{\mathbf{j}}}_a\,\underline{\mathbf{P}}^0]_\nu + \\ & +e\delta_{ab}\delta(t)\sum_{\nu}\left|[\underline{\underline{\mathbf{j}}}_{a/b}\,\underline{\mathbf{P}}^0]_\nu\right| \end{aligned} \tag{4.1.3}$$

($\theta(t)$ is the Heaviside function). The current operators $\underline{\underline{j}}_{a/b}$ used here project each initial state to the possible final states after an electron has traversed the junction a weighted with the corresponding tunneling rate and taking into account a positive/negative sign depending on the electron flow. Thus the current operators are essentially non-diagonal. An explicit representation of these operators can be found in Eq. (3.2.2) for a two-level system. The first two terms of the right-hand side in (4.1.3) contain the correlation between tunneling events at different times. The appearance of the term defined for negative times ensures the symmetry property of the correlation function (4.1.3):[1] $C_{ab}(t) = C_{ba}(-t)$. The last term describes the

[1] Proof : defining the correlation function with the help of time average $C_{ab}(t) = \langle I_a(t'+t)I_b(t')\rangle_{t'}$ then (presuming the equivalence of time and ensemble average) $C_{ab}(-t) = \langle I_a(t'-t)I_b(t')\rangle_{t'} = \langle I_a(\tau)I_b(\tau+t)\rangle_\tau = C_{ba}(t)$

self-correlation of a tunneling event at the same barrier (for further discussions of (4.1.3) see also Refs. [DAV92, HER93, KOR94]). Note that for frequencies ω much smaller than any other inverse time-scale of the stochastic process (here the inverse tunneling rates Γ) which is the typical experimental regime (e.g. in Refs. [NAU02, NAU03, NAU04, NAU04a]), the absolute value of correlations does not depend on the barriers where they are measured, i.e. $S_{ee}(\omega \to 0) = S_{cc}(\omega \to 0) = -S_{ec}(\omega \to 0) = -S_{ce}(\omega \to 0)$ holds (follows from flux conservation for low frequencies [BUE92, BLA00], for finite frequencies see Sec. 4.1.3).

For uncorrelated tunneling events one obtains **Poissonian noise**. For a brief derivation of its SPD we consider the time-dependent current as a series of delta-like pulses at random distributed[2] times t_k:

$$I(t) = e \sum_k \delta(t - t_k) \tag{4.1.4}$$

We utilize the time average in the definition of the autocorrelation function and with (4.1.4) it is

$$\langle I(t'+t)I(t')\rangle_{t'} - \langle I\rangle^2 = e^2 \lim_{T\to\infty} \frac{1}{T} \int_0^T dt' \sum_{k,l} \delta(t'+t-t_k)\delta(t'-t_l) - \langle I\rangle^2 \tag{4.1.5}$$

Carrying out the integration on the r.h.s leads to

$$e^2 \lim_{T\to\infty} \frac{1}{T} \sum_{k,l} \delta(t + t_l - t_k) - \langle I\rangle^2 \tag{4.1.6}$$

Now, the sum can be split up in one part for $k \neq l$ which cancels (after a further time averaging in order to get rid of the delta-functions in the summation) with the $\langle I\rangle^2$-term. There remains the $k = l$-part which becomes

$$\lim_{T\to\infty} e^2 \frac{K}{T} \delta(t) \tag{4.1.7}$$

where K is the number of events in the time interval T. Hence, the quotient times e gives the stationary current for large T and we obtain the autocorrelation function[3]: $e\langle I\rangle\delta(t)$. According to the Wiener-Khinchin theorem (4.1.1) the Fourier transform of this function yields the SPD for Poissonian noise [SCH18]

[2] Obeying the definition of a Poisson process.
[3] This is equivalent to the last term in (4.1.3)

$$S_{\text{Poisson}} = 2e\langle I\rangle \tag{4.1.8}$$

Note here that the SPD S_{Poisson} does not depend on frequency. This is caused by the assumption of delta-like events in the stochastic process (4.1.4). In reality the finite width of pulses given e.g. by the time of traversing a barrier provides a high-frequency cut-off which prevents the divergence of the full power.

As a measure of deviation from the Poissonian value of noise the dimensionless **Fano factor** α is introduced [FAN47]:

$$\alpha(\omega) \equiv \frac{S_P(\omega)}{S_{\text{Poisson}}} \quad \begin{cases} < 1 & \text{sub-Poissonian noise} \\ = 1 & \text{Poissonian noise} \\ > 1 & \text{super-Poissonian noise} \end{cases} \tag{4.1.9}$$

4.1.2. Thermal noise

There is another important source of fluctuations in conductors which is dominant in thermal equilibrium and caused by random fluctuations of particles at finite temperature T: thermal noise or the so-called Johnson-Nyquist noise. Naively one would expect that the full noise is a simple superposition of thermal and shot noise. By means of the introduced way to obtain the correlation function in the last section a double-barrier system with a single level is considered. Here, thermal noise is a consequence of thermal fluctuations in the reservoirs.

In the linear-response regime the conductance defined as $G = \lim_{V\to 0} I/V$ is an equilibrium quantity given by $G = \frac{e^2}{4k_BT}\frac{\Gamma_e\Gamma_c}{\Gamma_e+\Gamma_c}$ [BEE91a] for on-resonance transport (the level has the same energy as the chemical potentials).

The zero-frequency[4] SPD vs. current is shown in Fig. 4.1. For $V \to 0$ or $I \to 0$ the SPD approaches a constant value which can be associated with the fluctuation-dissipation theorem: $S_P(0) = 4k_BTG$. It relates the equilibrium fluctuations to the generalized susceptibility, in this case the conductance G. Interestingly, if one inserts the equilibrium conductance for the double-barrier system into the fluctuation-dissipation theorem one obtains a SPD which is independent of temperature: $S_P(0) = e^2\frac{\Gamma_e\Gamma_c}{\Gamma_e+\Gamma_c}$. This is specific to tunneling through double-barrier system in this semi-classical ME description[5].

For high bias-voltages $V \gg k_BT$ the SPD becomes proportional to the current which is the regime of shot noise. The proportionality factor is given by $2e\alpha$. In Fig. 4.1 the system is chosen to be symmetric so that the Fano factor α is one half.

[4] I.e. $\hbar\omega \ll eV$, for higher frequencies the thermal noise is proportional to $\hbar|\omega|$ [BLA00]. This so-called zero-point noise cannot be obtained by the ME approach as a semi-classical technique.

[5] Note that in a purely quantum mechanical description (Chap. 5) the noise vanishes for zero temperature and symmetric barriers.

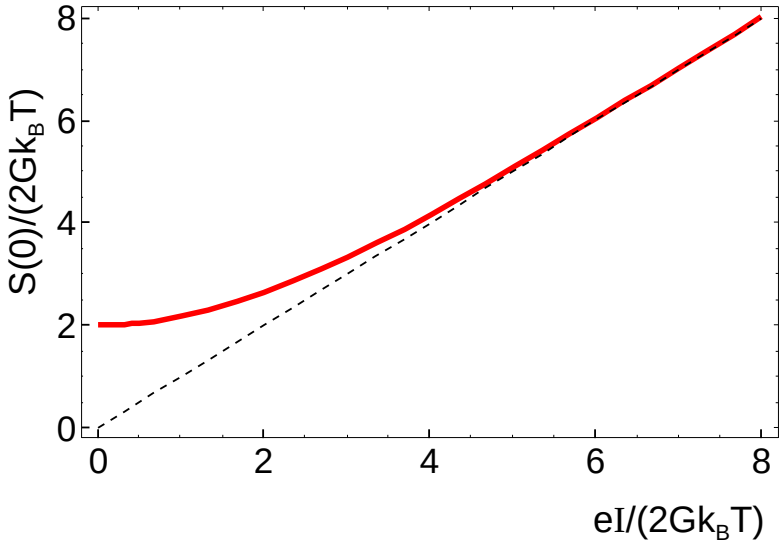

Figure 4.1.: Zero-frequency spectral power density vs. average current I, Eq. 4.1.10 (red curve). Low bias: fluctuation-dissipation theorem $S = 4k_BTG$; high bias: shot noise $S \propto I$ (Fano factor $\alpha = 0.5$). Dashed line is a guide for the eye.

The noise behavior depicted in Fig. 4.1 can be represented analytically over the whole range of bias-voltages [BLA00]

$$S(0) = \alpha S_{\text{Poisson}} \coth\left(\frac{eI}{2Gk_BT}\right) \tag{4.1.10}$$

Hence, there is a cross-over from thermal to shot noise for $eV \simeq k_BT$. In the strong nonlinear regime $eV \gg k_BT$ considered throughout this work thermal noise gives no contribution.

4.1.3. Finite-frequency noise

The total SPD $S_P(\omega)$ has to be calculated from the correlation function of the total current $I(t)$, i. e. particle plus displacement current [BLA00]. The current conservation (see Sec. 3.1) and the Ramo-Shockley theorem [SHO38] gives the total time-dependent current as $I(t) = l_eI_e(t) + l_cI_c(t)$ ($l_e \equiv \frac{C_e}{C_e+C_c}$ and $l_c \equiv \frac{C_c}{C_e+C_c}$ with the barrier capacitances $C_{e/c}$, $l_e + l_c = 1$). Then, one can express the total SPD in terms of the spectra of particle currents (4.1.1)

$$S_P(\omega) = l_e^2S_{ee}(\omega) + l_c^2S_{cc}(\omega) - l_el_c[S_{ec}(\omega) + S_{ce}(\omega)] \tag{4.1.11}$$

Note, that since the cross-correlation functions (4.1.3) $C_{ab}(t)$ for $a \neq b$ are not symmetric with respect to $t = 0$ the respective spectra have non-vanishing imaginary

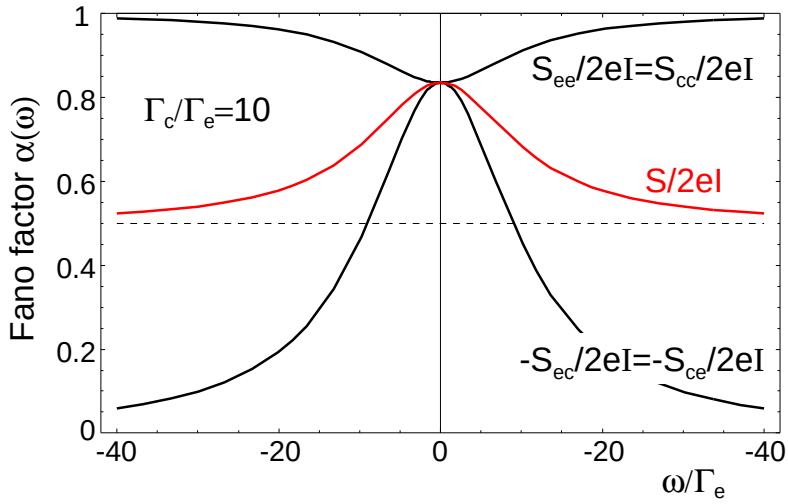

Figure 4.2.: Frequency-dependent Fano factor vs. frequency for the total current (red curve) and particle currents (black curves) for a double-barrier system, $l_e = l_c = 0.5$.

parts for $\omega \neq 0$. But in the last term of the r.h.s. of (4.1.11) they cancel out. In Fig. 4.2 the full spectrum for tunneling through a single level in a double-barrier system (red curve) together with the spectra of particle currents (black curves) are shown. As already outlined, all absolute values of spectral densities match at $\omega = 0$ due to current conservation. There, the Fano factor depends on the symmetry of the barriers Γ_c/Γ_e only (here chosen to be 10): $\alpha(0) = \frac{\Gamma_e^2+\Gamma_c^2}{(\Gamma_e+\Gamma_c)^2}$ as a consequence of Pauli's exclusion principle. This important relation will be discussed in a more detail with respect to Eq. (4.2.1) in the following section.

For large $|\omega|$ the spectra tend towards different values. The correlations at the same barrier (S_{ee} and S_{cc}) approach the Poissonian value because on a very short time scale there are no correlations between different tunneling events. The respective correlation functions are negative for all times t due to Pauli's exclusion principle so that the respective Lorentzian in Fig. 4.2 has a negative sign (compare Sec. 4.2.2 where also positive correlations will be discussed). The noise at different barriers (S_{ec} and S_{ce}) approaches zero for large $|\omega|$. Finally, the full noise $S(\omega)$ for $|\omega| \gg \Gamma_{e/c}$ is determined by the ratio of barrier capacitances $l_e/l_c = C_e/C_c$: $\alpha(\omega) = \frac{C_e^2+C_c^2}{(C_e+C_c)^2}$. In the case of Fig. 4.2 l_e/l_c is chosen to be unity. Then, the Fano factor approaches one half, i.e. for a simultaneous symmetry of tunneling rates $\Gamma_e/\Gamma_c = 1$ the full noise would appear frequency independent [BLA00].

Further literature on frequency-dependent noise: sequential tunneling through metallic QDs is investigated in [HAN93] in a similar approach; coherent tunneling through coupled QDs is studied in [SUN99]. Very recently asymmetric noise spectra were studied in [ENG04] and the shot noise spectrum of an open dissipative quantum

two-level system (coupled QDs) was investigated in [AGU04]. In Ref. [BLA00] a Langevin equation technique is used to obtain the frequency-dependent noise for double-barrier tunneling.

4.2. Application to coupled quantum dots with Coulomb interaction

4.2.1. Sub-Poissonian noise - parallel quantum dots

The results presented in this section are published in [KIE03a, KIE03b]. We consider two single particle states $\varepsilon_{1/2}$ which are connected to the emitter/collector contact and are coupled electro-statically by a Coulomb interaction of strength U (see Fig. 3.1). The transition matrix $\underline{\underline{M}}$ entering the ME (3.1.3) is explicitly given by (3.2.1). For the current operators at the collector and emitter barrier entering the autocorrelation function (4.1.3) and the average current (3.1.5) we use (3.2.2).

In contrast to the considerations in Sec. 3.2 here we allow for a finite energy difference between the single particle levels: $\Delta E \equiv \varepsilon_2 - \varepsilon_1 > 0$. The coupling to the emitter and collector contact is assumed to be the same for both states: $\Gamma_e \equiv \Gamma_e^{(1)} = \Gamma_e^{(2)}$ and $\Gamma_c \equiv \Gamma_c^{(1)} = \Gamma_c^{(2)}$.

In the following we discuss the average current and the Fano factor for three cases for the Coulomb interaction energy U: $U = 0$, $U < \Delta E$, and $U > \Delta E$.

4.2.1.1. Noninteracting states: $U = 0$

In Figs. 4.3 and 4.5 the results of a calculation for variation of U in the range of a few k_BT are shown (for fixed $k_BT = \Delta E/23$ and $\gamma = \Gamma_c/\Gamma_e$ =5). The mean current $\langle I \rangle$ vs. bias voltage V is plotted in Fig. 4.3a. For $U = 0$ there are two steps due to tunneling through the respective states. The width of the current steps is determined by the Fermi distribution of the emitter electrons. Note that typical energy scales are as follows: the bias voltage V is of the order of tens of mV, ΔE can be of the order of a few meV, k_BT is of the order of tens of μeV for temperatures in the range of a few Kelvin.

The corresponding Fano factor α (4.1.9) is shown in Fig. 4.3b. On the first plateau in the current-voltage curve of Fig. 4.3a where only tunneling through one single particle state occurs the Fano factor becomes

$$\alpha_i \equiv \alpha_i(0) = 1 - \frac{2}{\gamma_i + 2 + \frac{1}{\gamma_i}} f_e^{(i)} \qquad (4.2.1)$$

$$\text{with} \quad \gamma_i \equiv \frac{\Gamma_c^{(i)}}{\Gamma_e^{(i)}}$$

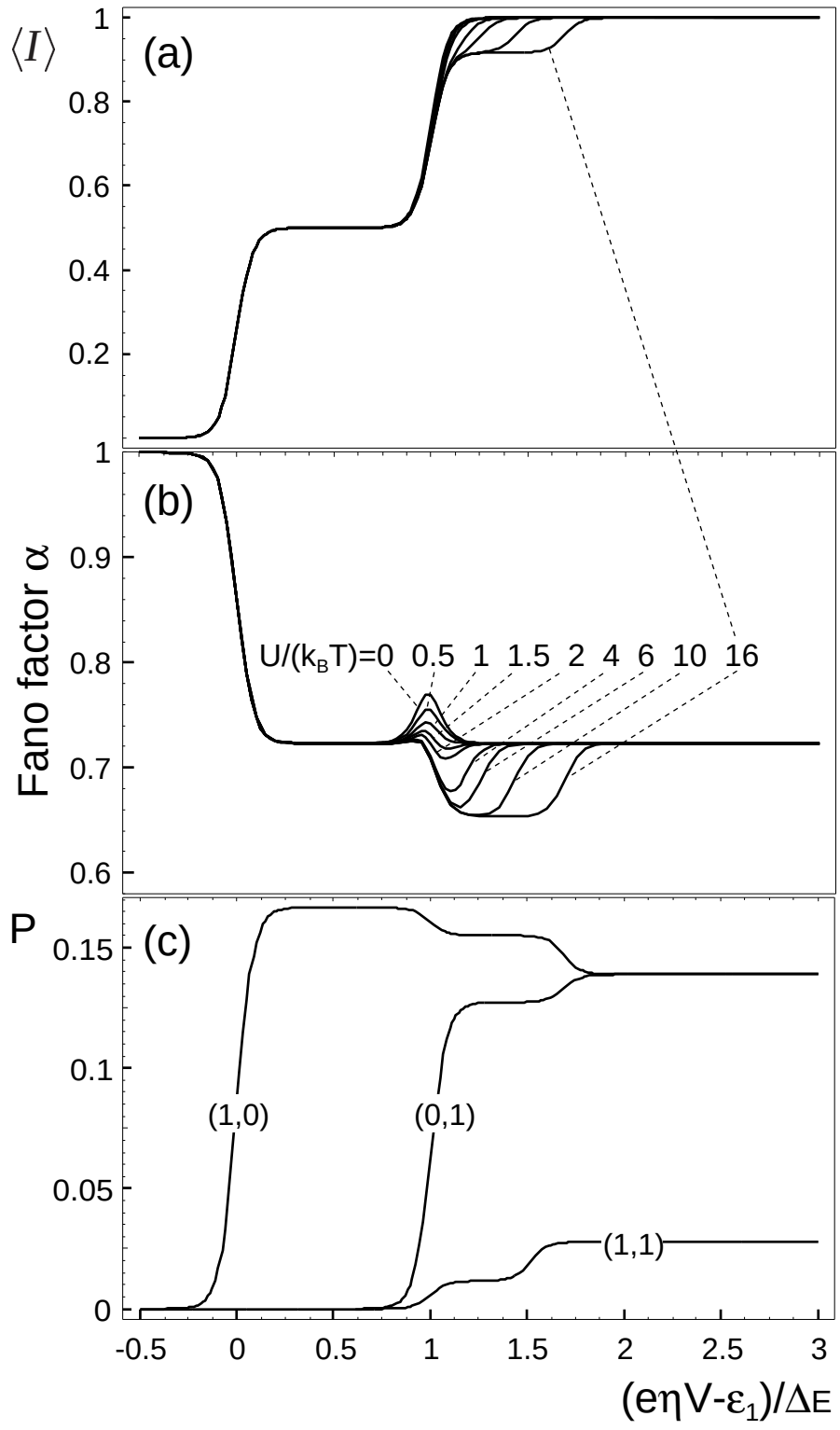

Figure 4.3.: a) Normalized mean current $\langle I \rangle$ vs. bias voltage V. b) Fano factor α vs. bias voltage V for different values of the Coulomb interaction energy U. c) Occupation probabilities $P_{(1,0)}$, $P_{(0,1)}$, and $P_{(1,1)}$ vs. bias voltage V for U/k_BT =16. Parameters: $k_BT = \Delta E/23$, $\gamma = \Gamma_c/\Gamma_e$ =5. Taken from [KIE03b].

where $i = 1$ denotes the energetically lowest single particle state. For $f_e^{(1)} = 1$ Eq. (4.2.1) is the well-known relation derived by L. Y. Chen *et al.* [CHE91]. It reflects the sensitivity of the Fano factor to Pauli's exclusion principle: If an electron has just passed the emitter barrier, the QD state is filled, so that no further electron can pass the barrier. This leads to an anti-correlation of the tunneling events, corresponding to a suppression of noise. As shown in Fig. 4.6a (black curve) the Fano factor α is equal to one half for symmetric tunneling barriers ($\gamma = 1$) and approaches unity for strong asymmetry. In the latter case the barrier with large Γ is effectively transparent so that the QD state is in equilibrium with the respective contact. The thicker barrier is then effectively a single tunnel barrier yielding Poissonian noise. For bias voltages below the current onset where $f_e^{(1)} \approx 0$ the tunneling current becomes uncorrelated so that $\alpha_1 = 1$. At the second step where the second single particle state is filled the Fano factor (Fig. 4.3b) has a peak which is also an effect of Pauli's exclusion principle: A new channel for the current opens, where electrons can fill both states $(1,0)$ and $(0,1)$. In this case, the Pauli blocking becomes less effective for the partially filled second state and the shot-noise suppression given by (4.2.1) is weaker. We obtain a simple analytical expression for an arbitrary number of noninteracting QD states which can account for the Fano factor behavior at the current steps (for a derivation for two states see Appendix C):

$$\alpha = \frac{\sum_i \langle I_i \rangle \alpha_i}{\langle I \rangle} \tag{4.2.2}$$

with α_i from Eq. (4.2.1), where the current through the single particle state i is: $\langle I_i \rangle = e\frac{\Gamma_c^{(i)}}{1+\gamma_i} f_e^{(i)}$, and the net current is $\langle I \rangle = \sum_i \langle I_i \rangle$. Eq. (4.2.2) was applied to the measured Fano factor modulation of tunneling through self-organized QDs (Fig. 2.7, [NAU02]) in a bias regime where only a few QD ground states are active in transport. It can qualitatively reproduce the measured Fano factor dependence on the bias voltage as shown in Fig. 4.4. For details, we refer the reader to [KIE03a].

4.2.1.2. $U < \Delta E$

With increasing Coulomb interaction $U \neq 0$ the Fano factor peak at the onset of the second resonance vanishes (see Fig. 4.3b) while the current changes only slightly. This underlines again the strong sensitivity of shot noise to correlations.

Further increase of U leads to an additional step whose bias voltage is proportional to U. The respective occupation probabilities $P_{(1,0)}$, $P_{(0,1)}$, and $P_{(1,1)}$ for $U = 16k_BT$ are shown in Fig. 4.3c: at the first plateau the electrons tunnel through the energetically lowest state $(1,0)$; the second plateau is generated by tunneling through both single particle states with different probabilities and with lower probability through the two-particle state which is determined by the coupling to the collector. This correlated state originates from aligning the emitter Fermi energy

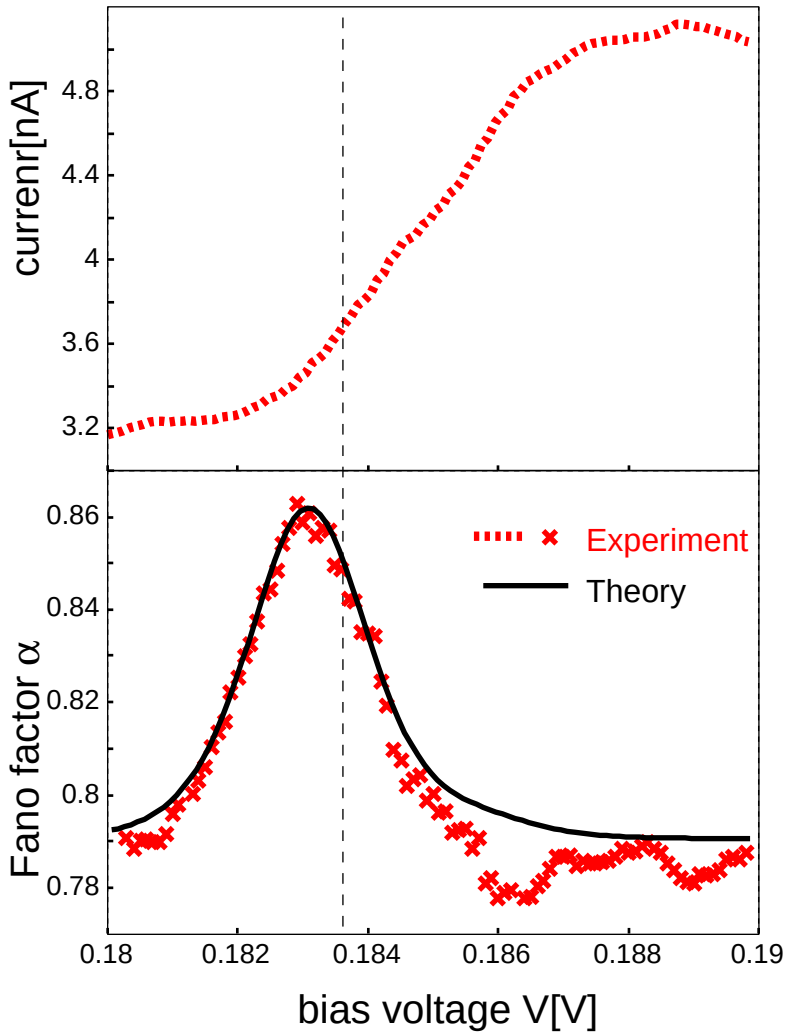

Figure 4.4.: Upper trace: current-voltage characteristic. Lower trace: Fano factor α vs. bias voltage. Red: experiment compare Fig. 2.7. Black: theory (4.2.2). Taken from [KIE03a].

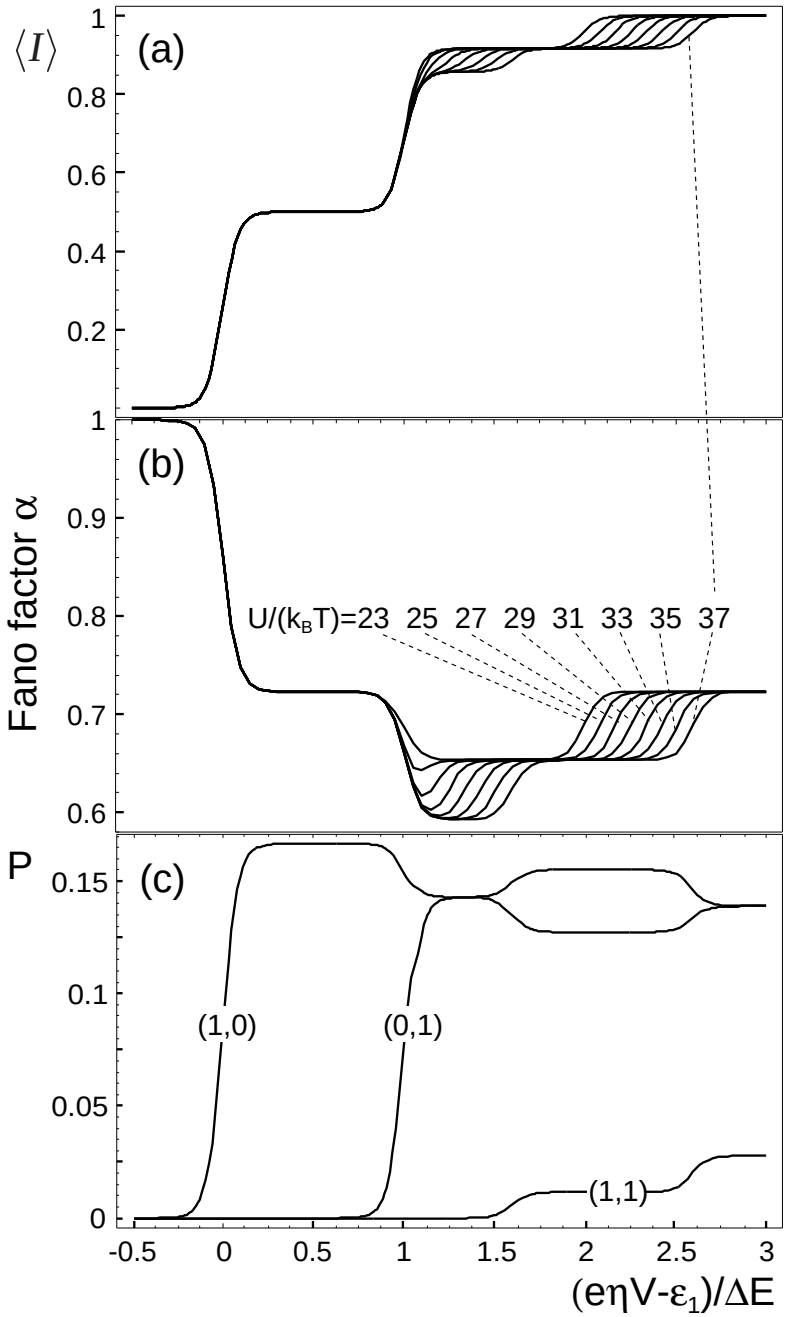

Figure 4.5.: Same as Fig. 4.3, but for different values of U. c) U/k_BT =37. Taken from [KIE03b].

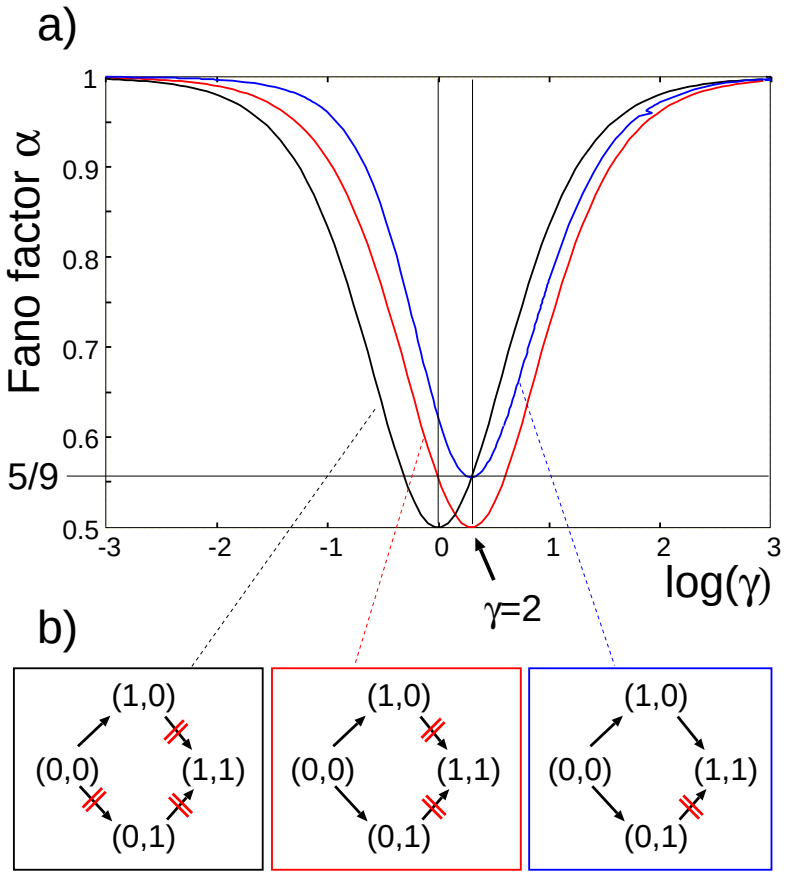

Figure 4.6.: a) Fano factor α vs. ratio of tunneling rates $\gamma = \Gamma_c/\Gamma_e$. black curve: first current plateau in Fig. 4.5; red curve: second current plateau; blue curve: third current plateau. $U = 37k_BT$. Taken from [KIE03b]. b) see text.

with the energy $\varepsilon_1 + \Delta E$ of the second single particle state which can then be filled. If the system is in state $(0,1)$, a second electron may enter the $i = 1$ level, as $U < \Delta E$. In contrast, the level $i = 2$ is not accessible from the state $(1,0)$ as long as $\eta V < \varepsilon_1 + \Delta E + U$. This explains the asymmetry between the occupation probabilities $P_{(1,0)}$ and $P_{(0,1)}$. The height of this second plateau depends on the ratio of the tunneling rates: $\propto (1+\gamma)^{-1}$ with $\gamma := \Gamma_c/\Gamma_e$.

At the second plateau in the CVC the Fano factor differs from the case of $U = 0$, where only Pauli's exclusion principle plays a role. The Coulomb interaction prevents double occupancy and therefore it can lead to additional negative correlations in the tunneling current. For the considered case, the state $(1,1)$ can be occupied from the state $(0,1)$ by adding an electron in the level $i = 1$ because $U < \Delta E$. The transition from $(0,1)$ to $(1,1)$ is energetically not possible, i.e. one current channel is blocked by the Coulomb interaction. This is sketched in the blue box of Fig. 4.6b).

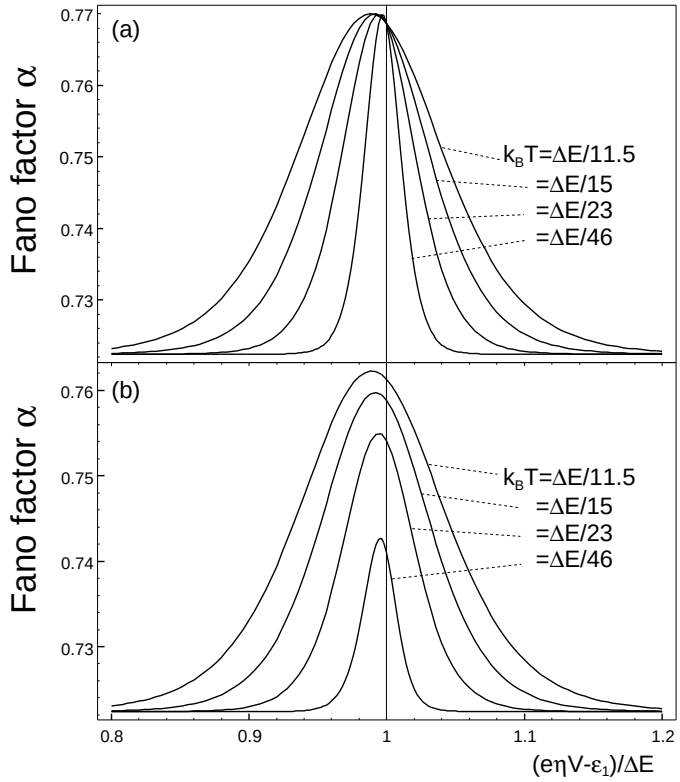

Figure 4.7.: Temperature dependence of the Fano factor vs. bias voltage V for γ =5. a) $U = 0$. b) $U = \Delta E/46$. Taken from [KIE03b].

The dependence on the ratio of tunneling rates γ in the range of V, given by $\Delta E < e\eta V - \varepsilon_1 < \Delta E + U$, corresponding to the second plateau in Fig. 4.3, is shown by the blue curve in Fig. 4.6a. In contrast to the noninteracting regime the minimum is now at $\gamma = 2$ so that the Fano factor becomes asymmetric with respect to an interchange of Γ_e and Γ_c. This clearly demonstrates the influence of the Coulomb interaction on the current direction. An analytical expression for the Fano factor in this regime was recently obtained in [THI03] and gives $\alpha = 5/9$ at the minimum in Fig. 4.6:

$$\alpha = \frac{\Gamma_e^3 + \Gamma_c^3 + 3\Gamma_e^2\Gamma_c}{(\Gamma_e + \Gamma_c)^3} \tag{4.2.3}$$

In the experiment of Ref. [NAU02] the question arises whether the QD states which are contributing to transport are Coulomb interacting. One way of determining this question would be the analysis of the Fano factor dependence upon the tunneling rate ratio γ as shown in Fig. 4.6a. However, in the experimental setup of Ref. [NAU02] these rates are determined by the growth procedure. Therefore, they cannot be varied in the same sample.

Instead, we propose a method on how to obtain the information about Coulomb correlations via the temperature dependence of the Fano factor. In Fig. 4.7 the Fano factor α vs. bias voltage V for different temperatures T in the bias range of the second current step of Fig. 4.3 is plotted. For noninteracting QD states (Fig. 4.7a) the Fano factor peak gets broader and experiences a slight shift to lower bias voltages for increasing temperature. A qualitatively different picture results for interacting QD states in Fig. 4.7b even for small Coulomb energies [6] ($U = \Delta E/46$): with increasing temperature the peak increases and also shifts to lower voltages. Hence, a unique fingerprint of Coulomb interaction of QD states even for very small U shows up in the temperature dependence of the Fano factor peaks. As temperature can be easily varied in experiment, the role of Coulomb interaction can be determined in this manner.

4.2.1.3. $U > \Delta E$

For $U > \Delta E$ a fourth step arises in the current vs. bias voltage characteristic in Fig. 4.5a). Now, the second current plateau corresponds to a different state as in the previous section. Due to $U > \Delta E$ only the two single particle states can be filled with the same probability (compare Fig. 4.5c) and the occupancy of the doubly-occupied state is forbidden (red box in Fig. 4.6b) so that a Coulomb correlated state emerges. The respective Fano factor dependence upon γ is (as also discussed in Ref. [NAZ96])

$$\alpha = 1 - \frac{2\tilde{\Gamma}_e\Gamma_c}{(\tilde{\Gamma}_e + \Gamma_c)^2} \quad \text{with} \quad \tilde{\Gamma}_e = 2\Gamma_e \tag{4.2.4}$$

and is shown by the red curve in Fig. 4.6. The effect of Coulomb correlation on the Fano factor consists of substituting Γ_e by $2\Gamma_e$ in Eq. (4.2.1) since the two single particle states are independently available [GLA88c] and leads to a shift of the minimum of the full curve in Fig. 4.6 by $\gamma = 2$. For γ =1 the Fano factor is α =5/9. Note, that tunneling through such a correlated state was found experimentally (Fig. 2.8).

Related literature: In [THI03] the authors start with an Anderson Hamiltonian (5.1.21) and apply a diagrammatic technique [KOE98] to obtain the current and the SPD in first-order perturbation in the contact couplings. It turns out that their results fully agree with ours. I.e. our method of simply setting-up a ME for the occupation probabilities of the Fock states is well-founded by a microscopic con-

[6] A spatial separation of 100 nm leads to U =1meV (This corresponds to $U = k_BT$ with T =10 K). A distance of 1 μm gives 0.1 meV (T =1K). Screening of the nearby highly-doped contacts can reduce these values significantly as shown in Appendix A. This can give fairly small interaction strengths even for QDs which are nearest neighbours.

sideration. In Refs. [EGU94, THI04] the additional influence of inelastic scattering on the noise is considered.

4.2.2. Super-Poissonian noise

So far we have only addressed negative correlations in the tunneling current due to Pauli's exclusion principle and Coulomb interaction. Another fascinating phenomenon in electronic tunneling is the effect of positive correlations which is accompanied by bunching of tunneling events [BUE03]. In Ref. [IAN98] it was experimentally shown for the first time that in the bias regime of negative differential conductance of a double-barrier resonant tunneling diode the respective noise becomes super-Poissonian[7]. In contrast, superlattices which also provide negative differential conductance do not exhibit super-Poissonian noise [SON03]. Therein the authors conclude that charge accumulation rather than a system instability is responsible for the noise enhancement. We can also show that the Coulomb interaction is crucial for the observation of super-Poissonian noise in tunneling through QDs. In the following we discuss in a simple and generic picture the emergence of super-Poissonian noise caused by Coulomb blocking.

4.2.2.1. Parallel quantum dots

The content of this section is published in [KIE04]. We consider the case where both energies of the single particle states of the QD system (Fig. 3.1) are equal: $\varepsilon_1 = \varepsilon_2$, the tunneling rates to the emitter are equal: $\Gamma_e^{(1)} = \Gamma_e^{(2)} \equiv \Gamma_e$, and a bias voltage V is applied such that both single particle states $(1,0)$ and $(0,1)$ can be occupied but the occupancy of the doubly-occupied state $(1,1)$ is energetically forbidden (red box in Fig. 4.6b)[8]. Then the zero-frequency Fano factor is derived analytically to be

$$\alpha(0) = 1 + \frac{2\left[\gamma_1^2 + \gamma_2^2 - \gamma_1\gamma_2(2 + \gamma_1 + \gamma_2)\right]}{\left(\gamma_1 + \gamma_2 + \gamma_1\gamma_2\right)^2} \tag{4.2.5}$$

with the ratios of collector and emitter tunneling rates $\gamma_i \equiv \Gamma_c^{(i)}/\Gamma_e$ (i = 1,2). The dependence of the Fano factor on γ_1 and γ_2 is depicted in Fig. 4.8. The Fano factor is symmetric with respect to an interchange of γ_1 and γ_2. Two different regions corresponding to $\alpha \leq 1$ and $\alpha > 1$ are labeled by N and P, respectively. The region N indicates negative correlations in the tunneling current for $\gamma_i \geq 1$ (i = 1,2). In this regime, mutual Coulomb blocking of the single particle states $(1,0)$ and $(0,1)$ is negligible since the levels are mostly empty in time average due to the stronger collector coupling. If either one ratio or both ratios become smaller than unity the

[7] Applying a magnetic field can also cause super-Poissonian noise in double barrier resonant tunneling diodes [KUZ98].

[8] This can be accompanied with NDC as considered in Sec. 3.2 and [KIE03b]

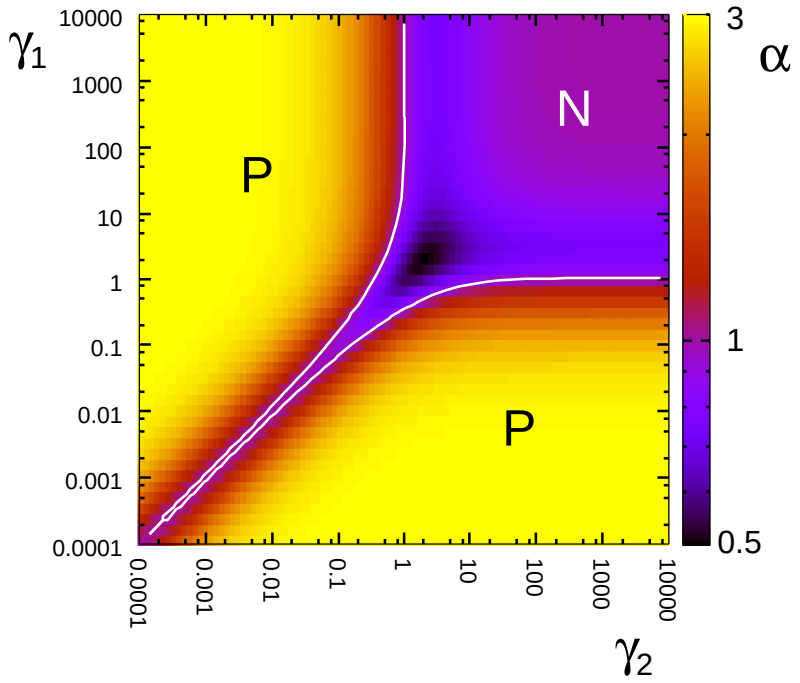

Figure 4.8.: Fano factor $\alpha(0)$ vs. $\gamma_1 = \Gamma_c^{(1)}/\Gamma_e$ and $\gamma_2 \equiv \Gamma_c^{(2)}/\Gamma_e$ (white lines correspond to $\alpha(0) = 1$ and confine the regions P and N). Taken from [KIE04].

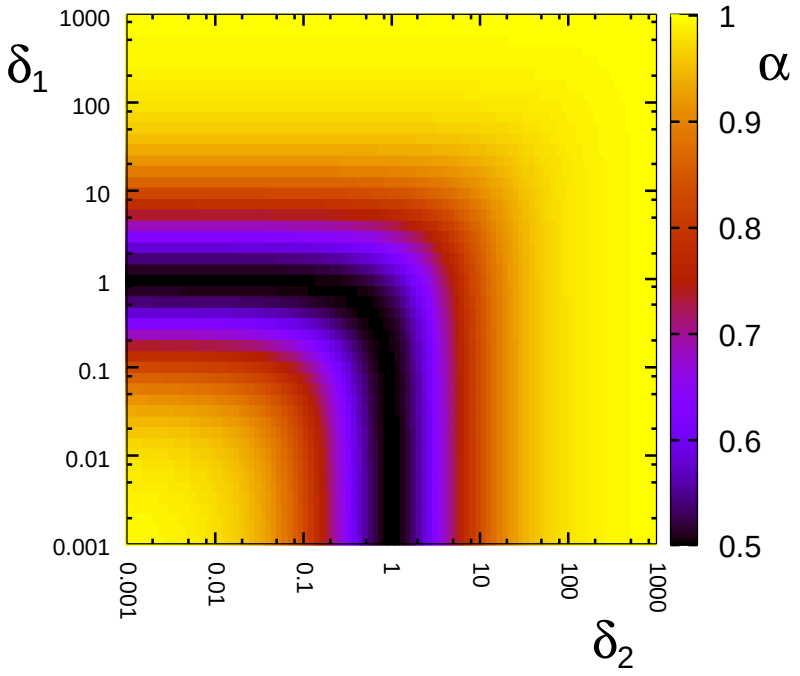

Figure 4.9.: Fano factor $\alpha(0)$ vs. $\delta_1 = \Gamma_e^{(1)}/\Gamma_c$ and $\delta_2 \equiv \Gamma_e^{(2)}/\Gamma_c$

tunneling is positively correlated (region P in Fig. 4.8) except for $\gamma_1 \simeq \gamma_2$ where α approaches unity. Hence, the conditions for positive correlations are: $\gamma_1 < 1$ or $\gamma_2 < 1$, and $\gamma_1 \neq \gamma_2$. For the inverse ratios $\delta_i \equiv \Gamma_e^{(i)}/\Gamma_c$ ($\Gamma_c = \Gamma_c^{(1)} = \Gamma_c^{(2)}$) the Fano factor is shown in Fig. 4.9. As can be seen the Fano factor is always below unity.

To illustrate the effect of positive correlations we consider a realization of time-dependent currents $I_1(t)$ and $I_2(t)$ through the levels 1 and 2, respectively, in Fig. 4.10b. There, it is assumed that $\gamma_1 \ll \gamma_2 = 1$. If an electron jumps from the emitter into level 1 (black peak) this level becomes occupied. Until the level becomes empty by tunneling of the electron out in the collector (grey peak) no electrons can jump in level 2 (Coulomb blocking). Only if level 1 is empty, a current I_2 is flowing. Hence, a bunching of tunneling events in current $I_2(t)$ occurs.

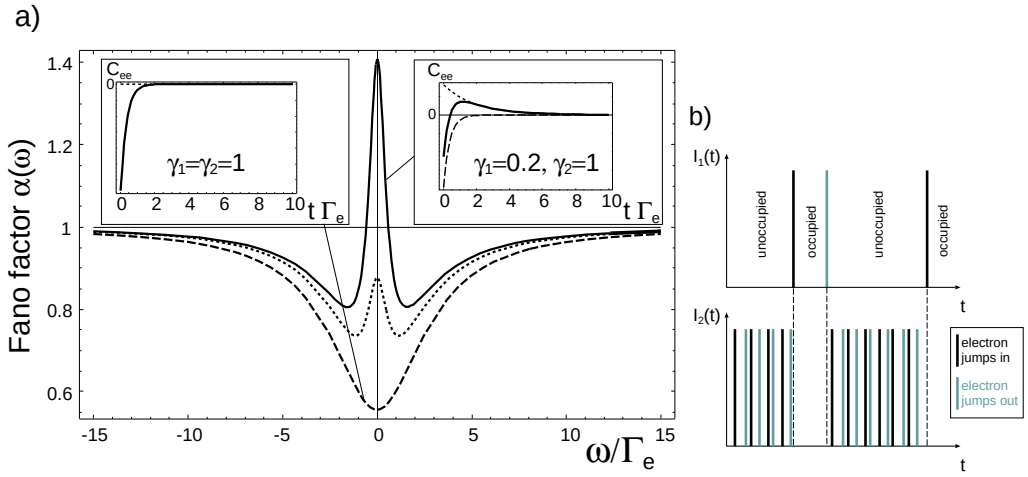

Figure 4.10.: a) Fano factor α vs. frequency ω for $\gamma_1 = 1$ and $\gamma_2 = 1$ (dashed curve), $\gamma_1 = 0.4$ (dotted curve), and $\gamma_1 = 0.2$ (full curve). Insets: current-current correlation functions at the emitter barrier C_{ee} vs. time t (full curves); dashed curve: negative part of C_{ee}, dotted curve: positive part of C_{ee}. b) Schematic realisations of current I_i vs. time t through level $i = 1$ (upper plot) and $i = 2$ (lower plot) for $\gamma_1 \ll \gamma_2 = 1$. Taken from [KIE04].

In Fig. 4.10 the frequency-dependent Fano factor $\alpha(\omega)$ and in the insets of Fig. 4.10 the current-current correlation function $C_{ee}(t)$ at the emitter barrier are shown. The dashed curve $\alpha(\omega)$ represents the case $\gamma_1 = \gamma_2 = 1$. It exhibits a minimum at $\omega = 0$ and approaches unity for $\omega \to \pm\infty$. The corresponding correlation function in the left inset is negative for all times, i.e. only negative correlations are present (region N in Fig. 4.8). By lowering γ_1 below one a maximum at $\omega = 0$ and two minima symmetric to $\omega = 0$ arise (dotted curve: $\gamma_1 = 0.4$, $\gamma_2 = 1$; full curve: $\gamma_1 = 0.2$, $\gamma_2 = 1$). The correlation function (full curve in the right inset of Fig. 4.10) belonging to the full curve $\alpha(\omega)$ ($\alpha > 1$, P-region in Fig. 4.8) now has two contributions with different signs: positive (dotted curve) and negative (dashed curve).

The positive part of the correlation function is due to the bunching of tunneling events as discussed with respect to Fig. 4.10b and the negative part is due to anti-bunching caused by Pauli's exclusion principle which is still present in the bunches of tunneling through the current carrying level. Therefore, the frequency-dependent Fano factor in Fig. 4.8 consists of a sum of two Lorentzians with positive and negative sign and different FWHM corresponding to the two time scales related to the respective collector tunneling rates.

Note that there are several recent publications which address super-Poissonian noise in tunneling through QDs: theory of coupled metallic QDs [GAT02], experiment in a single electron transistor setup[SAF03], theory for three ferromagnetic terminal QD setup [COT04], and Ref. [THI04] which is closely related to the present considerations and the additional study of relaxation effects.

Before we will continue with super-Poissonian noise in tunnel-coupled QDs in the next section the following analogy it is worth to emphasize: As already mentioned there is the observation of super-Poissonian noise in the double-barrier resonant tunneling diode [IAN98]. At first glance there might be no connection to the super-Poissonian noise behavior in QDs as shown here. But, by closer inspection we can identify some similarities: first of all in both cases the positive correlations occur in the NDC region of the CVC. Although the underlying mechanism for the occurrence of NDC is different, the bunching effect in both systems is caused by Coulomb repulsion. For the QD system it was elaborately explained above. For the tunneling diode it will be shown in a rather heuristic picture as follows: If the lowest sub-band energy of the 2DEG in the quantum well passes the emitter conduction band edge at a certain bias voltage the current starts to decrease by further increasing the bias - NDC occurs. The potential in the well region depends on the number of electrons there due to the Coulomb repulsion, i.e. the more electrons enter the well states the higher the potential. Consequently, there can be two different currents in the NDC region depending on the charging state of the well: (i) low current for the uncharged well and (ii) high current for charged well. This leads to the well-known bistability behavior. Bunching of tunneling events as the necessary condition for the occurrence of super-Poissonian noise arise whenever the device is in the high current state which is interrupted by random switching[9] to the low current state.

4.2.2.2. Quantum dot stack

The results of this section will be published in [KIE05c]. Inspired by recent experiments [BAR04] we want to discuss here under which circumstances it is possible to observe positive correlations in the tunneling current through vertically coupled QDs - a system which we already considered in detail in Sec. 3.3 with respect to

[9] Random telegraph noise [GAR02]

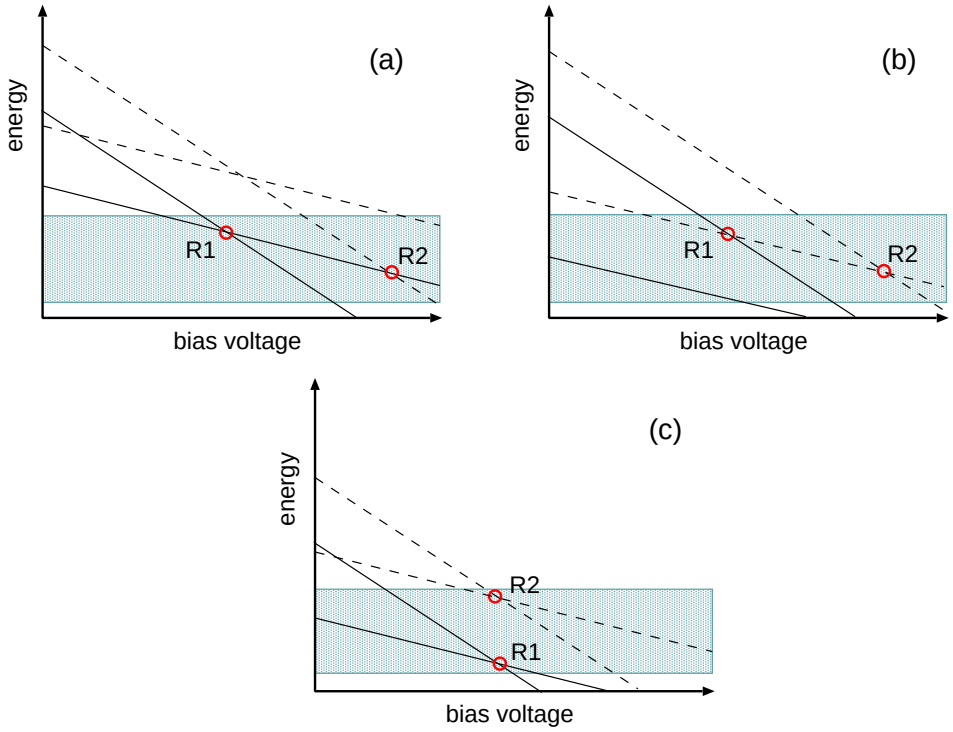

Figure 4.11.: Sketches of possible resonances which lead to a current peak (see text). $U_1 = U_2$.

the average current. As introduced there, the model is based on the ME where we treat the coupling between the QDs with Fermi's golden rule. Even though in this framework any effects due to coherence were neglected the average current for non-interacting electrons provides full agreement with the coherent result. Additionally in this section the SPD is calculated along the lines of Sec. 4.1.1.

We use the notations introduced in Sec. 3.3: The emitter/collector contact is treated in local equilibrium with temperature T and chemical potentials $\mu_{e/c}$, respectively. The difference in the chemical potentials is the applied bias voltage $eV = \mu_e - \mu_c$. We assume that both QD1 and QD2 contain one spin-degenerate state, e.g. the ground state. The respective energy levels are bias voltage dependent: $\varepsilon_{1/2}(V) = \varepsilon_{1/2}(0) + e\eta_{1/2}V$ with constant leverage factors $\eta_{1/2}$. Electrons can enter QD1/QD2 from the emitter/collector contact with rate $\Gamma_{e/c}$, respectively. The Coulomb interaction energy for two electrons in QD1/QD2 is $U_{1/2}$, respectively. Electrons in different QDs repel each other with the energy U_{inter}. The rate for tunneling between the QDs is $\Gamma_{\text{inter}} = 4|\Omega|^2/(\Gamma_e + \Gamma_c)$ with the tunnel matrix element Ω.

Let us first sketch different experimentally relevant scenarios for resonances which can lead to a peak in CVC. We neglect U_{inter} for simplicity.

Three important situations are depicted in Fig. 4.11a-c. The solid lines correspond to the single particle level in QD1 (small slope) and QD2 (large slope). The dashed lines are the addition energies due to double-occupancy (compare Fig. 3.5). Important for the emergence of a current peak is that the intersection point (circle) of a line of QD1 and a line of QD2 lies in the energy region where the emitter can provide electrons (shaded regions) while the collector states are empty. In this range empty collector states exist so that electrons can leave the QD system. We consider the following cases:

a) R1: The single particle levels intersect. The respective CVC and the Fano factor are shown in Fig. 4.12. Here, the Fano factor indicates sub-Poissonian noise around the resonance and Poissonian noise far from the resonance. To ensure that an electron can travel unhindered through the structure the contributing states have to be empty. This induces negative correlations by Pauli's principle. Furthermore, since double-occupancy of each QD is impossible there is an additional source of negative correlations due to Coulomb blockade. This effect was pointed out by Elattari and Gurvitz in [ELA02]. Interestingly, for an asymmetric coupling to the collector and emitter there is a local maximum of the Fano factor vs. bias voltage at the current peak maximum which is not present for symmetric coupling. This behavior can also be obtained in a noninteracting coherent description which is considered in Sec. 5.4.

   R2: This resonance is not active for tunneling since the single particle state in QD2 is below the band edge in the emitter and therefore the two-particle state in QD2 cannot be occupied.

b) R1: Resonance of two-particle state in QD1 and the single particle state in QD2. Here, a quite similar mechanism to a) takes place. Since the single particle state in QD1 can be occupied from the emitter electrons can tunnel into the doubly-occupied state of QD1 and subsequently into the single particle state in QD2. The tunneling events are negatively correlated since the occupation of QD2 is ruled by Pauli's principle. Additional negative correlations stem from the forbidden double-occupancy in QD2.

   R2: not active for the same reasons as in a).

c) R1: Resonance of single particle levels. R2: Resonance of two-particle levels.

   $U_1 \neq U_2$: current peaks at different bias voltages occur with noise behaviors as already discussed in a) and b).

   $U_1 \approx U_2$: (as depicted in Fig. 4.11c) The CVC and the Fano factor for such a regime is shown in Fig. 4.13. The parameters were estimated with respect to the experiment [BAR04]. Two transport channels contribute in one current peak: R1 and R2 (Fig. 4.13a). Since R2 lies slightly below μ_e the current peak broadens with increasing temperature. The Fano factor shows all quantitative

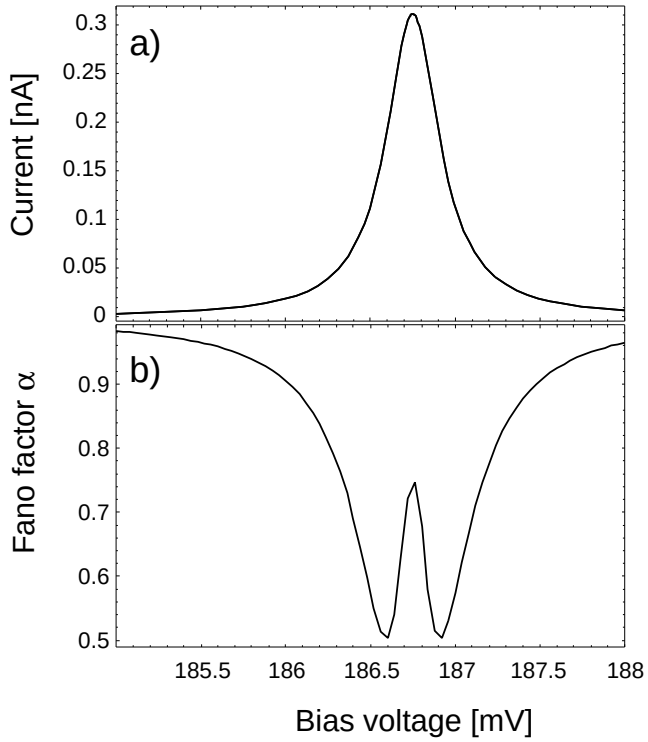

Figure 4.12.: a) Current vs. bias voltage. b) Fano factor vs. bias voltage. Parameters: Γ_e =40μeV, Γ_c =1.5μeV ,Ω =10μeV, $\varepsilon_1(0)$ =48 meV,$\varepsilon_2(0)$ =104.025 meV, η_1 =0.25, η_2 =0.55, $U_1 = U_2 = U_{\text{inter}}$ =0, μ_e =11.7 meV, T=1.4 K.

features of the experimental data: super-Poissonian noise at the edges of the current peak, Poissonian noise at the current peak maximum, and the observed temperature dependence.

How can one understand this behavior? For this purpose we look at the time evolution of the occupations in QD1 and QD2 and the current given by the jumps of electrons into the collector. To obtain a realisation for the stochastic process we apply a Monte-Carlo simulation with the same parameters leading to the ME results in Fig. 4.13 (for details of the Monte-Carlo simulation see [KIE02b]). Sections of the realisation are shown in Fig. 4.14a) for a bias voltage V =186.75 mV (at the voltage of current peak maximum in Fig. 4.13a) and b) V =186.9 mV (at the voltage of right Fano factor maximum in Fig. 4.13b). The upper graphs correspond to the occupation in QD1, the middle graph shows the occupation of QD2, and the lower graph contains the jumps of electrons into the collector. For both voltages it can be seen that QD1 is mostly occupied with one electron. Therefore QD1 can easily be occupied with two electrons. Crucial for the occurrence of a tunneling current is the occupation of the single particle state in QD2. This aspect yields

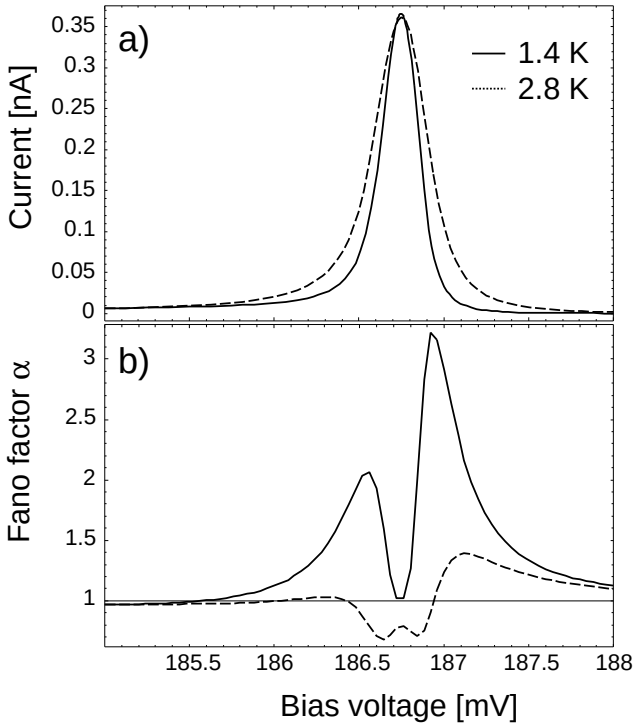

Figure 4.13.: a) Calculated current vs. bias voltage. b) Fano factor vs. bias voltage. Parameters: Γ_e =40μeV, Γ_c =1μeV ,Ω =15μeV, $\varepsilon_1(0)$ =48 meV,$\varepsilon_2(0)$ =104.025 meV, η_1 =0.25, η_2 =0.55, $U_1 = U_2$ =10 meV, U_{inter} =0, μ_e =11.7 meV, T=1.4 K (solid line), T=2.8K (dashed line).

the main difference in the processes at both voltages. The probability that one electron can enter the single particle level in QD2 is highest when the levels are exactly aligned (V =186.75 mV) - this becomes apparent in the time series of the QD2 occupation and consequently in the respective current: the tunneling events are statistically distributed in time and the noise is Poissonian. In contrast, for a slight misalignment of the levels the probability for entering QD2 with one electron decreases. Such events are more rare now. But, whenever one electron enters QD2 the R2 channel is opened which results in a bunching of tunneling events (shaded regions in Fig. 4.13b). In order to obtain a Fano factor larger than unity it is necessary that the average time between bunches is larger than the average time between tunneling events within such bunch [KIE04]. This is due to the unavoidable presence of Pauli's principle.

Far from the resonance the occupation of the single particle state in QD2 as well as the occupation of the two-particle state in QD2 are very unlikely. Technically, the electrons tunnel via the tails of the Lorentzian which is contained in the Fermi's golden rule treatment. Therefore the Fano factor becomes unity far from the resonance.

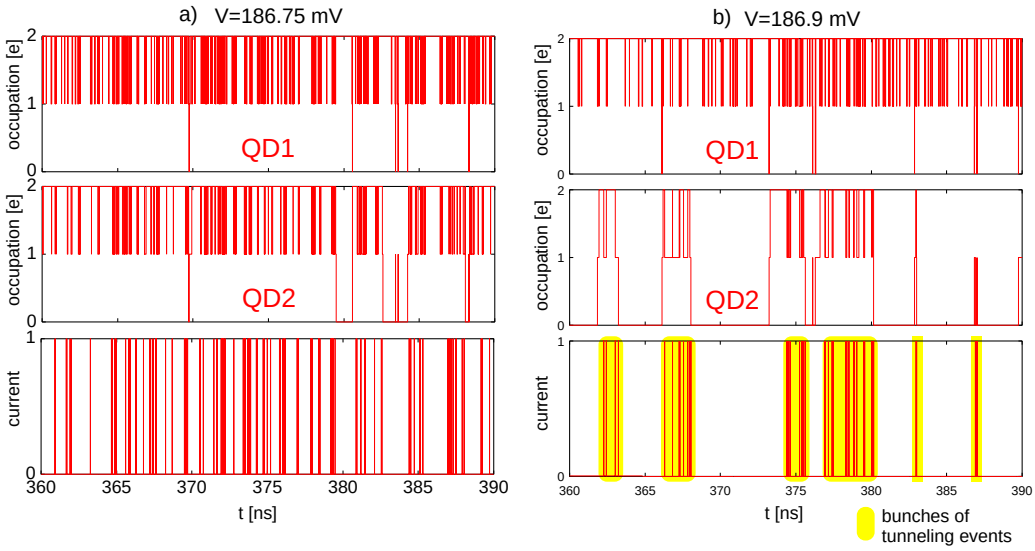

Figure 4.14.: Monte-Carlo simulation of the occupations in QD1 and QD2 and the electron jumps in the collector (current). a) bias voltage V =186.75 mV, b) V =186.9 mV. Parameters are the same as in Fig. 4.13

The temperature dependence of the Fano factor can be understood as follows: As already mentioned the R2 resonance lies slightly below μ_e. For increasing temperatures the occupation of the emitter at the energy of R2 decreases. I.e. the contribution of the R2 channel to the tunneling current decreases. Hence, the electrons are primarily transmitted through the R1 channel. This corresponds to the regime a), where the noise was shown to be sub-Poissonian (Fig. 4.12b). Thus, negative correlations rise and the Fano factor reduces.

So far, the Coulomb repulsion U_{inter} between electrons in different QDs was not taken into account. We observe that for $U_{\text{inter}} > 0$ the discussed effects in Fig. 4.13 become less pronounced already for relatively small U_{inter}.

Several ad-hoc assumptions had to be made whose validity concerning an experimental realisation has to be checked:

1. $\varepsilon_2(0) - \varepsilon_1(0) \approx$50 meV and $U_1 = U_2$:

   The large difference of the single particle levels in QD1 and QD2 under flat-band condition could be due to different QD sizes assuming both states are the ground states. Then the charging energies would be expected to be different. As known from the growth of selforganized QDs the composition of QDs, i.e. the amount of matrix material (AlAs) in the QD (InAs), can be quite different even if individual QDs have the same extension. Then the binding energies would be different but the charging energy remains the same.

Another possibility may be that the level in QD2 is an excited state, e.g. with p-symmetry. Then the QDs could have the same size. But, tunneling between such states is very unlikely due to selection rules which forbid such transition [SPR03].

2. U_i =10 meV ($i = 1, 2$):

   In our model we presume that the single particle resonance and the two-particle resonance contribute in the same current peak. Therefore the charging energies have to be smaller than the chemical potential in the emitter (typical values are around 10 meV). The Coulomb charging for ground states of InAs QDs in GaAs matrix is about 20 meV (Tab. I in [KIE03]). InAs QDs in AlAs are typically smaller [HAP02] so that the charging is expected to be even larger. But, the highly doped contacts are close to the layer of QDs (few nm) so that screening effects can strongly reduce the Coulomb matrix elements (see Appendix A).

To conclude we have proposed a mechanism to observe super-Poissonian noise in tunneling through two coupled QDs. The crucial ingredient is the Coulomb interaction of electrons in individual QDs within one QD stack, i.e. the tunneling of electrons through the resonance of single particle states and the two-particle states at the same bias voltage. We have discussed several aspects of the experimental realization. Unfortunately the experimental data [BAR04] are not reliable enough at the moment to serve as a basis for further investigations.

5. Coherent Tunneling

In this chapter we will investigate the nonlinear electronic transport through a single QD and through tunnel-coupled QDs with the emphasis on quantum effects and scattering. The starting point is defined by the Hamiltonian of the whole system including the contact regions (electron reservoirs) and the interacting QD system which are coupled to each other so that a complicated many-particle problem can arise. In order to derive the stationary current and the zero-frequency SPD (shot noise) as the essential observables throughout this thesis we will use the technique of nonequilibrium Green's functions (NEGF). The advantage of introducing Green's functions is the determination of expectation values or correlation functions of observables without the explicit knowledge of the partition function. There are two different but equivalent formulations for the equation-of-motion of the NEGF: the Kadanoff-Baym method [KAD62] and the Keldysh method [KEL65]. In the following section we will briefly review the latter and the reader is referred to the textbooks [HAU96, MAH00] for a detailed study. It further contains the derivation of expressions for the stationary current along the lines of [JAU94, HAU96] and for the zero-frequency SPD [SOU04, SOU04a].

The main focus of our considerations is the impact of the Coulomb interaction on the current and noise behavior. For that purpose we utilize the Anderson model [AND61] which describes a single spin degenerate state with Coulomb repulsion coupled to electron reservoirs: in Sec. 5.2 we will consider the limits of this model which are exactly solvable: a noninteracting QD and an isolated interacting QD. Beyond that, we discuss the lowest-order approximation of the Anderson model, the Hartree-Fock approximation. Two different schemes will be examined regarding their applicability for the description of nonlinear transport.

In the end of this chapter, the tunneling through a noninteracting QD stack with respect to its shot noise behavior is considered which we directly compare with the noise obtained in a sequential tunneling picture (Chap. 4).

5.1. Theoretical framework: Non-equilibrium Green's functions

Before we define the Green's functions required in the following sections terms like contour-ordering etc. have to be clarified. For that purpose let us consider the following Hamiltonian in a general form

$$H = H_0 + V \tag{5.1.1}$$

where H_0 describes the unperturbed part of the system and V can include any kind of interaction (electron-electron, electron-phonon, electron-impurity etc.). It is assumed that H can be explicitly time-dependent, e.g. by time-varying potentials.

5.1.1. General treatment and definitions

The consideration of non-equilibrium processes in many-particle physics brings the following expectation value into the theory

$$\begin{aligned} \langle a_\alpha^\dagger(t_2) a_\beta(t_1)\rangle &= \mathrm{Tr}\Big\{\rho(t_0) a_{H\alpha}^\dagger(t_2) a_{H\beta}(t_1)\Big\} \\ &= \mathrm{Tr}\Big\{\rho(t_0) U_D^{-1}(t_2,t_0) a_{D\alpha}^\dagger(t_2) U_D(t_2,t_1) a_{D\beta}(t_1) U_D(t_1,t_0)\Big\} \end{aligned} \tag{5.1.2}$$

where the annihilation and creation operators $a_{H\alpha}(t)$ and $a_{H\alpha}^\dagger(t)$, respectively, of the single particle state α are treated at different times $t_{1/2}$. On the right-hand side in the first line of (5.1.2) the expectation value is expressed with the density operator $\rho(t_0)$. By setting $t_0 \to -\infty$ the density operator $\rho(-\infty)$ is given by $|\Psi_0\rangle\langle\Psi_0|$ where $|\Psi_0\rangle$ is the ground state of the unperturbed Hamiltonian[1] H_0. The time dependence of $a_{H\alpha}^\dagger(t_2)$ and $a_{H\beta}(t_1)$ is defined in the Heisenberg picture. In the last line of (5.1.2) these Heisenberg operators are replaced by the respective operators in the Dirac picture[2]. The time evolution operator in the Dirac picture is

$$U_D(t,t') = U_0^{-1}(t,t_0) U_S(t,t') U_0(t',t_0) \tag{5.1.3}$$

where $U_0(t,t_0) = \exp\left[-\frac{i}{\hbar} H_0(t-t_0)\right]$ describes the free evolution. The time evolution in the Schrödinger picture is

$$\begin{aligned} i\hbar|\dot{\Psi}_S(t)\rangle = H|\Psi_S(t)\rangle \quad \Rightarrow \quad |\Psi_S(t)\rangle = U_S(t,t_0)|\Psi_S(t_0)\rangle \\ \text{with} \quad U_S(t,t_0) = \exp\left[-\frac{i}{\hbar} H(t-t_0)\right] \end{aligned} \tag{5.1.4}$$

and $U_S(t,t_0)$ can be expanded in a Born series[3]:

[1] It is usually bilinear in the operators, but not always.
[2] $A_H(t) = U_D^{-1}(t,t_0) A_D(t) U_D(t,t_0)$
[3] The index t on H_t denotes the explicit time-dependence.

$$\begin{aligned} U_S(t,t_0) &= 1+\frac{1}{i\hbar}\int_{t_0}^{t} dt_1 H_{t_1} + \frac{1}{(i\hbar)^2}\int_{t_0}^{t} dt_1 \int_{t_1}^{t} dt_2 H_{t_2} H_{t_1} + \\ &\quad + \frac{1}{(i\hbar)^3}\int_{t_0}^{t} dt_1 \int_{t_1}^{t} dt_2 \int_{t_2}^{t} dt_3 H_{t_3} H_{t_2} H_{t_1} + \cdots \\ &= 1+\frac{-i}{\hbar}\int_{t_0}^{t} dt_1 H_{t_1} + \frac{(-i)^2}{2\hbar^2}\hat{T}\int_{t_0}^{t} dt_1 \int_{t_0}^{t} dt_2 H_{t_2} H_{t_1} + \\ &\quad + \frac{(-i)^3}{3!(\hbar)^3}\hat{T}\int_{t_0}^{t} dt_1 \int_{t_0}^{t} dt_2 \int_{t_0}^{t} dt_3 H_{t_3} H_{t_2} H_{t_1} + \cdots \\ &= \hat{T}\exp\left(-\frac{i}{\hbar}\int_{t_0}^{t} dt' H_{t'}\right) \end{aligned} \tag{5.1.5}$$

with the time-ordering operator $\hat{T}$ (operation rules: (i) "late goes left", (ii) adds a minus sign if two fermionic operators change the sequence, and (iii) for equal times the annihilation operator goes to the right).

The equation of motion for the Dirac time evolution operator (5.1.3) is

$$\frac{d}{dt}U_D(t,t_2) = -\frac{i}{\hbar}V_D(t)U_D(t,t_2) \tag{5.1.6}$$

and one obtains

$$U_D(t_1,t_2) = \hat{T}\exp\left(-\frac{i}{\hbar}\int_{t_2}^{t_1} dt' V_D(t')\right) \quad \text{for} \quad t_1 > t_2 \tag{5.1.7}$$

In Eq. (5.1.2)the inverse of the Dirac time evolution operator $U_D^{-1}(t_2,t_0)$ appears, which contains the anti-time ordering operator:

$$U_D^{-1}(t_2,t_0) = \hat{T}^{\text{anti}}\exp\left(-\frac{i}{\hbar}\int_{t_2}^{t_0} dt' V_D(t')\right) \tag{5.1.8}$$

Now one defines the contour-ordered operator on the contour C (see Fig. 5.1) [KEL65, HAU96]

$$\hat{T}_C \equiv \begin{cases} \hat{T} & \text{for } \mathrm{Im}(\tau) > 0 \\ \hat{T}^{\text{anti}} & \text{for } \mathrm{Im}(\tau) < 0 \end{cases} \tag{5.1.9}$$

with $\tau \in \mathbb{C}$. This is necessary since in the non-equilibrium situation the state of the system for $t \to \infty$ is not known. The interactions can generally drive the system into a different state than the initial state in contrast to the equilibrium theory. Technically, one only knows the S-matrix for $t \to -\infty$. Therefore, the state is first evolved forward and then backwards in time. In order to distinguish between

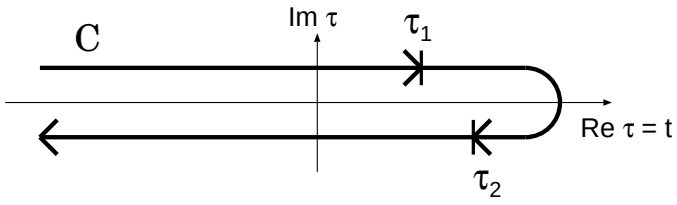

Figure 5.1.: Contour ordering

these two branches one introduces the contour where the sign of the imaginary part labels the branch.

Hence, the expectation value in (5.1.2) can be written as

$$\begin{aligned}\langle a_\alpha^\dagger(\tau_2)a_\beta(\tau_1)\rangle &= \langle\Psi_0|\hat{T}_C a_{H\alpha}^\dagger(\tau_2)a_{H\beta}(\tau_1)|\Psi_0\rangle \\ &= \langle\Psi_0|\hat{T}_C e^{[-i/\hbar\int_C d\tau V_D(\tau)]}a_{D\alpha}^\dagger(\tau_2)a_{D\beta}(\tau_1)|\Psi_0\rangle \end{aligned} \tag{5.1.10}$$

Now we can define the contour-ordered Green's function which is the central quantity of the non-equilibrium formalism (analog to the time-ordered Green's functions in the equilibrium theory)

$$G_{\alpha\beta}^C(\tau_\alpha,\tau_\beta) \equiv -i\langle\hat{T}_C a_{H\alpha}^\dagger(\tau_\alpha)a_{H\beta}(\tau_\beta)\rangle \tag{5.1.11}$$

With the second line in (5.1.10) an expansion in the interaction term V of (5.1.1) becomes possible. In literature (e.g. in [MAH00]) the time evolution operator in the Dirac picture given by the contour-ordered exponential in (5.1.10) is usually called S-matrix[4] and consequently, an S-matrix expansion can be carried out:

$$\begin{aligned}\langle S_C a_{D\alpha}^\dagger(\tau_\alpha)a_{D\beta}(\tau_\beta)\rangle &= \langle\hat{T}_C a_{D\alpha}^\dagger(\tau_\alpha)a_{D\beta}(\tau_\beta)\rangle + \\ &+\int d\tau_1\langle\hat{T}_C\frac{-i}{\hbar}V_D(\tau_1)a_{D\alpha}^\dagger(\tau_\beta)a_{D\beta}(\tau_\beta)\rangle + \\ &+\frac{1}{2}\int d\tau_1\int d\tau_2\langle\hat{T}_C\left(\frac{-i}{\hbar}\right)^2 V_D(\tau_1)V_D(\tau_2)a_{D\alpha}^\dagger(\tau_\beta)a_{D\beta}(\tau_\beta)\rangle + \cdots\end{aligned} \tag{5.1.12}$$

with $S_C \equiv \hat{T}_C \exp\left[-i/\hbar\int_C d\tau V_D(\tau)\right]$.

Depending on the special form of V_D expectation values of more than two operators are generated in (5.1.12). These can be factorized by using Wick's theorem [WIC50] provided that the Dirac operators have an exponential time dependence[5]. Utilizing diagrammatic techniques for the resulting perturbation expansion (5.1.12) and by clever regrouping of diagrams one can obtain the *Dyson equation*

[4]Note that in Chap. 6 and 7 we also deal with objects called S-matrices.

[5]This only holds for a H_0 which is bilinear in the creation/annihilation operators.

$$G^C_{\alpha\beta}(\tau_\alpha,\tau_\beta) = G^{C0}_{\alpha\beta}(\tau_\alpha,\tau_\beta) + \int_C\int_C d\tau_1 d\tau_2 \sum_{\rho\sigma} G^{C0}_{\alpha\rho}(\tau_\alpha,\tau_1)\Sigma^C_{\rho\sigma}(\tau_1,\tau_2)G^C_{\sigma\beta}(\tau_2,\tau_\beta) \tag{5.1.13}$$

with the self-energy functional $\Sigma^C_{\rho\sigma}(\tau_1,\tau_2)$ which contains the interactions and the free Green's function $G^{C0}_{\alpha\beta}(\tau_\alpha,\tau_\beta) \equiv -i\langle \hat{T}_C a^\dagger_{D\alpha} a_{D_\beta}\rangle$. Note, that it is not always possible to find a self-energy functional for the interaction under consideration, e.g. the Coulomb interaction.

In physical problems only real times should occur. Hence, one has to introduce real-time Green's functions. The following important functions are defined in the formalism

$$\begin{aligned} G^>_{\alpha\beta}(t_\alpha,t_\beta) \equiv G^C_{\alpha\beta}(t_\alpha - i0^+, t_\beta + i0^+) &= -i\langle a_{H\alpha}(t_\alpha) a^\dagger_{H\beta}(t_\beta)\rangle \\ G^<_{\alpha\beta}(t_\alpha,t_\beta) \equiv G^C_{\alpha\beta}(t_\alpha + i0^+, t_\beta - i0^+) &= i\langle a^\dagger_{H\beta}(t_\beta) a_{H\alpha}(t_\alpha)\rangle \end{aligned} \tag{5.1.14}$$

which gives for $\alpha = \beta$ the occupation of the states and for $\alpha \neq \beta$ the transition current from state α to β (for equal times).

$$\begin{aligned} G^{\rm ret}_{\alpha\beta}(t_\alpha,t_\beta) &\equiv \Theta(t_\alpha - t_\beta)\left[G^>_{\alpha\beta}(t_\alpha,t_\beta) - G^<_{\alpha\beta}(t_\alpha,t_\beta)\right] \\ &= -i\Theta(t_\alpha - t_\beta)\langle\{a_{H\alpha}(t_\alpha), a^\dagger_{H\beta}(t_\beta)\}\rangle \\ G^{\rm adv}_{\alpha\beta}(t_\alpha,t_\beta) &\equiv \Theta(t_\beta - t_\alpha)\left[G^<_{\alpha\beta}(t_\alpha,t_\beta) - G^>_{\alpha\beta}(t_\alpha,t_\beta)\right] \\ &= i\Theta(t_\beta - t_\alpha)\langle\{a_{H\alpha}(t_\alpha), a^\dagger_{H\beta}(t_\beta)\}\rangle \end{aligned} \tag{5.1.15}$$

where $\{\cdot,\cdot\}$ is the anti-commutator. The retarded and advanced Green's functions $G^{\rm ret}_{\alpha\beta}$ and $G^{\rm adv}_{\alpha\beta}$, respectively, in (5.1.15) describe the evolution of an excitation in state β at t_β forward and backward in time, respectively.

With the help of *Langreth*'s rules [LAN76a] (see below, Eq. (5.1.31)) the Dyson equation for the contour-ordered Green's function (5.1.13) can be transformed in Dyson equations for the real-time Green's functions (5.1.14),(5.1.15):

$$G^{\rm ret}_{\alpha\beta}(t_\alpha,t_\beta) = G^{{\rm ret},0}_{\alpha\beta}(t_\alpha,t_\beta) + \int\int dt_1\, dt_2 \sum_{\rho\sigma} G^{{\rm ret},0}_{\alpha\rho}(t_\alpha,t_1)\Sigma^{\rm ret}_{\rho\sigma}(t_1,t_2)G^{\rm ret}_{\sigma\beta}(t_2,t_\beta) \tag{5.1.16}$$

$$\begin{aligned} G^<_{\alpha\beta}(t_\alpha,t_\beta) = G^{<0}_{\alpha\beta}(t_\alpha,t_\beta) + \int\int dt_1\, dt_2 \sum_{\rho\sigma} \big[& G^{{\rm ret},0}_{\alpha\rho}(t_\alpha,t_1)\Sigma^{\rm ret}_{\rho\sigma}(t_1,t_2)G^<_{\sigma\beta}(t_2,t_\beta) \\ & + G^{{\rm ret},0}_{\alpha\rho}(t_\alpha,t_1)\Sigma^<_{\rho\sigma}(t_1,t_2)G^{\rm adv}_{\sigma\beta}(t_2,t_\beta) \\ & + G^{<0}_{\alpha\rho}(t_\alpha,t_1)\Sigma^{\rm adv}_{\rho\sigma}(t_1,t_2)G^{\rm adv}_{\sigma\beta}(t_2,t_\beta)\big] \end{aligned} \tag{5.1.17}$$

(analogously for $G^{>}$ and G^{adv}). Throughout this chapter we want to discuss stationary quantities. I.e. the defined functions in (5.1.14) and (5.1.15) only depend on time differences: $G(t_1, t_2) = G(t_1 - t_2)$. Then a Fourier transform can be carried out

$$\tilde{G}_{\alpha\beta}(\varepsilon) = \frac{1}{\hbar}\int dt \exp\left(\frac{i}{\hbar}\varepsilon t\right) G_{\alpha\beta}(t) \quad \text{with} \quad t \equiv t_1 - t_2 \tag{5.1.18}$$

so that an energy ε is obtained which is independent of all intrinsic energy scales (e.g. levels or level widths) and therefore it can be used to probe the DOS in the system. Fourier transforming Eq. (5.1.16) and bringing it in matrix notation yields

$$\mathbf{G}^{\mathrm{ret}}(\varepsilon) = \mathbf{G}^{\mathrm{ret},0}(\varepsilon) + \mathbf{G}^{\mathrm{ret},0}(\varepsilon)\mathbf{\Sigma}^{\mathrm{ret}}(\varepsilon)\mathbf{G}^{\mathrm{ret}}(\varepsilon) \tag{5.1.19}$$

(This form of Dyson's equation will be used in Sec. 5.3.2.)

The Dyson equation for the lesser Green's function (5.1.17) yields in the Keldysh formulation [KEL65, HAU96]

$$\mathbf{G}^{<}(\varepsilon) = \mathbf{G}^{\mathrm{ret}}(\varepsilon)\mathbf{\Sigma}^{<}(\varepsilon)\mathbf{G}^{\mathrm{adv}}(\varepsilon) \tag{5.1.20}$$

An alternative way for calculating the Green's functions is the equation-of-motion (EOM) technique where the time derivative of the time-ordered Green's functions are taken. This will be demonstrated explicitly in Sec. 5.2.

5.1.2. Transport observables

The aim is the modeling of tunneling through a QD system coupled to noninteracting electron reservoirs e/c (emitter/collector, respectively). Both will be treated in local equilibrium with temperature T, i.e. their occupation is ruled by the Fermi distributions f_e and f_c with the chemical potentials μ_e and μ_c, respectively. Different chemical potentials in the reservoirs induced by an applied bias voltage $eV = \mu_e - \mu_c$ can drive the QD system out of equilibrium. This is the regime we are interested in and where we want to calculate the observables: average current and spectral power density in the framework of NEGF introduced in the last section.

In the following we consider a single QD with two energy levels (e.g. two spin-states $\sigma \in \{\uparrow, \downarrow\}$). But it can easily be extended to a QD system with an arbitrary number of states.

The respective **Hamiltonian** reads

$$H = H_{\mathrm{QD}} + H_{\mathrm{R}} + H_{\mathrm{T}} \tag{5.1.21}$$

The Hamiltonian for the QD splits into a noninteracting part and a part which includes the Coulomb interaction with charging energy U:

$$\begin{aligned} H_{\mathrm{QD}} &= H^0_{\mathrm{QD}} + H^U_{\mathrm{QD}} \\ \text{with} \quad H^0_{\mathrm{QD}} &= \sum_\sigma \varepsilon_\sigma d^\dagger_\sigma d_\sigma \\ \text{and} \quad H^U_{\mathrm{QD}} &= U n_\uparrow n_\downarrow \end{aligned} \tag{5.1.22}$$

ε_σ is the energy level of the single-particle state σ in the QD. $d^\dagger_\sigma$ (d_σ) creates (annihilates) an electron in the QD state σ, and $n_\uparrow = d^\dagger_\uparrow d_\uparrow$, $n_\downarrow = d^\dagger_\downarrow d_\downarrow$ are occupation number operators.

The Hamiltonian for the reservoirs reads

$$H_{\mathrm{R}} = \sum_{k\sigma\eta} \varepsilon_{k\sigma\eta} c^\dagger_{k\sigma\eta} c_{k\sigma\eta} \tag{5.1.23}$$

$\varepsilon_{k\sigma\eta}$ is the single-particle energy of an electron in the emitter/collector reservoir $\eta = e, c$ in state $k\sigma$ with wavevector k and spin σ. $c^\dagger_{k\sigma\eta}$ ($c_{k\sigma\eta}$) is the respective creation (annihilation) operator.

The tunneling Hamiltonian in (5.1.21) can be written as

$$H_{\mathrm{T}} = \sum_{k\sigma\eta} (t_{k\sigma\eta} c^\dagger_{k\sigma\eta} d_\sigma + t^*_{k\sigma\eta} d^\dagger_\sigma c_{k\sigma\eta}) \tag{5.1.24}$$

with the matrix elements $t_{k\sigma\eta}$ which couple a QD state σ to a state $k\sigma$ in the reservoir $\eta = e, c$.

The Hamiltonian (5.1.21) with all presented terms is known as the famous Anderson model [AND61]. Basically, it describes the coupling of delocalized electron states to a localized electron state which can be met e.g. in the consideration of magnetic impurites in metals. The related Kondo effect which shows up for very small temperatures can also be observed in the tunneling through QDs (for a nice introduction see e.g. [KOU01]).

5.1.2.1. Stationary current

In this section a general form of the tunneling current from the leads through the QD is derived in terms of the Green's functions (5.1.14) and (5.1.15) for the QD system (replacing the operators a by d and $a^\dagger$ by $d^\dagger$) [JAU94, HAU96]. The definition of the current from the emitter into the QD is $I_e(t) = \langle \hat{I}_e(t) \rangle$ with the current operator $\hat{I}_e(t) = -e\dot{N}_e = -\frac{i}{\hbar} e[H, N_e]$ and the number operator in the emitter contact $N_e = \sum_{k\sigma} c^\dagger_{k\sigma e} c_{k\sigma e}$. Calculating the commutator $[H, N_e]$ with (5.1.21) and taking the average one obtains the current in the form[6]

$$I_e = -I_c = 2e\mathrm{Re} \sum_{k\sigma} t_{k\sigma} G^<_{\sigma,k\sigma e}(t,t) \tag{5.1.25}$$

[6]Note here that N_e commutes with H_{R} and H_{QD}

(Re denotes the real part)

with the lesser Green's function $G^{<}_{\sigma,k\sigma e}(t,t) = i\langle c^{\dagger}_{k\sigma e}(t)d_{\sigma}(t)\rangle$ which has to be determined in the following. Under the assumption of a bilinear Hamiltonian for the reservoirs H_{R} (5.1.23) a general expression for the contour-ordered Green's function can be derived. Following the lines of the last section it reads

$$G^{C}_{\sigma,k\sigma e}(\tau,\tau') = -i\langle S_C d_{D\sigma}(\tau)c^{\dagger}_{Dk\sigma e}(\tau')\rangle \tag{5.1.26}$$

where

$$S_C = \hat{T}_C \exp\left[-\frac{i}{\hbar}\int_C d\tau_1 \tilde{H}_{\mathrm{T}}(\tau_1)\right] \tag{5.1.27}$$

is the contour-ordered S-matrix and $\tilde{H}_{\mathrm{T}}$ is the tunneling Hamiltonian (5.1.24) in the Dirac picture. Now, the expansion (5.1.12) can be carried out (all creation and annihilation operators are in the Dirac picture so that we can omit the index D):

$$\begin{aligned} G^{C}_{\sigma,k\sigma e}(\tau,\tau') &= -i\left\langle \hat{T}_C d_{\sigma}(\tau)c^{\dagger}_{k\sigma e}(\tau')\sum_{n=0}^{\infty}\frac{(-i)^{n+1}}{(n+1)!}\right. \\ &\left.\times\left[\int_C d\tau_1 \sum_{k_1,\sigma_1,\eta_1}\left(t_{k_1\sigma_1}c^{\dagger}_{k_1\sigma_1\eta_1}(\tau_1)d_{\sigma_1}(\tau_1) + t^{*}_{k_1\sigma_1}d^{\dagger}_{\sigma_1}(\tau_1)c_{k_1\sigma_1\eta_1}(\tau_1)\right)\right]^{n+1}\right\rangle \end{aligned} \tag{5.1.28}$$

The zeroth order term does not contribute because annihilation and creation operators have to pair each other to give a nonzero expectation value. The only assumption of our further procedure is based on noninteracting leads (i.e. a bilinear Hamiltonian H_{R}). Then, Wick's theorem [WIC50] can be applied to contract $c^{\dagger}_{k\sigma e}(\tau')$ with one of the $(n+1)$ operators $c_{k_1\sigma_1\eta_1}(\tau_1)$ under the integral. The $(n+1)$ possible choices cancel a factor $(n+1)$ in the factorial in the denominator of (5.1.28). This leads to

$$\begin{aligned} G^{C}_{\sigma,k\sigma e}(\tau,\tau') &= \sum_{k_1\sigma_1\eta_1} t^{*}_{k_1\sigma_1}\int_C d\tau_1(-i)\left\langle \hat{T}_C c^{\dagger}_{k\sigma e}(\tau')c_{k_1\sigma_1\eta_1}(\tau_1)\right\rangle \\ &\quad\times(-i)\left\langle S_C d_{\sigma}(\tau)d^{\dagger}_{\sigma_1}(\tau_1)\right\rangle \end{aligned} \tag{5.1.29}$$

The first average in (5.1.29) gives $\delta_{k\sigma e,k_1\sigma_1\eta_1}$ so that the sum disappears and it follows

$$G^{C}_{\sigma,k\sigma e}(\tau,\tau') = t^{*}_{k\sigma}\int_C d\tau_1 G^{C}_{\sigma\sigma}(\tau,\tau_1)g^{C}_{k\sigma e}(\tau_1,\tau') \tag{5.1.30}$$

with $g^C_{k\sigma e}(\tau_1,\tau') \equiv -i\left\langle \hat{T}_C c_{k\sigma e}(\tau_1) c^\dagger_{k\sigma e}(\tau')\right\rangle$ and $G^C_{\sigma\sigma}(\tau,\tau_1) \equiv -i\left\langle S_C d_\sigma(\tau) d^\dagger_\sigma(\tau_1)\right\rangle$.

Now, Langreth's analytic continuation rules [LAN76a, HAU96] can be applied to (5.1.30), i.e. the contour-ordered Green's functions will be analytical continued to the real time axis (see appendix A in [JAU94] for a motivation) in order to obtain $G^<_{\sigma k\sigma e}(t,t)$ in (5.1.25). For the generic expression $A = \int BC$ as in (5.1.30) with the integration taken on the contour, the lesser component on the real time axis is given by:

$$A^<(t,t') = \int dt_1 \left[B^{\mathrm{ret}}(t,t_1)C^<(t_1,t') + B^<(t,t_1)C^{\mathrm{adv}}(t_1,t')\right] \tag{5.1.31}$$

Then the current (5.1.25) can be written as

$$I_e = 2e\mathrm{Re}\int dt_1 \sum_\sigma \left[G^{\mathrm{ret}}_{\sigma\sigma}(t,t_1)\Sigma^{e<}_{\sigma\sigma}(t_1,t) + G^<_{\sigma\sigma}(t,t_1)\Sigma^{e,\mathrm{adv}}_{\sigma\sigma}(t_1,t)\right] \tag{5.1.32}$$

where $\Sigma^{e(<,\mathrm{adv})}_{\sigma\sigma}(t_1,t) \equiv \sum_k |t_{k\sigma}|^2 g^{(<,\mathrm{adv})}_{k\sigma e}(t_1,t)$ with the lesser and advanced Green's functions for the uncoupled emitter contact obtained by using the Fermi distribution f_e in the emitter and (5.1.24)

$$\begin{aligned} g^<_{k\sigma e}(t_1,t) &\equiv i\left\langle c^\dagger_{k\sigma e}(t) c_{k\sigma e}(t_1)\right\rangle = i f_e(\varepsilon_{k\sigma e}) \exp\left[-\frac{i}{\hbar}\varepsilon_{k\sigma e}(t_1-t)\right] \\ g^{\mathrm{adv}}_{k\sigma e}(t_1,t) &\equiv i\Theta(t-t_1)\left\langle \{c_{k\sigma e}(t_1), c^\dagger_{k\sigma e}(t)\}\right\rangle = i\Theta(t-t_1)\exp\left[-\frac{i}{\hbar}\varepsilon_{k\sigma e}(t_1-t)\right] \end{aligned} \tag{5.1.33}$$

($\{\cdot,\cdot\}$ denotes the anti-commutator and the time dependence of the operators is in the Dirac picture).

Assuming the stationary limit so that the Green's functions depends only on $t - t_1$, using the Fourier transform of the right-hand side of (5.1.32) by means of (5.1.18) with the energy ε yields

$$I_e = 2e\mathrm{Re}\int \frac{d\varepsilon}{2\pi} \sum_\sigma \left[G^{\mathrm{ret}}_{\sigma\sigma}(\varepsilon)\Sigma^{e<}_{\sigma\sigma}(\varepsilon) + G^<_{\sigma\sigma}(\varepsilon)\Sigma^{e,\mathrm{adv}}_{\sigma\sigma}(\varepsilon)\right] \tag{5.1.34}$$

This can be rearranged by introducing the coupling matrix

$$\mathbf{\Gamma}^e = \begin{pmatrix} \Gamma^{(\uparrow)}_e & 0 \\ 0 & \Gamma^{(\downarrow)}_e \end{pmatrix} \tag{5.1.35}$$

with $\Gamma_e^{(\sigma)} = 2\pi \sum_k |t_{k\sigma}|^2 \delta(\varepsilon - \varepsilon_{k\sigma e})$ and the Fourier transform of the Green's functions (5.1.33) $g^{\rm adv}_{k\sigma e}(\varepsilon) = (\varepsilon - \varepsilon_{k\sigma e} - i0^+)^{-1}$, $g^{\rm ret}_{k\sigma e}(\varepsilon) = \left(g^{\rm adv}_{k\sigma e}(\varepsilon)\right)^*$, and $g^<_{k\sigma e}(\varepsilon) = 2\pi i f_e(\varepsilon)\delta(\varepsilon - \varepsilon_{k\sigma e})$:

$$I_e = ie \int \frac{d\varepsilon}{2\pi} {\rm Tr} \left\{ \mathbf{\Gamma}^e \left[(\mathbf{G}^{\rm ret} - \mathbf{G}^{\rm adv}) f_e + \mathbf{G}^< \right] \right\} \tag{5.1.36}$$

with the matrices $[\mathbf{G}^{\rm ret/adv}]_{\sigma\sigma'} = G^{\rm ret/adv}_{\sigma\sigma'}$ and Tr being the trace taken over the spin index σ, and the Fermi function $f_e(\varepsilon)$. The advantage of using Eq. (5.1.36) instead of Eq. (5.1.25) is that one only needs to know the Green's functions for the QD itself. The contacts enter by means of the Fermi functions and the coupling matrix (5.1.35). Note that the only approximation which led to (5.1.36) is the assumption of noninteracting contacts.

5.1.2.2. Spectral power density

The starting point for the calculation of noise is the auto-correlation function with the operator for current fluctuations around the average current $\Delta\hat{I}_\eta(t) \equiv \hat{I}_\eta(t) - \langle I_\eta \rangle$ at the time t (Eq. (49) in Ref. [BLA00] except for a factor of one half)

$$\begin{aligned} C_{\eta\eta'}(t,t') &= \left\langle \{\Delta\hat{I}_\eta(t), \Delta\hat{I}_{\eta'}(t')\} \right\rangle \\ &= \left\langle \{\hat{I}_\eta(t), \hat{I}_{\eta'}(t')\} \right\rangle - 2I_\eta^2 \end{aligned} \tag{5.1.37}$$

($\{\cdot,\cdot\}$ is the anti-commutator) with $I_\eta = I_{\eta'}$ in the stationary limit $t \to \infty$. Note this is the symmetrized version of current-current correlations. Additionally for finite frequencies, asymmetric shot noise can also be detected since the noise frequency ω corresponds to an energy quantum $\hbar\omega$ being transferred from the measurement apparatus to the system. This was considered recently in [ENG04].

Substituting the current operator from Sec. 5.1.2.1

$$\hat{I}_\eta(t) = ie \sum_{k\sigma} \left[t_{k\sigma} c^\dagger_{k\sigma\eta}(t) d_\sigma(t) - t^*_{k\sigma} d^\dagger_\sigma(t) c_{k\sigma\eta}(t) \right] \tag{5.1.38}$$

in Eq. (5.1.37) yields[7]

[7] along the lines of [SOU04]

$$
\begin{aligned}
C_{\eta\eta'}(t,t') &= (ie)^2 \sum_{kk'\sigma\sigma'} \Big[t_{k\sigma} t_{k'\sigma'} \left\langle c^\dagger_{k\sigma\eta}(t) d_\sigma(t) c^\dagger_{k'\sigma'\eta'}(t') d_{\sigma'}(t') \right\rangle \\
&\quad - t_{k\sigma} t^*_{k'\sigma'} \left\langle c^\dagger_{k\sigma\eta}(t) d_\sigma(t) d^\dagger_{\sigma'}(t') c_{k'\sigma'\eta'}(t') \right\rangle \\
&\quad - t^*_{k\sigma} t_{k'\sigma'} \left\langle d^\dagger_\sigma(t) c_{k\sigma\eta}(t) c^\dagger_{k'\sigma'\eta'}(t') d_{\sigma'}(t') \right\rangle \\
&\quad + t^*_{k\sigma} t^*_{k'\sigma'} \left\langle d^\dagger_\sigma(t) c_{k\sigma\eta}(t) d^\dagger_{\sigma'}(t') c_{k'\sigma'\eta'}(t') \right\rangle \Big] \\
&\quad + \text{h.c.} - 2I^2_\eta
\end{aligned} \tag{5.1.39}
$$

The expectation values in (5.1.39) can be defined as real time Green's functions as in (5.1.14) so that (5.1.39) can be rewritten as

$$
\begin{aligned}
C_{\eta\eta'}(t,t') &= (e)^2 \sum_{kk'\sigma\sigma'} \big[t_{k\sigma} t_{k'\sigma'} g^{(1)>}(t,t') \\
&\quad - t_{k\sigma} t^*_{k'\sigma'} g^{(2)>}(t,t') \\
&\quad - t^*_{k\sigma} t_{k'\sigma'} g^{(3)>}(t,t') \\
&\quad + t^*_{k\sigma} t^*_{k'\sigma'} g^{(4)>}(t,t') \big] \\
&\quad + \text{h.c.} - 2I^2_\eta
\end{aligned} \tag{5.1.40}
$$

Now, we define the contour-ordered Green's functions in order to carry out the S-matrix expansion as in (5.1.12):

$$
\begin{aligned}
g^{(1)C}(\tau,\tau') &= i^2 \left\langle \hat{T}_C c^\dagger_{k\sigma\eta}(\tau) d_\sigma(\tau) c^\dagger_{k'\sigma'\eta'}(\tau') d_{\sigma'}(\tau') \right\rangle \\
g^{(2)C}(\tau,\tau') &= i^2 \left\langle \hat{T}_C c^\dagger_{k\sigma\eta}(\tau) d_\sigma(\tau) d^\dagger_{\sigma'}(\tau') c_{k'\sigma'\eta'}(\tau') \right\rangle \\
g^{(3)C}(\tau,\tau') &= i^2 \left\langle \hat{T}_C d^\dagger_\sigma(\tau) c_{k\sigma\eta}(\tau) c^\dagger_{k'\sigma'\eta'}(\tau') d_{\sigma'}(\tau') \right\rangle \\
g^{(4)C}(\tau,\tau') &= i^2 \left\langle \hat{T}_C d^\dagger_\sigma(\tau) c_{k\sigma\eta}(\tau) d^\dagger_{\sigma'}(\tau') c_{k'\sigma'\eta'}(\tau') \right\rangle
\end{aligned} \tag{5.1.41}
$$

We carry out the expansion exemplarily for $g^{(1)C}(\tau,\tau')$ which reads in the Dirac picture (denoted by a tilde):

$$
g^{(1)C}(\tau,\tau') = i^2 \left\langle S_C \tilde{c}^\dagger_{k\sigma\eta}(\tau) \tilde{d}_\sigma(\tau) \tilde{c}^\dagger_{k'\sigma'\eta'}(\tau') \tilde{d}_{\sigma'}(\tau') \right\rangle \tag{5.1.42}
$$

with

$$
S_C = \hat{T}_C \exp\left(-\frac{i}{\hbar} \int_C d\tau_1 \tilde{H}_T(\tau_1) \right) \tag{5.1.43}
$$

The S-matrix expansion in (5.1.42) similar to (5.1.28) reads

$$
\begin{aligned}
g^{(1)C}(\tau,\tau') &= i^2 \sum_{n=0}^{\infty} \frac{(-i)^{n+2}}{(n+2)!} \\
&\quad \times \Big\langle \hat{T}_C \tilde{c}^{\dagger}_{k\sigma\eta}(\tau) \tilde{d}_{\sigma}(\tau) \tilde{c}^{\dagger}_{k'\sigma'\eta'}(\tau') \tilde{d}_{\sigma'}(\tau') \\
&\quad \times \left[\int_C d\tau_1 \sum_{k_1\sigma_1\eta_1} t_{k_1\sigma_1} \tilde{c}^{\dagger}_{k_1\sigma_1\eta_1}(\tau_1) \tilde{d}_{\sigma_1}(\tau_1) + t_{k_1\sigma_1} \tilde{d}^{\dagger}_{\sigma_1}(\tau_1) \tilde{c}_{k_1\sigma_1\eta_1}(\tau_1) \right]^{n+2} \Big\rangle
\end{aligned}
\tag{5.1.44}
$$

The zero and first order term in the expansion (5.1.44) give no contribution. Due to the bilinear form of the Hamiltonian of the leads Wick's theorem can be applied in order to contract $\tilde{c}^{\dagger}_{k\sigma\eta}(\tau)$ with one of the $(n+2)$ operators $\tilde{c}_{k_i\sigma_i\eta_i}(\tau_i)$. The remaining $(n+1)$ operators $\tilde{c}_{k_j\sigma_j\eta_j}(\tau_j)$ $(i \neq j)$ must be contracted with $\tilde{c}^{\dagger}_{k'\sigma'\eta'}(\tau')$. The number of all possible contractions is then $(n+2)(n+1)$. Each of them gives the same result by changing the labels. Then, one finds

$$
\begin{aligned}
g^{(1)C}(\tau,\tau') &= t^*_{k\sigma} t^*_{k'\sigma'} \int_C \int_C d\tau_1 d\tau_2 g^C_{k\sigma\eta}(\tau_1,\tau) g^C_{k'\sigma'\eta'}(\tau',\tau_2) \\
&\quad \times \Big\langle S_C \tilde{d}_{\sigma}(\tau) \tilde{d}_{\sigma'}(\tau') \tilde{d}^{\dagger}_{\sigma}(\tau_1) \tilde{d}^{\dagger}_{\sigma'}(\tau_2) \Big\rangle
\end{aligned}
\tag{5.1.45}
$$

with the Green's function for the contacts η and η': $g^C_{k\sigma\eta}(\tau_1,\tau) \equiv -i\langle \hat{T}_C \tilde{c}_{k\sigma\eta}(\tau_1) \tilde{c}^{\dagger}_{k\sigma\eta}(\tau)\rangle$.

Finally we arrive at an expression for the contour-ordered Green's function where the contact and QD degrees of freedom are apparently decoupled. Here a four-operator Green's function (two-particle Green's function) for the QD occurs, which essentially differs from the current formula in the previous section where only single-particle Green's functions enter. Due to the Coulomb interaction in the QD the Hamiltonian is not bilinear in the operators. Therefore Wick's theorem can only be applied without Coulomb interaction, i.e. $U = 0$ or in the Hartree-Fock approximations which will be discussed in detail in Sec. 5.3. According to Wick's theorem then the four-operator Green's function can be factorized as

$$
\Big\langle S_C \tilde{d}_{\sigma}(\tau) \tilde{d}_{\sigma'}(\tau') \tilde{d}^{\dagger}_{\sigma}(\tau_1) \tilde{d}^{\dagger}_{\sigma'}(\tau_2) \Big\rangle = G_{\sigma\sigma}(\tau,\tau_1) G_{\sigma'\sigma'}(\tau',\tau_2) - G_{\sigma\sigma'}(\tau,\tau_2) G_{\sigma'\sigma}(\tau',\tau_1)
\tag{5.1.46}
$$

with $G_{\sigma\sigma}(\tau,\tau_1) = -i \Big\langle \hat{T}_C d_{\sigma}(\tau) d^{\dagger}_{\sigma}(\tau_1) \Big\rangle$.

The other Green's functions in (5.1.41) are obtained in the same manner and read

$$
\begin{aligned}
g^{(2)C}(\tau,\tau') &= -\delta_{k\sigma\eta,k'\sigma'\eta'} g^C_{k\sigma\eta}(\tau',\tau) G_{\sigma\sigma'}(\tau,\tau') + \\
&\quad + t^*_{k\sigma} t_{k'\sigma'} \int\int d\tau_1\, d\tau_2\, g^C_{k\sigma\eta}(\tau_1,\tau) g^C_{k'\sigma'\eta'}(\tau',\tau_2) \times \\
&\quad \times \{G_{\sigma\sigma}(\tau,\tau_1) G_{\sigma'\sigma'}(\tau_2,\tau') - G_{\sigma\sigma'}(\tau,\tau') G_{\sigma'\sigma}(\tau_2,\tau_1)\} \\
g^{(3)C}(\tau,\tau') &= \left[g^{(2)C}(\tau,\tau')\right]^* \\
g^{(4)C}(\tau,\tau') &= \left[g^{(1)C}(\tau,\tau')\right]^*
\end{aligned}
\tag{5.1.47}
$$

The first term in the integrand of $g^{(1)C}(\tau,\tau')$ and $g^{(2)C}(\tau,\tau')$ correspond to disconnected diagrams and cancel exactly with $2I_\eta^2$ in (5.1.37) as proven in [SOU04]. The remaining terms correspond to connected diagrams and contribute to the noise. From Eqs. (5.1.45),(5.1.47) the auto-correlation function (5.1.37) can now be written as (the superscript C is skipped for clarity)

$$
\begin{aligned}
C_{\eta\eta'}(t,t') &= e^2 \sum_{k\sigma} |t_{k\sigma}|^2 \delta_{\eta\eta'} [g^>_{k\sigma\eta}(t,t') G^<_{\sigma\sigma}(t',t) + G^>_{\sigma\sigma}(t,t') g^<_{k\sigma\eta}(t',t)] - \\
&\quad - e^2 \sum_{kk'\sigma\sigma'} |t_{k\sigma}|^2 |t_{k'\sigma'}|^2 \int_C \int_C d\tau_1\, d\tau_2 \;\times \\
&\quad \times \{G_{\sigma\sigma'}(t,\tau_2) g_{k'\sigma'\eta'}(\tau_2,t') G_{\sigma'\sigma}(t',\tau_1) g_{k\sigma\eta}(\tau_1,t) \\
&\quad - G_{\sigma\sigma'}(t,t') g_{k'\sigma'\eta'}(t',\tau_2) G_{\sigma'\sigma}(\tau_2,\tau_1) g_{k\sigma\eta}(\tau_1,t) \\
&\quad - g_{k\sigma\eta}(t,\tau_1) G_{\sigma\sigma'}(\tau_1,\tau_2) g_{k'\sigma'\eta'}(\tau_2,t') G_{\sigma'\sigma}(t',t) \\
&\quad + g_{k\sigma\eta}(t,\tau_1) G_{\sigma\sigma'}(\tau_1,t') g_{k'\sigma'\eta'}(t',\tau_2) G_{\sigma'\sigma}(\tau_2,t)\}^> + \text{h.c.}
\end{aligned}
\tag{5.1.48}
$$

Here, the first two terms are already analytically continued with respect to Langreth's rules[8], e.g. one presented in Eq. (5.1.31). In the term containing the contour integrals the analytical continuation to the real time axis still has to be carried out, which is indicated by the superscript $>$. In particular, the products of at most three contour-ordered Green's function have to be evaluated since there are only two contours. The detailed straightforward calculation will be skipped here. After the analytical continuation a Fourier transform has to performed and with the Wiener-Khinchin theorem (Appendix B) the spectral power density (SPD), which is the Fourier transform of the autocorrelation function, in the zero-frequency limit then becomes

$$
\begin{aligned}
S_{ee}(0) &= 2e^2 \int \frac{d\varepsilon}{2\pi} \mathrm{Tr}\, \{i[f_e \mathbf{\Gamma}_e \mathbf{G}^> - (1-f_e)\mathbf{\Gamma}_e \mathbf{G}^<] \\
&\quad + \mathbf{G}^> \mathbf{\Gamma}_e \mathbf{G}^< \mathbf{\Gamma}_e + (\mathbf{G}^{\mathrm{ret}} - \mathbf{G}^{\mathrm{adv}}) \mathbf{\Gamma}_e [f_e \mathbf{G}^> - (1-f_e)\mathbf{G}^<] \mathbf{\Gamma}_e \\
&\quad - f_e(1-f_e)[\mathbf{G}^{\mathrm{adv}} \mathbf{\Gamma}_e \mathbf{G}^{\mathrm{adv}} \mathbf{\Gamma}_e + \mathbf{G}^{\mathrm{ret}} \mathbf{\Gamma}_e \mathbf{G}^{\mathrm{ret}} \mathbf{\Gamma}_e]\}
\end{aligned}
\tag{5.1.49}
$$

[8] In this special case, the last line of Tab. 4.1. in [HAU96] is used.

This expression for the DC noise was independently derived in Ref. [ZHU02][9] and in a scalar form in [DON02]. Noise conservation holds here, i.e. $S_{ee}(0) = S_{cc}(0) = -S_{ec}(0) = -S_{ce}(0)$, as already discussed in Sec. 4.1.1.

5.2. Exactly solvable limits of the Anderson Model

There is no exact solution for the problem given by the Anderson Hamiltonian (5.1.21). One has to rely on approximations depending on the physical situation one wishes to model.

Nevertheless there are two limits where one can find exact results which will be demonstrated in the following two sections.

5.2.1. Noninteracting quantum dot

Let us assume there is no Coulomb interaction in the QD: $U = 0$ so that the Hamiltonian (5.1.21) becomes bilinear in the operators. To obtain the retarded Green's function the EOM technique is used. For this reason the time evolution of the operators appearing in the Green's function is needed in the Heisenberg picture:

$$\frac{i}{\hbar}\dot{d}_\sigma = [H, d_\sigma] = \varepsilon_\sigma d_\sigma + \sum_{k\eta} t^*_{k\sigma\eta} c_{k\sigma\eta} \tag{5.2.1}$$

$$\frac{i}{\hbar}\dot{c}_{k\sigma\eta} = [H, c_{k\sigma\eta}] = \varepsilon_{k\sigma\eta} c_{k\sigma\eta} + t_{k\sigma\eta} d_\sigma \tag{5.2.2}$$

Then, the EOM for the time-ordered Green's function

$$G^t_{\sigma\sigma'}(t,t') \equiv -i\langle \hat{T} d_\sigma(t) d^\dagger_{\sigma'}(t')\rangle \tag{5.2.3}$$

with the time ordering operator $\hat{T}$ introduced in Sec. 5.1.1 is

$$\left(\frac{i}{\hbar}\frac{\partial}{\partial t} - \varepsilon_\sigma\right) G^t_{\sigma\sigma'}(t,t') = \delta_{\sigma\sigma'}\delta(t-t') + \sum_{k\eta} t^*_{k\sigma\eta} G^t_{k\sigma\eta,\sigma'}(t,t') \tag{5.2.4}$$

with the QD-contact Green's function $G^t_{k\sigma\eta,\sigma'}(t,t') = -i\langle \hat{T} c_{k\sigma\eta}(t) d^\dagger_{\sigma'}(t')\rangle$. For this function we also set up an EOM

$$\left(\frac{i}{\hbar}\frac{\partial}{\partial t} - \varepsilon_{k\sigma\eta}\right) G^t_{k\sigma\eta,\sigma'}(t,t') = t_{k\sigma\eta} G^t_{\sigma\sigma'}(t,t') \tag{5.2.5}$$

[9] Therein the authors claim that "it can take into account the many-body effects conveniently" which is doubtful in general regarding the approximation (5.1.46), i.e. the Hartree-Fock approximation.

with the formal solution

$$G^t_{k\sigma\eta,\sigma'}(t,t') = \int dt_1\, G^t_{\sigma\sigma'}(t,t_1) t_{k\sigma\eta} g^t_{k\sigma\eta}(t_1,t') \tag{5.2.6}$$

with the contact Green's function $g^t_{k\sigma\eta} = (\frac{i}{\hbar}\frac{\partial}{\partial t} - \varepsilon_{k\sigma\eta})^{-1}$ [HAU96]. Inserting (5.2.6) in (5.2.5), transformation to contour-ordered Green's functions, and Fourier transformation yields a Dyson equation for the QD Green's function of the form (the energy argument is skipped)

$$G^C_{\sigma\sigma'} = G^{C0}_{\sigma\sigma'} + \sum_{\alpha\beta} G^{C0}_{\sigma\alpha} \sum_{k\eta} \left(t^*_{k\alpha\eta} t_{k\beta\eta} g^C_{k\beta\eta}\right) G^C_{\beta\sigma'} \tag{5.2.7}$$

By comparison of Eq. (5.2.7) with Eq. (5.1.13) we can identify the self-energy due to the coupling of the QD to the reservoirs

$$\Sigma^C_{\alpha\beta} = \sum_{k\eta} t^*_{k\alpha\eta} t_{k\beta\eta} g^C_{k\beta\eta} \tag{5.2.8}$$

Then, the retarded/advanced self-energy for a single level can be written as

$$\Sigma^{\mathrm{ret/adv}}(\varepsilon) = \sum_{k\eta} |t_{k\eta}|^2 g^{\mathrm{ret/adv}}_{k\eta}(\varepsilon) = \sum_{k\eta} \frac{|t_{k\eta}|^2}{\varepsilon - \varepsilon_{k\eta} \mp 0^+} = \Lambda(\varepsilon) \mp \frac{i}{2}\Gamma(\varepsilon) \tag{5.2.9}$$

The real part of the self-energy $\Lambda(\varepsilon) = \Lambda_e(\varepsilon) + \Lambda_c(\varepsilon)$ is typically incorporated in the eigen-energies of the uncoupled system and the imaginary part $\Gamma(\varepsilon) = \Gamma_e(\varepsilon) + \Gamma_c(\varepsilon)$ is often considered as energy-independent, which is called the *wide-band approximation*. The lesser/greater self-energy reads

$$\begin{aligned}
\Sigma^<(\varepsilon) &= \sum_{k\eta} |t_{k\eta}|^2 g^<_{k\eta}(\varepsilon) = i[\Gamma_e(\varepsilon) f_e(\varepsilon) + \Gamma_c(\varepsilon) f_c(\varepsilon)] \\
\Sigma^>(\varepsilon) &= \sum_{k\eta} |t_{k\eta}|^2 g^>_{k\eta}(\varepsilon) = -i[\Gamma_e(\varepsilon)(1 - f_e(\varepsilon)) + \Gamma_c(\varepsilon)(1 - f_c(\varepsilon))]
\end{aligned} \tag{5.2.10}$$

with the distribution functions $f_{e/c}$ in the emitter/collector reservoir, respectively. For a many-level QD these self-energies can easily be generalized to matrices.

In the following, the current (5.1.36) and the noise (5.1.49) in tunneling through a single spin-degenerate QD level in the high-bias regime ($f_c = 0$) and wide-band approximation is considered. The spin-degeneracy is lifted for instance by a magnetic field B so that $\Delta E \equiv \varepsilon_\downarrow - \varepsilon_\uparrow = g^* \mu_B B$ (Zeeman-splitting; $g^* \ldots$ effective Landé factor, $\mu_B \ldots$ Bohr's magneton). Fig. 5.2 shows the current (upper panel)

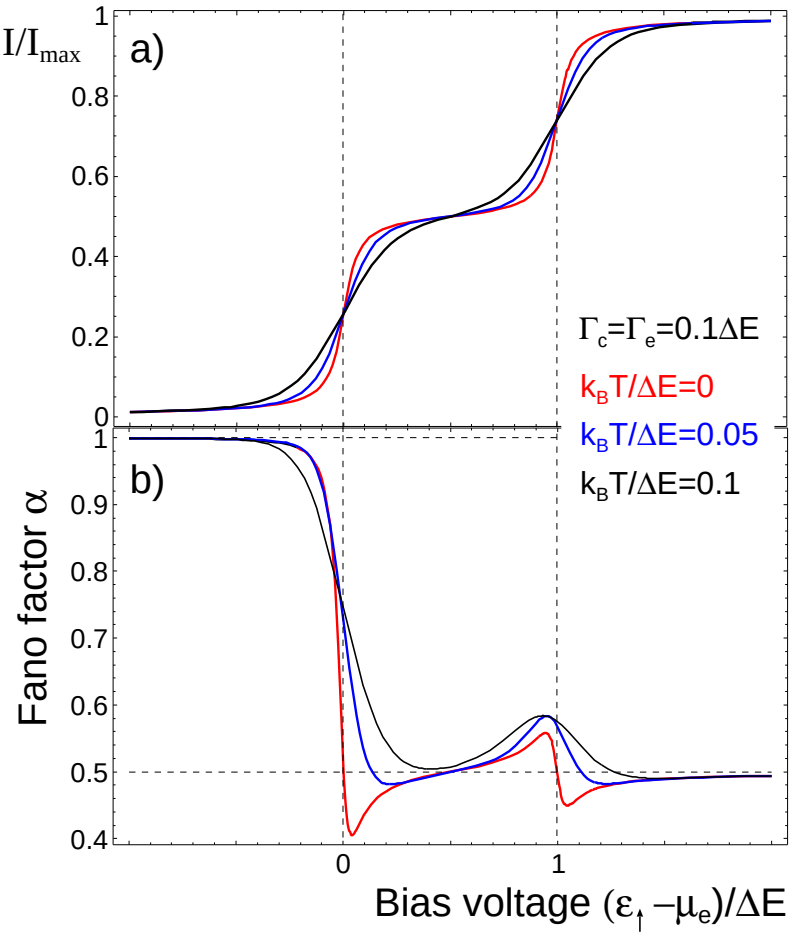

Figure 5.2.: a) Normalized current vs. bias voltage $\propto (\varepsilon_\uparrow - \mu_e)$. b) Fano factor α vs. bias voltage for various temperatures k_BT, $\Delta E = \varepsilon_\downarrow - \varepsilon_\uparrow$, and symmetric barriers $\Gamma_e = \Gamma_c$.

and the Fano factor (lower panel) defined by (4.1.9) vs. bias voltage ($\propto \varepsilon_\uparrow - \mu_e$, where the emitter chemical potential μ_e is given by the applied bias voltage) for various temperatures. The barriers are assumed to be symmetric: $\Gamma_e = \Gamma_c = 0.1\Delta E$. The current shows two steps of same height since for noninteracting electrons the current is the simple superposition of its components. For zero-temperature the shape of the current steps is determined by the antiderivative of the DOS, here Lorentzians with FWHM: $\Gamma_e + \Gamma_c$. Analytically, the current for N noninteracting levels i coupled to emitter/collector by $\Gamma^{(i)}_{e/c}$ vs. bias voltage ($V \propto \varepsilon_i - \mu_e$) can be expressed as

$$I(V) = \sum_i I_i(V) \quad \text{with} \quad I_i(V) = \frac{e}{\pi} \frac{\Gamma_e^{(i)} \Gamma_c^{(i)}}{\Gamma_e^{(i)} + \Gamma_c^{(i)}} \left[\arctan\left(\frac{2(\varepsilon_i - \mu_e)}{\Gamma_e^{(i)} + \Gamma_c^{(i)}} \right) + \frac{\pi}{2} \right] \tag{5.2.11}$$

For increasing temperatures the current steps further smear out due to the thermal excitations of emitter electrons. For $k_B T \gg \Gamma_{e/c}$ the intrinsic level broadening does not play any role and the sequential tunneling limit is reached (Chap. 3) where the shape of the current steps is fully determined by the thermal occupation of the reservoirs.

Really interesting behavior is provided by the noise at the respective current steps as shown by the Fano factor vs. bias voltage in Fig. 5.2b. For both levels far above the emitter chemical potential μ_e tunneling of electrons are rare events so that its statistics becomes Poissonian with a Fano factor of unity. For zero-temperature (red curve) the Fano factor is one half when the levels exactly pass the emitter chemical potential. This value corresponds to the symmetric barrier geometry and is given by Eq. (4.2.1) for arbitrary ratios of emitter to collector coupling. Close to these bias points correlations beyond Pauli's exclusion principle occur which result in a Fano factor even below one half on the higher bias side[10]. The simple picture of sequential transfer of electrons through two barriers is not sufficient to understand these correlations. While one can relate the sequential tunneling to classical noise even though Pauli's principle is involved[11] one can attribute these new correlations to *quantum noise*. The zero-temperature Fano factor vs. bias voltage ($V \propto \varepsilon_i - \mu_e$) for tunneling through a single level ε_i yields analytically[12]

$$\alpha_i(V) = 1 - \frac{2\Gamma_e^{(i)}\Gamma_c^{(i)}}{(\Gamma_e^{(i)} + \Gamma_c^{(i)})^2} \left\{ 1 + \frac{(\Gamma_e^{(i)} + \Gamma_c^{(i)})(\varepsilon_i - \mu_e)}{\left[\left(\frac{\Gamma_e^{(i)} + \Gamma_c^{(i)}}{2} \right)^2 + (\varepsilon_i - \mu_e)^2 \right] \left[\pi + 2 \arctan\left(\frac{2(\varepsilon_i - \mu_e)}{\Gamma_e^{(i)} + \Gamma_c^{(i)}} \right) \right]} \right\} \tag{5.2.12}$$

(red curve in Fig. 5.2a). From (5.2.12) it can be recognized that the Fano factor cannot be separated in a contribution caused by Pauli's principle alone and a quantum noise contribution. Using (5.2.11) and (5.2.12) the full Fano factor for the

[10] A Fano factor below 0.5 was also observed theoretically in [WEI99] for double-barrier tunneling, but therein it is discussed as an artefact of the wide-band approximation. Nevertheless, respective experimental evidence for $\alpha < 0.5$ in double-barrier resonant tunneling diodes can be found in [ALE03]. The question whether the observation of a Fano factor below one half is a signature of coherent tunneling is subject of a controversial debat [BLA04b, ALE04].

[11] The double-barrier tunneling can be treated successfully by means of a Langevin equation technique[BLA00].

[12] A similar expression was published in [ALE03].

tunneling through several levels is given by (4.2.2) which produces the peculiar bias dependence at the second current step (red curve) in Fig. 5.2. Increasing temperature leads to a bias dependence of the Fano factor (blue and black curves) which is already known from the discussions in Sec. 4.2.1.1 in the sequential tunneling limit $\Gamma_{ec} \ll k_B T$.

Remark: For zero-temperature and noninteracting electrons the general noise expression (5.1.49) can be rewritten as $\int d\varepsilon\, T_{ec}(\varepsilon)[1 - T_{ec}(\varepsilon)](f_e - f_c)^2$ with the transmission function from emitter to collector $T_{ec} = \mathrm{Tr}[\Gamma_e G^{\mathrm{ret}} \Gamma_c G^{\mathrm{adv}}]$. This equation appears in Sec. 6.2 and it will be considered from a more fundamental point of view in Sec. 7.1.

5.2.2. Isolated interacting quantum dot

Although no electronic transport would occur without coupling to the contacts, i.e. $|t_{k\sigma\eta}| = 0$ in (5.1.24) the following consideration is necessary on the one hand because it gives insight into the nature of Coulomb interaction and on the other hand the resulting Green's function will needed for further investigations in Sec. 5.3.2.

The Heisenberg EOM for the QD annihilation operator is

$$\frac{i}{\hbar}\dot{d}_\sigma = \varepsilon_\sigma d_\sigma + U d_\sigma n_{\sigma'} \tag{5.2.13}$$

The EOM for the time-ordered Green's function (5.2.3) then yields

$$\left(\frac{i}{\hbar}\frac{\partial}{\partial t} - \varepsilon_\sigma\right) G^t_{\sigma\sigma}(t,t') = \delta(t-t') + U G^{t(2)}(t,t') \tag{5.2.14}$$

with the higher-order Green's function $G^{t(2)}(t,t') \equiv -i\langle \hat{T} d_\sigma(t) n_{\sigma'}(t) d^\dagger_{\sigma'}(t')\rangle$. For this function generated by the Coulomb interaction the EOM yields ($\dot{n}_{\sigma'} = 0$)

$$\left(\frac{i}{\hbar}\frac{\partial}{\partial t} - \varepsilon_\sigma - U\right) G^{t(2)}(t,t') = \delta(t-t')\langle n_{\sigma'}\rangle \tag{5.2.15}$$

with $\sigma' = -\sigma$. Note, that the second-order Green's function does not further couple to higher-order functions so that an exact result for (5.2.3) can be obtained here. Fourier transforming Eqs. (5.2.14), (5.2.15) and eventually putting them together leads to

$$G^t_{\sigma\sigma}(\varepsilon) = \frac{\langle n_{\sigma'}\rangle}{\varepsilon - \varepsilon_\sigma - U} + \frac{1 - \langle n_{\sigma'}\rangle}{\varepsilon - \varepsilon_\sigma} \tag{5.2.16}$$

The retarded Green's function is then obtained from (5.2.16) with the replacement $\varepsilon \to \varepsilon + i0^+$:

$$G^{\mathrm{ret}}_{\sigma\sigma}(\varepsilon) = \frac{\langle n_{\sigma'}\rangle}{\varepsilon - \varepsilon_\sigma - U + i0^+} + \frac{1 - \langle n_{\sigma'}\rangle}{\varepsilon - \varepsilon_\sigma + i0^+} \tag{5.2.17}$$

The DOS is given as the imaginary part of the retarded Green's function (5.2.17) and has a nice and simple interpretation in this example: it consists of poles at ε_σ and $\varepsilon_\sigma + U$ which are weighted by the occupation of the opposite spin state; as soon as the opposite spin state gets more occupied ($\langle n_{\sigma'}\rangle > 0$) the DOS at ε_σ looses its weight taking into account the effect of Coulomb repulsion. Before we start with the considerations of both the contact coupling and the Coulomb interaction in the following section it is worth to emphasize that any approximation should provide the mentioned DOS behavior for weak contact coupling.

5.3. Hartree-Fock approximations

In this section we study the lowest-order approximation for the Anderson model (5.1.21) considering all terms therein. There are different approximation schemes available which are termed Hartree-Fock approximation in the literature. They have in common that the part of the Hamiltonian describing the Coulomb interaction (5.1.22) is transformed into a bilinear Hamiltonian. This can either be done directly as considered in Sec. 5.3.1 or implicitly as described in Sec. 5.3.2. Both approximations lead to different results, whereas we show that the former is not convenient to describe nonlinear transport. In contrast, the latter provides reasonable results for the current but not for the noise as will be discussed in detail.

5.3.1. Factorization of the Coulomb term

The Coulomb interaction term in the Anderson Hamiltonian (5.1.22) can be decoupled as follows

$$\begin{aligned} H^U_{\mathrm{QD}} &= U n_\uparrow n_\downarrow = U(n_\uparrow + \langle n_\uparrow\rangle - \langle n_\uparrow\rangle)(n_\downarrow + \langle n_\downarrow\rangle - \langle n_\downarrow\rangle) \\ &= U[(n_\uparrow - \langle n_\uparrow\rangle)(n_\downarrow - \langle n_\downarrow\rangle) + n_\uparrow\langle n_\downarrow\rangle + n_\downarrow\langle n_\uparrow\rangle - \langle n_\uparrow\rangle\langle n_\downarrow\rangle] \\ &\approx U(n_\uparrow\langle n_\downarrow\rangle + n_\downarrow\langle n_\uparrow\rangle) \end{aligned} \tag{5.3.1}$$

The approximation (wich provides a special form of *mean-field approximation*) which leads to the last line in (5.3.1) neglects the fluctuations of the level occupations around their average values (first term in second line) and the last term which does not affect the EOM since it is a c-number. Hence, the Hamiltonian (5.1.22) becomes bilinear and with the substitution $\varepsilon_\sigma \to \varepsilon_\sigma + U\langle n_{-\sigma}\rangle$ one can directly use the results for a noninteracting QD in Sec. 5.2.1. The retarded Green's function obtained from the Dyson equation (5.1.19) with the retarded self-energy for the contact coupling (5.2.9) reads

$$G^{\mathrm{ret}}(\varepsilon) = \mathrm{Diag}\left[\frac{1}{\varepsilon - \varepsilon_\uparrow - U\langle n_\downarrow\rangle + i\frac{\Gamma_e^{(\uparrow)}+\Gamma_c^{(\uparrow)}}{2}}, \frac{1}{\varepsilon - \varepsilon_\downarrow - U\langle n_\uparrow\rangle + i\frac{\Gamma_e^{(\downarrow)}+\Gamma_c^{(\downarrow)}}{2}}\right] \quad (5.3.2)$$

The average densities $\langle n_\sigma\rangle$ which enter this function have to be calculated from the lesser Green's function as

$$\langle n_\sigma\rangle = -i\int \frac{d\varepsilon}{2\pi} G^<_{\sigma\sigma}(\varepsilon, \langle n_{-\sigma}\rangle) \quad (5.3.3)$$

The lesser Green's function itself depends on the retarded Green's function via the Keldysh relation (5.1.20) and thus on the densities which then have to be determined self-consistently. Explicitly, the lesser Green's function reads

$$G^<_{\sigma\sigma}(\varepsilon) = i[\Gamma_e^{(\sigma)} f_e + \Gamma_c^{(\sigma)} f_c(\varepsilon)]|G^{\mathrm{ret}}_{\sigma\sigma}|^2 \quad (5.3.4)$$

This can be cast into a more convenient form as

$$\begin{aligned} G^<_{\sigma\sigma}(\varepsilon) &= -\frac{\Gamma_e^{(\sigma)} f_e(\varepsilon) + \Gamma_c^{(\sigma)} f_c(\varepsilon)}{\Gamma_e^{(\sigma)} + \Gamma_c^{(\sigma)}}[G^{\mathrm{ret}}_{\sigma\sigma}(\varepsilon) - G^{\mathrm{adv}}_{\sigma\sigma}(\varepsilon)] \\ &= iF_\sigma(\varepsilon)A_\sigma(\varepsilon) \end{aligned} \quad (5.3.5)$$

with $F_\sigma(\varepsilon) \equiv \frac{\Gamma_e^{(\sigma)} f_e(\varepsilon)+\Gamma_c^{(\sigma)} f_c(\varepsilon)}{\Gamma_e^{(\sigma)}+\Gamma_c^{(\sigma)}}$ and $A_\sigma(\varepsilon) = -i[G^{\mathrm{ret}}_{\sigma\sigma}(\varepsilon) - G^{\mathrm{adv}}_{\sigma\sigma}(\varepsilon)]$. I.e. the lesser Green's function is the product of the (non-equilibrium) distribution $F_\sigma(\varepsilon)$ and the spectral function $A_\sigma(\varepsilon)$ [13] very similar to the equilibrium situation where F_σ has to be replaced by the equilibrium occupation. Then, the integral in (5.3.3) takes the form for high bias ($f_c = 0$)

$$I_\sigma(x) = \int \frac{d\varepsilon}{2\pi} \frac{\Gamma_e^{(\sigma)}}{1 + \exp\left(\frac{\varepsilon-\mu_e}{k_B T}\right)} \frac{1}{(\varepsilon - x)^2 + \left(\frac{\Gamma_e^{(\sigma)}+\Gamma_c^{(\sigma)}}{2}\right)^2} \quad (5.3.6)$$

Hence, with (5.3.6) the self-consistency equations for $\langle n_{\uparrow/\downarrow}\rangle$ are

$$\begin{aligned} \langle n_\uparrow\rangle &= I_\uparrow(\varepsilon_\uparrow + U\langle n_\downarrow\rangle) \\ \langle n_\downarrow\rangle &= I_\downarrow(\varepsilon_\downarrow + U\langle n_\uparrow\rangle) \end{aligned} \quad (5.3.7)$$

This is a coupled set of strongly nonlinear equations and there might exist more than one solution. The graphical solution of (5.3.7) for symmetric barriers $\Gamma_e^{(\uparrow)} =$

[13] This relation takes the form of the fluctuation-dissipation theorem where $G^<$ contains information about fluctuations and the spectral function quantifies dissipation in the system [HAU96].

$\Gamma_c^{(\uparrow)} = \Gamma_e^{(\downarrow)} = \Gamma_c^{(\downarrow)}$ and $\varepsilon_\uparrow = \varepsilon_\downarrow$ in the bias regime where only one spin state can be occupied due to Coulomb repulsion (Coulomb blockade) $\varepsilon_{\uparrow/\downarrow} < \mu_e < U$ is shown in Fig. 5.3. Indeed, three crossing points as the possible solutions for the densities appear: there are two polarized solutions which correspond to unphysical situations since only one spin state can be occupied in the considered regime and there is one unpolarized solution which is physical correct [14].

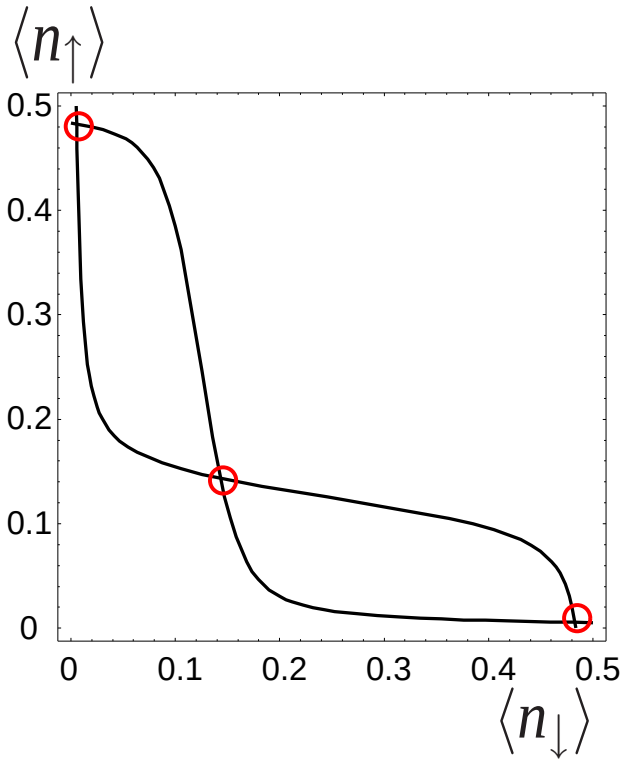

Figure 5.3.: Graphical solution of Eqs. (5.3.7) for $\Gamma_e^{(\uparrow)} = \Gamma_c^{(\uparrow)} = \Gamma_e^{(\downarrow)} = \Gamma_c^{(\downarrow)}$, $\varepsilon_\uparrow = \varepsilon_\downarrow$, and $\varepsilon_{\uparrow/\downarrow} < \mu_e < U$

These different density configurations correspond to two different coexisting currents through the system which can lead to bistability effects in the current-voltage characteristic as discussed e.g. in [MII96, MAK96, MII97, NAT98, KIE99a, SPR03][15]. By a slight lifting of the spin degeneracy or choosing proper initial values for the self-consistent loop in the numerical calculation one can exclude the unphysical solution and hence one gets rid of the artificial bistability. Another more crucial

[14] In this Coulomb blockade regime both single-particle states are occupied with the same probability since they are equally coupled to the reservoirs and the two-particle state cannot be occupied, i.e. $\langle n_\uparrow \rangle = P_{10} + P_{11} = P_{01} + P_{11} = \langle n_\downarrow \rangle$.

[15] With respect to the analysis in the present section it can be assumed that in all these references the bistability effect is artificial and caused by the mean-field approximation.

problem is connected to the DOS. In the Sec. 5.2.2 it was pointed out that the DOS should exhibit poles fixed at ε_σ and $\varepsilon_\sigma + U$. In the mean-field approximation considered here there are also poles at ε_σ but the poles caused by the Coulomb repulsion U shift linearly with the occupation of the opposite spin state which is in obvious conflict to the mentioned results. Furthermore, for symmetric coupling the occupations can approach maximally one half (only in the high-bias limit $f_c = 0$) which would give a repulsion with half the Coulomb energy. To conclude, the mean-field approximation investigated here is not suitable to describe high-bias transport through QDs and the appearing bistability effects in the average current are purely artificial.

Nevertheless, for weak-bias transport (linear-response regime) the mean-field approximation is applicable and yields results in agreement with the experimentally observed Coulomb blockade oscillations. In this regime the QD is in equilibrium with the reservoirs so that the physically correct solution for the occupations can be found by minimizing the free energy of the QD: $F = \langle\varepsilon\rangle - TS$ ($\langle\varepsilon\rangle$ is the total energy of the system, S is the entropy) [BAL99].

5.3.2. Truncation of the hierarchy

The following EOM procedure is adopted from [LAC81, HAU96] and can be retraced there in detail. Here only a brief sketch of the derivation will be given. For the derivation of the Heisenberg operators now the full Anderson Hamiltonian (5.1.21) without any approximation therein is considered. The EOM for the relevant operators are

$$\begin{aligned}
i\dot{d}_\sigma &= \varepsilon_\sigma d_\sigma + U d_\sigma n_{\sigma'} + \sum_{k\eta} t^*_{k\sigma\eta} c_{k\sigma\eta} \\
i\dot{d}^\dagger_{\sigma'} &= -\varepsilon_{\sigma'} d^\dagger_{\sigma'} - U n_\sigma d^\dagger_{\sigma'} - \sum_{k\eta} t_{k\sigma'\eta} c^\dagger_{k\sigma'\eta} \\
i\dot{c}_{k\sigma\eta} &= \varepsilon_{k\eta} c_{k\sigma\eta} + t_{k\sigma\eta} d_\sigma \\
i\dot{c}^\dagger_{k\sigma'\eta} &= -\varepsilon_{k\eta} c^\dagger_{k\sigma'\eta} - t^*_{k\sigma'\eta} d_{\sigma'} \\
i\dot{n}_{\sigma'} &= \sum_{k\eta} [-t_{k\sigma'\eta} c^\dagger_{k\sigma'\eta} d_{\sigma'} + t^*_{k\sigma'\eta} d^\dagger_{\sigma'} c_{k\sigma'\eta}]
\end{aligned} \tag{5.3.8}$$

This leads to the following Fourier transformed EOM equations for the time-ordered Green's functions defined in Sec. 5.2.1

$$(\varepsilon - \varepsilon_\sigma) G^t_{\sigma\sigma}(\varepsilon) = 1 + U G^{t(2)}(\varepsilon) + \sum_{k\eta} t^*_{k\sigma\eta} \Xi^{\sigma\sigma}_{k\eta}(\varepsilon) \tag{5.3.9}$$

where $\Xi^{\sigma\sigma}_{k\eta}(\varepsilon)$ is the Fourier transform of $\Xi^{\sigma\sigma}_{k\eta}(t,t') \equiv -i\langle \hat{T} c_{k\sigma\eta}(t) d^\dagger_\sigma(t')\rangle$. Its EOM reads

$$(\varepsilon - \varepsilon_{k\sigma\eta})\Xi^{\sigma\sigma}_{k\eta}(\varepsilon) = t_{k\sigma\eta} G^t_{\sigma\sigma}(\varepsilon) \tag{5.3.10}$$

Putting this back in (5.3.9) leads to

$$[\varepsilon - \varepsilon_\sigma - \Sigma(\varepsilon)] G^t_{\sigma\sigma}(\varepsilon) = 1 + U G^{t(2)}(\varepsilon) \tag{5.3.11}$$

where $\Sigma(\varepsilon)$ is the self-energy due to the coupling to the contacts. In the end, the EOM for $G^{t(2)}$ is needed and with (5.3.8) it becomes

$$(\varepsilon - \varepsilon_\sigma - U) G^{t(2)}(\varepsilon) = \langle n_{\sigma'} \rangle + \sum_{k\eta} \left[t^*_{k\sigma\eta} \Xi^1_{k\eta}(\varepsilon) + t_{k\sigma\eta} \Xi^2_{k\eta}(\varepsilon) - t^*_{k\sigma\eta} \Xi^3_{k\eta}(\varepsilon) \right] \tag{5.3.12}$$

with the Fourier transforms of the following correlation functions

$$\begin{aligned} \Xi^1_{k\eta}(t,t') &\equiv -i\langle \hat{T} c_{k\sigma\eta}(t) n_{\sigma'}(t) d^\dagger_\sigma(t') \rangle \\ \Xi^2_{k\eta}(t,t') &\equiv -i\langle \hat{T} c^\dagger_{k\sigma'\eta}(t) d_\sigma(t) d_{\sigma'}(t) d^\dagger_\sigma(t') \rangle \\ \Xi^3_{k\eta}(t,t') &\equiv -i\langle \hat{T} c_{k\sigma'\eta}(t) d^\dagger_{\sigma'}(t) d_\sigma(t) d^\dagger_\sigma(t') \rangle \end{aligned} \tag{5.3.13}$$

Continuation of the EOM scheme for these new functions would generate higher-order Green's functions so that an infinite number of equations occur. In order to truncate this infinite hierarchy, we carry out an approximation (Hartree-Fock approximation) at this step of the hierarchy, such that the Fourier transform of the first function in (5.3.13) is factorized and the others are neglected

$$\begin{aligned} \Xi^1_{k\eta}(\varepsilon) &\approx \langle n_{\sigma'} \rangle \Xi^{\sigma\sigma}_{k\eta}(\varepsilon) \\ \Xi^2_{k\eta} &= 0 \\ \Xi^3_{k\eta} &= 0 \end{aligned} \tag{5.3.14}$$

Finally, this yields

$$G^t_{\sigma\sigma}(\varepsilon) = \frac{\varepsilon - \varepsilon_\sigma - U(1 - \langle n_{\sigma'} \rangle)}{(\varepsilon - \varepsilon_\sigma)(\varepsilon - \varepsilon_\sigma - U) - \Sigma(\varepsilon)[\varepsilon - \varepsilon_\sigma - U(1 - \langle n_{\sigma'} \rangle)]} \tag{5.3.15}$$

with $\sigma' = -\sigma$. This function exhibits fixed poles at ε_σ and $\varepsilon_\sigma + U$ which leads to the correct form of the DOS in agreement with the considerations in Sec. 5.2.2. Note that there is another way to obtain (5.3.15) (i.e. its retarded version) [GRO91]: one utilizes Dyson's equation (5.1.19) where (5.2.17) enters as the "free" Green's function and (5.2.9) enters as the self-energy for the contact coupling[16].

[16] In Ref. [HAU96] the authors claim that the Hartree-Fock approximation which leads to (5.3.15) corresponds to replacing 0^+ by the self-energy (5.2.9) in (5.2.17). This is only valid for $\langle n_{\sigma'} \rangle \approx 1$, but not in general.

Before the nonlinear current and noise is discussed within the approximation (5.3.14) it is necessary to show that this description is equivalent to a treatment with a bilinear Hamiltonian as demanded for the applicability of the noise expression (5.1.49) [SOU04a]. For that purpose, one can rewrite the Dyson equation (5.1.19) in the form (the energy argument is skipped in the following)

$$\mathbf{G}^{\mathrm{ret}} = [(\tilde{\mathbf{G}}^{\mathrm{ret},0})^{-1} - \mathbf{\Sigma}^{\mathrm{ret},T}]^{-1} \tag{5.3.16}$$

where $\tilde{\mathbf{G}}^{\mathrm{ret},0}$ is given by (5.2.17) containing the Coulomb interaction and $\mathbf{\Sigma}^{\mathrm{ret},T}$ is the self-energy due to tunneling (5.2.9). In order to define a total self-energy $\mathbf{\Sigma}^{\mathrm{ret}}$ which contains both the Coulomb interaction and the coupling to the contacts a "zero"is added in (5.3.16)

$$\mathbf{G}^{\mathrm{ret}} = [(\mathbf{G}^{\mathrm{ret},0})^{-1} - (\mathbf{G}^{\mathrm{ret},0})^{-1} + (\tilde{\mathbf{G}}^{\mathrm{ret},0})^{-1} - \mathbf{\Sigma}^{\mathrm{ret},T}]^{-1} \tag{5.3.17}$$

Then, the self-energy contribution due to Coulomb interaction is defined by $\mathbf{\Sigma}^{\mathrm{ret},C} \equiv (\tilde{\mathbf{G}}^{\mathrm{ret},0})^{-1} - (\mathbf{G}^{\mathrm{ret},0})^{-1}$ and the Dyson equation becomes

$$\mathbf{G}^{\mathrm{ret}} = [(\mathbf{G}^{\mathrm{ret},0})^{-1} - \mathbf{\Sigma}^{\mathrm{ret}}]^{-1} \tag{5.3.18}$$

with the total self-energy $\mathbf{\Sigma}^{\mathrm{ret}} \equiv \mathbf{\Sigma}^{\mathrm{ret},C} + \mathbf{\Sigma}^{\mathrm{ret},T}$, and

$$\begin{aligned} \mathbf{\Sigma}^{\mathrm{ret},C} &= \mathrm{Diag}[\varepsilon - \varepsilon_\uparrow, \varepsilon - \varepsilon_\downarrow] - \mathrm{Diag}\left[\frac{(\varepsilon - \varepsilon_\uparrow)(\varepsilon - \varepsilon_\uparrow - U)}{\varepsilon - \varepsilon_\uparrow - U(1 - \langle n_\downarrow \rangle)}, \frac{(\varepsilon - \varepsilon_\downarrow)(\varepsilon - \varepsilon_\downarrow - U)}{\varepsilon - \varepsilon_\downarrow - U(1 - \langle n_\uparrow \rangle)}\right] \\ &= \mathrm{Diag}\left[\frac{U\langle n_\downarrow \rangle(\varepsilon - \varepsilon_\uparrow)}{\varepsilon - \varepsilon_\uparrow - U(1 - \langle n_\downarrow \rangle)}, \frac{U\langle n_\uparrow \rangle(\varepsilon - \varepsilon_\downarrow)}{\varepsilon - \varepsilon_\downarrow - U(1 - \langle n_\uparrow \rangle)}\right] \end{aligned} \tag{5.3.19}$$

This self-energy due to Coulomb interaction can be obtained by a bilinear Hamiltonian as shown in the following. The starting point is to replace the non-quadratic part of the Hamiltonian (5.1.21) namely $H_{\mathrm{QD}}^U = U n_\uparrow n_\downarrow$ by

$$H_{\mathrm{QD}}^U = \sum_\sigma \chi_\sigma d_\sigma^\dagger d_\sigma + \sum_\sigma \nu_\sigma v_\sigma^\dagger v_\sigma + \sum_{\sigma\sigma'} (t_{\sigma\sigma'}^U v_{\sigma'}^\dagger d_\sigma + \mathrm{h.c.}) \tag{5.3.20}$$

The parameters χ_σ,ν_σ, and $t_{\sigma\sigma'}^U$ have to be determined. The so-introduced bilinear Hamiltonian describes the Coulomb interaction of the QD with annihilation/creation operators $d_\sigma/d_\sigma^\dagger$, resp., as tunneling between the QD and a virtual QD with annihilation/creation operators $v_\sigma/v_\sigma^\dagger$, respectively. With the new Hamiltonian for the full system the respective self-energy is then obtained by EOM following the lines of Sec. 5.2.1. Comparing the resulting self-energy with (5.3.19) gives [SOU04a]

$$\begin{aligned} \chi_\sigma &= U\langle n_{-\sigma}\rangle \\ \nu_\sigma &= \varepsilon_\sigma + U(1-\langle n_{-\sigma}\rangle) \\ |t^U_{\sigma\sigma}|^2 &= U^2\langle n_{-\sigma}\rangle(1-\langle n_{-\sigma}\rangle) \end{aligned} \tag{5.3.21}$$

and finally for the Hamiltonian (5.3.20)

$$\begin{aligned} H^U_{\mathrm{QD}} &= \sum_\sigma U\langle n_{-\sigma}\rangle d^\dagger_\sigma d_\sigma + \sum_\sigma [\varepsilon_\sigma + U(1-\langle n_{-\sigma}\rangle)] v^\dagger_\sigma v_\sigma \\ &\quad + \sum_\sigma U\sqrt{\langle n_{-\sigma}\rangle(1-\langle n_{-\sigma}\rangle)}(e^{i\varphi} d^\dagger_\sigma v_\sigma + \text{h.c.}) \end{aligned} \tag{5.3.22}$$

with an arbitrary phase factor $e^{i\varphi}$. The first term in (5.3.22) corresponds to the mean-field approximation of the last section and the remaining terms give linear corrections. Summarizing these considerations we note that the approximation (5.3.14) is equivalent to a description with a bilinear Hamiltonian so that Eq. (5.1.49) can be used to calculate the noise.

The lesser Green's function is given by (5.3.5) as derived in [CHE90a]. The densities $\langle n_\sigma\rangle$ have to be determined self-consistently by (5.3.3) since the lesser Green's function depends on the densities via the retarded Green's function. Even though the coupled equations for the densities are strongly nonlinear similar to (5.3.7) it turns out that there is always one unique solution of this system of equations in contrast to the the previous section.

Now the current (5.1.36) and the zero-frequency noise (5.1.49) for tunneling through a single level where the spin-degeneracy is lifted by a magnetic field ($\propto \Delta E$) and in the high-bias regime ($f_c = 0$) is discussed. Fig. 5.4 shows the respective results vs. bias voltage ($\propto \varepsilon_\uparrow - \mu_e$) for symmetric contact coupling $\Gamma_e = \Gamma_c = 0.1\Delta E$, temperature $k_B T = \Gamma_{e/c}$, and with Coulomb interaction strength $U/\Delta E = 3$. The normalized average current (a) shows four steps due to the alignment of $\varepsilon_\uparrow$, $\varepsilon_\uparrow + \Delta E$, $\varepsilon_\uparrow + U$, and $\varepsilon_\uparrow + \Delta E + U$ with the emitter chemical potential μ_e. The current plateau heights depend only on the couplings $\Gamma_{e/c}$ and for the i-th plateau in Fig. 5.4a they are

1. $\frac{\Gamma_e\Gamma_c}{\Gamma_e+\Gamma_c}$
2. $\frac{2\Gamma_e\Gamma_c}{2\Gamma_e+\Gamma_c}$
3. $\frac{\Gamma_e\Gamma_c(\Gamma_e+2\Gamma_c)}{(\Gamma_e+\Gamma_c)^2}$
4. $\frac{2\Gamma_e\Gamma_c}{\Gamma_e+\Gamma_c}$

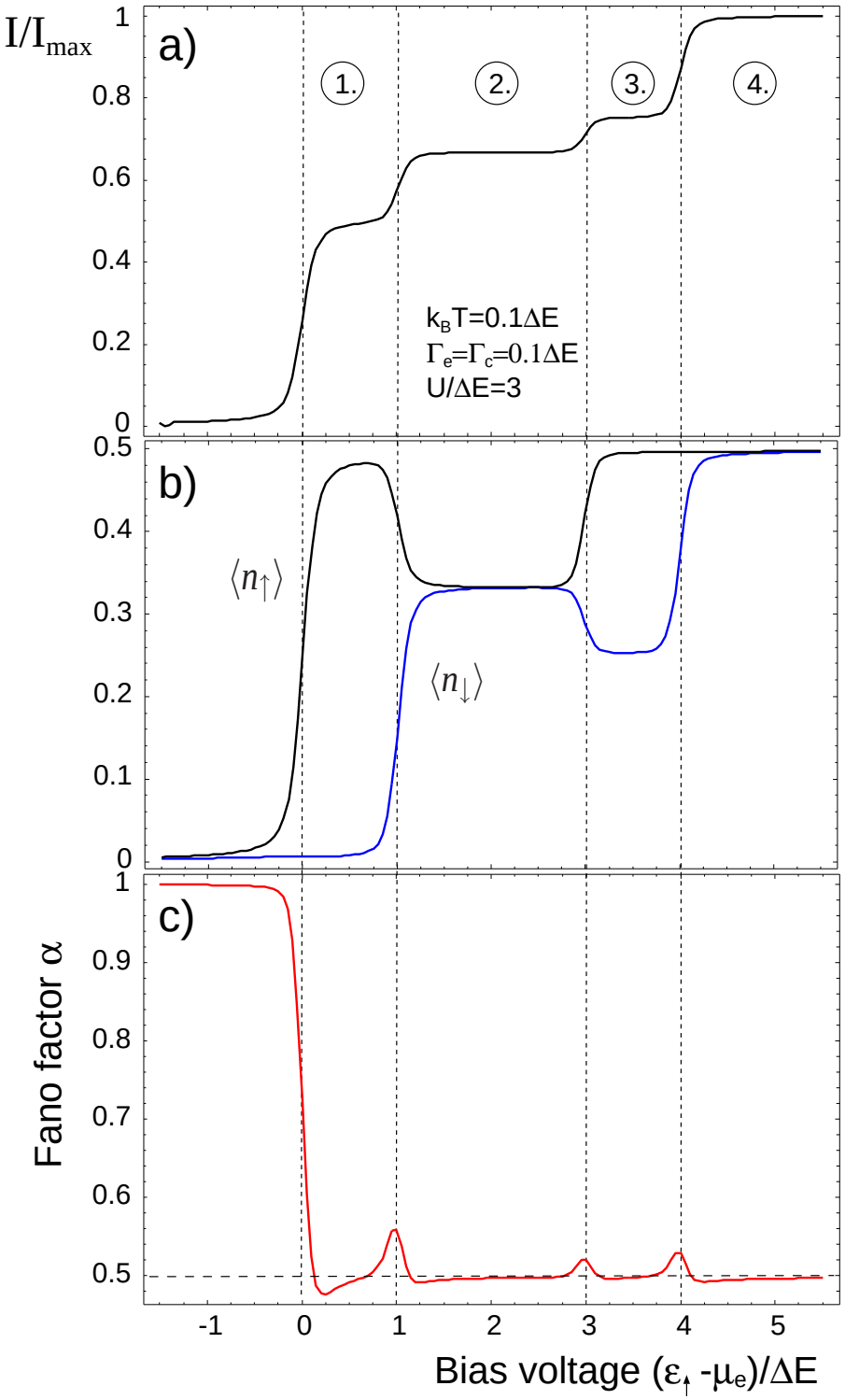

Figure 5.4.: a) Normalized current vs. bias voltage $\propto \varepsilon_\uparrow - \mu_e$. b) Electron densities $\langle n_{\uparrow/\downarrow} \rangle$ vs. bias voltage. c) Fano factor α vs. bias voltage. $\Delta E = \varepsilon_\downarrow - \varepsilon_\uparrow$. Charging energy $U = 3\Delta E$. Temperature $k_B T = 0.1\Delta E$. Symmetric barriers: $\Gamma_e = \Gamma_c = 0.1\Delta E$.

This current plateau behavior and the step positions are in agreement with the results of the sequential tunneling model in Sec. 4.2.1, particularly Fig. 4.5, just like the self-consistently determined densities $\langle n_{\uparrow/\downarrow}\rangle$ shown in the middle panel of Fig. 4.5 which can be compared with the sequential treatment by $\langle n_\uparrow\rangle = P_{(1,0)} + P_{(1,1)}$ and $\langle n_\uparrow\rangle = P_{(0,1)} + P_{(1,1)}$. Up to now, we notice that the algorithm to describe nonlinear coherent transport through a QD considered in this section is the approximation scheme one has to deal with in lowest-order to obtain reasonable results for the densities and consequently for the current for $k_BT \simeq \Gamma$. The respective Fano factor vs. bias voltage is shown in Fig. 5.4c. We already noticed that on the plateaus the sequential (Sec. 4.2.1) and coherent description provide identical results for the current. We conjecture without a proof that this should also hold for the noise. We recall the results for the Fano factor from Sec. 4.2.1 (Fig. 4.5b) for the i-th plateau

1. $\frac{\Gamma_e^2+\Gamma_c^2}{(\Gamma_e+\Gamma_c)^2}$
2. $\frac{4\Gamma_e^2+\Gamma_c^2}{(2\Gamma_e+\Gamma_c)^2}$
3. $\frac{\Gamma_e^3+\Gamma_c^3+3\Gamma_e^2\Gamma_c}{(\Gamma_e+\Gamma_c)^3}$
4. $\frac{\Gamma_e^2+\Gamma_c^2}{(\Gamma_e+\Gamma_c)^2}$

The Fano factor on the first and fourth plateau in Fig. 5.4c is one half which is obviously correct since symmetric coupling was assumed. The second and third plateau corresponds to Coulomb correlated tunneling (compare discussions in Sec. 4.2.1). In Fig. 5.4c the Fano factor appears to be one half in these bias regions which conflicts with the sequential tunneling result. Although we ensured that the approximations which lead to the noise expression (5.1.49) and the approximation (5.3.14) are consistent with each other, the actual reason for the observed discrepancy is unclear yet. A very likely explanation could be that the approximation (5.3.14) neglects quantum fluctuations due to the Coulomb interaction (In fact, the Fano factor on the second and third plateau in Fig. 5.4 refers only to Pauli's exclusion principle.). In the mean-field approximation (5.3.1) in Sec. 5.3.1 the fluctuations of the occupations were explicitly removed. We expect something similar here. Hence, in order to avoid this difficulty we believe one has to go beyond approximation (5.3.14), e.g. one applies the EOM technique to the second-order Green's functions (5.3.13) and factorizes the generated third-order functions [HAU96]. But then, the question arises which lesser Green's function to calculate the densities has to be used - (5.3.5) does not work here anymore. E.g. in [MEI93] the authors take the densities from a completely different approach. A better substantiated procedure is proposed by Niu et al. [NIU99] who apply the EOM to obtain the lesser Green's function. Furthermore, it is not clear whether the noise formula (5.1.49) with approximation (5.1.46) is then still applicable. Zhu et al.[ZHU02, ZHU03] claim that (5.1.49) has a bigger range of validity than (5.1.46)

would imply. In order to avoid the approximation (5.1.46) one has to carry out the analytical continuation of the two-particle Green's function in (5.1.48). This is a really cumbersome and tedious task. The two-particle Green's function which then enters the final noise expression can be obtained e.g. by the EOM as elaborately performed above.

Related literature:

- [HER92a]: The authors derive an expression for the noise starting from the Anderson Hamiltonian (5.1.21) by means of the Keldysh formalism which is valid for arbitrary interaction in the QD as they claim. For its evaluation they use the approximation scheme for the Green's functions we discussed in Sec. 5.3.1 which is not convenient for the description of nonlinear transport as we showed there. It would be very interesting to utilize the approximation of the present section to calculate the noise within the framework of [HER92a].

- [YAM94]: The current and the noise are derived in second-order tunnel coupling to the contacts (5.1.24). The noise is discussed separately for its equilibrium (Johnson-Nyquist noise) and non-equilibrium components (shot noise). A direct comparison with our method due to the perturbative character of their results cannot be drawn.

- [WAN98a]: The authors calculate the noise in the frame of Keldysh formalism for a one-dimensional double-barrier structure which one can associate with a QD coupled to a quantum wire. They also use the Hartree approximation (5.3.1) considering the noise in the linear response regime with the typical Coulomb oscillations in the resulting current. At the current peaks the equilibrium noise vanishes for zero temperature and symmetric barriers in contrast to the consideration of equilibrium noise for double barrier tunneling in Sec. 4.1.2. In a simple noninteracting picture where the noise is proportional to $T(1-T)$ with the transmission function T being unity for symmetric barriers the noise vanishes. Nevertheless for zero temperature the Hartree approximation cannot be applied since Kondo correlations take place. Furthermore, their nonlinear transport results are questionable because of the already mentioned problems.

- A very recent work uses a diagrammatic technique [KOE98] which allows to calculate the current and the noise perturbatively order by order. The first-order perturbation agrees with our results presented in Sec. 4.2.1 [THI03] and the second-order results can be found in [THI04a] which provide really interesting behavior: They consider a situation where they start from an initially occupied QD (not considered here). Then the transport below the current onset is governed by co-tunneling processes and the shot noise is super-Poissonian there.

5.4. Tunnel-coupled noninteracting quantum dots

In this section we consider the noise for tunneling through a stack of coupled QDs which we already discussed in Sec. 3.3. Thereby we concentrate on the noninteracting case. The consideration of the Coulomb interaction for this system in the

approximation scheme of Sec. 5.3.2 is an extensive task and still in progress - first steps can be found in [GNO04]. One of the difficulties is the calculation of the lesser Green's function. It turns out that (5.3.5) which worked for the single QD system cannot be utilized here since the non-equilibrium occupation function F of the QDs is unknown[17].

For noninteracting electrons the Green's functions read in particular

$$G^{\mathrm{ret/adv}}(\varepsilon) = \left[\varepsilon\mathbb{1} - H - \Sigma^{\mathrm{ret/adv}}\right]^{-1} \tag{5.4.1}$$

being Dyson's equation with the Hamiltonian for the coupled QDs without coupling to any contacts as

$$H = \begin{pmatrix} \varepsilon_1 & \Omega^* \\ \Omega & \varepsilon_2 \end{pmatrix} \tag{5.4.2}$$

For simplicity we consider non-degenerate single-particle levels $\varepsilon_1/\varepsilon_2$ for QD1/QD2, respectively, and their mutual coupling Ω. The retarded/advanced selfenergy for the contact coupling in (5.4.1) is then given by (5.2.9)

$$\Sigma^{\mathrm{ret/adv}} = \begin{pmatrix} \pm i\Gamma_e/2 & 0 \\ 0 & \pm i\Gamma_c/2 \end{pmatrix} \tag{5.4.3}$$

In order to obtain the lesser/greater Green's function by means of the Keldysh relation (5.1.20) $G^{</>}(\varepsilon) = G^{\mathrm{ret}}(\varepsilon)\Sigma^{</>}(\varepsilon)G^{\mathrm{adv}}(\varepsilon)$ the lesser/greater selfenergies are for high-bias $f_e = 1$ and $f_c = 0$ (5.2.10)

$$\begin{aligned} \Sigma^{<}(\varepsilon) &= \begin{pmatrix} i\Gamma_e & 0 \\ 0 & 0 \end{pmatrix} \\ \Sigma^{>}(\varepsilon) &= \begin{pmatrix} 0 & 0 \\ 0 & -i\Gamma_c \end{pmatrix} \end{aligned} \tag{5.4.4}$$

The average current provides the same result as the ME and the density matrix description (3.3.5) outlined in Sec. 3.3.2.1. Utilizing Eq. (5.1.49) we obtain the SPD which is shown in Fig. 5.5a as a function of the coupling between the QDs $|\Omega|$ (red curve) for on-resonance transport $\varepsilon_1 = \varepsilon_2$ and symmetric coupling $\Gamma_e = \Gamma_c$. A pronounced local minimum in S_P is present at $\Omega \approx \Gamma/2$. This value corresponds to the highest transparency for electrons traversing the QD system[18]. This can be seen in the inset of Fig. 5.5 where the transmission function $T_{ec}^{\max}$ (first line in Eq. (6.4.8))

[17] In Ref. [PAL96] such a function was proposed without a derivation which yields wrong results for the densities.

[18] In some sense it corresponds to the phenomenon of critical damping in the damped harmonic oscillator.

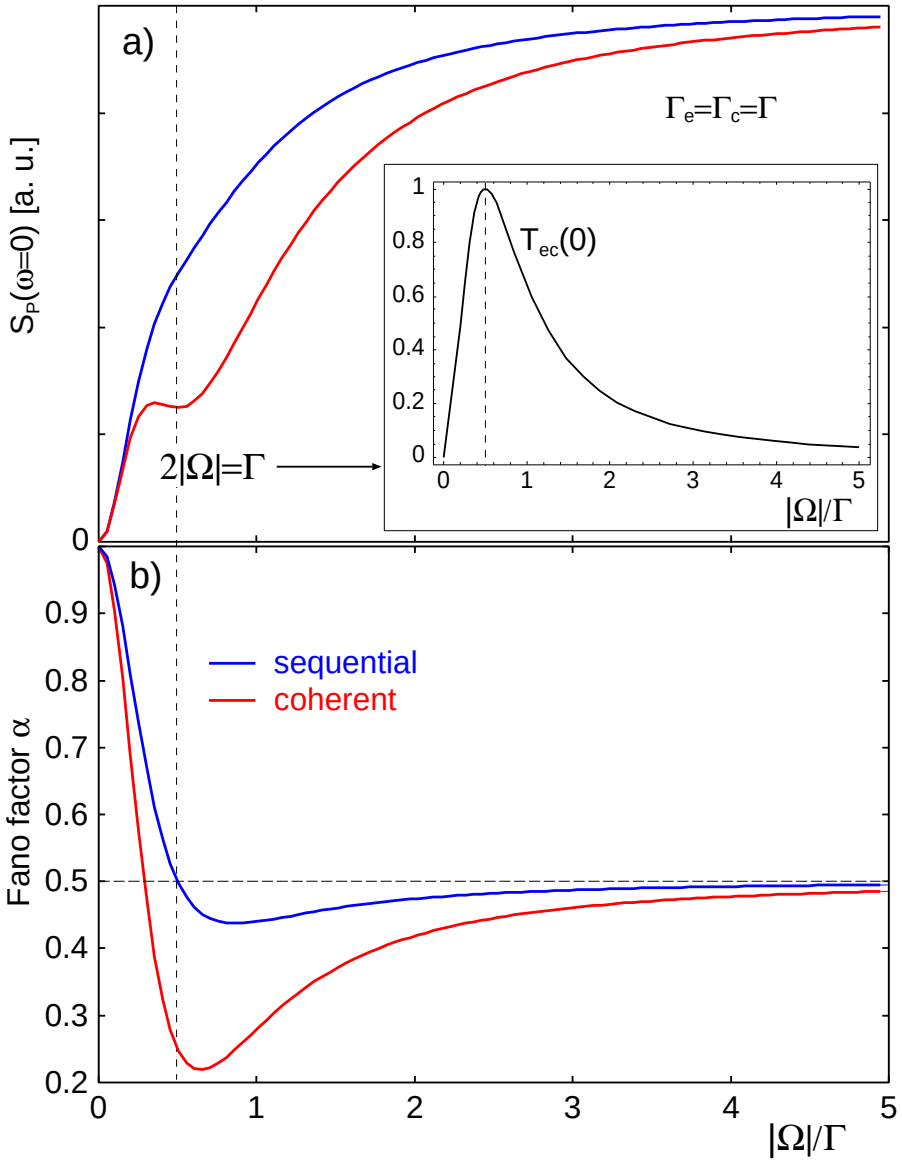

Figure 5.5.: a) Zero-frequency spectral power density S_P, b) Fano factor α vs. tunnel coupling Ω with ME (blue curves) and NEGF (red curves), Inset in a): Transmission function at $\varepsilon = 0$. Symmetric contact coupling $\Gamma_e = \Gamma_c$, on-resonance $\varepsilon_1 = \varepsilon_2$. Inset of b) see text.

is plotted. We compare this with the noise calculated for sequential tunneling along the lines of Sec. 4.1.1 (blue curve in Fig. 5.5). For small and large Ω the sequential and coherent tunneling noise merge. In those regimes the zero-frequency SPD is not able to give information about coherence in the tunneling current. For intermediate couplings the noise in both descriptions deviates - the sequential tunneling SPD is monotonically increasing for all $|\Omega|$. This result is very interesting for two reasons:

i) The SPD for small frequencies which is associated with the long time behavior of the auto-correlation function is already sensitive to coherence in the tunneling process. In [SUN99] and [AGU04] the full spectrum of tunneling through a coupled QD system was studied[19] - at the frequency of the coherent Rabi oscillations $2|\Omega|$ an additional noise suppression in form of a dip occurs which is a clear indication of coherence. Nevertheless the low-frequency noise is easier to measure in experiments and therefore worth to analyze in this respect.

ii) Zero-frequency current fluctuations can serve as a sensitive indicator for the investigation of decoherence in the tunneling process. This statement provides the base for the considerations in Chap. 6 and 7

The corresponding Fano factors were obtained analytically for symmetric coupling $\Gamma \equiv \Gamma_e = \Gamma_c$ and on-resonance transport $\varepsilon_1 = \varepsilon_2$ as

$$\alpha_{\mathrm{NEGF}} = \frac{\Gamma^4 - 2\Gamma^2|\Omega|^2 + 8|\Omega|^4}{(4|\Omega|^2 + \Gamma^2)^2} \tag{5.4.5}$$

for coherent tunneling (in agreement with [KOH04] where the authors used Eq. (6.2.6)) and

$$\alpha_{\mathrm{ME}} = \frac{\Gamma^4 + 2\Gamma^2|\Omega|^2 + 8|\Omega|^4}{(4|\Omega|^2 + \Gamma^2)^2} \tag{5.4.6}$$

for sequential tunneling. Both are plotted as a function of tunnel coupling $|\Omega|$ in Fig. 5.5b. For $|\Omega| \ll \Gamma$ the tunneling through the QDs follows Poissonian statistics corresponding to $\alpha = 1$, i.e. for weak coupling the transport is well described by sequential tunneling (see discussion in Sec. 3.3.2.1). For increasing $|\Omega|$ negative correlations take place so that the Fano factors decrease. At $2|\Omega| = \Gamma$ (corresponding to $\Gamma_{\mathrm{inter}} = \Gamma/2$) the Fano factor for sequential tunneling is one half and for coherent tunneling it becomes one quarter. Associating the Fano factor with the charge which is effectively transferred through the system [ELA02] this corresponds to tunneling of half and quarter elementary charges, respectively. For the latter we will show in Sec. 7.3.2 that the respective statistics of tunneling events becomes

[19] They did not study the zero-frequency SPD in detail.

even Poissonian. There is a minimum of the sequential tunneling Fano factor at some higher coupling $|\Omega|/\Gamma = \sqrt{3}/2$ which gets slightly below one half[20].

For coherent tunneling the strong suppression of the Fano factor below one half clearly refers to quantum noise [21].

For $|\Omega| \gg \Gamma$ the Fano factor of one half is approached in both descriptions. In the coherent picture the coupled QD system (triple-barrier system) behaves as a double-barrier system with the two extended states being the eigenstates of the Hamiltonian (5.4.2) with the separation energy $2|\Omega|$. For large Ω there are two independent channels which are available for transport and Pauli's exclusion principle induces the corresponding negative correlations for them.

For asymmetric contact couplings $\Gamma_e \neq \Gamma_c$ there is an interesting effect which we already noticed in the noise of sequential tunneling in Fig. 4.12. For symmetric coupling the maximum noise suppression appears for on-resonance transport $\Delta E = 0$. It turns out that at a certain ratio of the contact couplings $\Gamma_c/\Gamma_e < 1$ the maximum suppression starts to exhibit at the edges of the resonance so that a local maximum of the Fano factor for $\Delta E = 0$ arises as it can be seen in Fig. 5.6. This ratio depends on the tunnel coupling between the QDs $|\Omega|$: for $|\Omega| = \Gamma_e$ it is around 0.3 (Fig. 5.6a) and for $|\Omega| = 0.5\Gamma_e$ it is almost 0.2 (Fig. 5.6b). I.e. the larger $|\Omega|$ the larger the respective treshold ratio is. This behavior also emerges in the sequential tunneling description (Fig. 4.12) which should provide us a picture to understand this effect at least qualitatively. This will be addressed in the future.

[20] This was also observed in [EGU94] in a similar context.

[21] H. Sprekeler proposed to utilize a description by *piecewise deterministic processes* [BRE02] wherein one could consider the tunneling between the QDs as deterministic and the coupling to the contacts as stochastic process. The combination should give a better understanding of quantum noise.

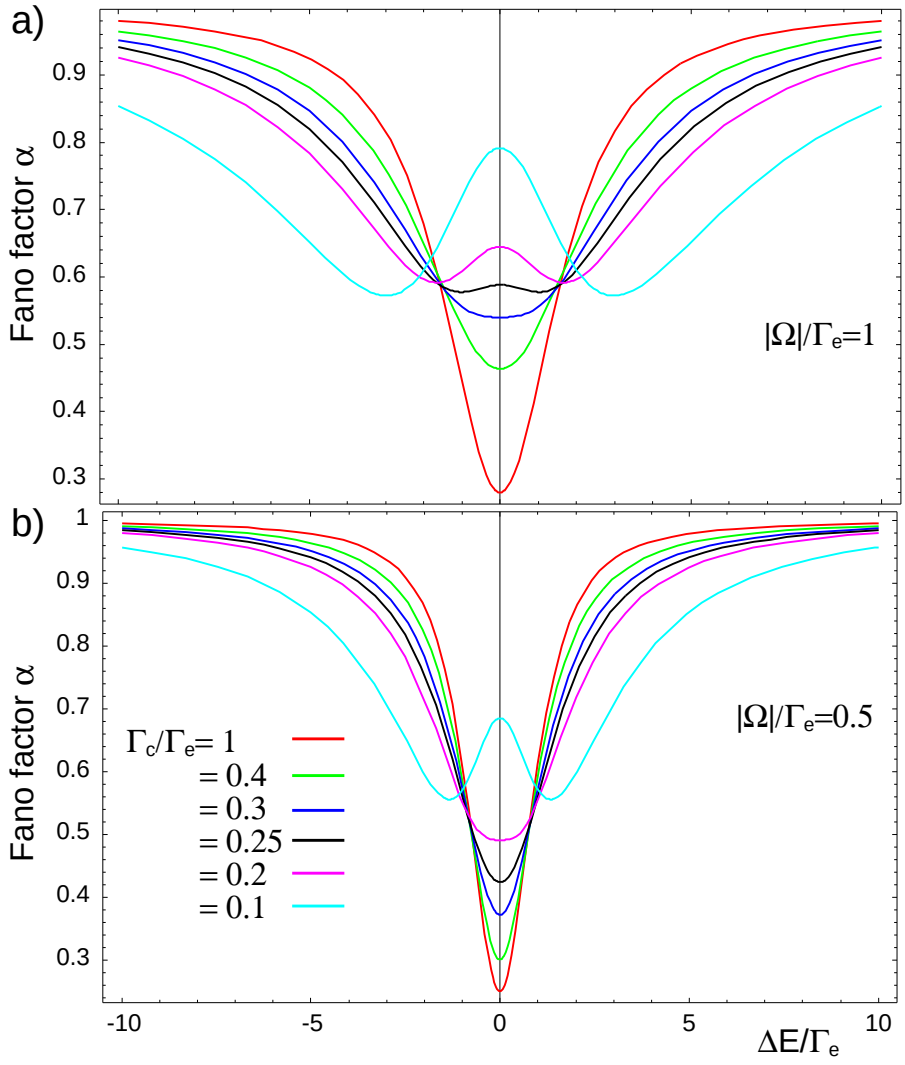

Figure 5.6.: Fano factor vs. level separation $\Delta E = \varepsilon_1 - \varepsilon_2$ for various asymmetric contact couplings. a) $\Omega/\Gamma_e = 1$, b)$\Omega/\Gamma_e = 0.5$.

6. Dephasing

In this chapter the influence of dephasing on the average current and the noise in tunneling through single and tunnel-coupled QDs is studied. In the previous chapters the limits of fully incoherent (sequential) and fully coherent transport through QDs were examined. In particular, for tunnel-coupled QDs without Coulomb interaction it was observed that the average current turns out to be the same in both descriptions (see Sec. 3.3.2). In contrast, the shot noise is different for intermediate couplings between the QDs (see Sec. 5.4). One of the aims of the present chapter is to examine the possibility of a continuous transition from the coherent to the incoherent tunneling noise. For that purpose, we will mainly utilize the SMF. Within this approach dephasing can be treated phenomenologically by attaching additional fictitious terminals to the QD system. The underlying escape model will be briefly reviewed. For the consideration of the shot noise we will show that it is very crucial how to implement the fictitious terminals in the calculation. The corresponding results will be compared with the findings of other formalisms.

6.1. Escape model

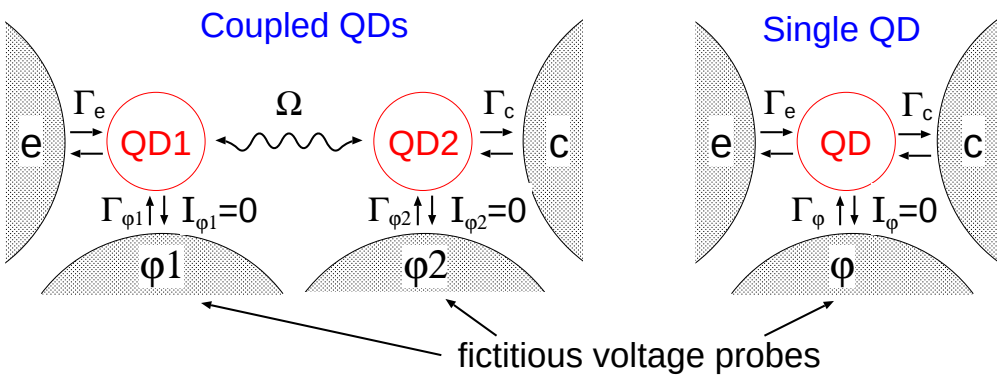

Figure 6.1.: Coupled QD system and single QD with fictitious voltage probes.

Here, the dephasing is introduced by fictitious voltage probes [BUE86a, BUE88, DAT95] as depicted in Fig. 6.1. QDs 1/2 (left picture) and the single QD (right picture) are coupled to (e)mitter/(c)ollector contacts with constant rates $\Gamma_{e/c}$, respectively, and QDs 1/2 are mutually coupled with the tunnel matrix element Ω.

Furthermore, QD 1/2 and the single QD are connected to fictitious terminals $\varphi 1/\varphi 2$ and φ, respectively, with dephasing rates $\Gamma_{\varphi 1/\varphi 2}$ and Γ_{φ}. The key concept is that a particle can be scattered out from the current carrying state into these fictitious terminals and gets reinjected. This justifies the term "escape model". During this scattering process the phase information gets lost and the actual coherent process of particle transfer through the QD system "dephases"partially depending on the dephasing rate Γ_{φ}. At first glance this seems purely phenomenological. But, as shown later in this chapter, it can be substantiated by real electron-phonon scattering processes at least in lowest order perturbation theory. Conceptionally important is the fact that the particle exchange of the QDs with those terminals only takes place under the condition that the respective net current vanishes: $I_{\varphi 1/\varphi 2} = 0$ and $I_{\varphi} = 0$.

6.2. Scattering matrix approach: Current and noise

In order to calculate the current fluctuations we use the scattering matrix formalism (SMF) introduced by Büttiker [BUE92, BLA00]. The expression for the average current at terminal α is

$$\langle I_\alpha \rangle = \frac{e}{h} \sum_{\beta\gamma} \sum_{mn} \int d\varepsilon \, A^{mn}_{\beta\gamma}(\alpha, \varepsilon) \delta_{\beta\gamma} \delta_{mn} f_\beta(\varepsilon) \tag{6.2.1}$$

with the spectral function

$$A^{mn}_{\beta\gamma}(\alpha, \varepsilon) \equiv \delta_{mn}\delta_{\alpha\beta}\delta_{\alpha\gamma} - s^{\dagger}_{\alpha\beta}(m, \varepsilon) s_{\alpha\gamma}(n, \varepsilon) \tag{6.2.2}$$

where $s_{\alpha\beta}(n, \varepsilon)$ denotes an element of the S-matrix s and describes the energy dependent scattering of a mode n from terminal α to terminal β; f_β denotes the distribution function in terminal β. The zero-frequency spectral power density reads

$$S_{\alpha\beta}(0) = \frac{2e^2}{h} \sum_{\gamma\delta} \sum_{mn} \int d\varepsilon \, A^{mn}_{\gamma\delta}(\alpha, \varepsilon) A^{mn}_{\delta\gamma}(\beta, \varepsilon) f_\gamma(\varepsilon)[1 - f_\delta(\varepsilon)] \tag{6.2.3}$$

Before we study the influence of dephasing let us consider a two-terminal QD system, i.e. without fictitious voltage-probes. Then the S-matrix is simply given by (single-mode: $m = n = 1$)

$$s = \begin{pmatrix} r & t \\ t & r \end{pmatrix} \tag{6.2.4}$$

where r/t is the reflection/transmission coefficient, respectively, for the full QD system (chosen to be equal for forward and backward scattering). Using (6.2.1) one obtains the current

$$\begin{aligned}\langle I_e\rangle &= \frac{e}{h}\int d\varepsilon\,[A_{ee}(e,\varepsilon)f_e(\varepsilon)+A_{cc}(e,\varepsilon)f_c(\varepsilon)]\\ &= \frac{e}{h}\int d\varepsilon\,[T_{ec}(\varepsilon)(f_e(\varepsilon)-f_c(\varepsilon))]\end{aligned}\tag{6.2.5}$$

($T_{ec}(\varepsilon)\equiv tt^*$). The noise (6.2.3) becomes

$$\begin{aligned}S_{ee}(0) &= \frac{2e^2}{h}\int d\varepsilon\,\big\{A_{ee}(e,\varepsilon)^2 f_e(\varepsilon)[1-f_e(\varepsilon)]+A_{ec}(e,\varepsilon)A_{ce}(e,\varepsilon)f_e(\varepsilon)[1-f_c(\varepsilon)]\\ &\quad +A_{ce}(e,\varepsilon)A_{ec}(e,\varepsilon)f_c(\varepsilon)[1-f_e(\varepsilon)]+A_{cc}(e,\varepsilon)^2 f_c(\varepsilon)[1-f_c(\varepsilon)]\big\}\\ &= \frac{2e^2}{h}\int d\varepsilon\,\{T_{ec}(\varepsilon)[f_e(\varepsilon)(1-f_e(\varepsilon))+f_c(\varepsilon)(1-f_c(\varepsilon))]+\\ &\quad +T_{ec}(\varepsilon)[1-T_{ec}(\varepsilon)][f_e(\varepsilon)-f_c(\varepsilon)]^2\big\}\end{aligned}\tag{6.2.6}$$

This is the well-known zero-frequency spectral power density for a two terminal conductor with transmission $T_{ec}(\varepsilon)$ [BLA00]. Here, the first two terms correspond to equilibrium noise (thermal noise, see also Sec. 4.1.2) and the third term is the non-equilibrium or shot noise contribution. Due to its structure[1] $T(1-T)$ or TR with the reflection $R=1-T$ it is also called partition noise since the scatterer divides the incident carrier stream in two streams: the reflected and the transmitted one.

6.2.1. Scattering matrix for quantum dot systems

Here we consider the S-matrix for the system with dephasing, i.e. we include the fictitious voltage-probes (Fig. 6.1).

A preliminary discussion for the implementation of dephasing in the S-matrix approach is necessary. Caution has to be taken since the reinjection of a dephased particle in the conductor from a fictitious terminal also randomizes the momentum, i.e. the particle can go in different directions with the same probability. This momentum relaxation provides an additional resistance in the conductor which is not desired. One can introduce phase-relaxation without introducing any momentum-relaxation by using a unidirectional pair of fictitious voltage probes (see Fig. 6.2) as outlined in Refs. [BUE88, DAT95]. The idea is that those probes reinject particles in the opposite direction from where they came from in order to preserve the sense of current flow.

The S-matrix for such a twin-probe configuration can be written as [BUE88]

[1] More fundamentally discussed in Sec. 7.1.

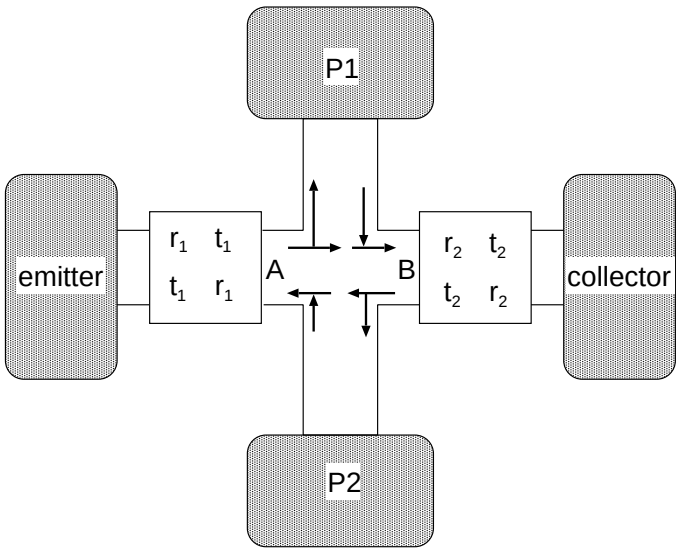

Figure 6.2.: Twin-probe configuration for dephasing in a double-barrier system [DAT95].

$$s_{\text{dephas}} = \begin{pmatrix} 0 & \sqrt{1-\epsilon} & \sqrt{\epsilon} & 0 \\ \sqrt{1-\epsilon} & 0 & 0 & \sqrt{\epsilon} \\ \sqrt{\epsilon} & 0 & 0 & -\sqrt{1-\epsilon} \\ 0 & \sqrt{\epsilon} & -\sqrt{1-\epsilon} & 0 \end{pmatrix} \tag{6.2.7}$$

This matrix connects the four incoming amplitudes with the four outgoing amplitudes at the terminals A, B, P1 and P2 (for a double-barrier system shown in Fig. 6.2). The parameter $\epsilon \in [0, 1]$ characterizes the coupling strength of the terminals P1, P2 to the conductor and is later related to the inelastic scattering rate Γ_φ. It ranges from complete coherence $\epsilon = 0$ to complete incoherence $\epsilon = 1$. Note, that the signs of the matrix elements are chosen such that the S-matrix is unitary.

In order to obtain the full S-matrix of the double-barrier system with dephasing as sketched in Fig. 6.2 connecting the emitter, collector, P1 and P2 terminals one has to combine the S-matrices of the barriers $i = 1, 2$

$$s_i = \begin{pmatrix} r_i & t_i \\ t_i & r_i \end{pmatrix} \tag{6.2.8}$$

(r_i is the reflection coefficient, t_i is the transmission coefficient) and the S-matrix (6.2.7) such that the terminals A and B are eliminated. After a lengthy straightforward calculation one obtains

$$s = \frac{1}{Z}\begin{pmatrix} r_1 Z + \alpha^2 r_2 t_1 t_1 & \alpha t_1 t_2 & \beta t_1 & \alpha\beta r_2 t_1 \\ \alpha t_1 t_2 & r_2 Z + \alpha^2 r_1 t_2 t_2 & \alpha\beta r_1 t_2 & \beta t_2 \\ \beta t_1 & \alpha\beta r_1 t_2 & \beta^2 r_1 & -\alpha(1 - r_1 r_2) \\ \alpha\beta r_2 t_1 & \beta t_2 & -\alpha(1 - r_1 r_2) & \beta^2 r_2 \end{pmatrix} \quad (6.2.9)$$

with $Z \equiv 1 - \alpha^2 r_1 r_2$, $\alpha \equiv \sqrt{1-\epsilon}$, and $\beta \equiv \sqrt{\epsilon}$. Then, the transmission from terminal m to n can be calculated by

$$T_{mn} = |s_{mn}|^2 \quad (6.2.10)$$

The full transmission through the system (Fig. 6.2) can be separated into the coherent part and the incoherent part (sequential tunneling) [BUE86a]:

$$T = T_{\text{coh}} + T_{\text{incoh}} \quad (6.2.11)$$

Using (6.2.9) the coherent part yields

$$T_{\text{coh}} = |s_{12}|^2 = \frac{(1-\epsilon) T_1 T_2}{|Z|^2} \quad (6.2.12)$$

with $T_{1/2} \equiv |t_{1/2}|^2$. The incoherent part can be formulated with the help of rates for forward and backward scattering due to the fictitious probes: S_f and S_b, respectively, [BUE86a]

$$T_{\text{incoh}} = \frac{S_b S_f}{S_b + S_f} \quad (6.2.13)$$

S_b is the transmission probability for an electron emerging from the inelastic scatterer to traverse the conductor backward against the direction of carrier flow. S_f is the transmission probability for a carrier emerging form the inelastic scatterer to traverse the sample forward in the direction of current flow. Hence, S_b is given by

$$\begin{aligned} S_b &= T_{P2e} + T_{P1e} = |s_{31}|^2 + |s_{41}|^2 \\ &= \frac{\epsilon T_1}{|Z|^2}\left[1 + (1-\epsilon) R_2\right] \end{aligned} \quad (6.2.14)$$

Analogously for S_f:

$$\begin{aligned} S_f &= T_{P2c} + T_{P1c} = |s_{42}|^2 + |s_{32}|^2 \\ &= \frac{\epsilon T_2}{|Z|^2}\left[1 + (1-\epsilon) R_1\right] \end{aligned} \quad (6.2.15)$$

with $R_i = 1 - T_i$ $(i = 1, 2)$.

For $\epsilon = 0$ one recovers the well-known result for the coherent transmission through two barriers

$$\begin{aligned} T_{\epsilon=0} &= \left| \frac{t_1 t_2}{1 - r_1 r_2} \right|^2 \\ &= \frac{T_1 T_2}{1 + R_1 R_2 - 2\sqrt{R_1 R_2}\cos(\Phi)} \end{aligned} \tag{6.2.16}$$

Here, Φ is the phase shift acquired in one round-trip between the barriers.

For $T_{1/2} \ll 1$ and the assumption of energies ε only close to the resonances ($\Phi(\varepsilon_r) = 2\pi n$) this can be rewritten in a Breit-Wigner form:

$$T_{ec}(\varepsilon) = \frac{\Gamma_e \Gamma_c}{(\varepsilon - \varepsilon_r)^2 + \left(\frac{\Gamma_e + \Gamma_c}{2}\right)^2} \tag{6.2.17}$$

with $\Gamma_{e/c} = \hbar\nu T_{1/2}$ where ν is the attempt frequency defined by $\hbar\nu = \frac{d\varepsilon}{d\Phi}$ (for a square well it is $\nu = \frac{v}{2w}$ with the electron velocity v given by the confinement energy and the well width w).

Now, the question arises whether it is possible to obtain such an expression for $\epsilon > 0$ and whether one can relate the parameter ϵ to the dephasing rate Γ_φ. Following the lines of the Appendices in Ref. [BUE88] one allows for a complex Φ (complex energy). Then the amplitude Z vanishes at the complex energy $\varepsilon = \varepsilon_r - i(\Gamma_e + \Gamma_c + \Gamma_\varphi)/2$. Here, the elastic width is given by

$$\Gamma_e + \Gamma_c = -\hbar\nu \log(R_1 R_2) \tag{6.2.18}$$

and the dephasing width becomes

$$\Gamma_\varphi = -2\hbar\nu \log(1 - \epsilon) \tag{6.2.19}$$

In the limit $\mathcal{O}(\epsilon) = \mathcal{O}(T_1) = \mathcal{O}(T_2) \ll 1$ the Breit-Wigner formula yields generally (Appendix C in [BUE88])[2]

$m \neq n$:

$$|s_{mn}|^2 = \frac{\Gamma_m \Gamma_n}{(\varepsilon - \varepsilon_r)^2 + \frac{\Gamma^2}{4}} \tag{6.2.20}$$

$m = n$:

$$|s_{mn}|^2 = \frac{(\varepsilon - \varepsilon_r)^2 + (\frac{\Gamma}{2} - \Gamma_n)^2}{(\varepsilon - \varepsilon_r)^2 + \frac{\Gamma^2}{4}} \tag{6.2.21}$$

with $\Gamma = \sum_n \Gamma_n$ enclosing the inelastic width $\Gamma_\varphi = \hbar\nu\epsilon$ (consistent with (6.2.19) for $\epsilon \ll 1$).

[2]Note, that Eq. (6.2.21) corrects Eq. (C5) in [BUE88] where a prefactor 2 is missing.

6.3. Single quantum dot

Here we calculate the current and noise for the single QD geometry shown in Fig. 6.1: The current (6.2.1) is

$$\langle I_e \rangle^{\varphi} = \frac{e}{h} \int d\varepsilon \left\{ [1 - |s_{ee}|^2] f_e(\varepsilon) - |s_{e\varphi}|^2 f_{\varphi} - |s_{ec}|^2 f_c(\varepsilon) \right\} \tag{6.3.1}$$

where the second term stems from the fictitious voltage probe φ. Using (6.2.20) and (6.2.21) one obtains

$$\langle I_e \rangle^{\varphi} = \frac{e}{h} \int d\varepsilon \left\{ \frac{\Gamma_e \Gamma_c}{(\varepsilon - \varepsilon_r)^2 + \left(\frac{\Gamma_e + \Gamma_c + \Gamma_{\varphi}}{2} \right)^2} [f_e(\varepsilon) - f_c(\varepsilon)] \right.$$
$$\left. + \frac{\Gamma_e \Gamma_{\varphi}}{(\varepsilon - \varepsilon_r)^2 + \left(\frac{\Gamma_e + \Gamma_c + \Gamma_{\varphi}}{2} \right)^2} [f_e(\varepsilon) - f_{\varphi}(\varepsilon)] \right\} \tag{6.3.2}$$

or more clearly arranged

$$\langle I_e \rangle^{\varphi} = \frac{e}{h} \int d\varepsilon \left\{ T_{ec}(\varepsilon) [f_e(\varepsilon) - f_c(\varepsilon)] + T_{e\varphi} [f_e(\varepsilon) - f_{\varphi}(\varepsilon)] \right\} \tag{6.3.3}$$

What does the noise (6.2.3) look like? The (lengthy) answer for zero-temperature is

$$
\begin{aligned}
S^{\varphi}_{ee}(0) &= \frac{2e^2}{h}\int d\varepsilon \\
&\quad \{A_{e\varphi}(e,\varepsilon)A_{\varphi e}(e,\varepsilon)f_e(\varepsilon)[1-f_\varphi(\varepsilon)] \\
&\quad +A_{\varphi e}(e,\varepsilon)A_{e\varphi}(e,\varepsilon)f_\varphi(\varepsilon)[1-f_e(\varepsilon)] \\
&\quad +A_{c\varphi}(e,\varepsilon)A_{\varphi c}(e,\varepsilon)f_c(\varepsilon)[1-f_\varphi(\varepsilon)] \\
&\quad +A_{\varphi c}(e,\varepsilon)A_{c\varphi}(e,\varepsilon)f_\varphi(\varepsilon)[1-f_c(\varepsilon)] \\
&\quad +A_{\varphi\varphi}(e,\varepsilon)^2 f_\varphi(\varepsilon)[1-f_\varphi(\varepsilon)] \\
&\quad +A_{ec}(e,\varepsilon)A_{ce}(e,\varepsilon)f_e(\varepsilon)[1-f_c(\varepsilon)] \\
&\quad +A_{ce}(e,\varepsilon)A_{ec}(e,\varepsilon)f_c(\varepsilon)[1-f_e(\varepsilon)]\} \qquad (6.3.4) \\
&= \frac{2e^2}{h}\int d\varepsilon \\
&\quad \big\{|s_{ee}|^2|s_{e\varphi}|^2[f_e(\varepsilon)(1-f_\varphi(\varepsilon))+f_\varphi(\varepsilon)(1-f_e(\varepsilon))] \\
&\quad +|s_{ec}|^2|s_{e\varphi}|^2[f_c(\varepsilon)(1-f_\varphi(\varepsilon))+f_\varphi(\varepsilon)(1-f_c(\varepsilon))] \\
&\quad +|s_{e\varphi}|^2|s_{e\varphi}|^2 f_\varphi(\varepsilon)[1-f_\varphi(\varepsilon)] \\
&\quad +|s_{ee}|^2|s_{ec}|^2[f_e(\varepsilon)(1-f_c(\varepsilon))+f_c(\varepsilon)(1-f_e(\varepsilon))]\big\} \qquad (6.3.5) \\
&= \frac{2e^2}{h}\int d\varepsilon \\
&\quad \{T_{e\varphi}(\varepsilon)[1-T_{ec}(\varepsilon)-T_{e\varphi}(\varepsilon)][f_e(\varepsilon)(1-f_\varphi(\varepsilon))+f_\varphi(\varepsilon)(1-f_e(\varepsilon))] \\
&\quad +T_{e\varphi}(\varepsilon)T_{ec}(\varepsilon)[f_c(\varepsilon)(1-f_\varphi(\varepsilon))+f_\varphi(\varepsilon)(1-f_c(\varepsilon))] \\
&\quad +T_{e\varphi}(\varepsilon)^2 f_\varphi(\varepsilon)[1-f_\varphi(\varepsilon)] \\
&\quad +T_{ec}(\varepsilon)[1-T_{ec}(\varepsilon)-T_{e\varphi}(\varepsilon)][f_e(\varepsilon)(1-f_c(\varepsilon))+f_c(\varepsilon)(1-f_e(\varepsilon))]\} \\
&\qquad (6.3.6)
\end{aligned}
$$

Before we are going to discuss numerically the average current (6.3.3) and the noise (6.3.6) one important issue of this formalism has to be stressed. In the beginning of this chapter it was emphasized that the net current at the fictitious terminal has to vanish: $I_\varphi = 0$. In order to fulfill this condition one can either set $i_\varphi(\varepsilon) = 0$ or $\int d\varepsilon\, i_\varphi(\varepsilon) = 0$. The former means that electrons which are removed from an energy channel have to be reinjected in the same channel - one calls this *quasi-elastic* scattering [JON97]. The latter allows the electrons to reshuffle their energy which justifies the term *inelastic scattering*. This adjusts self-consistently the distribution function of the fictitious terminal f_φ.

We consider a single non-degenerate level ε_r in the QD and symmetric barriers $\Gamma_e = \Gamma_c$. The collector chemical potential is chosen such that $f_c = 0$ (high-bias limit). The temperature is assumed to be zero so that $f_e(\varepsilon) = \Theta(\varepsilon - \mu_e)$.

This results in an average current (upper graph) and Fano factor (lower graph) as depicted in Fig. 6.3. The solid lines correspond to the situation without fictitious voltage probe ($\Gamma_\varphi = 0$): the current shows a step whose derivation is given by the

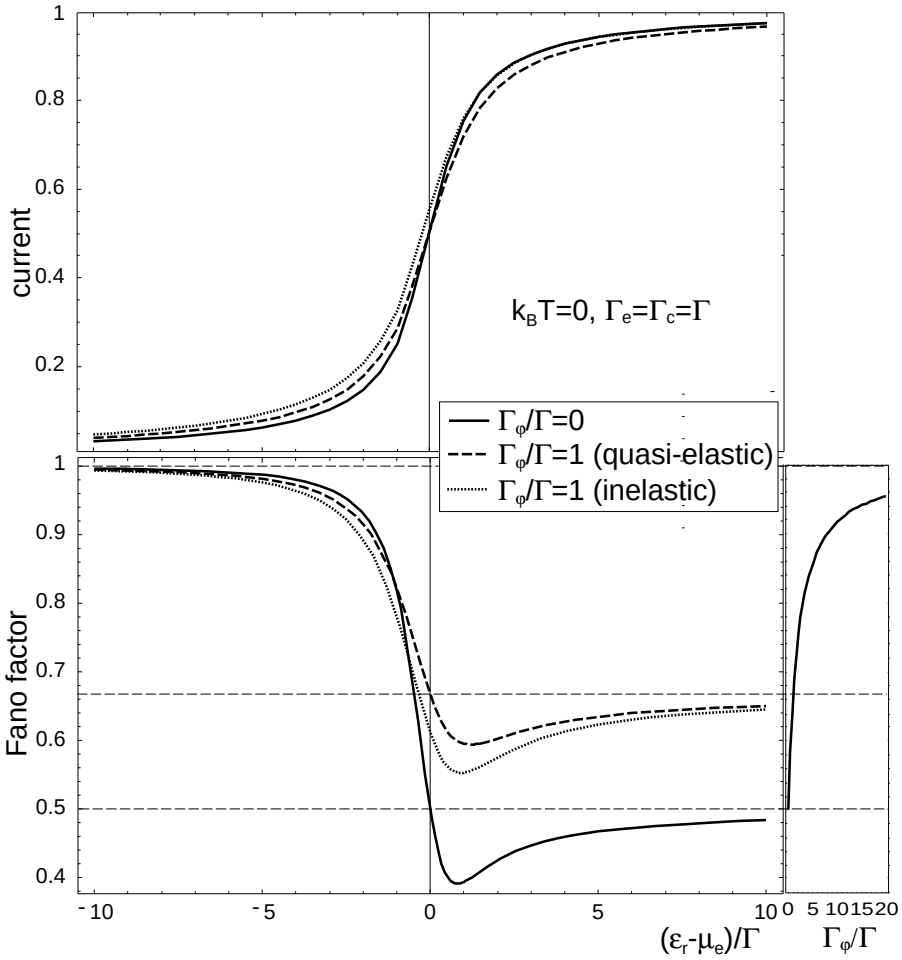

Figure 6.3.: Average normalized current (upper graph) and Fano factor (lower graph) vs. bias voltage for a single QD with voltage probe. Solid lines: without voltage probe. Dashed lines: with voltage probe $\Gamma_\varphi/\Gamma = 1$ (quasi-elastic scattering). Dotted lines: with voltage probe $\Gamma_\varphi/\Gamma = 1$ (inelastic scattering). Right inset of lower graph: High-bias Fano factor vs. dephasing rate Γ_φ.

Lorentzian function centered around ε_r (5.2.11). The corresponding Fano factor is unity for a bias far below the resonance and reaches 0.5 for on-resonance transport due to Pauli's exclusion principle (see Sec. 4.2.1). Around the resonance an additional suppression is present which leads to a Fano factor below 0.5 on the r.h.s. of the resonance. This effect is discussed in Sec. 5.2.1.

The essential effect for $\Gamma_\varphi > 0$ is a broadening and decaying of the transmission function resonance. Hence, the current step in Fig. 6.3 gets softened (dashed and dotted curves). But, the high-bias current value is unaffected by dephasing. As we already outlined the demand of a zero net-current at the fictitious voltage probe can be satisfied either by strict energy conservation (quasi-elastic scattering: dashed curves) or by enabling energy reshuffling during the scattering process (inelastic scattering: dotted curve). Although one would expect the same current for both, the latter leads to a slightly different behavior: the resonance is not symmetric with respect to ε_r. For zero-temperature an electron cannot be reinjected in states above μ_e because no absorption of e.g. phonons is present[3]. The Fano factor is again unity for biases below the resonance. In contrast to the case without dephasing now the Fano factor is above 0.5 for fully on-resonance transport (high-bias), i.e. the current becomes less correlated. This can be understood by the fact that the additional voltage probe takes out a particle and reinjects it after a certain time range given by Γ_φ^{-1}. During this time interval the current carrying state is unoccupied and Pauli's exclusion principle is less effective. We obtain an analytical expression for the high-bias Fano factor

$$\alpha = \frac{S_{ee}(0)}{2e\langle I_e\rangle} = 1 - \frac{2\Gamma_e\Gamma_c}{\Gamma_e+\Gamma_c}\left(\frac{1}{\Gamma_e+\Gamma_c+\Gamma_\varphi}\right) \tag{6.3.7}$$

Technically, the dependence of the high-bias Fano factor on Γ_φ (6.3.7) is caused by the change of the occupation statistics of the "transport channels"whereon the noise is sensitive.

In the following section we compare the result (6.3.7) with the results of other formalisms.

6.3.1. Relation to other formalisms

Formula (6.3.7) agrees with Eq. (11) in Ref. [DAV95]. Therein, the authors use a Fabry-Pèrot picture where they add a small random phase to the wave function on each round trip between the barriers. To obtain the noise they use $\int d\varepsilon T(1-T)$ (see Eq. (6.2.6) for zero-temperature and high-bias). Putting in an phase-averaged $\langle T\rangle$ leads directly to (6.3.7). Nevertheless, it is argued in [DAV95] that the correct average should be taken as $\langle T(1-T)\rangle$ which leads to a factor of one half in front of Γ_φ in (6.3.7). For a discussion see Sec. II D in [DAV95]. Note, that their form

[3]For this we multiplied the energy-independent f_φ by f_e. Without this assumption the DC noise becomes super-Poissonian for biases below the resonance.

of decoherence also broadens and lowers the resonant transmission function while conserving its area in agreement with our approach.

Next we return to NEGF which we introduced in Chap. 5. For a single QD with one state the Green's functions are scalar functions. In [DAT95] the dephasing rate Γ_φ is introduced for electron-phonon scattering in lowest-order perturbation theory. The average current is calculated with Eq. (5.1.25) and the zero-frequency SPD derived in Sec. 5.1.2.2 with Eq. (5.1.49). It turns out that the NEGF provides the same results as our fictitious terminal approach (Fig. 6.3). Hence the phenomenological dephasing approach we use is substantiated by electron-phonon scattering by means of a microscopic scattering model. For details of the electron-phonon scattering in tunneling through QDs see Ref. [GNO04].

Hence, we found the agreement with respect to the noise and the average current between three different approaches where dephasing in tunneling through a single QD is introduced:

(i) Fictitious terminal with vanishing net-current $\langle I_\varphi \rangle = 0$. The Fano factor (6.3.7) is obtained by means of Eqs. (6.3.3),(6.3.6) - **SMF**.

(ii) Phase-randomization in Fabry-Pèrot picture. The noise is obtained via $\int d\varepsilon \langle T \rangle (1 - \langle T \rangle)$ [DAV95].

(iii) Electron-phonon scattering in lowest-order perturbation theory and energy-independent scattering rate Γ_φ. The Fano factor (6.3.7) is obtained by Eqs. (5.1.25),(5.1.49) - **NEGF** [DAT95]

The physical picture behind the observation that phase-breaking elastic scattering can bring the noise towards its classical value is not clearly understood yet regarding items (ii) and (iii). In both pictures the occupation statistics of the current-carrying state is not apparently changed by the scattering, although Pauli's exclusion principle becomes less effective with increasing Γ_φ (6.3.7).

So far we found that internal elastic scattering which is accompanied by phase randomization changes the high-bias Fano factor for tunneling through a single QD.

In contrast, there is the crucial observation that the high-bias Fano factor independently calculated in the limits of pure sequential tunneling (e.g. by Langevin equation [BLA00] or by the ME discussed in Chap. 4) and pure coherent tunneling (e.g. NEGF discussed in Sec. 5.2.1) appear to be identical given by Eq. (4.2.1)[4]. Taking this into account in the fictitious terminal scheme (SMF) for the noise calculation one has to ensure that the occupation statistics of the current carrying states is not changed by taking out a particle. This can be guaranteed by the additional demand of the instantaneous reinjection of a particle in the current carrying channel as it will be shown in the following section.

[4]for $i = 1$ and $f_e^1 = 1$.

6.3.2. Instantaneous reinjection - Pure dephasing

Here we demand that the net-current for any energy (quasi-elastic) **and** at any instant of time vanishes $i_\varphi(t) = 0$ so that the occupation statistics of the "transport channels"is not changed by dephasing - *pure dephasing* [5]:

The energy-resolved currents are (the energy-arguments are skipped in the following)

$$\begin{aligned} i_e &= -(1-f_\varphi)T_{e\varphi} - T_{ec} \\ i_c &= T_{ec} + T_{c\varphi}f_\varphi \\ i_\varphi &= (1-f_\varphi)T_{e\varphi} - T_{c\varphi}f_\varphi \end{aligned} \tag{6.3.8}$$

There are two sources of fluctuations if we consider that the distribution function f_φ fluctuates: $f_\varphi + \delta f_\varphi$ - the "bare"fluctuations δi_α and fluctuations due to δf_φ. The total fluctuations Δi_α become

$$\begin{aligned} \Delta i_e &= \delta i_e + \delta f_\varphi T_{e\varphi} \\ \Delta i_c &= \delta i_c + \delta f_\varphi T_{c\varphi} \\ \Delta i_\varphi &= \delta i_\varphi - \delta f_\varphi (T_{e\varphi} + T_{c\varphi}) \end{aligned} \tag{6.3.9}$$

The idea behind the introduction of a fluctuating distribution in the fictitious terminal is to ensure that an removed electron will be instantaneously reinjected in the current-carrying state. Therefore, zero-fluctuations at the fictitious probe are demanded and one gets

$$\Delta i_\varphi = 0 \Longrightarrow \delta f_\varphi = \frac{\delta i_\varphi}{T_{e\varphi} + T_{c\varphi}} \tag{6.3.10}$$

This is inserted back in the expression Δi_e. Then, the current correlations (per unit energy) are

$$S_P(\varepsilon) = \langle (\Delta i_e)^2 \rangle = S_{ee} + 2\frac{T_{e\varphi}}{T_{e\varphi} + T_{c\varphi}} S_{e\varphi} + \left(\frac{T_{e\varphi}}{T_{e\varphi} + T_{c\varphi}} \right)^2 S_{\varphi\varphi} \tag{6.3.11}$$

with the "bare"noise correlations $S_{\alpha\beta} = \langle \delta i_\alpha \delta i_\beta \rangle$ obtained within the standard technique (6.2.3). S_{ee} is given by Eq. (6.3.6), $S_{e\varphi}$ and $S_{\varphi\varphi}$ can be obtained analogously [6]:

$$\begin{aligned} S_{ee}(\varepsilon) &= [T_{ec} + T_{e\varphi}(1-f_\varphi)][1 - T_{ec} - T_{e\varphi}(1-f_\varphi)] \\ S_{e\varphi}(\varepsilon) &= -(1-f_\varphi)T_{e\varphi} + [T_{ec} + T_{e\varphi}(1-f_\varphi)][T_{e\varphi}(1-f_\varphi) - T_{c\varphi}f_\varphi] \\ S_{\varphi\varphi}(\varepsilon) &= (1-f_\varphi)T_{e\varphi} + T_{c\varphi}f_\varphi - [T_{e\varphi}(1-f_\varphi) - T_{c\varphi}f_\varphi]^2 \end{aligned} \tag{6.3.12}$$

[5] The following procedure is adopted from [SAM04].

[6] For the cross-correlations $\alpha \neq \beta$ the property $\sum_\delta s_{\alpha\delta} s^\dagger_{\beta\delta} = 0$ is used such that the products of S-matrices can be replaced by transmission functions.

Using the generalized Breit-Wigner resonances (6.2.20)

$$T_{ec} = \frac{\Gamma_e\Gamma_c}{(\varepsilon-\varepsilon_r)^2+\Gamma^2/4}, \qquad T_{e\varphi} = \frac{\Gamma_e\Gamma_\varphi}{(\varepsilon-\varepsilon_r)^2+\Gamma^2/4}, \qquad T_{c\varphi} = \frac{\Gamma_c\Gamma_\varphi}{(\varepsilon-\varepsilon_r)^2+\Gamma^2/4} \tag{6.3.13}$$

with $\Gamma \equiv \Gamma_e + \Gamma_c + \Gamma_\varphi$, Eqs. (6.3.12) can be simplified to

$$\begin{aligned} S_{ee}(\varepsilon) &= [T_{ec} + T_{e\varphi}(1-f_\varphi)][1 - T_{ec} - T_{e\varphi}(1-f_\varphi)] \\ S_{e\varphi}(\varepsilon) &= -(1-f_\varphi)T_{e\varphi} \\ S_{\varphi\varphi}(\varepsilon) &= (1-f_\varphi)T_{e\varphi} + T_{c\varphi}f_\varphi \end{aligned} \tag{6.3.14}$$

As one can see in (6.3.14), the current correlations at the same terminal are positive and the cross-correlation is negative. This holds generally following Büttiker who states that in the absence of interactions the zero-frequency cross-correlations are always negative [BUE92, BLA00]. This is a consequence of the fermionic statistics of electrons. With Coulomb interactions inside the QD the cross-correlations can also be positive which is not necessarily accompanied by super-Poissionian noise (Sec. 4.2.2,[KIE04]) as shown for a three-terminal QD in [COT04].

The distribution function f_φ reads for elastic scattering $f_\varphi(\varepsilon) = \frac{T_{e\varphi}(\varepsilon)}{T_{e\varphi}(\varepsilon)+T_{c\varphi}(\varepsilon)}$ and is energy-dependent; for inelastic scattering it becomes $f_\varepsilon = \frac{\Gamma_e}{\Gamma_e+\Gamma_c}$ which is energy-independent.

Performing the energy integration for both gives

$$S_P = \frac{2e^2}{h}\int d\varepsilon\, S(\varepsilon) = \frac{2e^2}{\hbar}\frac{\Gamma_e\Gamma_c(\Gamma_e^2+\Gamma_c^2)}{(\Gamma_e+\Gamma_c)^3} \tag{6.3.15}$$

which turns out to be independent on the dephasing strength Γ_φ. This is in agreement with the observation that purely sequential and coherent descriptions provide the same Fano factor in the high bias regime.

To conclude, we considered dephasing by elastic scattering and pure dephasing. For the former, the shot noise goes towards its Poissonian value by increasing the dephasing rate due to the change of the occupation statistics of the current carrying states. This is in contradiction to the key observation, that the high-bias Fano factor is independent of the degree of quantum coherence. Pure dephasing as considered here accounts for this fact.

6.4. Tunnel-coupled quantum dots

6.4.1. Current

In [DAT95] the equivalence of the SMF and NEGF approach was shown. In order to set up the link to the discussions in Sec. 5.4 the current through the tunnel-coupled QDs will be calculated by means of the NEGF approach. The retarded/advanced self energy is now extended by the coupling of both QDs to the fictitious terminals and is given by

$$\Sigma^{\mathrm{ret/adv}} = \begin{pmatrix} \pm i(\Gamma_e + \Gamma_\varphi)/2 & 0 \\ 0 & \pm i(\Gamma_c + \Gamma_\varphi)/2 \end{pmatrix} \tag{6.4.1}$$

where we assumed equal dephasing rates in both QDs $\Gamma_\varphi \equiv \Gamma_{\varphi 1} = \Gamma_{\varphi 2}$. The lesser/greater selfenergies are (high-bias limit: $f_e = 1$ and $f_c = 0$)

$$\begin{aligned} \Sigma^{<}(\varepsilon) &= \Sigma^{<}_{\varphi 1}(\varepsilon) + \Sigma^{<}_{\varphi 2}(\varepsilon) + \Sigma^{<}_{C} \\ &\text{with} \\ \Sigma^{<}_{\varphi 1}(\varepsilon) &= \begin{pmatrix} i\Gamma_\varphi f_{\varphi 1}(\varepsilon) & 0 \\ 0 & 0 \end{pmatrix} \quad , \quad \Sigma^{<}_{\varphi 2}(\varepsilon) = \begin{pmatrix} 0 & 0 \\ 0 & i\Gamma_\varphi f_{\varphi 2}(\varepsilon) \end{pmatrix} \end{aligned} \tag{6.4.2}$$

and

$$\begin{aligned} \Sigma^{>}(\varepsilon) &= \Sigma^{>}_{\varphi 1}(\varepsilon) + \Sigma^{>}_{\varphi 2}(\varepsilon) + \Sigma^{>}_{C} \\ &\text{with} \\ \Sigma^{>}_{\varphi 1}(\varepsilon) &= \begin{pmatrix} -i\Gamma_\varphi (1 - f_{\varphi 1}(\varepsilon)) & 0 \\ 0 & 0 \end{pmatrix} \quad , \quad \Sigma^{>}_{\varphi 2}(\varepsilon) = \begin{pmatrix} 0 & 0 \\ 0 & -i\Gamma_\varphi (1 - f_{\varphi 2}(\varepsilon)) \end{pmatrix} \end{aligned} \tag{6.4.3}$$

where the functions describing the emitter/collector coupling $\Sigma_C^{</>}$ are given by (5.4.4). The occupations of the fictitious terminals $f_{\varphi 1/\varphi 2}(\varepsilon)$ have to be determined by the demand of vanishing net-currents at these terminals. The average current at terminal α is

$$\begin{aligned} \langle I_\alpha \rangle &= \frac{e}{h} \int d\varepsilon \, i_\alpha(\varepsilon) \\ \text{with} \quad i_\alpha(\varepsilon) &= \mathrm{Tr}\left[\Sigma^{<}_{\alpha}(\varepsilon) G^{>}(\varepsilon) - \Sigma^{>}_{\alpha}(\varepsilon) G^{<}(\varepsilon)\right] \end{aligned} \tag{6.4.4}$$

Eq. (6.4.4) can be rewritten in a form which can also be obtained in SMF. For that purpose we use $\Sigma^{<} - \Sigma^{>} = i\Gamma$. After some basic algebra this yields

$$i_e = \frac{e}{h}\left[T_{e\varphi 1}(\varepsilon)(1-f_{\varphi_1}(\varepsilon)) + T_{e\varphi 2}(\varepsilon)(1-f_{\varphi_2}) + T_{ec}(\varepsilon)\right] \tag{6.4.5}$$

with the transmission functions defined by

$$\begin{aligned} T_{\alpha\beta}(\varepsilon) &= \mathrm{Tr}[\Gamma_\alpha G^{\mathrm{ret}} \Gamma_\beta G^{\mathrm{adv}}] \qquad \alpha,\beta = e, c, \varphi 1, \varphi 2 \\ \Gamma_e &= \begin{pmatrix} \Gamma_e & 0 \\ 0 & 0 \end{pmatrix} \quad , \quad \Gamma_c = \begin{pmatrix} 0 & 0 \\ 0 & \Gamma_c \end{pmatrix} \\ \Gamma_{\varphi 1} &= \begin{pmatrix} \Gamma_\varphi & 0 \\ 0 & 0 \end{pmatrix} \quad , \quad \Gamma_{\varphi 2} = \begin{pmatrix} 0 & 0 \\ 0 & \Gamma_\varphi \end{pmatrix} \end{aligned} \tag{6.4.6}$$

In Eq. (6.4.5) the total current is now split into a non-coherent part (first two terms) and a coherent part (last term). This is one of the advantages of the SMF.

For quasi-elastic and inelastic scattering the on-resonance ($\Delta E \equiv \varepsilon_1 - \varepsilon_2 = 0$) current vs. dephasing rate Γ_φ is shown in Fig. 6.4 (the inset depicts the current vs. ΔE for various Γ_φ).

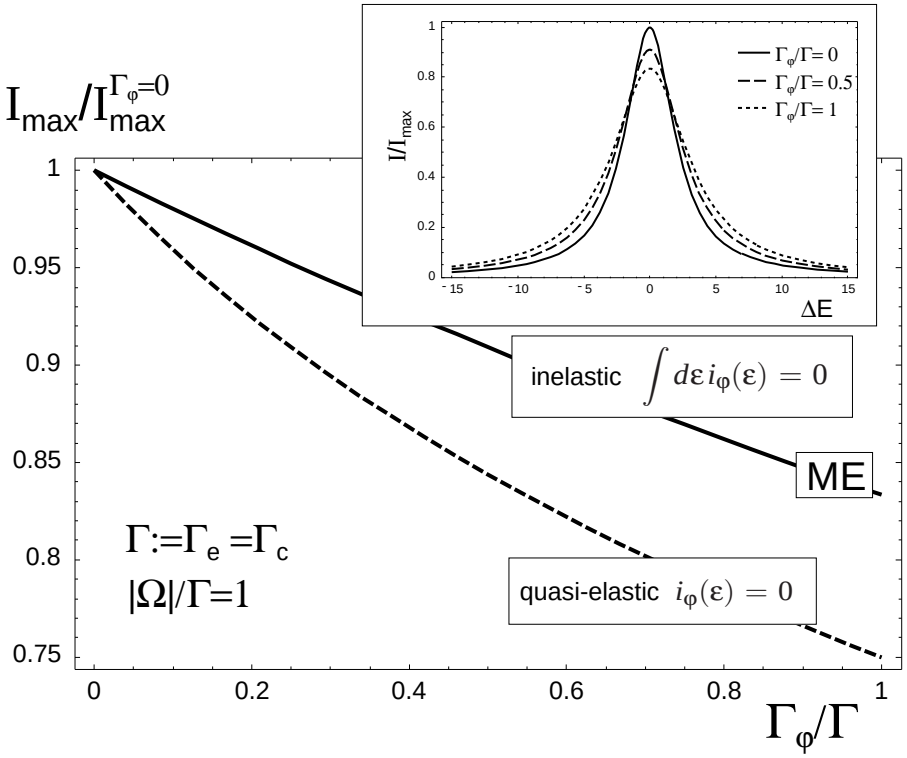

Figure 6.4.: On-resonance current vs. dephasing Γ_φ with NEGF and ME (6.4.7). Inset: NEGF current vs. level separation $\Delta E = \varepsilon_1 - \varepsilon_2$ for different Γ_φ.

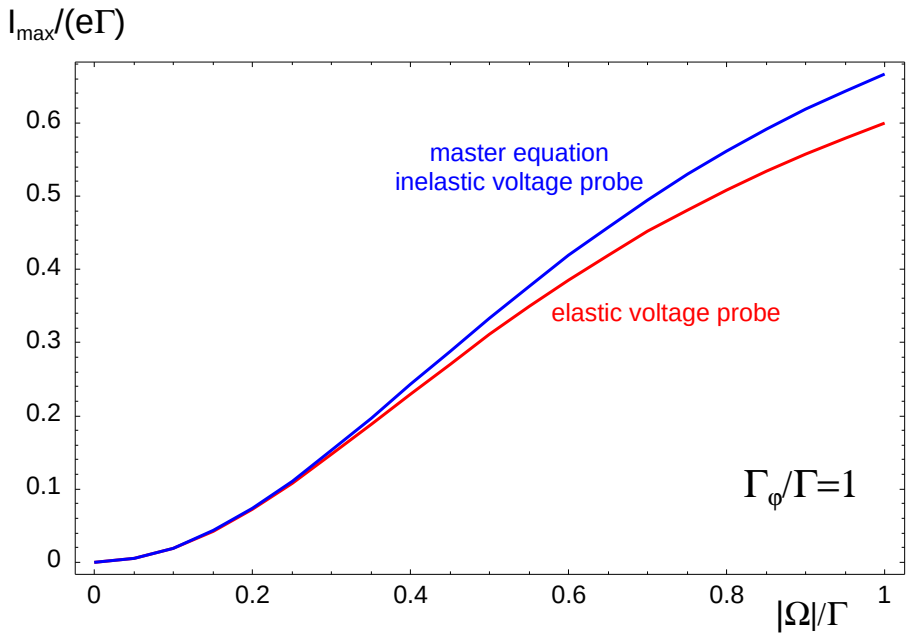

Figure 6.5.: On-resonance current vs. tunnel coupling $|\Omega|$ for $\Gamma_\varphi/\Gamma = 1$. blue curve: master equation (6.4.7) and inelastic scattering. red curve: elastic scattering.

We compare the current with the current obtained by the ME in Sec. 3.3.1 wherein we replace $\Gamma_{\rm inter} = \frac{4|\Omega|^2}{\Gamma_e+\Gamma_c}$ by $\frac{4|\Omega|^2}{\Gamma_e+\Gamma_c+2\Gamma_\varphi}$ which means that each of both QD levels is additionally broadened by Γ_φ. The on-resonance ME current is then

$$I_e^{\rm ME} = \frac{4e\Gamma_e\Gamma_c|\Omega|^2}{\Gamma_e\Gamma_c(\Gamma_e+\Gamma_c+2\Gamma_\varphi)+4(\Gamma_e+\Gamma_c)|\Omega|^2} \tag{6.4.7}$$

Astonishingly, it turns out that the on-resonance current with inelastic scattering fully agrees with the ME result for all Γ_φ (full line in Fig. 6.4) and all $|\Omega|$ (blue line in Fig. 6.5). This peculiar issue will be the subject of future investigations. In the remainder of this chapter we deal with dephasing by quasi-elastic scattering. The corresponding on-resonance current turns out to be smaller (dashed line in Fig. 6.4). In a rather heuristic view we understand the difference for both cases as follows. If the electrons can reshuffle their energy during the scattering back and forth to the voltage probe they can more easily find a free channel to tunnel through. If strict energy conservation is demanded the channel has to be free before an electron can travel through the system. Hence, for this case the current should appear smaller.

Importantly, for small tunnel couplings $|\Omega|/\Gamma \ll 1$ Fermi's golden rule current (6.4.7) can also provide a good approximation for the elastic scattering current as shown in Fig. 6.5. We will see in the next chapter that the full statistics of charge transfer in the presence of elastic scattering and for small interdot coupling can

be approximated by the simple Fermi's golden rule treatment and appears to be Poissonian.

6.4.2. Shot noise

The transmission functions for the coupled QD system sketched in Fig. 6.1 are (the same dephasing rate Γ_φ for both QDs is assumed.)

$$\begin{aligned}
T_{ec}(\varepsilon) &= |s_{ec}(\varepsilon)|^2 = \frac{1}{|Z|^2}\Gamma_e\Gamma_c|\Omega|^2 \\
T_{e\varphi1}(\varepsilon) &= |s_{e\varphi1}(\varepsilon)|^2 = \frac{1}{|Z|^2}\Gamma_e\Gamma_\varphi\left[(\varepsilon-\varepsilon_2)^2+\left(\frac{\Gamma_c+\Gamma_\varphi}{2}\right)^2\right] \\
T_{e\varphi2}(\varepsilon) &= |s_{e\varphi2}(\varepsilon)|^2 = \frac{1}{|Z|^2}\Gamma_e\Gamma_\varphi|\Omega|^2 \\
T_{c\varphi1}(\varepsilon) &= |s_{c\varphi1}(\varepsilon)|^2 = \frac{1}{|Z|^2}\Gamma_c\Gamma_\varphi|\Omega|^2 \\
T_{c\varphi2}(\varepsilon) &= |s_{c\varphi2}(\varepsilon)|^2 = \frac{1}{|Z|^2}\Gamma_c\Gamma_\varphi\left[(\varepsilon-\varepsilon_1)^2+\left(\frac{\Gamma_e+\Gamma_\varphi}{2}\right)^2\right] \\
T_{\varphi1\varphi2}(\varepsilon) &= |s_{\varphi1\varphi2}(\varepsilon)|^2 = \frac{1}{|Z|^2}\Gamma_\varphi^2|\Omega|^2
\end{aligned} \tag{6.4.8}$$

with

$$Z \equiv \left(\varepsilon-\varepsilon_1+i\frac{\Gamma_e+\Gamma_\varphi}{2}\right)\left(\varepsilon-\varepsilon_2+i\frac{\Gamma_c+\Gamma_\varphi}{2}\right)-|\Omega|^2 \tag{6.4.9}$$

The energy-resolved currents at the terminals read (high-bias: $f_e=1$, $f_c=0$), suppressing the energy arguments,

$$\begin{aligned}
i_e &= -T_{ec}-T_{e\varphi1}(1-f_{\varphi1})-T_{e\varphi2}(1-f_{\varphi2}) \\
i_c &= T_{ec}+T_{c\varphi1}f_{\varphi1}+T_{c\varphi2}f_{\varphi2} \\
i_{\varphi1} &= T_{e\varphi1}(1-f_{\varphi1})-T_{c\varphi1}f_{\varphi1}+T_{\varphi2\varphi1}(f_{\varphi2}-f_{\varphi1}) \\
i_{\varphi2} &= T_{e\varphi2}(1-f_{\varphi2})-T_{c\varphi2}f_{\varphi2}+T_{\varphi1\varphi2}(f_{\varphi1}-f_{\varphi2})
\end{aligned} \tag{6.4.10}$$

Note, that current-conservation demands $\sum_\alpha i_\alpha = 0$ where the current is taken positive if it flows from the reservoir towards the conductor. The condition of no net-current at the fictitious terminals gives

$$i_{\varphi 1}=0 \Longrightarrow f_{\varphi 1}=\frac{T_{e\varphi 1}(T_{e\varphi 2}+T_{c\varphi 2})+T_{\varphi 1\varphi 2}(T_{e\varphi 1}+T_{e\varphi 2})}{(T_{e\varphi 1}+T_{c\varphi 1})(T_{e\varphi 2}+T_{c\varphi 2})+T_{\varphi 1\varphi 2}(T_{e\varphi 1}+T_{c\varphi 1}+T_{e\varphi 2}+T_{c\varphi 2})} \tag{6.4.11}$$

$$i_{\varphi 2}=0 \Longrightarrow f_{\varphi 2}=\frac{T_{e\varphi 2}(T_{e\varphi 1}+T_{c\varphi 1})+T_{\varphi 1\varphi 2}(T_{e\varphi 1}+T_{e\varphi 2})}{(T_{e\varphi 1}+T_{c\varphi 1})(T_{e\varphi 2}+T_{c\varphi 2})+T_{\varphi 1\varphi 2}(T_{e\varphi 1}+T_{c\varphi 1}+T_{e\varphi 2}+T_{c\varphi 2})} \tag{6.4.12}$$

Here, in contrast to the single QD the distributions $f_{\varphi 1/2}$ are energy-dependent.

The evaluation of the total current at the emitter barrier $\langle I_e\rangle = \frac{e}{h}\int d\varepsilon\, i_e(\varepsilon)$ leads to the dashed curve in Fig. 6.4. Note, that the total current through coupled QDs is not independent on the strength of dephasing Γ_φ. The zero-frequency SPD is calculated by means of Eq. (5.1.49). The numerical results for the on-resonance ($\varepsilon_1=\varepsilon_2$) and high-bias ($f_e=1$) Fano factor vs. interdot-coupling for various Γ_φ are shown in Fig. 6.6

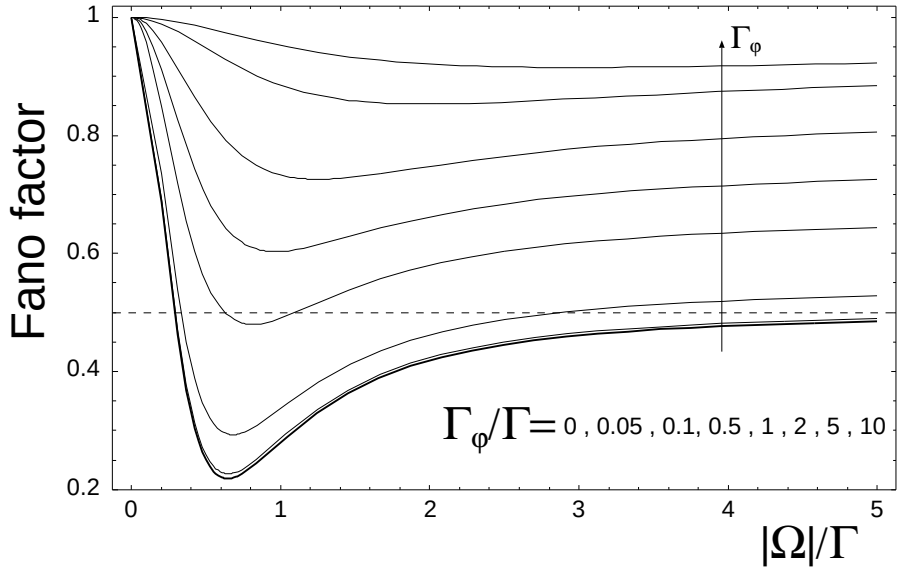

Figure 6.6.: On-resonance ($\varepsilon_1=\varepsilon_2$) Fano factor vs. interdot-coupling $|\Omega|$ for various dephasing rates Γ_φ. Fictitious terminals $f_{\varphi 1}/f_{\varphi 1}$ without fluctuations. High-bias limit $f_e=1$, $f_c=0$.

The Fano factor also goes towards unity with increasing Γ_φ for $|\Omega|\gg\Gamma_{e/c}$ as already discussed with respect to the preceding noise analysis of a single QD with voltage probe. What happens if we implement the voltage probe model with instantaneous vanishing net-currents $i_{\varphi 1}/i_{\varphi 2}$ as in Sec. 6.3.2?

We introduce fluctuations of the distribution functions: $f_{\varphi 1}\to f_{\varphi 1}+\delta f_{\varphi 1}$ and $f_{\varphi 2}\to f_{\varphi 2}+\delta f_{\varphi 2}$. Then, we obtain the total fluctuations Δi_α

$$\begin{aligned}
\Delta i_e &= \delta i_e + \delta f_{\varphi 1} T_{e\varphi 1} + \delta f_{\varphi 2} T_{e\varphi 2} \\
\Delta i_c &= \delta i_c + \delta f_{\varphi 1} T_{c\varphi 1} + \delta f_{\varphi 2} T_{c\varphi 2} \\
\Delta i_{\varphi 1} &= \delta i_{\varphi 1} - \delta f_{\varphi 1}(T_{e\varphi 1} + T_{c\varphi 1} + T_{\varphi 2\varphi 1}) + \delta f_{\varphi 2} T_{\varphi 2\varphi 1} \\
\Delta i_{\varphi 2} &= \delta i_{\varphi 2} - \delta f_{\varphi 2}(T_{e\varphi 2} + T_{c\varphi 2} + T_{\varphi 1\varphi 2}) + \delta f_{\varphi 1} T_{\varphi 1\varphi 2}
\end{aligned} \tag{6.4.13}$$

We demand zero-fluctuations at the fictitious terminals

$$\begin{aligned}
\Delta i_{\varphi 1} = 0 \implies \delta f_{\varphi 1} &= \frac{\delta i_{\varphi 2} T_{\varphi 1\varphi 2} + \delta i_{\varphi 1}(T_{c\varphi 2} + T_{e\varphi 2} + T_{\varphi 1\varphi 2})}{(T_{e\varphi 1} + T_{c\varphi 1})(T_{e\varphi 2} + T_{c\varphi 2}) + T_{\varphi 1\varphi 2}(T_{e\varphi 1} + T_{c\varphi 1} + T_{e\varphi 2} + T_{c\varphi 2})} \\
\Delta i_{\varphi 2} = 0 \implies \delta f_{\varphi 2} &= \frac{\delta i_{\varphi 1} T_{\varphi 1\varphi 2} + \delta i_{\varphi 2}(T_{c\varphi 1} + T_{e\varphi 1} + T_{\varphi 1\varphi 2})}{(T_{e\varphi 1} + T_{c\varphi 1})(T_{e\varphi 2} + T_{c\varphi 2}) + T_{\varphi 1\varphi 2}(T_{e\varphi 1} + T_{c\varphi 1} + T_{e\varphi 2} + T_{c\varphi 2})}
\end{aligned} \tag{6.4.14}$$

Inserting these expressions in Δi_e the total current correlations (per unit energy) at the emitter barrier becomes

$$S_P(\varepsilon) = \langle (\Delta i_e)^2 \rangle = S_{ee} + \frac{C_1}{A} S_{e\varphi 1} + \frac{C_2}{A} S_{e\varphi 2} + \frac{C_3}{A^2} S_{\varphi 1\varphi 2} + \frac{C_4}{A^2} S_{\varphi 1\varphi 1} + \frac{C_5}{A^2} S_{\varphi 2\varphi 2} \tag{6.4.15}$$

with the constants

$$\begin{aligned}
A &\equiv (T_{e\varphi 1} + T_{c\varphi 1})(T_{e\varphi 2} + T_{c\varphi 2}) + T_{\varphi 1\varphi 2}(T_{e\varphi 1} + T_{c\varphi 1} + T_{e\varphi 2} + T_{c\varphi 2}) \\
C_1 &= 2[T_{e\varphi 1}(T_{c\varphi 2} + T_{e\varphi 2} + T_{\varphi 1\varphi 2}) + T_{e\varphi 2} T_{\varphi 1\varphi 2}] \\
C_2 &= 2[T_{e\varphi 2}(T_{c\varphi 1} + T_{e\varphi 1} + T_{\varphi 1\varphi 2}) + T_{e\varphi 1} T_{\varphi 1\varphi 2}] \\
C_3 &= 2\{T_{e\varphi 1}^2 T_{\varphi 1\varphi 2}(T_{c\varphi 2} + T_{e\varphi 2} + T_{\varphi 1\varphi 2}) + T_{e\varphi 2}^2 T_{\varphi 1\varphi 2}(T_{c\varphi 1} + T_{e\varphi 1} + T_{\varphi 1\varphi 2}) \\
&\quad + T_{e\varphi 1} T_{e\varphi 2}[T_{\varphi 1\varphi 2}^2 + (T_{c\varphi 2} + T_{e\varphi 2} + T_{\varphi 1\varphi 2})(T_{c\varphi 1} + T_{e\varphi 1} + T_{\varphi 1\varphi 2})]\} \\
C_4 &= T_{e\varphi 1}^2 (T_{c\varphi 2} + T_{e\varphi 2} + T_{\varphi 1\varphi 2})^2 + T_{e\varphi 2}^2 T_{\varphi 1\varphi 2}^2 \\
&\quad + 2T_{e\varphi 1} T_{e\varphi 2} T_{\varphi 1\varphi 2}(T_{c\varphi 2} + T_{e\varphi 2} + T_{\varphi 1\varphi 2}) \\
C_5 &= T_{e\varphi 2}^2 (T_{c\varphi 1} + T_{e\varphi 1} + T_{\varphi 1\varphi 2})^2 + T_{e\varphi 1}^2 T_{\varphi 1\varphi 2}^2 \\
&\quad + 2T_{e\varphi 1} T_{e\varphi 2} T_{\varphi 1\varphi 2}(T_{c\varphi 1} + T_{e\varphi 1} + T_{\varphi 1\varphi 2})
\end{aligned} \tag{6.4.16}$$

The "bare"current correlations $S_{\alpha\beta} = \langle \delta i_\alpha \delta i_\beta \rangle$ (per unit energy) in Eq. (6.4.15) follow from (6.2.3) for $\alpha = \beta$:

$$
\begin{aligned}
S_{ee} &= [T_{ec} + T_{e\varphi 1}(1-f_{\varphi 1}) + T_{e\varphi 2}(1-f_{\varphi 2})][1 - T_{ec} - T_{e\varphi 1}(1-f_{\varphi 1}) - T_{e\varphi 2}(1-f_{\varphi 2})] \\
S_{\varphi 1\varphi 1} &= (1 - T_{\varphi 1\varphi 2} f_{\varphi 2} - T_{e\varphi 1})(T_{e\varphi 1} + T_{\varphi 1\varphi 2} f_{\varphi 2}) - (T_{\varphi 1\varphi 2} + T_{c\varphi 1} + T_{e\varphi 1})^2 f_{\varphi 1}^2 \\
&\quad + f_{\varphi 1}\{T_{c\varphi 1} + T_{\varphi 1\varphi 2}[1 - 2f_{\varphi 2}(1 - T_{\varphi 1\varphi 2} - T_{c\varphi 1})] - T_{e\varphi 1} \\
&\quad + 2(T_{\varphi 1\varphi 2} + T_{\varphi 1\varphi 2} f_{\varphi 2} + T_{c\varphi 1}) T_{e\varphi 1} + 2T_{e\varphi 1}^2\} \\
S_{\varphi 2\varphi 2} &= -T_{\varphi 1\varphi 2}^2 f_{\varphi 1}^2 + T_{e\varphi 2}(1 - T_{e\varphi 2}) - f_{\varphi 2}^2 (T_{e\varphi 2} + T_{c\varphi 2} + T_{\varphi 1\varphi 2})^2 \\
&\quad + f_{\varphi 2}[T_{\varphi 1\varphi 2} + T_{c\varphi 2} - T_{e\varphi 2} + 2T_{\varphi 1\varphi 2} T_{e\varphi 2} + 2T_{e\varphi 2}(T_{e\varphi 2} + T_{c\varphi 2})] \\
&\quad + f_{\varphi 1} T_{\varphi 1\varphi 2}[1 - 2T_{e\varphi 2} - 2f_{\varphi 2}(1 - T_{\varphi 1\varphi 2} - T_{c\varphi 2} - T_{e\varphi 2})]
\end{aligned} \tag{6.4.17}
$$

For the cross-correlations between different terminals $\alpha \neq \beta$ it turns out that the appearing products of S-matrices in (6.2.3) cannot be fully transferred to products of transmission functions $T_{\alpha\beta} = |s_{\alpha\beta}|^2$ in contrast to the analysis of the three-terminal single QD (Sec. 6.3.2):

$$
\begin{aligned}
S_{e\varphi 1} &= s_{ee}^\dagger s_{e\varphi 1} s_{\varphi 1\varphi 1}^\dagger s_{e\varphi 1}(1-f_{\varphi 1}) + s_{ee}^\dagger s_{e\varphi 2} s_{\varphi 1\varphi 2}^\dagger s_{e\varphi 1}(1-f_{\varphi 2}) \\
&\quad + s_{e\varphi 1}^\dagger s_{ec} s_{\varphi 1c}^\dagger s_{\varphi 1\varphi 1} f_{\varphi 1} + s_{e\varphi 2}^\dagger s_{ec} s_{\varphi 1c}^\dagger s_{\varphi 1\varphi 2} f_{\varphi 2} \\
&\quad - |s_{e\varphi 1}|^2[1 - |s_{\varphi 1\varphi 1}|^2] f_{\varphi 1}(1-f_{\varphi 1}) + |s_{e\varphi 2}|^2 |s_{\varphi 1\varphi 2}|^2 f_{\varphi 2}(1-f_{\varphi 2}) \\
&\quad + s_{e\varphi 1}^\dagger s_{e\varphi 2} s_{\varphi 1\varphi 2}^\dagger s_{\varphi 1\varphi 1} f_{\varphi 1}(1-f_{\varphi 2}) + s_{e\varphi 2}^\dagger s_{e\varphi 1} s_{\varphi 1\varphi 1}^\dagger s_{\varphi 1\varphi 2} f_{\varphi 2}(1-f_{\varphi 1}) \\
&\quad + s_{ee}^\dagger s_{ec} s_{\varphi 1c}^\dagger s_{\varphi 1e} \\
S_{e\varphi 2} &= s_{ee}^\dagger s_{e\varphi 1} s_{\varphi 2\varphi 1}^\dagger s_{e\varphi 2}(1-f_{\varphi 1}) + s_{ee}^\dagger s_{e\varphi 2} s_{\varphi 2\varphi 2}^\dagger s_{e\varphi 2}(1-f_{\varphi 2}) \\
&\quad + s_{e\varphi 1}^\dagger s_{ec} s_{\varphi 2c}^\dagger s_{\varphi 2\varphi 1} f_{\varphi 1} + s_{e\varphi 2}^\dagger s_{ec} s_{\varphi 2c}^\dagger s_{\varphi 2\varphi 2} f_{\varphi 2} \\
&\quad - |s_{e\varphi 2}|^2[1 - |s_{\varphi 2\varphi 2}|^2] f_{\varphi 2}(1-f_{\varphi 2}) + |s_{e\varphi 1}|^2 |s_{\varphi 1\varphi 2}|^2 f_{\varphi 1}(1-f_{\varphi 1}) \\
&\quad + s_{e\varphi 1}^\dagger s_{e\varphi 2} s_{\varphi 2\varphi 2}^\dagger s_{\varphi 1\varphi 2} f_{\varphi 1}(1-f_{\varphi 2}) + s_{e\varphi 2}^\dagger s_{e\varphi 1} s_{\varphi 2\varphi 1}^\dagger s_{\varphi 2\varphi 2} f_{\varphi 2}(1-f_{\varphi 1}) \\
&\quad + s_{ee}^\dagger s_{ec} s_{\varphi 2c}^\dagger s_{\varphi 2e} \\
S_{\varphi 1\varphi 2} &= s_{\varphi 1e}^\dagger s_{\varphi 1\varphi 1} s_{\varphi 2\varphi 1}^\dagger s_{e\varphi 2}(1-f_{\varphi 1}) + s_{\varphi 1e}^\dagger s_{\varphi 1\varphi 2} s_{\varphi 2\varphi 2}^\dagger s_{e\varphi 2}(1-f_{\varphi 2}) \\
&\quad + s_{\varphi 1\varphi 1}^\dagger s_{\varphi 1c} s_{\varphi 2c}^\dagger s_{\varphi 2\varphi 1} f_{\varphi 1} + s_{\varphi 1\varphi 2}^\dagger s_{\varphi 1c} s_{\varphi 2c}^\dagger s_{\varphi 2\varphi 2} f_{\varphi 2} \\
&\quad - |s_{\varphi 1\varphi 2}|^2[1 - |s_{\varphi 2\varphi 2}|^2] f_{\varphi 2}(1-f_{\varphi 2}) - [1 - |s_{\varphi 1\varphi 1}|^2] |s_{\varphi 1\varphi 2}|^2 f_{\varphi 1}(1-f_{\varphi 1}) \\
&\quad + s_{\varphi 1\varphi 1}^\dagger s_{\varphi 1\varphi 2} s_{\varphi 2\varphi 2}^\dagger s_{\varphi 1\varphi 2} f_{\varphi 1}(1-f_{\varphi 2}) + s_{\varphi 1\varphi 2}^\dagger s_{\varphi 1\varphi 1} s_{\varphi 2\varphi 1}^\dagger s_{\varphi 2\varphi 2} f_{\varphi 2}(1-f_{\varphi 1}) \\
&\quad + s_{\varphi 1e}^\dagger s_{\varphi 1c} s_{\varphi 2c}^\dagger s_{\varphi 2e}
\end{aligned} \tag{6.4.18}
$$

Following the discussion of the cross-correlations in a four-terminal geometry in Ref. [BLA00] these terms refer to the quantum (Fermi) statistics of the electrons. They are called exchange-interference terms and reflect the fact that one is not able to distinguish from which of the two fictitious terminals a carrier was incident. This "lack of knowledge"gives rise to additional noise contributions. One may associate this with a kind of two-particle stochastic process. To deal with the exchange-interference terms on has to characterize the entire scattering matrix of the system.

Typically some "ad-hoc"phases [BUE91] of the scattering matrix elements must be introduced which may enter the results (see e.g. the discussions considering the Hanbury-Brown-Twiss effect in Sec. II F 9. in Ref. [BLA00]). As we show in the Appendix D, the S-matrix of our QD system is independent of these phases [SAM04].

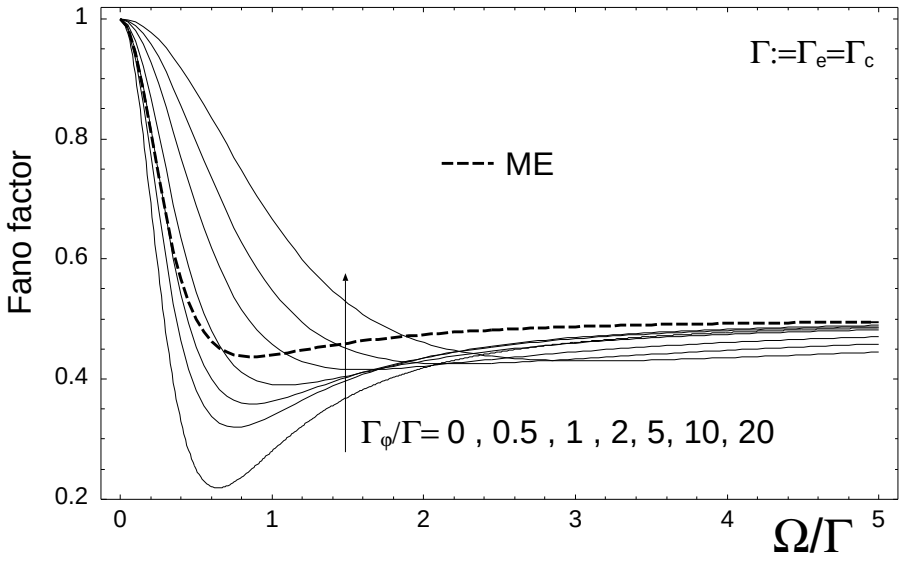

Figure 6.7.: On-resonance ($\varepsilon_1 = \varepsilon_2$) Fano factor (Eq. (6.4.15)) vs. interdot-coupling $|\Omega|$ for various dephasing rates Γ_φ. Fictitious terminals $f_{\varphi 1}/f_{\varphi 1}$ with fluctuations $\delta f_{\varphi 1}/\delta f_{\varphi 1}$, respectively. Dashed curve: master equation (ME) result for comparison. High-bias limit $f_e = 1$, $f_c = 0$

In Fig. 6.7 the resulting Fano factor calculated by Eq. (6.4.15) is shown. Here, in contrast to Fig. 6.6 the Fano factor approaches one half for large interdot-coupling $|\Omega| \gg \Gamma$ and for any amount of Γ_φ. Hence, the occupation statistics of the current carrying states is not changed by the fictitious terminals as it is expected for pure dephasing. The local minimum in the Fano factor for $\Gamma_\varphi = 0$ increases and shifts to larger $|\Omega|$ with increasing Γ_φ. The Fano factor minimum goes towards one half. The zero-frequency SPD $S_P(0)$ is shown in Fig. 6.8. The local minimum for $\Gamma_\varphi = 0$ at $\Gamma = 2|\Omega|$ which we identified as the fingerprint of quantum noise in Sec. 5.4 disappears with increasing Γ_φ.

By comparison with the SPD obtained for sequential tunneling through coupled QDs (blue curve in Fig. 5.5) we notice that this sequential tunneling limit cannot be approached by pure dephasing from coherent tunneling via an escape model. As a main reason we identify the decreasing of the current by increasing the decoherence which is accompanied by a reduction of the SPD (Fig. 6.8).

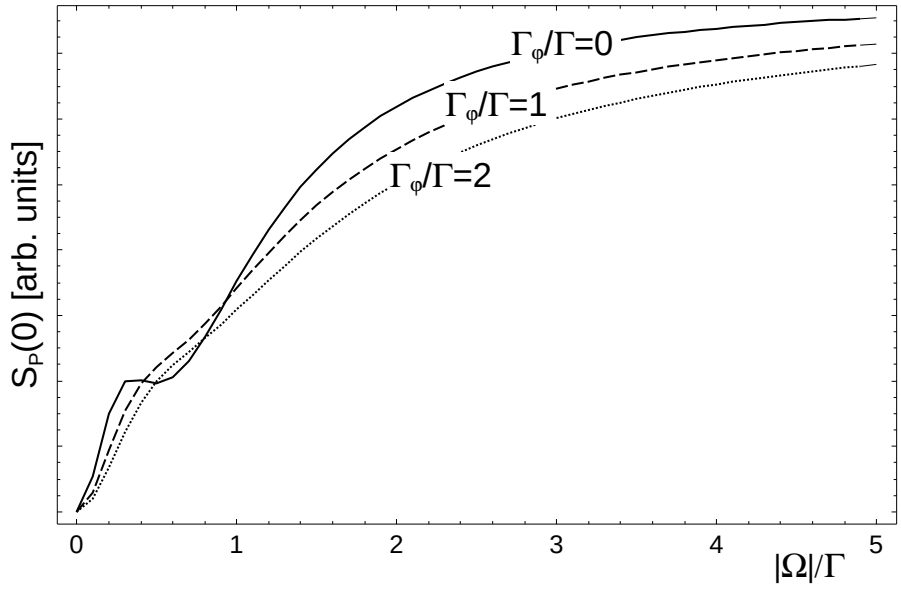

Figure 6.8.: On-resonance spectral power density (zero frequency) vs. interdot-coupling $|\Omega|$ for dephasing rates $\Gamma_\varphi/\Gamma = 0$ (solid line), $\Gamma_\varphi/\Gamma = 1$ (dashed line), and $\Gamma_\varphi/\Gamma = 2$ (dotted line). High-bias limit $f_e = 1$, $f_c = 0$

7. Current Fluctuations - Full Counting Statistics

Electronic transport through mesoscopic conductors mostly deals with time averaged currents. But, it turned out that the analysis of the accompanying current fluctuations can reveal a deeper insight in the transport mechanism. In the classical regime, the discreteness of the particles leads to the so-called shot noise which is sensitive to temporal correlations of the particle flow caused by Pauli's exclusion principles or the Coulomb interaction and their mutual interplay as elaborately discussed in Chap. 4. In the quantum limit the shot noise can also be influenced by electron correlations or entanglement.

Naturally the question arises whether it is possible to obtain even more information by considering higher-order correlators. Unfortunately, their calculation is a really hard task and even the second-order (shot noise) becomes quite cumbersome, e.g. by dealing with Coulomb interaction in the quantum limit (see Sec. 5.1.2.2). The adoption of the concept of *full counting statistics* (FCS) in mesoscopic electron transport from quantum optics allows to characterize comprehensively the statistics of the particle current, i.e. all moments of its distribution function are available in an elegant manner. The crucial quantity is the distribution function of the number N of transferred charges during the time interval t_0: $P(N, t_0)$. As soon as one knows this function one knows everything about the underlying stochastic process. This is equivalent to the determination of the *characteristic function* $F(\chi)$ (or the so-called *cumulant generating function*) which is defined by

$$\exp\left[-F(\chi)\right] = \sum_N P(N, t_0) \exp\left[iN\chi\right] \tag{7.0.1}$$

Note that is the definition for the two-terminal case, in which only the number N of transferred charges in one terminal matters. In the other terminal it is given by $-N$ due to charge conservation in the stationary case. In this chapter we also deal with more than two terminals. The generalization of (7.0.1) to this case can be found e.g. in Ref. [NAZ03]. From (7.0.1) it follows directly $F(0) = 0$ which ensures the probability normalization. From the characteristic function (7.0.1) the cumulants of k-th order can be obtained

$$C_k \equiv \langle\langle N^k \rangle\rangle = -(-i)^k \frac{\partial^k}{\partial \chi^k} F(\chi)\bigg|_{\chi=0} \tag{7.0.2}$$

Their meaning with respect to the distribution function $P(N, t_0)$ is illustrated in Fig. 7.1.

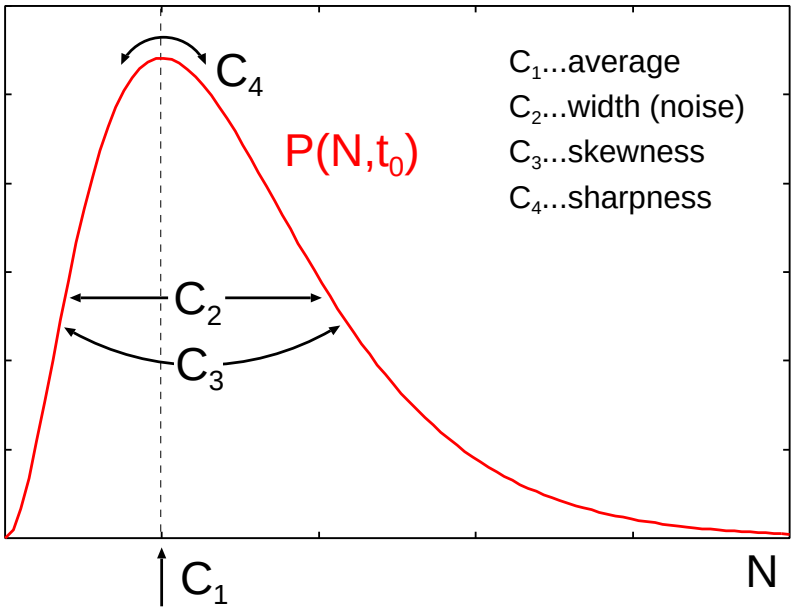

Figure 7.1.: An example of a probability distribution function $P(N, t_0)$ illustrating the meaning of different cumulants (7.0.2).

The first two cumulants are related to the average current $\langle I \rangle$ and zero-frequency SPD S_P of current fluctuations as

$$\langle I \rangle = -\frac{e}{t_0} C_1 \tag{7.0.3}$$

$$S_P = \frac{2e^2}{t_0} C_2 \tag{7.0.4}$$

where $\langle I \rangle = e\langle N \rangle / t_0$ has been used.

7.1. Single barrier tunneling: Binomial and Poissonian statistics

Let us consider a single potential barrier and assume that all states in both adjacent reservoirs e/c are either filled or empty at $T = 0$, i.e. there is no thermal noise present (see Sec. 4.1.2). Then, current fluctuations arise from scattering events in the barrier that connects both reservoirs. In the energy interval given by the difference of the chemical potentials in the reservoirs induced by a bias voltage V, the transmission probability T_{ec} is assumed to be independent of energy for

simplicity. In this case particle transfer is a Bernoulli process [LEV93, LEV96]: $K = t_0 eV/h$ particles try to pass the barrier independently of each other in a time interval t_0 and each of them succeeds with the probability T_{ec}. The number N of transmitted particles for a given number of trials K obeys binomial statistics with the distribution

$$P_{\text{binomial}}(N, t_0) = \left(\begin{array}{c} K \\ N \end{array} \right) T_{ec}^N (1 - T_{ec})^{K-N} \tag{7.1.1}$$

The respective cumulant generating function (7.0.1) is

$$F_{\text{binomial}}(\chi) = K \ \ln[1 + T_{ec}(e^{i\chi} - 1)] \tag{7.1.2}$$

The first three cumulants (7.0.2) are

$$\begin{aligned} C_1 &= KT_{ec} \\ C_2 &= KT_{ec}(1 - T_{ec}) \\ C_3 &= KT_{ec}(1 - T_{ec})(1 - 2T_{ec}) \end{aligned} \tag{7.1.3}$$

Using the relations (7.0.3),(7.0.4) on can easily reproduce the expressions for the current (6.2.5) and the last term in the SPD (6.2.6) under the assumption of energy-independent transmission.

In the limit $T_{ec} \ll 1$, the transfer of a particle is a rare event. In this limit and under the condition $KT_{ec} \to \langle N \rangle$ the quantum statistics becomes irrelevant and the FCS follows a Poissonian distribution with the characteristic function

$$F_{\text{Poissonian}} = t_0 \Gamma (e^{i\chi} - 1) \tag{7.1.4}$$

where the average transferred particle number $\langle N \rangle$ is replaced by $t_0\Gamma$ with the tunneling rate Γ which is widely used with respect to sequential tunneling in Chapter 3.

Note that all of these distributions tend to a Gaussian distribution for $K \to \infty$, as a consequence of the central limit theorem. Then, all cumulants higher than second order are suppressed. Therefore the measurement of higher-order cumulants is complicated. Nevertheless, in Refs. [REU03, BOM05] the third-order cumulant of a single tunnel junction was measured very recently.

7.2. Double barrier tunneling: Single quantum dot

Before we start with the consideration of the coupled QD system (triple barriers) let us briefly review the well-established results for the tunneling through a double barrier system [JON96, NAZ03]. Without performing the full derivation (where the

ingredients can be found in the following sections) we just give the characteristic function for high-bias noninteracting transport

$$F(\chi) = \frac{t_0}{2}\left(\Gamma_e + \Gamma_c - \sqrt{(\Gamma_e + \Gamma_c)^2 - 4\Gamma_e\Gamma_c(1 - e^{-i\chi})}\right) \tag{7.2.1}$$

Note that (7.2.1) holds regardless whether sequential or coherent tunneling is considered [BAG03a]. The normalized second and third cumulant namely the Fano factor and the normalized skewness, respectively, show minima at $\Gamma_e = \Gamma_c$ which corresponds to a generating function

$$F(\chi) = t_0\Gamma_{e/c}(e^{i\chi/2} - 1) \tag{7.2.2}$$

I.e. by comparison with (7.1.4) we can associate this with the Poissonian statistics of the transfer of "half charges". As outlined in Sec. 4.2.1 the Fano factor is one half for symmetric coupling without Coulomb interaction and caused by Pauli's exclusion principle which already gave a hint to half elementary charges. However, the detailed nature of the charge transfer was not accessible there. Now, we are in the position to identify it with a Poissonian process. For strong asymmetric couplings $\Gamma_e \ll \Gamma_c$ or $\Gamma_e \gg \Gamma_c$ Poissonian charge transfer appears, but with full charges so that the characteristic function is of the form (7.1.4) in which the smaller rate enters.

7.3. Triple barrier tunneling: Tunnel-coupled quantum dots

The specific aim of this section is the investigation of transport through two coupled QDs in series. It was shown in Sec. 3.3.2 and Ref. [SPR04] that the average (stationary) current through such system in the high-bias limit is identical in a coherent or sequential description if one presumes noninteracting electrons. The former approach is based on a reduced density matrix for the QD system (Sec. 3.3.2.1,[GUR96c]) which yields the same results as the SMF (Chap. 6) under the given assumptions, and the latter stems from a ME approach (Chap. 3). The main difference between both techniques can be seen in the time evolution of occupations in Fig. 3.4. While the coherent transients are governed by Rabi oscillations with a decay to the stationary occupations those oscillations are missing in the sequential treatment. In the long-time limit the occupations in both descriptions coincide which leads to the same average current as already mentioned. Interestingly, the zero-frequency SPD S_P is sensitive to this difference in time evolutions as discussed with respect to Fig. 5.5 in Sec. 5.4.

In the following, we want to apply the methods of FCS in order to obtain more information than contained in the first- and second-order cumulants. First, we address the FCS for the sequential tunneling using a ME technique. After that, the

FCS with SMF, and density matrix description for coherent transport is considered. Their results will be compared by means of the third-order cumulants. The last section of this chapter addresses the question how is the statistics influenced if pure dephasing (Chap. 6) is introduced in the coherent tunneling through coupled QDs and is it possible to reach the limit of sequential tunneling for strong dephasing.

7.3.1. Master equation approach - Sequential tunneling

In order to obtain the characteristic function we go along the lines of Refs. [BAG03, BAG03a]:

We have a ME[1] of the form $\partial_t|p\rangle = -\hat{M}|p\rangle$ with the matrix elements of $\hat{M}$:

$$M_{ij} = \delta_{ij}\gamma_i - \Gamma_{i\leftarrow j} \quad , \quad \gamma_i = \sum_{i\neq j}\Gamma_{i\leftarrow j} \tag{7.3.1}$$

where i and j denote the many-particle states of the QD system. For the following it is useful to present the $\hat{M}$ operator in the form:

$$\hat{M} = \hat{\gamma} - \hat{\Gamma} \quad , \quad \hat{\Gamma} = \sum_{k=1}^{M}\left(\hat{\Gamma}_k^{(+)} + \hat{\Gamma}_k^{(-)}\right) \tag{7.3.2}$$

where $\hat{\gamma}$ is the diagonal operator in the basis $|n\rangle = |n_1 \dots n_M\rangle$ ($n_\alpha \in \{0, 1\}$) and $\hat{\Gamma}_k^{(\pm)}$ refers to electron transfers with the transition labeled by $k = (\alpha, \beta)$ (α and β denote single particle states in the QD system)

$$\hat{\gamma} = \sum_{\{n\}}|n\rangle\gamma(n)\langle n| \quad , \quad \hat{\Gamma}_k^{(\pm)} = \sum_{\{n\}}|n'\rangle\Gamma_k^{(\pm)}\langle n| \tag{7.3.3}$$

The state $|n'\rangle = |n_1 \dots n'_\alpha \dots n'_\beta \dots n_M\rangle$ results from the state $|n\rangle$ by changing the corresponding occupation numbers $n'_\alpha = n_\alpha - \sigma_k$, $n'_\beta = n_\beta + \sigma_k$,where $\sigma_k = \pm 1$ denotes the direction of the transition. Now, one introduces the χ-dependent linear operator M_χ as

$$\hat{M}_\chi(t) = \hat{\gamma} - \hat{\Gamma}_\chi(t) \tag{7.3.4}$$

$$\hat{\Gamma}_\chi(t) = \sum_{k=1}^{N}\left(\hat{\Gamma}_k^{(+)}e^{i\chi_k(t)} + \hat{\Gamma}_k^{(-)}e^{-i\chi_k(t)}\right) + \sum_{k=N+1}^{M}\left(\hat{\Gamma}_k^{(+)} + \hat{\Gamma}_k^{(-)}\right) \tag{7.3.5}$$

Each operator $\hat{\Gamma}_k^{(\pm)}$ that corresponds to a transition through an external junction ($k = 1 \dots N$) is multiplied by an extra χ-dependent factor $e^{\pm i\chi_k(t)}$. The diagonal part and the operators for internal transitions with $k > N$ remains unchanged.

[1] Here we use the notation of Refs. [BAG03, BAG03a] which differs from the ME description in Chap. 3.

For the low frequency limit $\omega \ll \Gamma$ one can set $\chi_k(t) = \chi_k$ during the time interval of measurement $0 \leq t \leq t_0$ and $\chi_k(t) = 0$ otherwise. Then, the minimum eigenvalue $m_{\min}(\{\chi_i\})$ of the operator (7.3.4) gives the characteristic function

$$F(\{\chi_i\}) = t_0 m_{\min}(\{\chi_i\}) \tag{7.3.6}$$

For the QD stack (Sec. 3.3) the operator (7.3.4) becomes (probability vector $(P_{(0,0)}, P_{(0,1)}, P_{(1,0)}, P_{(1,1)})^T$)

$$M_\chi = \begin{pmatrix} \Gamma_e & -\Gamma_c e^{-i\chi_2} & 0 & 0 \\ 0 & \Gamma_e + \Gamma_c + Z & -Z & 0 \\ -\Gamma_e e^{i\chi_1} & -Z & Z & -\Gamma_c e^{-i\chi_2} \\ 0 & -\Gamma_e e^{i\chi_1} & 0 & \Gamma_c \end{pmatrix} \tag{7.3.7}$$

For $\Gamma_e = \Gamma_c \equiv \Gamma$, $\chi \equiv \chi_1 - \chi_2$, and $Z \equiv 2\Omega^2/\Gamma$ we obtain (*Mathematica*) the characteristic function:

$$F(\chi) = \frac{t_0}{6}\left\{(6\Gamma + 4Z) - \frac{(1+i\sqrt{3})(3\Gamma^2 + 4Z^2)}{G(\chi)} + (1 - i\sqrt{3})G(\chi)\right\} \tag{7.3.8}$$

with

$$\begin{aligned} G(\chi) \;=\; & \Big\{8Z^3 + 9\Gamma^2 Z(1 - 3e^{-i\chi}) + \\ & + \frac{1}{2}\sqrt{\left[16Z^3 + 18\Gamma^2 Z(1 - 3e^{-i\chi})\right]^2 - 4(3\Gamma^2 + 4Z^2)^3}\Big\}^{\frac{1}{3}} \end{aligned} \tag{7.3.9}$$

With the characteristic function (7.3.8) all cumulants (7.0.2) of the distribution function can be calculated now and reproduce the current (3.3.6) for $\Delta E = 0$ and $\Gamma_e = \Gamma_c$ and the noise behavior depicted in Fig. 5.5 (blue curve).

Regarding Eq. (7.0.1) the probability for N electrons traversing the left or right barrier during the measurement time t_0 yields

$$P(N, t_0) = \int_{-\pi}^{\pi} \frac{d\chi}{2\pi} \exp\left[-F(\chi) - iN\chi\right] \tag{7.3.10}$$

For the evaluation of the integral (7.3.10) one can use the saddle point approximation [BAG03a]: The saddle-point χ^* of the function $\Omega(\chi) = F(\chi) + i\chi I t_0/e$ with the current $I(\chi) = (ie/t_0)\partial_\chi F(\chi)$ (Eq. (7.0.3) taken at arbitrary χ) turns out to be purely imaginary. Within this approximation the probability for measuring a current during the time interval t_0 simply becomes $P(I) \approx \exp\left[-\Omega(\chi^*)\right]$ with $I(\chi)$ (see above) regarded as parametric relation between I and χ^*.

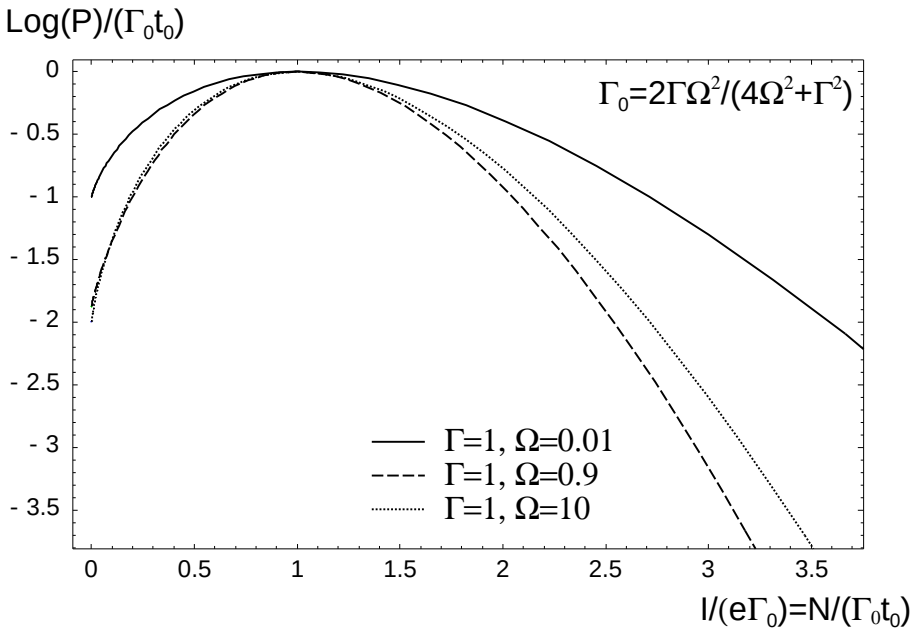

Figure 7.2.: Current statistics with ME for the double-dot system [SPR04] for different tunnel couplings Ω and symmetric coupling $\Gamma = \Gamma_e = \Gamma_c$ on resonance.

The statistics for the double-dot system is shown in Fig. 7.2 for different inter-dot couplings Ω. For all curves the unity probability occurs at the resonance current $I_0 = e\Gamma_0$ with the effective rate $\Gamma_0 = 2\Gamma\Omega^2/(4\Omega^2 + \Gamma^2)$. The solid line corresponds to an almost uncorrelated current due to small Ω and therefore to a Poissonian process.

7.3.2. Coherent approach

7.3.2.1. Levitov's formula - S-matrix description

The characteristic function (known as Levitov's formula [LEV93, LEV96]) for a mesoscopic conductor with n terminals is given as

$$F(\{\chi_i\}) = t_0 \int \frac{d\varepsilon}{2\pi\hbar} F_\varepsilon(\{\chi_i\}) \tag{7.3.11}$$

with

$$F_\varepsilon(\{\chi_i\}) = \ln \mathrm{Det}\left[\mathbb{1} - \hat{f} + \hat{f} s^\dagger \hat{\chi} s \hat{\chi}^{-1}\right] \tag{7.3.12}$$

with $\hat{f} \equiv \mathrm{Diag}[f_1, \ldots, f_n]$ and $\hat{\chi} \equiv \mathrm{Diag}[e^{i\chi_1}, \ldots, e^{i\chi_n}]$, where f_i and χ_i are the distribution functions and counting fields of the terminal i, respectively. s is the

$n \times n$ scattering matrix[2] (S-matrix: already introduced in Chap. 6).

For our double-dot system (7.3.11) becomes explicitly ($\chi = \chi_2 - \chi_1$)

$$F(\chi) = -\frac{t_0}{\pi} \int d\varepsilon \ln \{1 + T_{ec}(\varepsilon)[\exp(i\chi) - 1]\} \tag{7.3.13}$$

This is the generalization of the characteristic function of binomial statistics (7.1.2) for energy-dependent transmission. We assume the high-bias limit such that the contact occupations are $f_e = 1$ and $f_c = 0$. With the transmission function

$$T_{ec}(\varepsilon) = \frac{\Gamma_e \Gamma_c \Omega^2}{|(\varepsilon - \varepsilon_1 + i\Gamma_e/2)(\varepsilon - \varepsilon_2 + i\Gamma_c/2) - \Omega^2|^2} \tag{7.3.14}$$

for tunneling through the double QDs with one level ε_i for the i-th QD, for symmetric coupling $\Gamma = \Gamma_e = \Gamma_c$, and on-resonance transport ($\varepsilon_1 = \varepsilon_2 = 0$) we obtain the characteristic function

$$F(\chi) = \frac{t_0}{2}\left[2\Gamma - \sqrt{\Gamma^2 - 4i\Gamma\Omega\exp(-i\chi/2) - 4\Omega^2} - \sqrt{\Gamma^2 + 4i\Gamma\Omega\exp(-i\chi/2) - 4\Omega^2}\right] \tag{7.3.15}$$

Now, the distribution function of the tunneling current can be calculated in the same manner as in the last section. For different Ω they are displayed in Fig. 7.3.

In the limits of small and large Ω the statistics for sequential tunneling (Fig. 7.2) and coherent tunneling (Fig. 7.3) fully coincide. For intermediate Ω deviations are present as already outlined with respect to the noise (Sec. 5.4). The third-order cumulant (skewness) vs. Ω is shown in Fig. 7.4.

For very small Ω the skewness approaches zero for both sequential and coherent tunneling. Further, it can be seen that for all Ω the skewness of coherent tunneling is closer to zero than for sequential tunneling. In the region $0 < |\Omega|/\Gamma < 1$ the skewness of the coherent tunneling shows more structure than that of the sequential tunneling. A better interpretation can be obtained by considering the normalized skewness $c_3 \equiv C_3/\langle I \rangle$ in Fig. 7.4b where the third cumulant is divided by the average current. For $|\Omega| \to 0$ this value becomes unity in both approaches which refers to Poissonian statistics where all higher cumulants equal the average value of the distribution. There are three distinct extrema in the normalized skewness of coherent tunneling. Using its characteristic function (7.3.15) and putting $\Gamma^2/4|\Omega|^2 \equiv x$ we get the normalized third cumulant

$$c_3 = \frac{1 - 8x + 21x^2 - 14x^3 + 4x^4}{4(1+x)^4} \tag{7.3.16}$$

The extrema are found to be

[2]For simplicity we consider single-mode conductors.

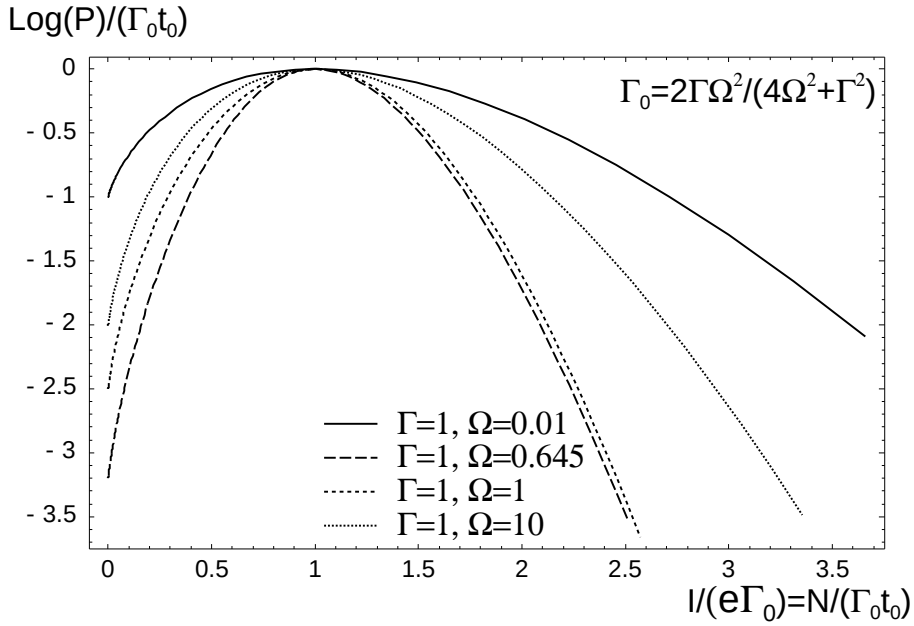

Figure 7.3.: Current statistics with coherent approach for the double-dot system [SPR04] for different tunnel couplings Ω and symmetric coupling $\Gamma = \Gamma_e = \Gamma_c$ on resonance.

$$x_1 = 1, \qquad x_2 = \frac{1}{10}\left(9 - \sqrt{41}\right) \approx 0.26, \qquad x_3 = \frac{1}{10}\left(9 + \sqrt{41}\right) \approx 1.54 \quad (7.3.17)$$

which corresponds to

$$\frac{|\Omega|}{\Gamma} = \left\{0.40, \frac{1}{2}, 0.98\right\} \quad (7.3.18)$$

From Fig. 7.4b) we see that $|\Omega|/\Gamma$ =0.4 and 0.98 correspond to local minima and $|\Omega|/\Gamma$ =1/2 is the local maximum. Inserting these extreme points back into the generating function we find for the local maximum, $x = 1$

$$F(\chi) = t_0\Gamma\left(e^{i\chi/4} - 1\right) \quad (7.3.19)$$

This is the characteristic function of the Poissonian transfer of "quarter charges". Note that the Fano factor which can be considered as the fraction of effectively transferred charges is 0.25 at this point (Fig. 5.5b) [KIE05b].

Unfortunately, the two local minima do not correspond to any particularly "simple"function. Thus, there is no simple explanation of the statistics at these two points.

In the large coupling limit $|\Omega| \gg \Gamma$ for both sequential and coherent tunneling approach the same limit value of 1/4 of the normalized skewness is reached which

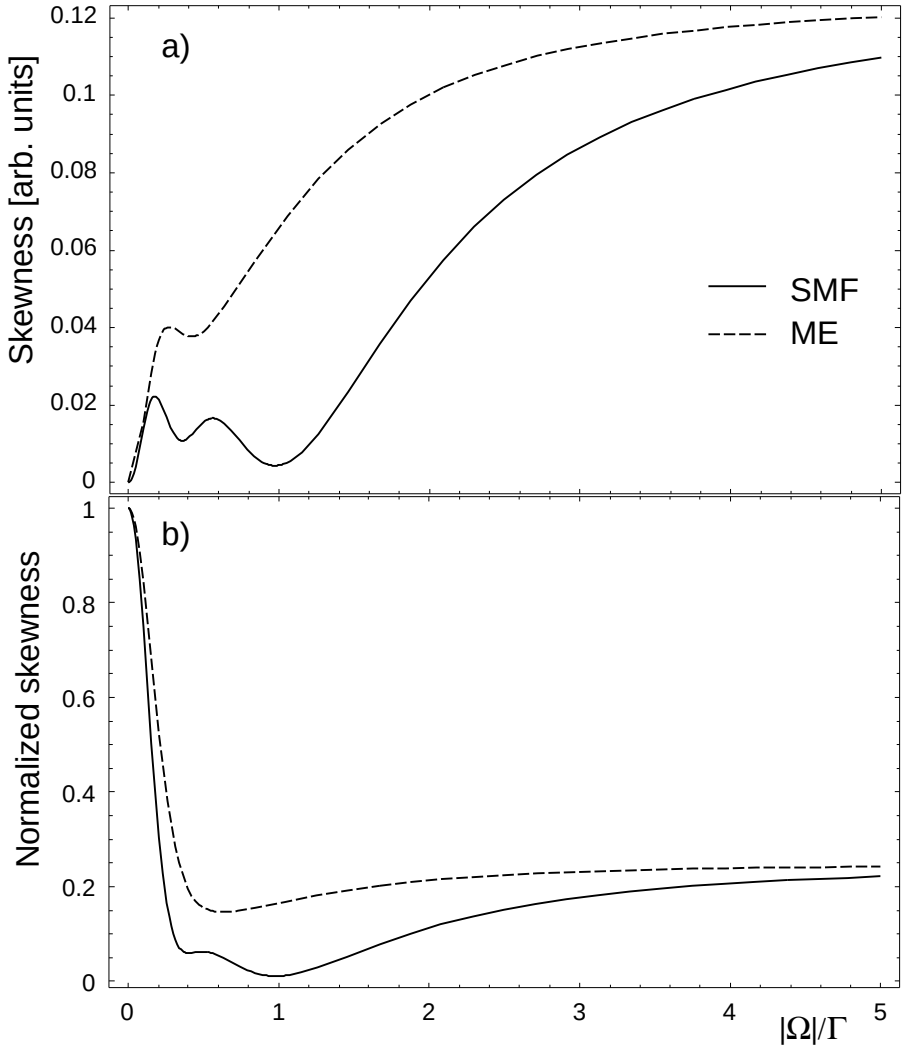

Figure 7.4.: a) Third-order cumulant of the distribution ("skewness") vs. tunnel coupling Ω, b) Normalized skewness in the ME approach: dashed curve; in the coherent approach (SMF): solid curve. $\Gamma = \Gamma_e = \Gamma_c$.

we also directly can read off from Eq. (7.3.16) setting $x = 0$. The corresponding transfer of charges is also Poissonian but here with "half charges"in agreement with the result for tunneling through a symmetric single QD.

7.3.2.2. Density matrix description

In this section we will show an alternative way to obtain the FCS for coherent tunneling through a QD system. Gurvitz et al. [GUR96c, GUR98] provide transport equations in terms of the dynamics of the elements of the reduced density matrix in Fock-space of the QD system. Such equations were already used in Sec. 3.3.2 regarding the noninteracting transport through coupled QDs. To illustrate the approach, we first consider a single QD with a single level. Keeping the notation of [GUR96c] the recurrency equations are

$$\begin{aligned} \dot{\rho}_{aa}^{(n)}(t) &= -\Gamma_e \rho_{aa}^{(n)}(t) + \Gamma_c \rho_{bb}^{(n-1)}(t) \\ \dot{\rho}_{bb}^{(n)}(t) &= \Gamma_e \rho_{aa}^{(n)}(t) - \Gamma_c \rho_{bb}^{(n)}(t) \end{aligned} \tag{7.3.20}$$

with the Fock states $|a\rangle \equiv |0\rangle$ (unoccupied level) and $|b\rangle \equiv |1\rangle$ (occupied level). The index n is the number of electrons that have been transferred to the collector reservoir during the time t. These equations must be supplemented by the initial conditions. To obtain the equations for the total probabilities (compare with the ME in Chap. 3) one just has to sum up Eqs. (7.3.20) $\rho_{aa/bb} = \sum_n \rho_{aa/bb}^{(n)}$. As a consequence, we can immediately find the probability of transferred charges n in time t

$$P(n,t) = \rho_{aa}^{(n)} + \rho_{bb}^{(n)} \tag{7.3.21}$$

or the cumulant generating function by using its definition (7.0.1)

$$e^{F(\chi)} = \sum_n \left[\rho_{aa}^{(n)} + \rho_{bb}^{(n)}\right] e^{in\chi} \tag{7.3.22}$$

We note that for $\chi = 0$, we have $e^{F(\chi)} = 1$ directly from probability conservation $\sum_n [\rho_{aa}^{(n)} + \rho_{bb}^{(n)}] = 1$. An expression for $F(\chi)$ one obtains in the following way. One first introduces the (discrete) Fourier transformed quantities

$$\rho_{aa}(\chi,t) = \sum_n \rho_{aa}^{(n)}(t) e^{in\chi}, \qquad \rho_{bb}(\chi,t) = \sum_n \rho_{bb}^{(n)}(t) e^{in\chi} \tag{7.3.23}$$

which gives the generating function

$$e^{F(\chi)} = \rho_{aa}(\chi,t) + \rho_{bb}(\chi,t) \tag{7.3.24}$$

Fourier transforming Eqs. (7.3.20) leads to

$$\begin{aligned}\dot{\rho}_{aa}(\chi,t) &= -\Gamma_e\rho_{aa}(\chi,t) + \Gamma_c e^{-i\chi}\rho_{bb}(\chi,t)\\ \dot{\rho}_{bb}(\chi,t) &= \Gamma_e\rho_{aa}(\chi,t) - \Gamma_c\rho_{bb}(\chi,t)\end{aligned} \tag{7.3.25}$$

Here, we note that the counting field term $e^{-i\chi}$ appears naturally from the transformation. Importantly, it appears at the place in the recurrency equations which describes the transfer of one electron out into the collector reservoir. In order to find the characteristic function one has to solve a coupled set of first order differential equations. We write Eqs. (7.3.25) on a vector form. We then have

$$\begin{aligned}\dot{\underline{\rho}}(\chi,t) &= \underline{\underline{A}}(\chi)\cdot\underline{\rho}(\chi,t), \qquad \underline{\rho}(\chi,t) = \begin{pmatrix}\rho_{aa}(\chi,t)\\ \rho_{bb}(\chi,t)\end{pmatrix}\\ \underline{\underline{A}}(\chi) &= \begin{pmatrix}-\Gamma_e & \Gamma_c e^{-i\chi}\\ \Gamma_e & -\Gamma_c\end{pmatrix}\end{aligned} \tag{7.3.26}$$

Diagonalizing $\underline{\underline{A}}$ gives

$$\underline{\underline{A}} = \underline{\underline{U}}\,\underline{\underline{\Lambda}}\,\underline{\underline{U}}^{-1}, \qquad \underline{\underline{\Lambda}} = \begin{pmatrix}\lambda_1 & 0\\ 0 & \lambda_2\end{pmatrix} \tag{7.3.27}$$

with

$$\lambda_{1/2} = \frac{1}{2}\left[\Gamma_e + \Gamma_c \pm \sqrt{(\Gamma_e+\Gamma_c)^2 - 4\Gamma_e\Gamma_c(1-e^{-i\chi})}\right] \tag{7.3.28}$$

Introducing the rotated vector $\underline{\tau}(\chi,t) \equiv \underline{\underline{U}}^{-1}\underline{\rho}(\chi,t)$ we get the equation

$$\dot{\underline{\tau}}(\chi,t) = \underline{\underline{\Lambda}}(\chi)\underline{\tau}(\chi,t) \tag{7.3.29}$$

which has the homogeneous solution

$$\tau_1(\chi,t) = c_1 e^{\lambda_1 t}, \qquad \tau_2(\chi,t) = c_2 e^{\lambda_2 t} \tag{7.3.30}$$

with the constants c_1 and c_2. To get the solution for $\underline{\rho}(\chi,t)$ we have to transform back with $\underline{U}$. The characteristic function is obtained by adding the solutions for $\rho_{aa}(\chi,t)$ and $\rho_{bb}(\chi,t)$ as in (7.3.24). In general, the result will be of the form

$$\rho_{aa}(\chi,t) + \rho_{bb}(\chi,t) = ce^{\lambda_1 t} + de^{\lambda_2 t} \tag{7.3.31}$$

where c and d are constants to be determined from the initial conditions. However, we can now make use of the normalization condition that tells us that $\rho_{aa}(\chi = 0,t) + \rho_{bb}(\chi = 0,t) = 1$ for any t. As a consequence, we see that in general only the term with the eigenvalue λ_i which is zero for $\chi = 0$ can contribute. In our example, this means λ_2. One can thus directly write ($d = 0$)

$$e^{F(\chi)} = \rho_{aa}(\chi, t) + \rho_{bb}(\chi, t) = ce^{\lambda_2 t} \tag{7.3.32}$$

The characteristic function is then given by

$$F(\chi) = t\lambda_2 + \ln c \tag{7.3.33}$$

where we in the long time limit of interest can neglect the second, time independent term and only keep the first term that grows linearly in time. We thus end up with the characteristic function

$$F(\chi) = t\frac{1}{2}\left[\Gamma_e + \Gamma_c - \sqrt{(\Gamma_e + \Gamma_c)^2 - 4\Gamma_e\Gamma_c(1 - e^{-i\chi})}\right] \tag{7.3.34}$$

which is the "standard" solution for tunneling through double barriers comprising a single level [NAZ03, BAG03, BAG03a]. This generating function we already introduced in Sec. 7.2 to characterize the statistics of charge transfer (7.2.1).

Now, we simply can apply this approach to the coupled QD system which provides the simplest nontrivial example. The respective transport equations for the elements of the reduced density matrix were already given in (3.3.7). As shown above we simply have to put the factor $e^{-i\chi}$ at the place which describes the transfer of one electron into the collector reservoir and use the Fourier transformed density matrix elements. Then, these equations reads (suppressing the χ- and t-arguments)

$$\begin{aligned}
\dot{\rho}_{aa} &= -\Gamma_e\rho_{aa} + e^{-i\chi}\Gamma_c\rho_{cc} \\
\dot{\rho}_{bb} &= \Gamma_e\rho_{aa} + e^{-i\chi}\Gamma_c\rho_{dd} + i\Omega(\rho_{bc} - \rho_{cb}) \\
\dot{\rho}_{cc} &= -\Gamma\rho_{cc} - i\Omega(\rho_{bc} - \rho_{cb}) \\
\dot{\rho}_{dd} &= -\Gamma_c\rho_{dd} + \Gamma_e\rho_{cc} \\
\dot{\rho}_{bc} &= i\Delta E\rho_{bc} + i\Omega(\rho_{bb} - \rho_{cc}) - \frac{1}{2}(\Gamma_e + \Gamma_c)\rho_{bc}
\end{aligned} \tag{7.3.35}$$

with the abbreviations for the Fock states: $|a\rangle \equiv |0,0\rangle$, $|b\rangle \equiv |1,0\rangle$, $|c\rangle \equiv |0,1\rangle$, and $|d\rangle \equiv |1,1\rangle$ and $\rho_{cb} = \rho_{bc}^*$. Note again that in contrast to the example of a single QD coherence now plays a important role since the off-diagonal elements of the density matrix appear in the transport equations (7.3.35). Writing these equations in a vector form and working with separate equations for the real and imaginary parts of ρ_{bc} gives the χ-dependent matrix $\underline{\underline{A}}$ (3.3.8) and putting $e^{-i\chi}$ at the corresponding place. Diagonalizing this 6×6-matrix one gets the same generating function (i.e. the eigenvalue that goes to zero for $\chi = 0$) as obtained in the preceding section by Levitov's formula (7.3.15). Hence, the density matrix approach introduced by Gurvitz et al. and the S-matrix approach provide the same statistics of noninteracting charge transfer through the coupled QDs. However, we did not address any additional interactions in the statistics of charge transfer so far. One of the strengths of the density matrix description is the incorporation of scattering starting from a

detailed microscopic picture, e.g. electron-phonon or electron-electron interactions. In contrast, the S-matrix approach has to rely mainly on a phenomenological treatment of interactions. For instance, phase-breaking scattering can be implemented by an escape model which was elaborately discussed in Chap. 6.

7.3.3. Pure dephasing - Stochastic Path Integral method

As shown in the considerations of Chap. 6, the "pure"dephasing in tunneling through localized states can be realized by attaching fictitious voltage probes which can destroy the phase of electrons by escaping. There was the difficulty that the noise goes towards its Poissonian value since the current carrying states are empty for the time range of escape. To avoid that fluctuating occupations of the additional terminals were assumed such that the electron is instantaneously reinjected in the system. This leads to a complicated structure for the noise expression which also contains cross-correlations which are fortunately phase insensitive. For the calculation of the FCS the fictitious terminal distributions and the respective counting fields have to be fluctuating quantities now. To solve this highly nontrivial problem one can use a Stochastic Path Integral approach (SPI) recently developed by S. Pilgram et al. [PIL03, JOR04]. A detailed description of this method would go beyond the scope of this thesis so that we refer the reader to [PIL03, JOR04].

The generating function for a given energy is given by (7.3.12) with

$$\hat{f} = \begin{pmatrix} 1 & 0 & 0 & 0 \\ 0 & f_{\varphi 1} & 0 & 0 \\ 0 & 0 & f_{\varphi 2} & 0 \\ 0 & 0 & 0 & 0 \end{pmatrix}, \qquad \hat{\chi} = \begin{pmatrix} 1 & 0 & 0 & 0 \\ 0 & e^{i\chi_1} & 0 & 0 \\ 0 & 0 & e^{i\chi_2} & 0 \\ 0 & 0 & 0 & e^{i\chi} \end{pmatrix} \tag{7.3.36}$$

for the coupled QD system depicted in Fig. 6.1. The S-matrix for this system is calculated by means of (D.0.2). The resulting generating function is a cumbersome object even if one assumes $\Gamma = \Gamma_e = \Gamma_c$, $\Gamma_\varphi = \Gamma_{\varphi 1} = \Gamma_{\varphi 2}$, and on-resonance transport $\Delta E = \varepsilon_1 - \varepsilon_2 = 0$ and we will skip its explicit form here. The quantities $f_{\varphi 1}$, $f_{\varphi 2}$, χ_1, and χ_2 are fluctuating in time. The distribution of transmitted charges can be formulated as a classical path integral over all possible fluctuation configurations. This integral is maximal at the "saddle point" where the fluctuations are small, i.e. where the derivative of the generating function with respect to $f_{\varphi 1}$, $f_{\varphi 2}$, χ_1, and χ_2 is zero. This gives the nonlinear coupled saddle point equations:

$$\frac{dF_\varepsilon}{df_{\varphi 1}} = 0, \quad \frac{dF_\varepsilon}{df_{\varphi 2}} = 0, \quad \frac{dF_\varepsilon}{d\chi_1} = 0, \quad \frac{dF_\varepsilon}{d\chi_2} = 0 \tag{7.3.37}$$

for the solutions $f_{\varphi 1}$, $f_{\varphi 2}$, χ_1, and χ_2. Unfortunately, these equations cannot be solved analytically. To obtain the cumulants of the distribution of the transmitted

charges we insert the χ-dependent quantities in the generating function, differentiate with respect to χ at $\chi = 0$ and perform the energy integration numerically. The dependencies of $f_{\varphi 1}$,$f_{\varphi 2}$, $\exp[i\chi_1]$, and $\exp[i\chi_2]$ on χ turn out to be quite simple: the real parts depend quadratically and the imaginary parts linearly on χ. For $\chi = 0$ the imaginary parts vanish, the real parts of $f_{\varphi 1}$ and $f_{\varphi 2}$ provide the average occupations of QD1 and QD2, and the real parts of $\exp[i\chi_1]$ and $\exp[i\chi_2]$ are unity. Hence, the $\chi = 0$-result of (7.3.37) provides us with the statistics for the dephasing model where only the net charge transfer to the fictitious terminals is demanded to be zero. We indeed recover the previous result for the Fano factor presented in Fig. 6.6 where the strong coupling value went towards unity with increasing Γ_φ. The noise calculated by means of the SPI approach fully agrees with the results obtained by the direct calculation of the SPD (6.4.15) presented in Fig. 6.8. Hence, the saddle-point approximation in the SPI approach is substantiated by reproducing the first and second cumulant within an independent calculation. Now, we are pretty confident that the computation of the next-order cumulants reveals reliable results. The third-order cumulant namely the skewness of the distribution function of transmitted electrons is shown in Fig. 7.5 for the SPI-approach with fluctuating $f_{\varphi 1}$,$f_{\varphi 2}$, $\exp[i\chi_1]$, and $\exp[i\chi_2]$.

The skewness vs. interdot coupling $|\Omega|$ is shown for various increasing Γ_φ's. For $\Gamma_\varphi = 0$ the result of coherent tunneling in Fig. 7.4 is reproduced. The distinct local extrema which we already discussed with respect to Fig. 7.4b) vanish and the normalized skewness increases. Only one global minimum survives and shifts to higher $|\Omega|$-values with increasing Γ_φ. In the large coupling limit $|\Omega| \gg \Gamma$ the normalized skewness value of 1/4 is independent on the dephasing strength Γ_φ in the same manner as the Fano factor (Fig. 6.7). For small coupling $|\Omega| \ll \Gamma$ the skewness approaches the first cumulant which again refers to Poissonian statistics of the tunneling process in this limit. To obtain an analytical result for the statistics in the low-coupling limit we introduce the small parameter $\gamma \equiv |\Omega|/\Gamma \ll 1$. Then, we can expand the quantities $f_{\varphi 1}$,$f_{\varphi 2}$, $\exp[i\chi_1]$, and $\exp[i\chi_2]$ to second order as

$$\begin{aligned} f_{\varphi 1} &= f_{\varphi 1}^{(0)} + \gamma f_{\varphi 1}^{(1)} + \frac{\gamma^2}{2} f_{\varphi 1}^{(2)} \\ f_{\varphi 2} &= f_{\varphi 2}^{(0)} + \gamma f_{\varphi 2}^{(1)} + \frac{\gamma^2}{2} f_{\varphi 2}^{(2)} \\ e^{i\chi_1} &= \Theta_1^{(0)} + \gamma \Theta_1^{(1)} + \frac{\gamma^2}{2} \Theta_1^{(2)} \\ e^{i\chi_2} &= \Theta_2^{(0)} + \gamma \Theta_2^{(1)} + \frac{\gamma^2}{2} \Theta_2^{(2)} \end{aligned} \tag{7.3.38}$$

Inserting these equations into the saddle point equations (7.3.37), we can solve them by order in γ. This gives to zeroth order

$$f_{\varphi 1}^{(0)} = 1, \qquad f_{\varphi 2}^{(0)} = 0, \qquad \Theta_1^{(0)} = 1 \qquad \Theta_2^{(0)} = e^{i\chi} \tag{7.3.39}$$

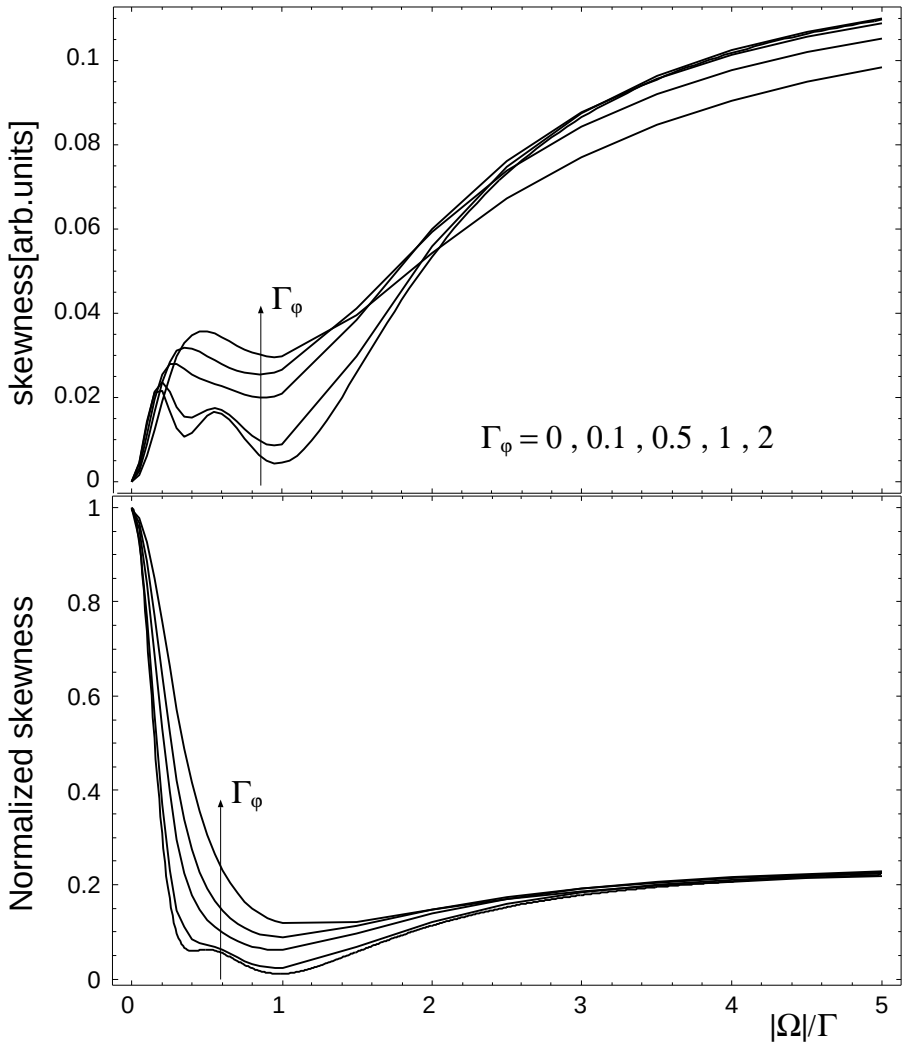

Figure 7.5.: Skewness and normalized skewness vs. tunnel coupling $|\Omega|$ for various Γ_φ by means of saddle point approximation in SPI approach.

which is the result for decoupled QDs as expected. To first order one finds the "trivial" result

$$f_{\varphi 1}^{(1)} = 0, \qquad f_{\varphi 2}^{(1)} = 0, \qquad \Theta_1^{(1)} = 0 \qquad \Theta_2^{(1)} = 0 \tag{7.3.40}$$

Inserting the expansion (7.3.38) into the generating function (7.3.12) with the obtained values in (7.3.39) and (7.3.40), and expanding the generating function to second order in γ, we get

$$F_\varepsilon = \frac{|\Omega|^2(\Gamma+\Gamma_\varphi)^2}{[(\varepsilon_1-\varepsilon)^2+(\Gamma+\Gamma_\varphi)^2/4][(\varepsilon_2-\varepsilon)^2+(\Gamma+\Gamma_\varphi)^2/4]}(e^{i\chi}-1) \tag{7.3.41}$$

which is independent on $f_{\varphi 1}^{(2)}$, $f_{\varphi 2}^{(2)}$, $\Theta_1^{(2)}$, and $\Theta_2^{(2)}$. Performing the energy integration, the total generating function becomes (on-resonance $\varepsilon_1 = \varepsilon_2$)

$$F(\chi) = \frac{2|\Omega|^2}{(\Gamma + \Gamma_\varphi)}(e^{i\chi} - 1) \tag{7.3.42}$$

We see that the statistics thus becomes Poissonian with the tunneling rate given by Fermi's Golden rule [SPR04] containing an additional effective broadening by Γ_φ of both QD levels due to dephasing.

8. Summary

The electronic transport through mesoscopic conductors with a discrete level spectrum, namely systems of QDs, was the subject of the present work. In particular, parallel QDs coupled via an electrostatic potential due to the Coulomb interaction or tunnel-coupled QDs in series were studied theoretically. They were connected to two electron reservoirs (emitter and collector) which are treated in local equilibrium. The difference of their chemical potentials given by an applied bias voltage drives the QD system out of equilibrium. The central observables for the transport characterization were the stationary current and the zero-frequency spectral power density. In addition, the skewness as the third-order cumulant of transport processes was considered.

Different approaches to describe the nonlinear transport through these systems were used and have been reviewed in detail: master equation (ME) approach, non-equilibrium Green's function (NEGF) technique, scattering matrix formalism (SMF), and density matrix description.

The emergence of multiple peaks in the current voltage characteristic of coupled QD systems was systematically elaborated in the sequential tunneling regime. As a major advantage, the Coulomb interaction can be implemented without approximations in this regime. For parallel QDs a negative differential conductance in the current-voltage characteristic can be caused by the mutual blocking of single particle states due to Coulomb interaction. Whereas for QDs in series current-voltage characteristic peaks are caused by the energetic alignment of excitations in both QDs. There, the Coulomb interaction can yield a multiple peak structure as frequently observed in experiments.

We further systematically discussed the shot noise behavior in the sequential tunneling regime. Scenarios for sub- and super-Poissonian noise, corresponding to negative and positive temporal correlations in the tunneling current, respectively, were presented. Particularly, we proposed an experimental setup to indicate Coulomb correlations in an ensemble of self-organized QDs by means of shot noise. A clear physical picture for bunching of tunneling events leading to super-Poissonian noise was drawn and a guidance for experimentalists to observe this phenomenon in tunnel-coupled QDs was provided.

In the framework of non-equilibrium Green's functions the quantum coherent description with Coulomb interaction beyond sequential tunneling was studied. For that purpose, lowest-order perturbation theory for the solution of the single-impurity Anderson model was considered. Two schemes of the Hartree-Fock approximation were reviewed. As an important result, we explicitly showed that the

factorization of the Coulomb interaction term in the Hamiltonian is generally not an appropriate starting point to describe nonlinear transport. In contrast, the factorization in the Green's function hierarchy yields a reasonable result for the average current, but the shot noise behavior turns out to be not sufficient by comparison with the sequential tunneling noise.

For noninteracting QDs analytical expressions for the current and the zero-frequency spectral power density were obtained: The Fano factor for coherent tunneling through a noninteracting symmetric QD becomes below one half in contrast to the sequential tunneling Fano factor, so that we attribute this to a signature of coherent tunneling.

A sequential (incoherent) and quantum coherent description of transport through two noninteracting QDs tunnel-coupled in series provide the same average current. In contrast to this key finding, we found that the zero-frequency spectral power density is different for intermediate coupling strengths between the QDs reflecting its sensitivity to quantum coherence in the tunneling process.

Starting from this observation, the continuous transition between the coherent and incoherent tunneling limit in the current fluctuations was tried to establish. For that purpose, we analyzed the effect of decoherence on the quantum coherent tunneling within a phenomenological escape model based on the scattering matrix formalism. Therein we considered dephasing by elastic scattering of particles from the current carrying state into fictitious terminals and back again, which completely randomizes their phase. Importantly, we found that decoherence by this elastic scattering changes the occupation-statistics of the current carrying states visible in the noise for large coupling between the QDs since it goes towards its Poissonian value. There are some indications that this also holds for electron-phonon interaction, as we discussed in the framework of non-equilibrium Green's functions in lowest-order Born approximation. But, this is not proven yet. Nevertheless, this finding contradicts with the result for the large coupling noise in the sequential tunneling limit. To get rid of this discrepancy we applied a scheme where the distributions in the fictitious terminals are allowed to fluctuate - for that reason we call this "pure" dephasing. In this scheme, we found that strong decoherence indeed smears out the coherent features in the noise for intermediate couplings between the QDs, but however, the incoherent tunneling limit is not reached within this framework[1].

In this context we utilized the concept of full counting statistics for a complete characterization of the sequential and coherent tunneling limits without Coulomb interaction. For the latter we provided the derivation of the full counting statistics by means of the density matrix description as an alternative to the scattering matrix description based on Levitov' formula. In both approaches the same statistics is obtained. As a result, we compared the third-order cumulant of the distribution of transferred charges (skewness) within the incoherent master equation and coherent

[1] Recently we found a way to achieve the continous transition between the coherent and incoherent tunneling limit in all cumulants of the transport process [KIE05a].

density matrix approach and found a very similar behavior by comparison with the shot noise (corresponding to the second-order cumulant). Moreover, we are able to identify Poissonian transfers of fractional charges for certain coupling strengths between the QDs. In the end, the stochastic path-integral method was applied to study the effect of pure dephasing on the full counting statistics. As well as the shot noise the skewness does not approach the sequential tunneling limit for intermediate couplings between the QDs for sufficient strong decoherence.

Finally to summarize, this work addressed the influence of Coulomb interaction and quantum coherence on the nonlinear transport through coupled QD systems. In order to obtain a detailed insight into the underlying physics we considered not only the stationary current, but also the corresponding current fluctuations. For simple few-level QD systems various models were compared with respect to the first three cumulants of the transport process. Explanations for some recent experimental observations were proposed and various intriguing physical effects in electronic transport were elaborately discussed as e.g. negative differential conductance, super-Poissonian shot noise, quantum noise, decoherence. The content of this thesis started from the sequential tunneling description which provides a handy and clear entrance into the subject of transport phenomena. It covered such sophisticated concepts as the non-equilibrium Green's function approach and ended with the current "hot"topic full counting statistics. In this sense, the present work offers a review of state-of-the-art concepts for the modeling of electronic transport through QDs and their mutual connections.

Brief review of the most important new results:

- Explanation and detailed discussion of the measured peak structure in the current-voltage characteristics of coupled QD systems

  [KIE02, KIE02a, KIE03, SPR04]

- Complete understanding of the interplay between Pauli's exclusion principle and Coulomb interaction in sequential tunneling through QDs by means of the shot noise behavior and quantitative explanation of experiments

  [KIE03a, KIE03b, NAU04a]

- Various mechanisms for the emergence of super-Poissonian noise in coupled QDs were elaborated in detail

  [KIE03b, KIE04, KIE05c]

- Systematic comparison and review of lowest-order approximations for Coulomb interaction in the framework of non-equilibrium Green's functions and their applicability for the calculation of current **and** zero-frequency noise

- Detailed examination of the impact of decoherence on the **zero-frequency** current fluctuations (current, shot noise, skewness of the distribution of transferred charges) of tunnel-coupled QDs by means of the scattering matrix formalism (escape model) and comparison with some other models

  [KIE05a, KIE05b]

Some important features of the used formalisms:

- **Master equation approach (ME):** incoherent description, works only for weak coupling between QDs and to the contacts $k_B T \gg \Gamma_{i/e/c}$, exact treatment of Coulomb interaction possible, clear and transparent approach
- **Non-equilibrium Green's functions (NEGF):** coherent description, in principle any kind of scattering processes (e.g. electron-electron, electron-phonon) can be implemented, but approximations necessary
- **Scattering matrix formalism (SMF):** coherent description, microscopic interactions only can be treated phenomenologically, best suited for the description of e.g. metallic, diffusive systems
- **Density matrix approach:** like the NEGF, but better linked to the ME approach

A. Screened Coulomb potential by highly-doped contacts

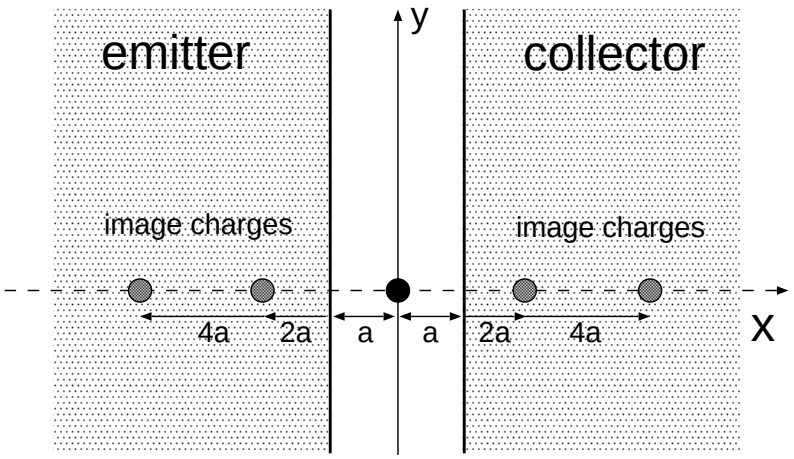

Figure A.1.: Sketch of a point charge between two infinite, parallel plates with its image charges. (z-coordinate perpendicular to $x-y$ plane).

A point charge e is symmetrically placed between two infinite, parallel, and grounded plates with distance a as sketched in Fig. A.1. What is the Coulomb potential of this charge in the $y-z$-plane? Using the method of images an infinite series of image charges at positions $x = \pm 2na$ ($n \in \mathbb{N}_0$) appear. Then, the potential in the $y-z$-plane reads

$$\phi(r) = \frac{e}{4\pi\epsilon}\left[\sum_{-\infty}^{\infty}\frac{(-1)^n}{\sqrt{r^2+(2na)^2}}\right] \tag{A.0.1}$$

with $r \equiv \sqrt{y^2+z^2}$. We rewrite (A.0.1) in the following form

$$\phi(r) = \frac{e}{4\pi\epsilon r} f(x) \tag{A.0.2}$$

with $x \equiv a/r$ and

$$\begin{aligned} f(x) &= \sum_{n=-\infty}^{\infty} \frac{(-1)^n}{\sqrt{1+(2nx)^2}} \\ &= \sum_{n=-\infty}^{\infty} F_n(x) \end{aligned} \tag{A.0.3}$$

Now, we are able to apply the *Poisson summation formula*:

$$\sum_n g_n = \sum_n \hat{g}_n \tag{A.0.4}$$

with $\hat{g}$ being the Fourier transform with respect to n of a once-differentiable, square integrable function g.

Hence, we just need the Fourier transform of $F_n(x)$ with respect to n which reads

$$\hat{F}_n(x) = \int dt e^{int} \frac{(-1)^n}{\sqrt{1+(2tx)^2}} = (-1)^n \frac{K_0\left(\frac{n}{2x}\right)}{x} \tag{A.0.5}$$

with the modified *Bessel function* of zeroth order K_0. It follows for the potential (A.0.1)

$$\phi(r) = \frac{e}{4\pi\epsilon a} \sum_{n=-\infty}^{\infty} (-1)^n K_0\left(\frac{nr}{2a}\right) \tag{A.0.6}$$

This result is shown in Fig. A.2 (black curve) by comparison with the unscreened potential ($\propto 1/r$) (red curve). In the limit $\frac{r}{a} \gg 1$ the potential (A.0.6) becomes

$$\phi_{r\gg a}(r) = \frac{1}{4\pi\epsilon} \frac{\exp\left(-\frac{r}{2a}\right)}{\sqrt{\pi r a}} \tag{A.0.7}$$

which is represented by the blue curve in Fig. A.2.

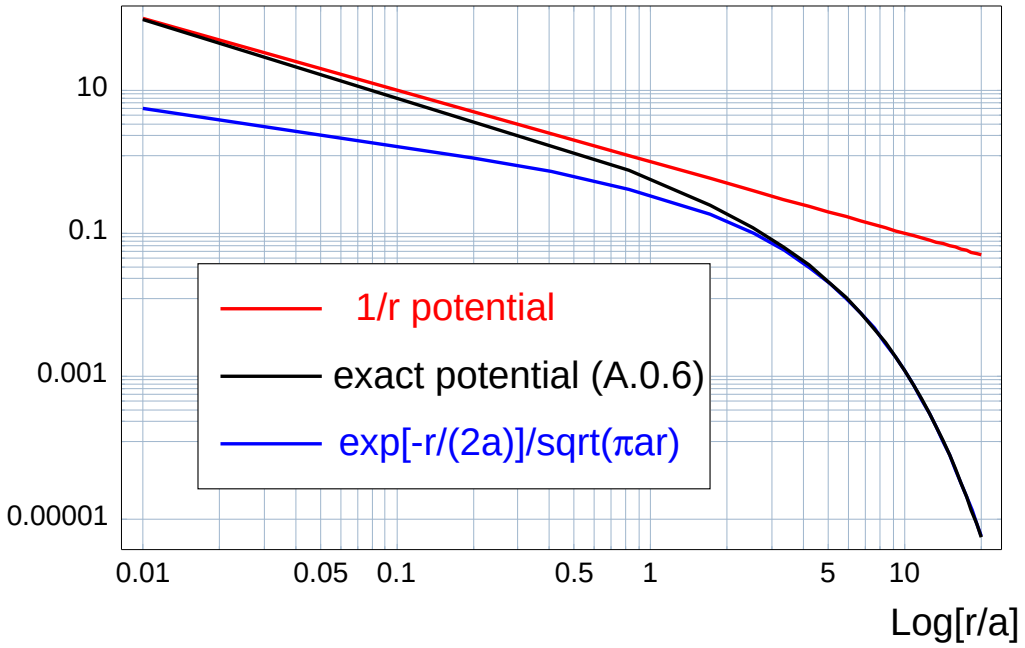

Figure A.2.: Screened Coulomb potential (A.0.6) vs. $\frac{r}{a}$ (black curve) by comparison with the unscreened potential $1/r$ (red curve) and the expression (A.0.7) for $r \gg a$ (blue curve).

B. Proof: Wiener-Khinchin theorem

Let $x(t)$ be a stationary random process, and let $R(\tau)$ be its autocorrelation function, i.e.:

$$R(\tau) := \langle x(t)x(t+\tau)\rangle - \langle x\rangle^2 \tag{B.0.1}$$

One assumes that $R(\tau)$ is absolutely integrable. Then, the Fourier transform $\hat{R}(\omega)$ exists

$$\hat{R}(\omega) := \int_{-\infty}^{\infty} R(\tau)e^{-i\omega\tau}d\tau \tag{B.0.2}$$

For each sample function $x(t)$, one defines its T-truncated Fourier transform $X_T(\omega)$ as

$$X_T(\omega) := \int_{-T/2}^{T/2} (x(t) - \langle x\rangle)e^{-i\omega t}dt \tag{B.0.3}$$

The corresponding truncated spectral power density is then $\frac{1}{T}\langle|X_T(\omega)|^2\rangle$. Since $x(t)$ is a random process, for each ω, the truncated spectral power density will be an ordinary random variable, and so one considers its expectation $S_T(\omega)$:

$$S_T(\omega) := \frac{1}{T}\langle|X_T(\omega)|^2\rangle \tag{B.0.4}$$

The spectral power density $S(\omega)$ of the random process is then defined as

$$S(\omega) := \lim_{T\to\infty} S_T(\omega) \tag{B.0.5}$$

Wiener-Khinchin Theorem: For all ω the limit in (B.0.5) exists, and

$$S(\omega) = \hat{R}(\omega) \tag{B.0.6}$$

Proof: (see also [SCH01] p.21)

$$\begin{aligned}
\langle|X_T(\omega)|^2\rangle &= \left\langle \left| \int_{-T/2}^{T/2} (x(t) - \langle x\rangle)e^{-i\omega t}dt \right|^2 \right\rangle \\
&= \left\langle \int_{-T/2}^{T/2}\int_{-T/2}^{T/2} (x(t)x(t') - \langle x\rangle^2)e^{-i\omega(t-t')}dtdt' \right\rangle
\end{aligned} \tag{B.0.7}$$

But since $\langle x(t)x(t')\rangle - \langle x\rangle^2 = R(t-t')$ and expectation is a linear operator, the last integral in (B.0.7) is

$$\int_{-T/2}^{T/2}\int_{-T/2}^{T/2} R(t-t')e^{-i\omega(t-t')}dtdt' \tag{B.0.8}$$

It holds with $\tau = t - t'$ and $\gamma = t + t'$

$$\int_{-T/2}^{T/2}\int_{-T/2}^{T/2} f(t-t')dtdt' = \int_{-T}^{T}(T-|\tau|)f(\tau)d\tau \tag{B.0.9}$$

Using this, the integral in (B.0.8) becomes

$$\int_{-T}^{T}(T-|\tau|)R(\tau)e^{-i\omega\tau}d\tau \tag{B.0.10}$$

Thus, combining (B.0.7)-(B.0.8)

$$\begin{aligned}\frac{1}{T}\langle|X_T(\omega)|^2\rangle &= \int_{-T}^{T}(1-\frac{|\tau|}{T})R(\tau)e^{-i\omega\tau}d\tau \\ &= \int_{-\infty}^{\infty} R_T(\tau)e^{-i\omega\tau}d\tau \end{aligned}\tag{B.0.11}$$

where

$$R_T(\tau) := \begin{cases}(1-\frac{|\tau|}{T})R(\tau) & \text{if} \quad |\tau| \le T \\ 0 & \text{if} \quad |\tau| \ge T\end{cases} \tag{B.0.12}$$

Since $|R_T(\tau)| \le |R(\tau)|$ and since $R(\tau)$ is absolutely integrable, it follows from the *Lebesgue dominated convergence theorem* [BRO81] that

$$\begin{aligned}\lim_{T\to\infty}\int_{-\infty}^{\infty} R_T(\tau)e^{-i\omega\tau}d\tau &= \int_{-\infty}^{\infty}\left(\lim_{T\to\infty} R_T(\tau)e^{-i\omega\tau}\right)d\tau \\ &= \int_{-\infty}^{\infty} R(\tau)e^{-i\omega\tau}d\tau \\ &= \hat{R}(\omega)\end{aligned}\tag{B.0.13}$$

■

C. Analytical evaluation of the Fano factor for two noninteracting states

The stationary probability that level i is occupied is $p_i \equiv \frac{\Gamma_e^{(i)} f_e^{(i)}}{\Gamma^{(i)}}$ or unoccupied $1-p_i$ ($\Gamma^{(i)} := \Gamma_e^{(i)} + \Gamma_c^{(i)}$). Then the stationary occupation probability of the noninteracting two-level system given by (3.1.4) reads

$$\underline{\mathbf{P}}^{\mathbf{0}} = \begin{pmatrix} (1-p_1)(1-p_2) \\ p_1(1-p_2) \\ p_2(1-p_1) \\ p_1 p_2 \end{pmatrix} \tag{C.0.1}$$

since in the uncorrelated case the occupation probability for each state factorizes into the occupation probabilities of the single levels. By inserting this vector into (3.1.5) one immediately sees that terms with $p_i p_j$ cancel and the current is the sum of the currents through each level i: $\langle I_i \rangle = e\Gamma_c^{(i)} p_i$. This also holds for an arbitrary number of levels: $\langle I \rangle = \sum_i \langle I_i \rangle$.

Now, let us consider the time propagator (4.1.2): its matrix elements $T_{\nu\mu}(t)$ describe the conditional probability to have state ν at time t under the condition of state μ at $t = 0$. The matrix element $T_{\nu\mu}(t) \equiv T_{\mu\to\nu}(t)$ can be factorized for each level i with the following conditional probabilities:

$$\begin{aligned} n_i &= 0 \to 1: \quad p_i(1 - e^{-\Gamma^{(i)}t}) \\ n_i &= 1 \to 0: \quad (1-p_i)(1 - e^{-\Gamma^{(i)}t}) \\ n_i &= 0 \to 0: \quad 1 - p_i(1 - e^{-\Gamma^{(i)}t}) \\ n_i &= 1 \to 1: \quad p_i + e^{-\Gamma^{(i)}t}(1-p_i) \end{aligned} \tag{C.0.2}$$

Due to the form of the current operator at the collector barrier in (3.2.2) the first row and last column of the matrix $\underline{\underline{\mathbf{T}}}(t)$ does not enter in the calculation of the current-current correlator (4.1.3). Carrying out the sum in (4.1.3) for two levels leads to

$$\begin{aligned}\langle I_c(t)I_c(0)\rangle = \quad & 2e\Gamma_c^{(1)}\left\{[\langle I_1\rangle p_1(1-p_2)+\langle I_2\rangle p_2(1-p_1)][T_{(0,0)\to(1,0)}+T_{(0,0)\to(1,1)}]\right.\\ & \left.+\langle I_2\rangle p_1[T_{(1,0)\to(1,0)}+T_{(1,0)\to(1,1)}]+\langle I_1\rangle p_2[T_{(0,1)\to(1,0)}+T_{(0,1)\to(1,1)}]\right\}\\ & +2e\Gamma_c^{(2)}\left\{[\langle I_1\rangle p_1(1-p_2)+\langle I_2\rangle p_2(1-p_1)][T_{(0,0)\to(0,1)}+T_{(0,0)\to(1,1)}]\right.\\ & \left.+\langle I_2\rangle p_1[T_{(1,0)\to(0,1)}+T_{(1,0)\to(1,1)}]+\langle I_1\rangle p_2[T_{(0,1)\to(0,1)}+T_{(0,1)\to(1,1)}]\right\}\\ & +e\langle I\rangle\delta(t)\end{aligned} \tag{C.0.3}$$

Replacing the $T_{\mu\to\nu}$ in (C.0.3) by using the rules (C.0.2) the correlator becomes

$$\begin{aligned}\langle I_c(t)I_c(0)\rangle = & -2\langle I_1\rangle^2 e^{-\Gamma^{(1)}t}-2\langle I_2\rangle^2 e^{-\Gamma^{(2)}t}+\langle I\rangle^2\\ & +e\langle I\rangle\delta(t)\end{aligned} \tag{C.0.4}$$

which can be generalized for an arbitrary number of levels

$$\begin{aligned}\langle I_c(t)I_c(0)\rangle = & -2\sum_i\langle I_i\rangle^2 e^{-\Gamma^{(i)}t}+\langle I\rangle^2\\ & +e\langle I\rangle\delta(t)\end{aligned} \tag{C.0.5}$$

The time-independent term in (C.0.4) and (C.0.5) cancels out in the calculation of the spectral power density (4.1.1) and we obtain

$$S(0)=2e\langle I\rangle-4\sum_i\frac{\langle I_i\rangle^2}{\Gamma^{(i)}} \tag{C.0.6}$$

Dividing Eq. (C.0.6) by $2e\langle I\rangle$ and using the Fano factor for tunneling through a single level i, i.e. $\alpha_i=1-\frac{2\langle I_i\rangle}{e\Gamma^{(i)}}$ (4.2.1), the Fano factor for an arbitrary number of noninteracting levels Eq. (4.2.2) is derived.

D. Phase independence of the S-matrix for coupled quantum dots with voltage probes

A QD system with m QDs coupled to n terminals, including also "fictitious" voltage probes, is considered. Each QD is connected to one terminal only. The system is described by a $n \times n$ scattering matrix s. Then the energy-resolved cumulant-generating function for charge transfer in the system is given by Levitov's formula (7.3.12). This function is invariant under unitary transformations (rotations) of the S-matrix

$$s \to UsU^\dagger \quad \text{with} \quad U \equiv \mathrm{diag}(e^{i\phi_1}, \ldots, e^{i\phi_n}) \tag{D.0.1}$$

with arbitrary phases ϕ_i For our specific consideration, the S-matrix can be written as

$$s = \mathbb{1} - i\hat{W}^\dagger G^{\mathrm{ret}} \hat{W} \tag{D.0.2}$$

where G^{ret} is the retarded Green's function ($m \times m$-matrix) of the system (compare Eq. (5.4.1)) and $\hat{W}$ describes the coupling of the QD system to the reservoirs.

For our QD system with "fictitious" terminals $\varphi 1/\varphi 2$ depicted in Fig. 6.1 we have

$$G^{\mathrm{ret}} = \left[\mathbb{1} - \hat{H} - \frac{i}{2}\hat{W}\hat{W}^\dagger\right]^{-1}, \quad \hat{H} = \begin{pmatrix} \varepsilon_1 & \Omega \\ \Omega^* & \varepsilon_2 \end{pmatrix} \tag{D.0.3}$$

and

$$\hat{W} = \begin{pmatrix} \sqrt{\Gamma_e} & \sqrt{\Gamma_{\varphi 1}} & 0 & 0 \\ 0 & 0 & \sqrt{\Gamma_{\varphi 2}} & \sqrt{\Gamma_c} \end{pmatrix} \tag{D.0.4}$$

All Γ's can in principle be complex. However, the Green's function (D.0.3) depends only on the modulus of the Γ's and Ω. Performing the rotation (D.0.1), the phases ϕ_i can be choosen such that all phases of the Γ's in $\hat{W}$ cancel out. Therefore, one can work right from the beginning with only real couplings Γ_i and the "phase problem" hence is solved.

Bibliography

[AGU04] R. Aguado and T. Brandes. *Shot noise spectrum of open dissipative quantum two-level systems.* Phys. Rev. Lett. **92**, 206601 (2004).

[ALE03] V. Ya. Aleshkin, L. Reggiani, N. V. Alkeev, V. E. Lyubchenko, C. N. Ironside, J. M. L. Figueiredo, and C. R. Stanley. *Giant suppression of shot noise in double barrier resonant diode: a signature of coherent transport.* Semicond. Sci. Technol. **18**, L35 (2003).

[ALE04] V. Ya. Aleshkin, L. Reggiani, N. V. Alkeev, V. E. Lyubchenko, C. N. Ironside, J. M. L. Figueiredo, and C. R. Stanley. *Reply to Comment on 'Giant suppression of shot noise in double barrier resonant diode: a signature of coherent transport'.* Semicond. Sci. Technol. **19**, 665 (2004).

[AND61] P. W. Anderson. *Localized Magnetic States in Metals.* Phys. Rev. **124**, 41 (1961).

[AVE91] D. V. Averin, A. N. Korotkov, and K. K. Likharev. *Theory of single-electron charging of quantum wells and dots.* Phys. Rev. B **44**, 6199 (1991).

[BAG03] D. A. Bagrets and Y. V. Nazarov. *Multiterminal Counting Statistics*, in *Quantum Noise in Mesoscopic Physics*, Y. Nazarov. (Kluwer Academic Publishers, Dordrecht, Boston, London, 2003).

[BAG03a] D. A. Bagrets and Y. V. Nazarov. *Full counting statistics of charge transfer in Coulomb blockade systems.* Phys. Rev. B **67**, 085316 (2003).

[BAL99] R. Baltin. *Fluctuations and correlations in the electron transport through Semiconductor Nanostructures.* (Ph.D. thesis, Ruprecht-Karls-Universität Heidelberg, 1999).

[BAR87] J. B. Barner and S. T. Ruggiero. *Observation of the Incremental Charging of Ag Particles by Single Electrons.* Phys. Rev. Lett. **59**, 807 (1987).

[BAR04] P. Barthold. *Transport- und Rauschmessung an einzelnen und vertikal gekoppelten selbstorganisierten Quantenpunktsystemen.* (diploma thesis, Universität Hannover, 2004).

[BEE91a] C. W. J. Beenakker. *Theory of Coulomb-blockade oscillations in the conductance of a quantum dot.* Phys. Rev. B **44**, 1646 (1991).

[BEE03] C. Beenakker and C. Schönenberger. *Quantum Shot Noise.* Physics Today **56**, 37 (2003).

[BIM99] D. Bimberg, M. Grundmann, and N.N. Ledentsov. *Quantum Dot Heterostructures.* (John Wiley & Sons Ltd., New York, 1999).

[BIR95] H. Birk, M. J. M. de Jong, and C. Schönenberger. *Shot noise suppression in the Single-Electron-Tunneling Regime.* Phys. Rev. Lett. **75**, 1610 (1995).

[BLA00] Ya. M. Blanter and M. Büttiker. *Shot noise in mesoscopic conductors.* Phys. Rep. **336**, 1 (2000).

[BLA04b] Ya. M. Blanter and M. Büttiker. *Comment on 'Giant suppression of shot noise in double barrier resonant diode: a signature of coherent transport'.* Semicond. Sci. Technol. **19**, 663 (2004).

[BOM05] Y. Bomze, G. Gershon, D. Shovkun, L.S. Levitov, and M. Reznikov. *Measurement of counting statistics of electron transport in a tunnel junction.* cond-mat/0504382.

[BOR01] M. Borgstrom, T. Bryllert, T. Sass, B.Gustafson, L.-E. Wernersson, W. Seifert, and L. Samuelson. *High peak to valley ratios observed in InAs/InP resonant tunneling quantum dot stacks.* Appl. Phys. Lett. **78**, 3232 (2001).

[BRE02] H.-P. Breuer and F. Petruccione. *The theory of open quantum systems.* (Oxford University Press, Great Clarendon Street, 2002).

[BRO81] I. N. Bronstein and K. A. Semendjajew. *Taschenbuch der Mathematik.* (Verlag Harry Deutsch, Thun und Frankfurt/Main, 20. Auflage, 1981).

[BRY02] T. Bryllert, M. Borgstrom, T. Sass, B. Gustafson, L. Landin, L.-E. Wernersson, W. Seifert, and L. Samuelson. *Designed emitter states in resonant tunneling through quantum dots.* Appl. Phys. Lett. **80**, 2681 (2002).

[BRY03] T. Bryllert, M. Borgstrom, L.-E. Wernersson, W. Seifert, and L. Samuelson. *Transport through an isolated artificial molecule formed from stacked self-assembled quantum dots.* Appl. Phys. Lett. **82**, 2655 (2003).

[BUE86a] M. Büttiker. *Role of quantum coherence in series resistors.* Phys. Rev. B **33**, 3020 (1986).

[BUE88] M. Büttiker. *Coherent and sequential tunneling in series barriers.* IBM J. Res. Develop. **32**, 63 (1988).

[BUE91] M. Büttiker. *The quantum phase of flux correlations in waveguides.* Physica B **175**, 199 (1991).

[BUE92] M. Büttiker. *Scattering theory of current and intensity noise correlations in conductors and wave guides.* Phys. Rev. B **46**, 12485 (1992).

[BUE03] M. Büttiker. *Reversing the Sign of Current-Current correlations*, in *Quantum Noise in Mesoscopic Physics*, Y. Nazarov. (Kluwer Academic Publishers, Dordrecht, Boston, London, 2003).

[CHA74] L. L. Chang, L. Esaki, and R. Tsu. *Resonant tunneling in semiconductor double barriers.* Appl. Phys. Lett. **24**, 593 (1974).

[CHE90a] L. Y. Chen and C. S. Ting. *Path-integral approach to transient transport of a double-barrier resonant-tunneling system.* Phys. Rev. B **41**, 8533 (1990).

[CHE91] L. Y. Chen and C. S. Ting. *Theoretical investigation of noise characteristics of double-barrier resonant tunneling structures.* Phys. Rev. B **43**, 4534 (1991).

[CHE91a] L. Y. Chen and C. S. Ting. *Coulomb staircase in the I-V characteristic of an ultrasmall double-barrier resonant-tunneling structure.* Phys. Rev. B **44**, 5916 (1991).

[COT04] A. Cottet, W. Belzig, and C. Bruder. *Positive cross-correlations due to Dynamical Channel-Blockade in a three-terminal quantum dot.* Phys. Rev. B **70**, 115315 (2004).

[DAT95] S. Datta. *Electronic Transport in Mesoscopic Systems.* (Cambridge University Press, Cambridge, 1995).

[DAV92] J. H. Davies, P. Hyldgaard, S. Hershfield, and J. W. Wilkins. *Classical theory of shot noise in resonant tunneling.* Phys. Rev. B **46**, 9620 (1992).

[DAV95] J. H. Davies, J. C. Egues, and J. W. Wilkins. *Effect of incoherence on current and shot noise in resonant tunneling: An exactly solvable model.* Phys. Rev. B **52**, 11259 (1995).

[DON02] B. Dong and X. L. Lei. *Effect of the Kondo correlation on shot noise in a quantum dot.* J. Phys.: Condens. Matter **14**, 4963 (2002).

[EAV02] L. Eaves, A. Patané, and P. C. Main. *Magneto-Tunneling spectroscopy of self-assembled quantum dots*, in *Nano-Optoelectronics: Concepts, Physics and Devices*, M. Grundmann. (Springer, Berlin, 2002).

[EGU94] J. C. Egues, S. Hershfield, and J. W. Wilkins. *Zero-frequency shot noise for tunneling through a system with internal scattering.* Phys. Rev. B **49**, 13517 (1994).

[ELA02] B. Elattari and S. A. Gurvitz. *Shot noise in coupled dots and the "fractional charges".* Phys. Lett. A **292**, 289 (2002).

[ENG04] H.-A. Engel and D. Loss. *Asymmetric quantum shot noise in quantum dots.* Phys. Rev. Lett. **93**, 136602 (2004).

[FAN47] U. Fano. *Ionization Yield of Radiations.II. The Fluctuations of the Number of the Ions.* Phys. Rev. **72**, 26 (1947).

[GAR02] C. W. Gardiner. *Handbook of Stochastic Methods for Physics, Chemistry and the Natural Sciences.* (Springer, Berlin, 2002).

[GAT02] M. Gattobigio, G. Iannacconne, and M. Macucci. *Enhancement and suppression of shot noise in capacitively coupled metallic double dots.* Phys. Rev. B **65**, 115337 (2002).

[GLA88c] L. I. Glazman and K. A. Matveev. *Coulomb correlations in the tunneling through resonance centers.* JETP Lett. **48**, 445 (1988).

[GNO04] C. Gnodtke. *Streuung beim Transport durch selbstorganisierte Quantenpunktstapel.* (diploma thesis, TU Berlin, 2004).

[GRA92a] H. Grabert and M. H. Devoret (Editors). *Single Charge Tunneling*, Vol. 294 of *NATO Advanced Study Institute, Series B: Physics.* (Plenum, New York, 1992).

[GRI00] T. G. Griffiths, E. Comforti, M. Heiblum, A. Stern, and V. Umansky. *Evolution of Quasiparticle charge in the Fractional Quantum Hall Regime.* Phys. Rev. Lett. **85**, 3918 (2000).

[GRO91] A. Groshev, T. Ivanov, and V. Valtchinov. *Charging effects of a single quantum level in a box.* Phys. Rev. Lett. **66**, 1082 (1991).

[GRU02] M. Grundmann (Ed.). *Nano-Optoelectronics: Concepts, Physics and Devices.* (Springer, Berlin, 2002).

[GUR96c] S. A. Gurvitz and Ya. S. Prager. *Microscopic derivation of rate equations for quantum transport.* Phys. Rev. B **53**, 15932 (1996).

[GUR96d] S. A. Gurvitz, H. J. Lipkin, and Ya. S. Prager. *Interference effects in resonant tunneling and the Pauli principle.* Phys. Lett. A **212**, 91 (1996).

[GUR98] S. A. Gurvitz. *Rate equations for quantum transport in multidot systems.* Phys. Rev. B **57**, 6602 (1998).

[HAN93] U. Hanke, Yu. M. Galperin, K.A. Chao, and N. Zou. *Finite-frequency shot noise in a correlated tunneling current.* Phys. Rev. B **48**, 17209 (1993).

[HAU96] H. Haug and A.-P. Jauho. *Quantum Kinetics in Transport and Optics of Semiconductors.* (Springer, Berlin, 1996).

[HEN94] L. E. Henrickson, A. J. Glick, G. W. Bryant, and D. F. Barbe. *Nonequilibrium-Green's function theory of transport in interacting quantum dots.* Phys. Rev. B **50**, 4482 (1994).

[HER92a] S. Hershfield. *Resonant tunneling through an Anderson impurity. II. Noise in the Hartree approximation.* Phys. Rev. B **46**, 7061 (1992).

[HER93] S. Hershfield, J. H. Davies, P. Hyldgaard, C. J. Stanton, and J. W. Wilkins. *Zero-frequency current noise for the double-tunnel-junction Coulomb blockade.* Phys. Rev. B **47**, 1967 (1993).

[HET02] M. H. Hettler, H. Schoeller, and W. Wenzel. *Non-linear transport through a molecular nanojunction.* Europhys. Lett. **57**, 571 (2002).

[HAP99] I. Hapke-Wurst, U. Zeitler, H. W. Schumacher, R. J. Haug, K. Pierz, and F. J. Ahlers. *Size determination of InAs quantum dots using magneto-tunneling experiments.* Semicond. Sci. Technol. **14**, L41 (1999).

[HAP02] I. Hapke-Wurst. *Resonanter Magnetotransport durch selbstorganisierte Quantenpunkte.* (Ph.D. Thesis, Universität Hannover, 2002).

[IAN98] G. Iannaccone, G. Lombardi, M. Macucci, and B. Pellegrini. *Enhanced Shot Noise in Resonant Tunneling: Theory and Experiment.* Phys. Rev. Lett. **80**, 1054 (1998).

[ITS96] I. E. Itskevich, T. Ihn, A. Thornton, M. Henini, T. J. Foster, P. Moriarty, A. Nogaret, P. H. Beton, L. Eaves, and P. C. Main. *Resonant magnetotunneling through individual self-assembled InAs quantum dots.* Phys. Rev. B **54**, 16401 (1996).

[JAU94] A.-P. Jauho, N. S. Wingreen, and Y. Meir. *Time-dependent transport in interacting and noninteracting resonant-tunneling systems.* Phys. Rev. B **50**, 5528 (1994).

[JON96] M. J. M. de Jong. *Distribution of transmitted charge through a double-barrier junction.* Phys. Rev. B **54**, 8144 (1996).

[JON97] M. J. M. deJong and C. W. J. Beenakker. *Shot noise in mesoscopic systems*, in *Mesoscopic Electron Transport*, L. L. Sohn, L. P. Kouwenhoven, and G. Schön. (Kluwer Academic Publishers, Dordrecht, Boston, London, 1997).

[JOR04] A.N. Jordan, E.V. Sukhorukov, and S. Pilgram. *Fluctuation Statistics in Networks: a Stochastic Path Integral Approach.* J. Math. Phys. **45**, 4386 (2004).

[KAD62] L. P. Kadanoff and G. Baym. *Quantum Statistical Mechanics.* (Benjamin, New York, 1962).

[KAM81] N. G. van Kampen. *Stochastic Processes in Physics and Chemistry.* (North-Holland, Amsterdam, 1981).

[KEL65] L. V. Keldysh. *Diagram technique for nonequilibrium processes.* Sov. Phys. JETP **20**, 1018 (1965). [Zh. Eksp. Theor. Fiz. **47**, 1515 (1964)].

[KIE98] G. Kießlich. *Transport durch gekoppelte Quantenpunkte.* (Studienarbeit, TU Berlin, 1998).

[KIE99a] G. Kießlich. *Resonantes Tunneln durch ein Ensemble von selbstorganisierten Quantenpunkten.* (diploma thesis, TU Berlin, 1999).

[KIE02] G. Kießlich, A. Wacker, and E. Schöll. *Nonlinear transport through an ensemble of quantum dots.* Physica B **314**, 459 (2002).

[KIE02a] G. Kießlich, A. Wacker, and E. Schöll. *Sequential Tunneling Through An Array Of Electrostatically Coupled Quantum Dots.* Physica E **12**, 837 (2002).

[KIE02b] G. Kießlich, A. Wacker, and E. Schöll. *Many-Particle Charging Effects and Recombination Current through a Quantum Dot Array.* phys. status solidi (b) **234**, 215 (2002).

[KIE03] G. Kießlich, A. Wacker, E. Schöll, S. A. Vitusevich, A. E. Belyaev, S. V. Danylyuk, A. Förster, N. Klein, and M. Henini. *Nonlinear charging effect of quantum dots in a p-i-n diode.* Phys. Rev. B **68**, 125331 (2003).

[KIE03a] G. Kießlich, A. Wacker, E. Schöll, A. Nauen, F. Hohls, and R. J. Haug. *Shot Noise in Tunneling through a Quantum Dot Array.* phys. status solidi (c) **0**, 1293 (2003).

[KIE03b] G. Kießlich, A. Wacker, and E. Schöll. *Shot Noise of coupled Semiconductor Quantum Dots.* Phys. Rev. B **68**, 125320 (2003).

[KIE04] G. Kießlich, H. Sprekeler, A. Wacker, and E. Schöll. *Positive Correlations in Tunnelling through coupled Quantum Dots.* Semicond. Sci. Technol. **19**, S37 (2004).

[KIE05a] G. Kießlich, P. Samuelsson, A. Wacker, and E. Schöll. *Counting statistics and decoherence in coupled quantum dots.* cond-mat/0507403.

[KIE05b] G. Kießlich, P. Samuelsson, A. Wacker, and E. Schöll. Decoherence and current fluctuations in tunneling through coupled quantum dots, in *Proc. 18th Internat. Conf. on Noise and Fluctuations (ICNF-2005)*. T. Gonzales, J. Mateos, and D. Pardo, Vol. 780, Seite 439, American Institute of Physics, Melville, NY, 2005.

[KIE05c] G. Kießlich, A. Wacker, and E. Schöll. Super-Poissonian current fluctuations in tunneling through coupled quantum dots. , in *Proc. 14th International Conference on Nonequilibrium Carrier Dynamics in Semiconductors*, Springer, Berlin, 2005. to be published.

[KLI94a] G. Klimeck, R. Lake, S. Datta, and G. W. Bryant. *Elastic and inelastic scattering in quantum dots in the Coulomb-blockade regime*. Phys. Rev. B **50**, 5484 (1994).

[KOE98] J. König. *Quantum fluctuations in the single-electron transistor*. (Ph.D. Thesis, Universität Karlsruhe, 1998).

[KOH04] S. Kohler, S. Camelet, M. Strass, J. Lehmann, G. Ingold, and P. Hänggi. *Charge transport through a molecule driven by a high-frequency field*. Chem. Phys. **296**, 243 (2004).

[KOR94] A. N. Korotkov. *Intrinsic noise of the single-electron transistor*. Phys. Rev. B **49**, 10381 (1994).

[KOU97] L. P. Kouwenhoven, C. M. Marcus, P. L. McEuen, S. Tarucha, R. M. Westervelt, and N. S. Wingreen. *Electron Transport in Quantum Dots*, in *Mesoscopic Electron Transport*, L. L. Sohn, L. P. Kouwenhoven, and G. Schön. (Kluwer Academic Publishers, Dordrecht, Boston, London, 1997).

[KOU97a] L. P. Kouwenhoven, G. Schön, and L. L. Sohn. *Introduction to Mesoscopic Electron Transport*, in *Mesoscopic Electron Transport*, L. L. Sohn, L. P. Kouwenhoven, and G. Schön. (Kluwer Academic Publishers, Dordrecht, Boston, London, 1997).

[KOU01] L. P. Kouwenhoven and L. Glazman. *Revival of the Kondo effect*. Physics World, january, 33 (2001).

[KUZ98] V. V. Kuznetsov, E. E. Mendez, J. D. Bruno, and J. T. Pham. *Shot noise enhancement in resonant-tunneling structures in a magnetic field*. Phys. Rev. B **58**, R10159 (1998).

[LAC81] C. Lacroix. *Density of states for the Anderson model*. J. Phys. F **11**, 2389 (1981).

[LAN76a] D. C. Langreth. *Linear and nonlinear response theory with application*, in *Linear and Nonlinear Electron Transport in Solids*, J. T. Devreese and V. E. van Doren. (Plenum Press, New York, 1976).

[LAN98] R. Landauer. *The noise is the signal.* Nature **392**, 658 (1998).

[LEV93] L. S. Levitov and G. B. Lesovik. *Charge distribution in quantum shot noise.* JETP Lett. **58**, 230 (1993).

[LEV96] L. S. Levitov, H. W. Lee, and G. B. Lesovik. *Electron counting statistics and coherent states of electric current.* J. Math. Phys. **37**, 4845 (1996).

[LEV01] A. Levine, E. E. Vdovin, A. Patanè, L. Eaves, P. C. Main, Yu. N. Khanin, Yu. V. Dubrovskii, M. Henini, and G. Hill. *Magneto-Tunnelling for Spatial Mapping of Orbital Wavefunctions of the Ground and Excited Electronic States in Self-Assembled Quantum Dots.* phys. status solidi (b) **224**, 715 (2001).

[LIU89] H. C. Liu and G. C. Aers. *Resonant Tunneling through one-, two-, and three-dimensionally confined quantum wells.* J. Appl. Phys. **65**, 4908 (1989).

[LOS98] D. Loss and D. P. Vincenzo. *Quantum computation with quantum dots.* Phys. Rev. A **57**, 120 (1998).

[MAH00] G. D. Mahan. *Many-Particle Physics.* (Plenum, New York, 2000).

[MAI03] N. C. Maire. *Schrotrauschen von InAs-Quantenpunkten.* (diploma thesis, Universität Hannover, 2003).

[MAK96] K. Makoshi and T. Mii. *Nonequilibrium Anderson model, Coulomb blockade and scanning tunneling spectroscopy.* Surface Science **357**, 335 (1996).

[MAT92a] K. A. Matveev and A. I. Larkin. *Interaction-induced singularities in tunneling via localized levels.* Phys. Rev. B **46**, 15337 (1992).

[MCE97] P. L. McEuen. *Artificial Atoms: New Boxes for Electrons.* Science **278**, 1729 (1997).

[MEI91] Y. Meir, N. S. Wingreen, and P. A. Lee. *Transport through a strongly interacting electron system: Theory of periodic conductance oscillations.* Phys. Rev. Lett. **66**, 3048 (1991).

[MEI93] Y. Meir, N. S. Wingreen, and P. A. Lee. *Low-Temperature Transport through a Quantum Dot: The Anderson Model Out of Equilibrium.* Phys. Rev. Lett. **70**, 2601 (1993).

[MEI95a] U. Meirav and E. B. Foxman. *Single-electron phenomena in semiconductors.* Semicond. Sci. Technol. **10**, 255–284 (1995).

[MEI02b] M. Meixner. *Simulation of self-organized growth kinetics of quantum dots.* (Ph.D. Thesis, TU Berlin, 2002).

[MEI03] M. Meixner and E. Schöll. *Kinetically enhanced correlation and anticorrelation effects in self-organized quantum dot stacks.* Phys. Rev. B **67**, 121202 (2003).

[MEI03a] M. Meixner, R. Kunert, and E. Schöll. *Control of strain-mediated growth kinetics of self-assembled semiconductor quantum dots.* Phys. Rev. B **67**, 195301 (2003).

[MII96] T. Mii and K. Makoshi. *Negative conductance in Coulomb blockade.* Jpn. J. Appl. Phys. **35**, 3706 (1996).

[MII97] T. Mii, K. Makoshi, and N. Shima. *Effects of Coulomb interaction in tunneling current through several energy levels.* Jpn. J. Appl. Phys. **36**, 3796 (1997).

[NAR97] M. Narihiro, G. Yusa, Y. Nakamura, T. Noda, and H. Sakaki. *Resonant tunneling of electrons via 20nm scale InAs quantum dot and magneto-tunneling spectroscopy of its electronic states.* Appl. Phys. Lett. **70**, 105 (1997).

[NAT98] K. Natori and N. Sano. *Current bistability in resonant tunneling through a semiconductor quantum dot.* Superlattices and Microstructures **23**, 1339 (1998).

[NAU02] A. Nauen, I. Hapke-Wurst, F. Hohls, U. Zeitler, R. J. Haug, and K. Pierz. *Shot noise in self-assembled InAs quantum dots.* Phys. Rev. B **66**, 161303 (2002).

[NAU03] A. Nauen. *Rauschmessungen an mikroskopischen Tunnelsystemen.* (Ph.D. Thesis, Universität Hannover, 2003).

[NAU04] A. Nauen, F. Hohls, J. Könemann, and R. J. Haug. *Shot noise in resonant tunneling through a zero-dimensional state with a complex energy spectrum.* Phys. Rev. B **69**, 113316 (2004).

[NAU04a] A. Nauen, F. Hohls, N. Maire, K. Pierz, and R. J. Haug. *Shot noise in tunneling through a single quantum dot.* Phys. Rev. B **70**, 033305 (2004).

[NAZ96] Y. Nazarov and J. J. R. Struben. *Universal excess noise in resonant tunneling via strongly localized states.* Phys. Rev. B **53**, 15466 (1996).

[NAZ03] Y. V. Nazarov (Ed.). *Quantum Noise in Mesoscopic Physics*. (Kluwer Academic Publishers, Dordrecht, Boston, London, 2003).

[NIU99] C. Niu, D.L. Lin, and T.-H. Lin. *Equation of motion for nonequilibrium Green functions*. J. Phys.: Condens. Matter **11**, 1511 (1999).

[PAC01] C. Pacher, C. Rauch, G. Strasser, E. Gornik, F. Elsholz, A. Wacker, G. Kießlich, and E. Schöll. *Anti-reflection coating for miniband transport and Fabry-Perot resonances in GaAs/AlGaAs superlattices*. Appl. Phys. Lett. **79**, 1486 (2001).

[PAL96] P. Pals and A. MacKinnon. *Coherent tunnelling through two quantum dots with Coulomb interaction*. J. Phys. Cond. Mat. **8**, 5401 (1996).

[PIL03] S. Pilgram, A.N. Jordan, E.V. Sukhorukov, and M. Büttiker. *Stochastic Path Integral Formulation of Full Counting Statistics*. Phys. Rev. Lett. **90**, 206801 (2003).

[REI02] S. R. Reimann and M. Manninen. *Electronic structure of quantum dots*. Rev. Mod. Phys. **74**, 1238 (2002).

[REU03] B. Reulet, J. Senzier, and D. E. Prober. *Environmental effects in the third moment of voltage fluctuations in a tunnel junction*. Phys. Rev. Lett. **91**, 196601 (2003).

[ROE87] G. Röpke. *Statistische Mechanik für das Nichtgleichgewicht*. (Physik-Verlag, Weinheim, 1st. Auflage, 1987).

[SWI03] R. Świrkowicz, J. Barnaś, and M. Wilczyński. *Nonequilibrium Kondo effect in quantum dots*. Phys. Rev. B **68**, 195318 (2003).

[SAF03] S. S. Safonov, A. K. Savchenko, D. A. Bagrets, O. N. Jouravlev, Y. V. Nazarov, E. H. Linfield, and D. A. Ritchie. *Enhanced shot noise in resonant tunnelling via interacting localized states*. Phys. Rev. Lett. **91**, 136801 (2003).

[SAM04] P. Samuelsson. *private communication*.

[SCH18] W. Schottky. *Über spontane Stromschwankungen in verschiedenen Elektrizitätsleitern*. Ann. Phys. (Leipzig) **57**, 541 (1918).

[SCH01] E. Schöll. *Nonlinear spatio-temporal dynamics and chaos in semiconductors*. (Cambridge University Press, Cambridge, 2001). Nonlinear Science Series, Vol. 10.

[SHC03] V. A. Shchukin, N. N. Ledentsov, and D. Bimberg. *Epitaxy of Nanostructures*. (Springer, Berlin, 2003).

[SHO38] W. Shockley. *Currents to conductors induced by a moving point charge.* J. Appl. Phys. **9**, 635 (1938).

[SON03] W. Song, E. E. Mendez, V. Kuznetsov, and B. Nielsen. *Shot noise in negative-differential-conductance devices.* Appl. Phys. Lett. **82**, 1568 (2003).

[SOU04] F. M. Souza, J. C. Egues, and A. P. Jauho. *Current and noise in a FM-QD-FM System with spin-flip scattering.* (to be published).

[SOU04a] F. M. Souza and G. Kießlich. *private communication.*

[SPR03] H. Sprekeler. *Transport durch Stapel von selbstorganisierten Quantenpunkten.* (diploma thesis, TU Berlin, 2003).

[SPR04] H. Sprekeler, G. Kießlich, A. Wacker, and E. Schöll. *Coulomb effects in tunneling through a quantum dot stack.* Phys. Rev. B **69**, 125328 (2004).

[STA96b] C. A. Stafford. *Nonlinear conductance in resonant tunneling.* Phys. Rev. Lett. **77**, 2770 (1996).

[STA04] J. Stangl, V. Holý, and G. Bauer. *Structural properties of self-organized semiconductor nanostructures.* Rev. Mod. Phys. **76**, 725 (2004).

[STI01] O. Stier. *Electronic and Optical Properties of Quantum Dots and Wires.* (Ph.D. Thesis TU-Berlin, Mensch & Technik Verlag, Berlin, 2001).

[SUN99] H. B. Sun and G. J. Milburn. *Quantum open-systems approach to current noise in resonant tunneling junctions.* Phys. Rev. B **59**, 10748 (1999).

[SUZ97] T. Suzuki, K. Nomoto, K. Taira, and I. Hase. *Tunneling spectroscopy of InAs wetting layer and self-assembled quantum dots: Resonant tunneling through two- and zero-dimensional electronic states.* Jpn. J. Appl. Phys. **36**, 1917 (1997).

[TAR96] S. Tarucha, D.G. Austing, T. Honda, R.J. van der Hage, and L.P. Kouwenhoven. *Shell filling and spin effects in a few electron quantum dot.* Phys. Rev. Lett. **77**, 3613 (1996).

[THI03] A. Thielmann, M. H. Hettler, J. König, and G. Schön. *Shot noise in tunneling transport through molecules and quantum dots.* Phys. Rev. B **68**, 115105 (2003).

[THI04] A. Thielmann, M. H. Hettler, J. König, and G. Schön. *Super-poissonian noise, negative differential conductance, and relaxation effects in transport through molecules, quantum dots and nanotubes.* Phys. Rev. B **71**, 045341 (2005).

[THI04a] A. Thielmann, M. H. Hettler, J. König, and G. Schön. *Cotunneling current and shot noise in quantum dots.* Phys. Rev. Lett. **95**, 146806 (2005).

[VDO00] E. E. Vdovin, A. Levin, A. Patanè, L. Eaves, P. C. Main, Yu. N. Khanin, Yu. V. Dubrovskii, M. Henini, and G. Hill. *Imaging the electron wave function in self-assembled quantum dots.* Science **290**, 122 (2000).

[WAN98a] Z. Wang, M. Iwanaga, and T. Myoshi. *Current Noise in Semiconductor Quantum Dots.* Jpn. J. Appl. Phys. **37**, 5894 (1998).

[WAR98] R. J. Warburton, B. T. Miller, C. S. Dürr, C. Bödefeld, K. Karrai, J. P. Kotthaus, G. Medeiros-Ribeiro, P. M. Petroff, and S. Huant. *Coulomb interactions in small charge-tunable quantum dots: A simple model.* Phys. Rev. B **58**, 16221 (1998).

[WEG99] M.R. Wegewijs and Yu.V. Nazarov. *Resonant tunneling through linear arrays of quantum dots.* Phys. Rev. B **60**, 14318 (1999).

[WEI95] D. Weinmann, W. Häusler, and B. Kramer. *Spin Blockades in Linear and Nonlinear through Quantum Dots.* Phys. Rev. Lett. **74**, 984 (1995).

[WEI99] Y. Wei, B. Wang, and J. Wang. *Nonlinear voltage dependence of shot noise.* Phys. Rev. B **60**, 16900 (1999).

[WET03] R. Wetzler, A. Wacker, and E. Schöll. *Self-consistent Coulomb effects and charge distribution of quantum dot arrays.* Phys. Rev. B **68**, 045323 (2003).

[WET03a] R. Wetzler, A. Wacker, and E. Schöll. *Coulomb scattering with remote continuum states in quantum dot devices.* J. Appl. Phys. **95**, 7966 (2004).

[WET03b] R. Wetzler. *Spatial Coulomb effects in semiconductor quantum dot devices.* (Ph.D. Thesis, TU Berlin, 2003).

[WET04b] R. Wetzler, R. Kunert, A. Wacker, and E. Schöll. *Inhomogeneous charging and screening effects in semiconductor quantum dot arrays.* New J. Phys. **6**, 81 (2004).

[WHA96] C. B. Whan, J. White, and T. P. Orlando. *Full capacitance matrix of coupled quantum dot arrays: Static and dynamical effects.* Appl. Phys. Lett. **68**, 2996 (1996).

[WIC50] G. C. Wick. *The evaluation of the collision matrix.* Phys. Rev. **80**, 268 (1950).

[WIE03] W. G. van der Wiel, S. De Franceschi, J. M. Elzerman, T. Fujisawa, S. Tarucha, and L. P. Kouwenhoven. *Electron transport through double quantum dots.* Rev. Mod. Phys. **75**, 1 (2003).

[YAM94] F. Yamaguchi and K. Kawamura. *Fluctuation of Current through a Quantum Dot far from Equilibrium: Effects of Strong Coulomb Interaction.* J. Phys. Soc. Jpn. **63**, 1258 (1994).

[ZHU02] J. Zhu and A. V. Balatsky. *Theory of current and shot noise spectroscopy in single-molecular quantum dots with phonon-mode.* Phys. Rev. B **67**, 165326 (2003).

[ZHU03] J. Zhu. *private communication.*

Publications

- **G. Kießlich, A. Wacker and E. Schöll**
  Geometry effects at conductance quantization in quantum wires
  phys. stat. sol. (b) 216, R5 (1999)

- **G. Kießlich, A. Wacker and E. Schöll**
  Geometry effects at conductance quantization in quantum wires
  Proc. 25th International Conference on the Physics of Semiconductors (ICPS-25), Osaka 2000

- **C. Pacher, C. Rauch, G. Strasser, G. Gornik, F. Elsholz, A. Wacker, G. Kießlich, and E. Schöll**
  Anti-reflection coating for miniband transport and Fabry-Perot resonances in GaAs/AlGaAs superlattices
  Appl. Phys. Lett. **79**, 1486 (2001)

- **G. Kießlich, A. Wacker and E. Schöll**
  Nonlinear transport through an ensemble of quantum dots
  Physica B 314, 459 (2002)

- **G. Kießlich, A. Wacker and E. Schöll**
  Sequential Tunneling Through An Array Of Electrostatically Coupled Quantum Dots
  Physica E 12, 837 (2002)

- **C. Pacher, G. Strasser, E. Gornik, F. Elsholz, G. Kießlich, A. Wacker and E. Schöll**
  Optics with ballistic electrons: anti-reflection coatings for GaAs/AlGaAs superlattices
  Physica E 12, 285 (2002)

- **G. Kießlich, A. Wacker and E. Schöll**
  Many-Particle Charging Effects and Recombination Current through a Quantum Dot Array
  phys. stat. sol. (b) 234, 215 (2002)

- **G. Kießlich, A. Wacker, E. Schöll, S. A. Vitusevich, A. E. Belyaev, M. Henini, A. Förster, N. Klein and S. V. Danylyuk**
  Nonlinear charging effect of quantum dots in a p-i-n diode
  Phys. Rev. B **68**, 125331 (2003)

- **G. Kießlich, A. Wacker, E. Schöll, A. Nauen, F. Hohls and R. J. Haug**
  Shot noise in tunneling through a quantum dot array
  physica status solidi (c) 0, 1293 (2003), cond-mat/0209523

- **G. Kießlich, A. Wacker, and E. Schöll**
  Shot noise of coupled semiconductor quantum dots
  Phys. Rev. B **68**, 125320 (2003), cond-mat/0303025

- **G. Kießlich, H. Sprekeler, A. Wacker, and E. Schöll**
  Positive Correlations in Tunneling through coupled Quantum Dots
  Semiconductor Science and Technology **19**, S37 (2004), cond-mat/0309027

- **H. Sprekeler, G. Kießlich, A. Wacker, and E. Schöll**
  Coulomb Effects in Tunneling through a Quantum Dot Stack
  Phys. Rev. B **69**, 125328 (2004), cond-mat/0309696

- **G. Kießlich, P. Samuelsson, A. Wacker, and E. Schöll**
  Decoherence and current fluctuations in tunneling through coupled quantum dots
  AIP Conf. Proc. 780, 439 (2005)

- **G. Kießlich, A. Wacker, and E. Schöll**
  Super-Poissonian current fluctuations in tunneling through coupled quantum dots
  appears in HCIS proceedings (2005)

- **G. Kießlich, P. Samuelsson, A. Wacker, and E. Schöll**
  Counting statistics and decoherence in coupled quantum dots
  submitted (2005), cond-mat/0507403

- **C. Gnodtke, G. Kießlich, A. Wacker, and E. Schöll**
  Phonon-assisted Tunneling through a Quantum Dot Stack
  in preparation (2005)

Index

Acknowledgements

The following persons I would like to thank for their particular contributions in the formation of this work:

- Prof. Dr. E. Schöll, PhD
- Prof. Dr. Andreas Wacker (Lund University, formerly TU Berlin)
- Henning Sprekeler, Christian Gnodtke
- Dr. André Nauen, Dr. Isabella Hapke-Wurst, Dr. Frank Hohls, Prof. Dr. R. Haug (Universität Hannover)
- Dr. Axel Thielmann und Dr. Matthias Hettler (Forschungszentrum Karlsruhe)
- Dr. Peter Samuelsson (Lund University, formerly University of Geneva)
- Fabricio M. Souza (Universidade de São Paulo, Brazil)
- Dr. S. A. Vitusevich and Prof. Dr. A. E. Belyaev (Forschungszentrum Jülich)
- Dr. H. Shtrikman, Prof. Dr. A. Yacoby, Prof. Dr. M. Heiblum (for the hospitality at the Weizmann Institute, Israel)
- AG Schöll, in particular: Michael Block, Frank Elsholz, Birte Hauschildt, Johanne Hizanidis, Dr. Oliver Holzner, Philipp Hövel, Roland Kunert, Dr. Kathy Lüdge, Jan Pomplun, Adrian Seufert, Grischa Stegemann
- all colleagues at the ITP
- my parents
- Claudia